University of Nottingham
UK | CHINA | MALAYSIA

# Microcarriers with Complex Architectures Manufactured by Two-Photon Lithography for Mechanobiological Manipulation and Expansion of Mesenchymal Stem Cells

**Jason Hutchinson**

Thesis submitted to the University of Nottingham in partial fulfilment of the requirements for the degree of Doctor of Philosophy

March 2022

# Abstract

Mesenchymal stem cells (MSCs) are a powerful tool in regenerative medicine owing to their innate capacity to differentiate into a range of cell lineages and this behaviour has been utilised as a means of tissue repair and regeneration. The prevalent issue in many treatments is the vast number of cells required for therapeutic effect, but this can be addressed through expansion of cell populations *in vitro* to suitable levels. Microcarriers are designed to provide a high level of cell growth surface within a small volume and have become one of the most promising expansion tools to date. However, transition to approaches that integrate biomechanical cues to modulate cell responses can lead to far greater outcomes than those that can be achieved through surface area alone. Such biophysical properties that can be integrated include geometry, roughness, topography, stiffness, and porosity which can promote specific biological responses through mechanotransduction pathways. This thesis focuses on employing this approach to microcarrier technology and examining the effects of such structures on cell control and enhancement of expansion yield to facilitate MSC production for therapeutic uses.

Two-photon lithography was employed to produce microcarriers with highly complex geometry at sub-micron feature size and optimisations allowed fabrication speed to be increased by up to 423-fold at the cost of structure resolution. Biocompatibility testing identified several suitable acrylate polymers with varying characteristics but highlighted the need for further materials exploration due to suboptimal adherence in most candidates. Novel fabrication techniques allowed cell culture isolation to structures without complication by anchoring substrates which addressed a continuing issue with two-photon derived samples that has been presented in the literature. A variety of produced designs exhibited significant increase in cell proliferation and consistent interaction with structure features with observable cellular preference for certain feature types and sizes. From these selected designs further morphological analysis of cells and DNA quantification determined microcarrier designs that lead to a significant increase in expansion yield in comparison to a conventional microcarrier design. Best expansion yields were seen in Buckminsterfullerene styled structures with

hollow interiors and porous outer shells and identified that expansion yield was not necessarily based on the amount of surface area alone. Analysis of stem cell phenotype changes across expansion periods indicated mixed results in the maintenance of phenotypes and requires further exploration.

This thesis demonstrated biomechanical based enhancement of expansion proficiency as well as novel techniques relating to two-photon lithography. However, for scale up of work and translation to clinical applications a significant increase in microcarrier production is necessary. Microcarriers that intelligently shape cellular proliferation and differentiation present an opportunity to act both *in vitro* and *in vivo* evolving beyond their primary function of expansion and acting as multifunctional tissue modulators.

# Acknowledgements

I would first like to thank my supervisor Professor Felicity Rose for the opportunity to undertake this challenge and for all the support, guidance and encouragement provided along the way. I would also like to thank my co-supervisors Professor Cameron Alexander and Professor Ricky Wildman for their continued guidance over the years. My gratitude goes to my supervisory team for all the support throughout this process and your efforts have made all the difference. My thanks also go to the EPSRC for funding this project and to the university of Nottingham for this opportunity. Acknowledgments also go to Tim Self and the school of life sciences imaging facilities along with the facilities and training provided by the nanoscale and microscale research centre.

A special thanks goes to Dr. Robert Owen for your help and knowledge throughout the last few years. I would also like to thank all the friends I've made along the way in the RMCT division, biodiscovery institute and two-photon group.

To my family, I would like to thank you for always encouraging and supporting me in every way possible. There will never be words for how grateful I am to you. Thank you for everything.

# Contents

# List of Figures

# List of Tables

# Abbreviations

| | |
|---|---|
| 2D | Two dimensional |
| 2GL | Two-photon grayscale lithography |
| 2PP | Two-photon Lithography |
| 3D | Three dimensional |
| 4D | Four dimensional |
| AA-2P | Ascorbic acid 2-phosphate |
| AAV | Adeno-associated virus |
| ALI | Acute lung injury |
| ALP | Alkaline phosphatase |
| ALS | Amyotrophic lateral sclerosis |
| ALT | Alanine transaminase |
| AM | Additive manufacturing |
| AMP | Adenosine monophosphate |
| ANOVA | Analysis of variance |
| AOM | Acousto-optic modulator |
| AST | Aspartate transaminase |
| BCA | Bicinchoninic acid |

| | |
|---|---|
| BDK | Benzyl dimethyl ketal |
| BDNF | Brain-derived neurotrophic factor |
| BM-MSCs | Bone marrow mesenchymal stem cells |
| BMP | Bone morphogenetic protein |
| BPD | Bronchopulmonary dysplasia |
| BSA | Bovine serum albumin |
| CCD | Charged-coupled device |
| CCL2 | (C-C motif) ligand 2 |
| CD | Cluster of differentiation |
| CFU-F | Colony forming unit fibroblast |
| CLI | Critical limb ischemia |
| CLP | Cecal ligation and puncture |
| COL1 | Collagen type I |
| COVID-19 | Coronavirus disease 2019 |
| COX2 | Cyclooxygenase 2 |
| CRP | C-reactive protein |
| CXCL | Chemokine (C-X-C motif) ligand |
| DAPI | 6-diamidino-2- phenylindole dihydrochloride |
| DASH | Disabilities of arm, shoulder and hand |
| DC | Dendritic cell |

| | |
|---|---|
| DEAE | Diethylaminoethyl |
| dH2O | Deionised water |
| DiLL | Dip-in laser lithography |
| DMAEMA | 2-(Dimethylamino)ethyl methacrylate |
| DMD | Duchenne’s muscular dystrophy |
| DMEM | Dulbecco's modified eagle medium |
| DMSO | Dimethyl sulfoxide |
| DNA | Deoxyribonucelic acid |
| DPP | Dynamic printing precision |
| dsDNA | Double stranded deoxyribonucleic acid |
| ECM | Extracellular matrix |
| EDTA | Ethylenediaminetetraacetic acid |
| ESC | Embryonic stem cell |
| ESEM | Environmental scanning electron microscopy |
| EthD-III | Ethidium homodimer III |
| ETOH | Ethanol |
| EV | Extracellular vesicle |
| FAK | Focal adhesion kinase |
| FBS | Fetal bovine serum |
| FDM | Fused deposition modelling |

| | |
|---|---|
| FIB-SEM | Focused ion beam scanning electron microscopy |
| GAGs | Glycosaminoglycans |
| GelMA | Gelatin methacrylate |
| GFP | Green fluorescent protein |
| GM | Goeppert-Mayer |
| GMP | Good manufacturing practices |
| GPI | Glycosylphosphatidylinositol |
| GvHD | Graft versus host disease |
| HA | Hydroxyapatite |
| HGF | Hepatocyte growth factor |
| HLA-DR | Human leukocyte antigen – DR isotype |
| HMDS | Hexamethyldisilazane |
| hTERT | Human telomerase reverse transcriptase |
| IBSP | Integrin Binding Sialoprotein |
| ICAM | Intercellular adhesion molecule |
| IFN-γ | Interferon-γ |
| IL | Interleukin |
| IL1-RA | Interleukin 1 receptor antagonist |
| iMSC | Immortalised mesenchymal stem cell |
| IPA | Isopropyl alcohol |

| | |
|---|---|
| IPSC | Induced pluripotent stem cell |
| ISCT | International society for cellular therapy |
| IV | Intravenous |
| IVD | Intervertebral disc |
| LESCs | Limbal epithelial stem cells |
| LP | Laser power |
| MAPTMS | 3-methylacryloxypropyltrimethoxysilane |
| MCA | Mesenchymoangioblast |
| MCP1 | Monocyte chemoattractant protein 1 |
| MED | Minimal effective dose |
| MEHQ | 4-Methoxyphenol |
| MRI | Magnetic resonance imaging |
| MS | Multiple sclerosis |
| MSC | Mesenchymal stem cell |
| NA | Numerical aperture |
| NIR | Near infrared |
| OCD | osteochondritis dissecans |
| PμSLA | Projection micro-stereolithography |
| PAG | Photoacid generation |
| PAX | Paired box protein |

| | |
|---|---|
| PBS | Phosphate buffered saline |
| PCL | Polycaprolactone |
| PDMS | Polydimethylsiloxane |
| PEG | Polyethylene glycol |
| PEGDA | Polyethylene glycol diacrylate |
| PETA | Pentaerythritol triacrylate |
| PETRA | Pentaerythritol tetraacrylate |
| PFA | Paraformaldehyde |
| PFD | Perfluorodecalin |
| PGMEA | Propylene glycol monomethyl ether acetate |
| pHEMA | Poly 2-hydroxyethyl methacrylate |
| PI | Photoinitiator |
| PLA | Polylactic acid |
| PLGA | Poly (Lactic-co-Glycolic) Acid |
| pNIPAAm | Poly N-isopropyl acrylamide |
| pNP | Para-nitrophenol |
| pNPP | Para-nitrophenol phosphate |
| PPARγ2 | Peroxisome Proliferator Activated Receptor Gamma 2 |
| RGD | Arginine-glycine-aspartic acid |
| RILI | Radiation induced lung injury |

| | |
|---|---|
| RNA | Ribonucleic acid |
| RT | Room temperature |
| RUNX2 | Runt-related transcription factor 2 |
| SA | Surface area |
| SA:V | Surface area to volume ratio |
| SCI | Spinal cord injury |
| SCPL | Solvent casting particle leaching |
| SD | Standard deviation |
| SEM | Scanning electron microscopy |
| SEMD | Spondyloepimetaphyseal dysplasia |
| SMA | Spinal muscular atrophy |
| SOX9 | SRY-Box Transcription Factor 9 |
| SS | Scanning speed |
| TCDMDA | Tricyclodecanedimethanol diacrylate |
| TGF-β1 | Transforming growth factor beta 1 |
| TMPETA | Trimethylopropane ethoxylate triacrylate |
| TNFα | Tumour necrosis factor α |
| TPA | Two photon absorption |
| TPMS | Triply periodic minimal surface |
| UV | Ultraviolet |

| | |
|---|---|
| VEGF | Vascular endothelial growth factor |
| WCA | Water contact angle |
| βGP | Beta-glycerol phosphate |
| δTPA | Two-photon absorption cross-section |

# 1. Introduction

Mesenchymal stem cells (MSCs) are progenitor cells capable of differentiating into a range of tissues and have been pursued in regenerative medicine and tissue engineering as a means of tissue repair and replacement. MSCs have been demonstrated for use across a wide range of tissue types and diseases including myocardial repair (1), gastrointestinal epithelia (2), kidney disease (3), liver (4), diabetes mellitus (5, 6), neurodegenerative diseases (7, 8) and complex immune diseases such as Parkinson's and multiple sclerosis (9). The use of MSCs for generation and repair of bone tissue (10-12) and cartilage (13-15) has been well explored across a number of studies. MSCs also have function as potent immunomodulators that have become more recently recognised and explored as a therapeutic.

Given the vast potential of MSCs in tissue repair they have been explored for use both academically and clinically in many different therapeutic scenarios and treatments across a broad range of tissue types and disorders. The prevalent issue in many of these treatments is the vast number of cells required for therapeutic effect that can range into the billions of cells per patient (16). The necessity for such substantial quantities of cells becomes problematic when the population of such cells in the human body is very low with the mononuclear cell fraction of bone marrow containing only 0.001% MSCs (17). As such expansion and growth of cell population *in vitro* to levels suitable to therapies is necessary.

One of the essential components for this process is a solid surface for growth given that MSCs are anchorage dependant cells. However, within early passages cells will only grow at a consistent rate for about three weeks after which proliferation decreases and cells begin to senesce and lose their multilineage differentiation capacity rendering them useless as a therapeutic agent (18, 19). As such rapid growth of cells facilitated by large surface areas (SA) are necessary for expansion to be achieved and these have been employed in the form of multi tray systems, roller bottles and other robotic assisted means to increase surface area and manufacturing throughput (20-22). Despite

the early success of some of these techniques when it comes to stem cell therapies, they still struggle to meet demand and come with a variety of drawbacks.

One of the most promising solutions to date is the production of microcarriers which are microparticle beads as a cell growth surface. Whilst the classical goal of microcarriers was to provide high surface area the established view of microcarriers as exclusively a provision of surface area is becoming obsolete. There is a need for new products that can integrate cues for cell differentiation to intelligently modulate cell responses and enhance proliferation and modulate phenotype. One route of achieving this through microcarriers is by adjusting the biophysical properties of the microcarriers. Such features include size, geometry, topography, stiffness, and porosity which can promote specific biological responses through mechanobiological persuasion, that is by subjecting cells to physical cues or stresses that trigger mechanotransduction pathways that lead to cell behaviour changes (23-26). Advanced additive manufacturing (AM) techniques such as two-photon lithography can provide this function and have been utilised in the presented research to address this unrealised goal.

# 1.1 Tissue engineering and MSCs

### 1.1.1 Tissue engineering – aims, approaches and history

The regenerative medicine approach aims to treat diseased and damaged tissues through replacement, repair or regeneration of tissues in order to restore normal function (27). Despite the terms relatively modern popularisation the goal of regenerative medicine has been long sought after and has only begun to be realised due to the advancement of medical technologies. The greatest tool in regenerative medicine is the application of tissue engineering strategies to restore and regenerate tissue function. Tissue engineering is born from a collection of disciplines including mechanical engineering, materials science and various biological fields (28). The term first coined in 1988 was described by Langer and Vacanti as “the application of principles and methods of engineering and life sciences towards the fundamental understanding of structure–function relationships in normal and pathological

mammalian tissues and the development of biological substitutes to restore, maintain or improve tissue function." (29).

The three main strategies employed by tissue engineering are the transplantation of cells or tissues to stimulate natural repair processes, the use of cells to deliver therapeutics such as genes or growth factors and also the use of biomaterials as support for tissue growth (30). Biomaterials can be historically defined as "substances other than food or drugs contained in therapeutic or diagnostic systems that are in contact with tissue or biological fluids"(31). These terms can be applied to early attempts to restore function to damaged or lost body parts such as through wood or bone prosthetics. Dating back to 1065BC, Egyptians demonstrated replacement of amputated toes with primitive but functional wooden prosthetics for balance and aesthetic purposes (32).These early attempts were acellular practices with inert materials acting as structural supports often in the form of prosthetics. Modernisation of this approach utilises a variety of materials including metals, ceramics and polymers which have been commonly used for plastic surgery, joint replacement, bone fracture repair, vascular stabilisation, and dentistry to name but a few (33). Many modern approaches seek to use materials that are cellularised and have active living components within or on the material itself which elevates them from simple structural supports and into living functional constructs.

The processes by which tissue engineered constructs are made typically form into either a top-down approach or bottom-up approach. Top-down approaches often employ the seeding of a therapeutic cellular component into a larger structured biomaterial seeking to add cellular function guided by the pre-patterned scaffold. Bottom-up approaches take the form of smaller modular units of regeneration that combine together over time with tissue ingrowth forming a larger construct (34). The advantage of cellular techniques is that the living component delivered can respond to changing environments and adapt over time to a variety of situations, this dynamic behaviour cannot be replicated for drugs that often have a single and continuous mode of effect (35). However, as technology and understanding grows the original concept of biomaterials functioning as simple structural substitutes is becoming obsolete. Advancements in materials design and in the understanding of complex biological

interactions is now driving materials development towards those that replicate or improve upon native tissue function and dynamics

### 1.1.2 Stem cell discovery

Arguably the greatest tool in regenerative medicine is the identification of the stem cell. Stem cells are generally defined as progenitor or undifferentiated cells that have the ability to indefinitely reproduce and differentiate into tissue specific cell types and lineages (8). The first use of stem cells therapeutically is uncertain as stem cells in bone marrow were unknowingly applied before the term or understanding of the underlying principle was identified. As such, stem cell use and discovery pre-dates the establishment of the regenerative medicine field. The name stem cell is first documented as early as 1868 by German biologist Haeckel, although this term was used in an evolutionary sense and described ancestral unicellular organisms. This first use of the term does not reflect what we have now come to understand as stem cells. Haeckel also later applied the term for fertilized eggs to describe the cell that stems into all others within the organism (36). This concept developed and solidified its roots in embryology through the works of Weismann, Boveri and Häcker but didn't become popularised in the English language until this work was reviewed and published in a book by Wilson in 1896. Around this time, research into haematopoiesis began to grow and these concepts of a undifferentiated progenitor cell population began to be explored in experiments and histological techniques developed by works of Ehrlich, Neumann, Müller and Maximow from 1868 onwards (37). Given the technological restriction of this era it wasn't until the early 1960s that work by Becker, McCulloch and Till fully demonstrated the existence of haematopoietic stem cells (38). The exact nature and functionality of these cells was fully reported in 1963 shortly after their initial observations. These experiments confirmed self-renewal and differentiation capabilities of the identified cell population (39). Despite the identification and characterisation provided in these papers from 1963 onwards, bone marrow transplants which contain stem cell populations had been utilised therapeutically as early as 1957 with success by both Thomas and Mathe (40, 41). The establishment of stem cell biology and function over the years paved the way for the development of the regenerative medicine approach that stem cell therapies later became associated with.

### 1.1.3 Stem cell potency and classification

The function of stem cells is to act as progenitors which can differentiate into the many cell types of the body. Stem cells have roles in adult tissue maintenance and repair as well as embryonic development. The capability of stem cells to form specific tissues is defined as its potency. Totipotent stem cells exhibit the capacity to generate all tissues of the body with no limitation growing entire bodies during foetal growth (42). Pluripotent cells have the capability to differentiate into cells of all three embryonic germ lines when chemically prompted (43). Multipotent cells exhibit potency to the extent that they can form a multitude of cells but only from one specific embryonic germ layer, most adult stem cells are of this type (44). Finally the lowest degree of stemness is unipotent cells that can differentiate into only one specific tissue lineage (8).

The classification and nomenclature of stem cells is derived primarily by location from which they are sourced and their level of potency. Embryonic stem cells isolated from the inner cell contents of blastocyst stage of embryos around three to five days after fertilisation are pluripotent and would naturally give rise to all the organs and tissues of the human body (45). Although these cells are incredibly useful for therapies due to their pluripotency, there are some difficulties to their use due to ethical consideration, fragility and necessity of feeder cells for culture (46). Another group of stem cells can be briefly described as somatic or tissue specific adult stem cells. These cells are multipotent and exhibit less stemness than embryonic cells but persist in small populations even in fully matured organisms. These cells, thought to be involved in tissue repair, remodelling and homeostasis, can be isolated from various sources within the body but are far outnumbered by mature adult cells (47). Another interesting stem cell type that was more recently established was the induced pluripotent stem cell (iPSC) which is unique given that they are adult cells transformed into a stem cell like state and therefore not naturally occurring. They provide a more sustainable and ethical cell source directly from the patient with an additional bonus that genetic material will match resulting in a lower chance of rejection when used as a therapy (48). However, cell reprogramming to induce the stem cell state can be quite costly and there is also an enhanced risk of immunogenicity and tumour formation which can make transplantation unsafe (49). Breakthroughs in this area have allowed iPSCs

programmed from adult cells to differentiate into mesenchymoangioblasts (MCAs) which have then been demonstrated to differentiate into mesenchymal stem cells (50).

### 1.1.4 Mesenchymal Stem cells

Of the described stem cell types, one of the most highly researched is the MSC that belongs to the somatic or adult stem cell population. The terminology mesenchymal stem cell, coined in the 1991 by Caplan, is often used to classify cell populations isolated from connective tissues that show stem cell properties (51). The discovery and initial description of MSCs arose years before the MSC term was coined through a series of experiments by Friedenstein in the 1970's regarding what they described as colony forming unit fibroblasts (CFU-Fs) from bone marrow that exhibit stem cell qualities. These experiments collectively reviewed in 1990 paved the way for what became known as the MSC (52, 53). The features of these cells include the ability to self-renew and differentiate along the mesodermal lineage of tissues which include the formation of osteogenic, adipogenic and chondrogenic cell types whilst also presenting specific spindle shape cell morphology and adherence to tissue culture plastic (54). Over the years following this discovery, cell populations that present with similar phenotypes have been extracted from a variety of tissues including skin (55), adipose (56), muscle (57) and even teeth (58).

There has been debate as to the exact nature of an MSC and as to whether this is the correct terminology to use. Many different populations of cells have fallen under this umbrella term each exhibiting varying levels of differentiation, gene expression, origin and markers which leads to an unclear understanding of the biology at play (59). As the understanding of MSCs and their characteristics in comparison to other stem cell populations grew many began to urge the use of new terminology to better reflect their true nature. In 2005 Horwitz *et al* presented a statement to the International Society Cellular Therapy (ISCT) advocating for the use for the term mesenchymal stromal cell to better reflect their belief that these cells were derived from the connective tissue referred to as stroma (60). This stromal origin theory was later disproved in 2008 when it was identified that MSCs were derived from perivascular origins (61). In response to this dispute, a further level of clarification was given in 2006 when the ISCT outlined three specific standards to classify as an MSC. These include the positive expression of

surface markers CD73, CD90 and CD105 and the absence of CD34, CD45, HLA-DR, CD14 or CD11B, CD79α or CD19 expression. The two other standards include adherence to tissue culture plastic and the capability of *in vitro* trilineage differentiation to adipogenic, chondrogenic and osteogenic lineages (62). These standards are still used currently. Despite this effort to classify this cell type, it is still reported that cells falling under these criteria can exhibit variance in biological features based on donor variation, source material, culture materials and conditions (63). The advancement of MSC characterisation and recognition of their potent immunomodulatory and signalling properties prompted Caplan to publish an article in 2017 strongly advocating the use of the term medicinal signalling cells that he had first proposed in 2010 (64, 65). This updated nomenclature would allow the popularised acronym MSC to continue but updated the MSC term to reflect that, in Caplan's opinion, MSCs are not stem cells. Despite this, the term mesenchymal stem cell has continued to be used and this debate continues.

Despite the terminology debate, these cell populations present an excellent source of cells for regenerative therapies that have potential for substantial therapeutic effect. Additional to these qualities, they also exhibit immunological influences including the important capacity to reduce inflammation and regulate immune (66), (67). MSCs have been shown to have therapeutic potential for treating heart (1), diabetes (5) (6), gastrointestinal (2), liver (68), kidney (3), immune (9) and neurodegenerative diseases (7), as well as to regenerate bone (10-12) and cartilage (13-15). An overview of this is depicted in figure 1.1.

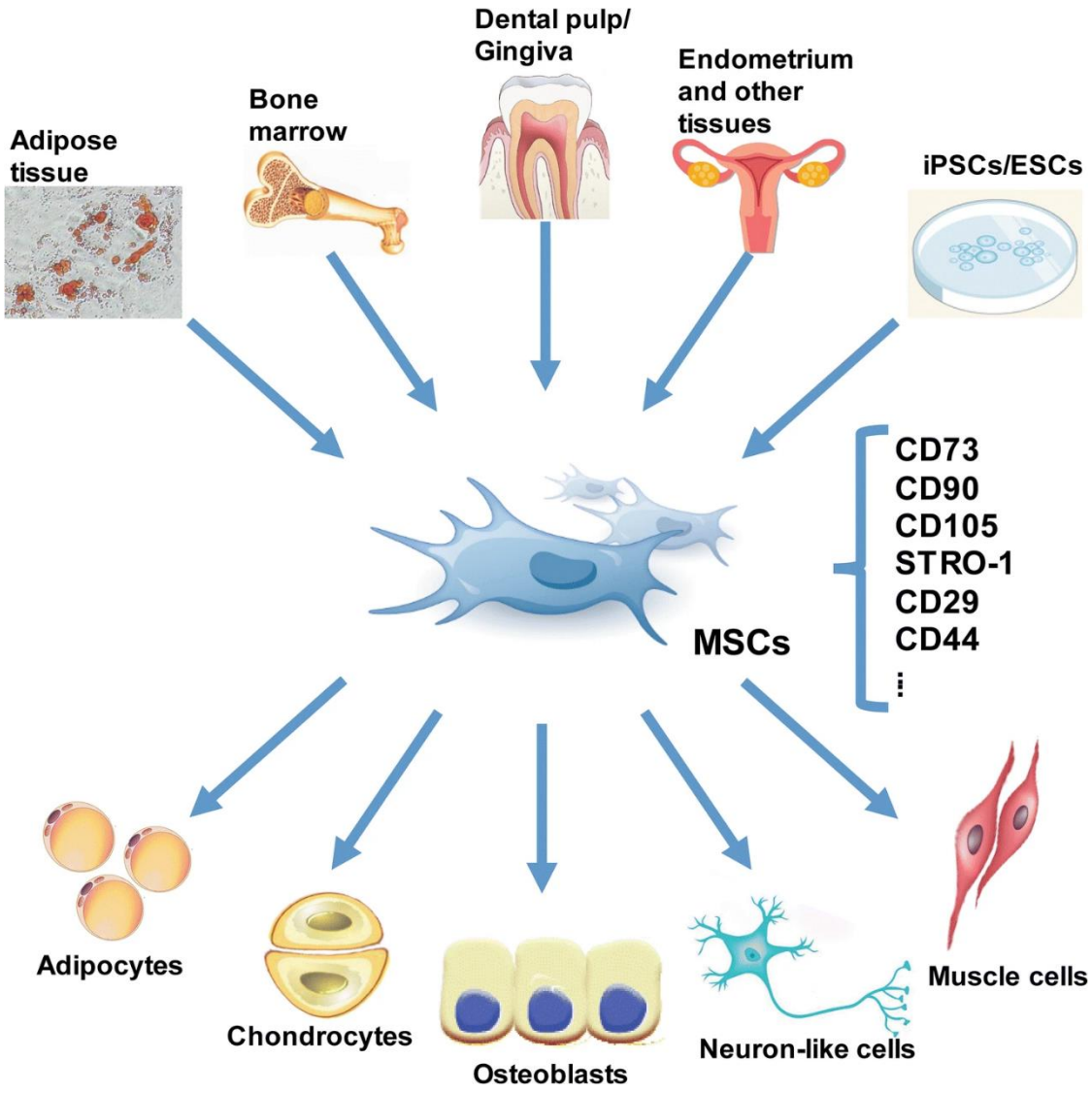


***Figure 1.1:*** *MSC source sites and differentiation routes. MSCs can be isolated from foetal, neonatal and a variety of adult tissues including bone marrow and adipose. These MSCs present certain surface markers and can differentiate into a variety of cell types from varying tissues. Reproduced with permission via creative commons license from Fan et al (69)*

## 1.2 MSC mechanism of action

There are several mechanisms by which MSCs can exert a therapeutic effect. This includes migration of cells to sites of injury, differentiation and engraftment into tissues, various paracrine factors including immunomodulation, mitochondrial transfer, extracellular vesicle production and antimicrobial activity. These mechanisms will be discussed further but are briefly summarised in figure 1.2.

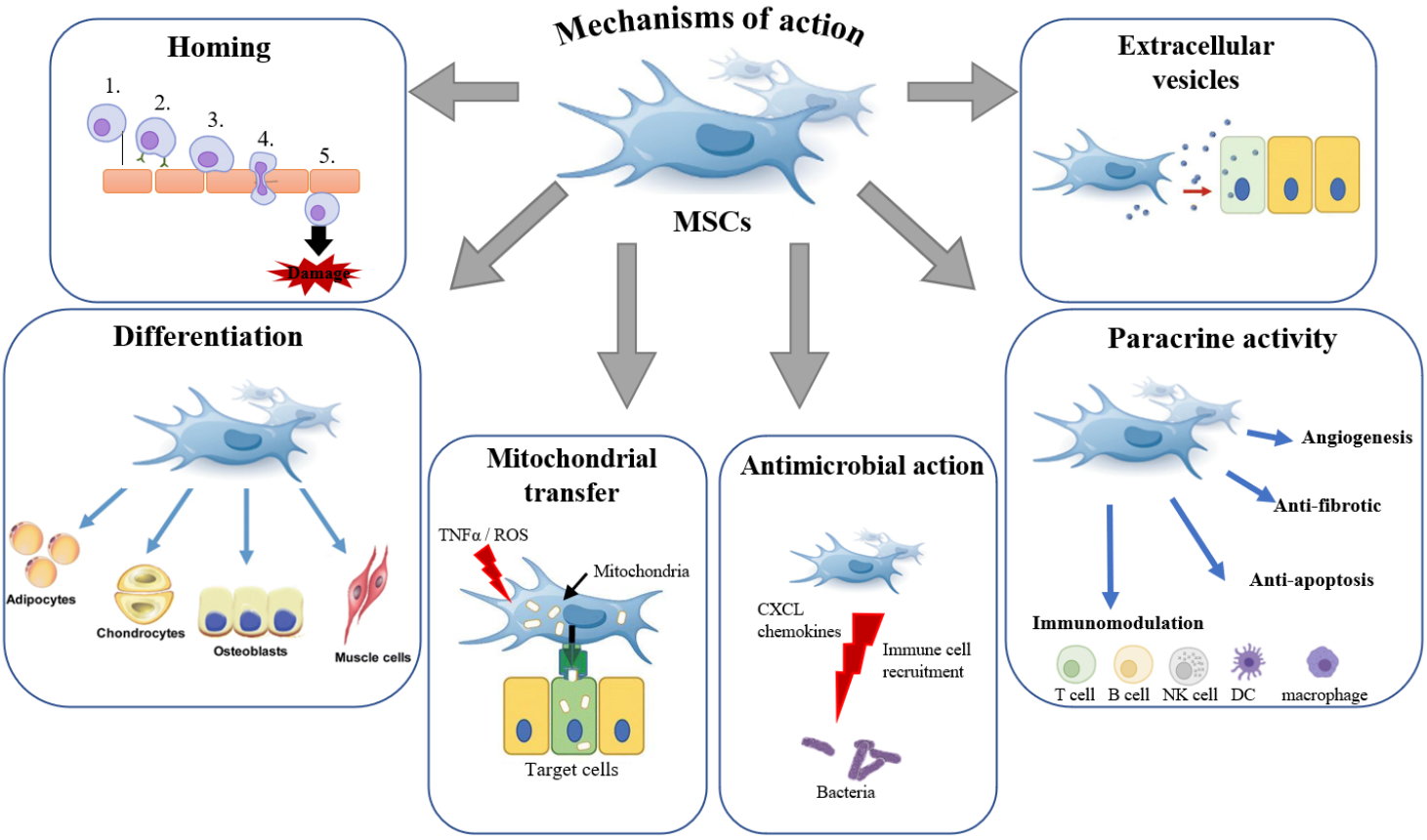


***Figure 1.2:*** *MSC mechanisms of action. MSCs can exert a therapeutic effect through migration of cells to sites of injury, differentiation and engraftment into tissues, various paracrine factors including immunomodulation, mitochondrial transfer, extracellular vesicle production and antimicrobial activity. Some elements modified with permission via creative commons license from Fan et al (69)*

### 1.2.1 Differentiation and engraftment

Early studies primarily focused on the migration and differentiation of transplanted cells that underwent direct engraftment or fusion with damaged cells. Some studies have shown that direct engraftment can occur following transplant, but they are often a low portion out of the total number of cells delivered (70-75). Other studies how found complete clearance and demonstrated that <1% of cells survive and engraft with the remainder unable to be detected for long after delivery. Despite the results of this study this value of clearance does not hold true in all therapies, including some previously discussed, and will vary based on transplantation methodology. There is continuing debate within the literature as to the insufficient confirmation of *in vivo* proliferation of transplanted MSCs for any substantial period of time following therapy

This situation is not unique to MSCs specifically and similar outcomes have been seen in other cell transplantations including hematopoietic stem cell and T-cell therapies (76). The reasons for this may include the sensitivity to the transplanted microenvironment as stem cell niches have very specific conditions and are scarcely available. There is also the potential issue of entrapment in small vessels such as in the lungs when administered systemically. MSCs exhibit strong cell to cell contacts and can lead to an inhibition of cell division leading to a slow uptake and quick clearance. This outcome can be improved when delivered to, or in, a matrix for cell colonisation, in which focal adhesion-based signalling and other increases in intracellular signalling pathways leads to an increased proliferative outcome (76). Other steps towards cell optimisation often taken for granted include oxygen levels in culture. Often laboratory culture of cells is conducted at 21% or atmospheric oxygen levels for ease of use, however oxygen values within tissue may be much lower than this. This can lead to a metabolic mismatch when cultured cells are suddenly implanted into a low oxygen environment and need to rapidly adapt. Studies have used low oxygen (1-5%) for MSC culture and found promising results with increased levels of cell survival *in vitro* at the cost of slower proliferation (77). Overall, synchronisation of culture microenvironment to destination conditions and metabolically priming cells for survival before implantation could be further considered for higher cell survival rates post-transplant.

Another reason for a low retention of delivered cells may be due to delivery method and the strains that are placed on cells during that transition. Most clinical grade therapies deliver cells via injection whether this is an IV administration or localised, and most commonly saline is the vehicle of choice for that delivery (78, 79). In some cases the loss of cells in the transplant area has been immediately documented within minutes of the injection (80). Previous studies indicate that cell damage, lack of retention and changes to stem cell differentiation may be due in part to the shear stresses and mechanical forces that occur during delivery through the needle (81). Increasing the proportion of viable cells sustained after delivery would aid in provision of a better therapeutic dose whilst easing expansion needs and overall increasing success of the therapy. The material surrounding the stem cells during and immediately after administration can be vital to cell proliferation and fate (82). Therefore, it was explored whether biomaterials could act as a protective agent to cells during delivery to maintain a higher cell survival and therefore dose. An *in vitro* study indicated a significant improvement in cell viability of 87% when a 2% gelatin support vehicle was used. This was in comparison to a 32% viable delivery when administered with a saline vehicle. Rheological properties or material chemistry were not responsible for protective effects but the ejection rate and carrier material effectively modulated stem cell differentiation into osteogenic lineages (79). This study demonstrated how important overlooked practices such as delivery through needles can be in the fate of a stem cell therapy and highlights the need for strict controls and standardised techniques across clinical studies.

### 1.2.2 Homing to the site of injury

MSCs also exhibit a homing ability to sites of injury, this has been explored in cell delivery models to increase the survival rate of transplanted cells. The mechanism of migration can be summarised in five stages: tethering, activation, arrest, transmigration and migration. These stages start with tethering to endothelial cells in the vasculature via interaction of endothelial cell selectins and MSC expressed CD44. This tethering leads to rolling of the MSC and begins pulling the cell out of circulation and onto the vasculature wall (83). Following this MSCs may become activated by chemokine receptors that are triggered by inflammatory signals and cause arrest of the cell on the

surface. Next matrix metalloproteinases are secreted by the MSC in order to migrate through the endothelial layer and basement membrane before further migration through the interstitium towards the inflammatory signals at the site of injury (84, 85).

This homing ability present in MSCs can be enhanced by drug pre-treatment with kinase inhibitors such as Ro-31-842, boosting migration to ICAM-1 abundant sites of injury and inflammation (86). This is an important step as migration is quite inefficient and only a small portion of cells will localise at the injury site if administered systemically (83).

### 1.2.3 Paracrine factors

Another feature of MSCs that make them an interesting tool for regenerative medicine is their potent paracrine function and release of soluble factors that has become more recently recognised and explored as the primary therapeutic agent. This is particularly important given that there is debate as to the level of cell engraftment possible. Paracrine factors include immunomodulatory, angiogenic, antifibrotic, anti-apoptotic and antioxidative factors (69).

Immunomodulatory capacity includes interactions with T cells, B cells, dendritic cells, neutrophils, natural killer cells, macrophages and through secretion of both anti-inflammatory and pro-inflammatory cytokines (87). This function of MSCs has been explored as potential treatment for autoimmune diseases such as rheumatoid arthritis, Crohn's disease, and type-1 Diabetes (88-90). Additionally, there is therapeutic potential in the treatment of sepsis via macrophage reprogramming induced via secretion of prostaglandin $E_2$ (91). Autoimmune suppression via MSC therapy can also offer a potential solution to organ transplantation and tissue graft rejection (92).

MSC therapy supports the polarization of macrophages to type two anti-inflammatory immune regulatory states and inhibits pro inflammatory type-1 polarized states by the action of MSC produced interleukin-1 receptor antagonist (IL1-RA) (93). Anti-inflammatory state macrophages produce large amounts of IL-10 and reduced levels of proinflammatory TNF- α which is mediated and enhanced by MSC secreted factors such as IL-6 and hepatocyte growth factor (HGF) (94). This enhanced production and

circulation of IL10 from macrophages further influences polarisation towards anti-inflammatory states in naïve and type-1 macrophages creating a positive feedback loop guiding towards immune regulatory pro healing states (95). Anti-inflammatory polarization has also been demonstrated upon phagocytosis of MSCs by macrophages (96). The removal of phagocytic cells from the population supresses MSC induced immunomodulation indicating that both soluble factors and cell-cell interactions play a critical role (97).

Similar immunomodulation via MSCs is seen in dendritic cells (DCs) where the presence MSCs reduces DC migration and maturation. MSCs also reduce secretion of TNF-α in pro-inflammatory DCs and increase production of IL10 in anti-inflammatory DCs similar to their effect on macrophage (66). In a cecal ligation and puncture (CLP) induced sepsis rat model the levels of overall mortality as wells as TNF-α, cytotoxic T cells and T helper cells was significantly reduced in groups treated with apoptotic MSCs (A-ADMSCs) in comparison to those without treatment(98). In further studies of sepsis induced acute lung injury (ALI) and sepsis induced acute kidney injury, intravenous apoptotic MSC transplantation reduced inflammation, oxidative stress and tissue damage. Interestingly a better therapeutic outcome was seen in the delivery of apoptotic cells that were provided by the administration of living MSCs (99). In a murine model of GVHD it was identified that host cytotoxic T cells induce apoptosis in transplanted MSCs via the action of perforin. This action in part triggers the immunomodulatory functions of MSCs previously described and is a vital step in generating this function. Hence the delivery of already apoptotic cells skips this stage leading to a more rapid and enhanced therapeutic effect (100). This mechanism of reliance on apoptosis of MSCs in order to deliver therapeutic function has recently become more understood and is beginning to be thought of as the primary route of therapeutic action rather than just their secretory profile (101).

Angiogenesis or the promotion of vasculature growth is another biological factor that can be modified by MSCs. It is believed that part of the therapeutic effects in ischemic disease, coronary artery disease, and wound repair are related to modulation of angiogenesis by MSCs. These aspects are affected by MSC secretion of vascular endothelial growth factor (VEGF), fibroblast growth factor (FGF), insulin-like growth factor (IGF), hepatocyte growth factor (HGF), placental growth factor (PGF),

monocyte chemotactic protein-1 (MCP-1), stromal cell-derived factor-1 (SDF-1), and angiopoietins which are all intrinsic to angiogenesis and vascularisation (69, 102, 103).

It is also known that the secretome of MSCs can also prevent scarring and has anti-fibrotic properties. Chronic inflammatory loops drive fibrosis and replace tissue structures with non-functional scar tissue. Secretion of interleukin-1 receptor antagonist (IL-1Ra) was shown in mouse live fibrosis models to reduce collagen deposition and reverse chronic inflammatory states (104). Similar inhibition of fibrotic outcomes has been shown in both lung injury and myocardial infarction models and is driven by reduction of oxidative stress, TGF-β1 levels, endoplasmic reticulum stress and fibrosis associated tissue inhibitor of matrix metalloproteinase-1 (TIMP1) (105-107).

An additional mode of action is the production of anti-apoptotic factors that restore cellular homeostasis in affected cells. MSCs can secrete VEGF, HGF, IGF-I, FGF, TGF-β, stanniocalcin-1 (STC1), and granulocyte–macrophage colony-stimulating factor (GM-CSF) which have been shown to inhibit apoptosis (107). Of these soluble factors VEGF is particularly linked with reduction of p53 associated apoptosis through the phosphorylation of focal adhesion kinase (FAK) which is integral in promoting cell survival (108). This has been explored *in vivo* in rat models as well as with human liver cells *in vitro* which indicated that BCL-2-associated X protein (BAX) downregulation and increased secretion of B-cell lymphoma-2 (BCL-2) tips the balance between these two factors promoting homeostasis and protecting against ischemia (109).

### 1.2.4 Mitochondrial transfer

Growing evidence of mitochondrial transfer from MSCs to damaged cells has been seen in the literature. Transfer of mitochondria are believed to rescue the damaged cells and return them to homeostasis. This is given that mitochondria play critical roles in ATP production, oxidative phosphorylation, and apoptosis. This transfer is believed to occur through the action of microvesicles, gap junctions, tunnelling nanotubes and cell fusion (69, 107, 110). Several studies have identified signals of this transfer process including mitochondrial DNA, products and signals. This mechanism has been shown to have protective effects in a variety of scenarios including, lung injury, allergic

reaction, ischemic cardiomyocytes, neurotoxicity, kidney injury and spinal cord damage (69).

Tunnelling nanotubes form through action of miro1 adaptor proteins that binds to various motor proteins upon activation to form a motor-adaptor complex that directs the migration of mitochondria (111). Studies with miro1 knockdown cells was found to limit mitochondrial transfer which led to a reduction in therapeutic effects within bronchial injury models (112). In contrast overexpression of miro1 is shown to give enhanced therapeutic function (69, 111). It has been demonstrated that presence of high levels of TNF-α and high levels of reactive oxygen species are responsible for triggering formation of tunnelling nanotube *in vivo* and as such indicate how this process is naturally triggered in sites of injury and inflammation (113). As such mitochondrial transfer is thought to be one of the many modes of action that give MSCs their therapeutic ability although further work is needed to fully identify all aspects of this function.

### 1.2.5 Extracellular vesicles

Non-cellular therapies have been explored in order to address concerns with direct cell implantation. This has led to the use of extracellular vesicles (EVs) produced by MSCs as a potential therapeutic product. These MSC derived membrane particles or exosomes still seem to have immunomodulatory potential even on their own. These particles are enzymatically active and are absorbed by monocytes and surface bound to the plasma membrane leading to apoptosis in proinflammatory populations (114). However, these did not exhibit T-cell interaction indicating that both cell contact dependent interactions as well as soluble factors such as cytokines are both implicated in total immunomodulatory function.

The contents of these vesicles that promote therapeutic function can be quite heterogeneous containing proteins, mRNA and microRNAs which are believed to be critical in many processes and constitute a form of intracellular communication (115). The most understood mechanism is that these EVs supress proinflammatory cytokines in sites of injury stabilising the immune environment and promote the production of

anti-inflammatory cytokines such as IL-10 and IL-4. This cytokine adjustment has been seen *in vivo* in animal models of autoimmune diabetes and liver injury (90, 116).

The mechanism of EVs are not limited to immunomodulation and cytokine balancing but have also been shown to promote angiogenesis and neovascularisation in wound healing. Through increased VEGF-A expression which stimulates the Wnt4/β-catenin pathway EVs were shown to increase proliferation of endothelial cells in both burn wound and diabetic wound models (117, 118). This is in combination to a variety of other activated signalling pathways that promote wound healing and repair processes (107).

Some of the EVs that can be produced by MSCs and have been implicated in therapeutic effect include apoptotic bodies. These are only released via apoptosis of the MSC which links into previous discussion of therapeutic effects being mediated by apoptosis of the delivered cells. Some apoptotic bodies have been characterised to include ubiquitin ligase RNF146 and miR328-3p which are known to maintain MSC multipotency, triggering activation and maintenance of native stem cell populations (119). Apoptotic bodies released from apoptotic MSCs in a myocardial infarction rat model were seen to promote both angiogenesis as well as lysosomal biogenesis and autophagy which resulted in improved cardiac function (120).

### 1.2.6 Antimicrobial action

*In vivo* studies of bacterial sepsis have indicated that MSCs also have a bactericidal effect as a result of their immunomodulatory properties and cytokine secretion which enhance phagocytic activity (91, 121, 122). *In vitro* studies of the secretory properties of MSCs demonstrated antimicrobial activity against *E. coli* and *S. epidermidis* with response to the latter microorganism being just as potent as commercial antimicrobial solutions (123). These initial experiments were conducted *in vitro* and so interference from host immune responses and extraneous chemical signals are uninvolved, signifying that the antibacterial effect is a direct result of one or more of the components of the MSCs secretome (124). Chemokines including CXCL1, CXCL6, CXCL8, CXCL10, CCL5 and CCL20 have been proven to have antibacterial activity against staphylococcal strains as well as *E.coli* and are actively secreted from the cells

attributing to the therapeutic effect (124, 125). This demonstrates the wide-reaching implications of MSC based treatments and the impact they can have on medicine if properly understood, controlled and implemented.

### 1.2.7 Immunomodulation case study: COVID-19

The immunomodulatory functions of MSCs have become so well recognised that they have been a potential source of treatment even for very high-profile cases such as COVID-19. COVID-19 induced pathology is brought about by excessive inflammation and the mass production of inflammatory signals sometimes referred to as “a cytokine storm”. It is this extreme response that leads to respiratory distress and overall organ inflammation, damage and scarring that is exhibited in severe cases (126). Since intravenously transplanted MSCs tend to accumulate within the lung vascular system the potential for MSC therapy for restoration of the pulmonary environment, protection of alveolar epithelial cells, prevention of fibrosis and overall reversion of chronic inflammatory lung dysfunction has been investigated (127).

Since the pandemic began and global scientific focus has shifted towards finding suitable therapies, there have been 127 stem cell based clinical trials registered on clinicaltrials.gov aiming to combat the disease through the administration of MSC therapies (128). Overall many studies have indicated an improved clinical outcome in patients treated with MSCs with reduced lung damage and quicker recovery (129). This treatment was found to be safe even in very high doses when patients followed up after 96 weeks post treatment, a high level of immune tolerance was seen and clinical trials progressed to phase three (130). Exosome treatment as previously described was also found to be a promising route for alleviating inflammatory states and improving clinical outcome (131). A case study of a critically ill patient showed an increase in neutrophil populations by 87% and a minor decrease in lymphocytes due to viral infection. Antiviral drugs did little to combat the symptoms at this point with severely under oxygenated muscle tissue leading to fatigue and the need for mechanical ventilation. Injection with MSCs along with α1 thymosin showed decreased CRP, serum albumin and AST/ALT ratio which marked overall improved vitality. As white blood cell and neutrophil levels decreased the increase of CD3+ ,CD4+ and CD8+ T

cell populations lead to improved lung function and the removal of mechanical ventilation (132).

Further early studies saw similar results across multiple patients treated with MSCs with clinical improvement in all patients 2-days post transplantation compared to those treated with conventional therapy. Inflammatory responses were reduced via increased presence of peripheral lymphocytes and T cells, TNF-α levels significantly decreased and IL-10 levels increased marking the action of MSCs and shifting of the environment away from the hyper inflammatory state.

### 1.2.8 Risk of cell transplantation

With transplantation of stem cells for various therapies, whether these are focusing on regenerative or immunomodulatory aspects, there are some risk factors associated and these are the major barriers to clinical application. Although a large number of trials and studies have been conducted with overwhelmingly positive outcomes the major safety concerns of tumorigenicity, inflammation and fibrosis are still present in a small number of cases (63).

MSCs do have the ability to form and support tumours, for example Ewing's sarcoma which is thought to be derived from MSC populations, which is a severe risk factor (133). Some studies have found tumours that have developed from tissue grafts some years later after treatment, this was the case for an ataxia-telangiectasia stem cell therapy that lead to the formation of a glioma (134). These incidents occasionally form due to a few factors including the excessive production of cytokines and growth factors by MSCS that, while often providing a positive effect, can also regulate tumour function enhancing growth (135). Another problematic factor is that the immunosuppression abilities of MSCs can in the case of tumour formation turn into immune evasion reducing the clearance of problematic cells and aiding in cell metastasis (136). Another tumorigenic risk factor is the pro-angiogenic properties of MSCs previously discussed, that are often useful for regenerating tissues but in the case of tumours can aid in vasculature growth, feeding the tumour and endorsing growth (137). Studies into MSC tumorigenesis have given mixed results with direct transplantation of large volumes of cells into rat models yielding no evidence of tumour

growth (138). The fear of proliferative action on already established tumours is also uncertain as studies of oesophageal cancer found stem cell fusion led to selective apoptosis in tumour cells and shifts towards a benign state (139). However soluble factors that promote growth or angiogenesis can be downstream from the tumour and cause proliferative effects without coming in contact close enough to allow cell fusion. This is similarly seen in the case of ovarian cancer studies where stimulation of tumours can occur due to soluble factors but reduction of tumour mass can occur upon direct contact of cells and fusion of MSCs (140).

MSCs immunomodulatory properties in the presence of pro-inflammatory environments can restore homeostasis. However, under certain circumstances where pro-inflammatory signals such as TNF-α and IFN-γ are low MSCs can instigate an inflammatory effect. Immunomodulatory function is very dependent on the local microenvironment and the triggering of anti-inflammatory states is induced by inflammatory cytokines which when not present can lead the aforementioned outcome (141). Further to this when dealing with allogenic transplantation there is debate as to the guarantee of immune privilege. This makes the process of autologous therapies more complicated as when dealing with the elderly, or those who are clinically vulnerable, where cells may be isolated in smaller numbers and be conditioned to behave in a suboptimal way. This has led to the increased uptake of allogenic transplants which provide a quicker, cheaper and often stronger therapeutic effect. However, the uncertainty of immunogenicity despite claims of the immune privileged status of MSCs and the more rapid clearance of allogenic cells make this a topic of debate and a barrier to common use among stem cell therapies (142).

## 1.3 MSC differentiation and their application to regenerative medicine therapies

As of October 2022, clinicaltrials.gov, an online database documenting clinical trials, indicates 9368 registered clinical trials involving stem cells across the globe and in a wide variety of therapies (143). Of these registered trials, 1467 specifically focus on the

use of mesenchymal stem cells for experimental treatments in a range of uses including bone fracture healing, multiple sclerosis (MS), cartilage injury and graft versus host disease (GvHD) (144). It's clear to see from the number of trials ongoing that the potential of MSCs for regenerative therapies cannot be disregarded.

The goal of the research in this thesis is to create a more effective expansion technology for MSCs, this will allow these to be employed for therapeutic strategies. These therapeutic strategies may be achieved by cell transplant alone, cell products or cells in combination with biomaterials. The necessity of cell expansion technologies is critical regardless of the approach taken or specific tissue treated. As such the studies presented below represent some of the uses of MSCs in a range of different approaches and tissues demonstrating the potential of these cells and the importance of expansion technology to support these various treatments.

### 1.3.1 Osseous tissue

One of the most explored tissue types for MSC therapy is osseous tissue or bone regeneration. Bone is a composite material consisting of both cellular, organic and inorganic components. Bone tissues come in a variety shapes and sizes and with different purposes depending on their location in the body. Bone tissue architecture involves the outer dense layer of cortical bone followed by a porous trabecular or cancellous bone interior ultimately opening to the medullary cavity in which bone marrow resides. Even at a cellular level the cells are packed in highly regulated osteon components which are cylindrical structures composing of osteocytes and collagen fibrils mineralised with hydroxyapatite (HA) and calcium carbonate tightly packed with blood vessels woven throughout (145). With such a complex structure and vital purpose, it is inevitable that diseases that compromise bone structure or function can have devastating consequences on the patient. Some of these issues faced include fracture, non-union, osteoporosis, arthritis, cancer and other uncommon diseases including osteomalacia (bone softening), osteodystrophy (bone growth abnormality) and Paget's disease (bone weakening and deformity) (146, 147). As such, a variety of studies have sought to use the potent osteogenic differentiation capabilities of MSCs, as well as the already impressive capabilities of bone healing, to repair damaged skeletal tissues.

A retrospective clinical study that analysed approximately 10 years' worth of patient data from those presenting with forearm non-union fractures was assessed to ascertain effectiveness of therapy type (148).This study can give insight into the types of therapies that have been used in treatment of bone fracture non-union and whether cellular components, growth factors or scaffolds are the most effective option. Data from 52 patients included case history, radiographs and CT scans which were used to classify patient injuries based on the non-union scoring system (NUSS). Patients were divided by the treatment types received and whether these therapies included only one therapeutic agent as a monotherapy or if multiple agents were used as a polytherapy. Monotherapy treatments include the delivery of one therapeutic agent only including either an MSC transplant, scaffold, or rh-BMP-7 but never in combination. Rh-BMP-7 is a bone morphogenic protein shown to aid in bone regeneration (149). Polytherapy strategies included the combination of all these factors in a polytherapy that attempts to better represent the triad of tissue engineering approaches previously discussed. In the case of bone fracture treatment, the model used is called the diamond concept and includes four factors known to promote bone healing. These factors are osteogenic cells, osteoconductive scaffold, growth factors and tailored mechanical environments (150). This concept is an improvement on the previous triangle concept that didn't recognise the importance of the mechanical environment. The retrospective clinical study found that monotherapy groups showed a 64% recovery rate after one year as measured by radiographic imaging and rating on the DASH score system that measures upper arm disability levels. Polytherapy groups however presented with an 89.5% recovery when scored by the same process (148). The study indicated the that to improve the efficacy of treatments a more comprehensive approach is needed that includes a multitude of regenerative aspects including cells, materials and growth factors.

Other studies have investigated improvement of natural osteogenic regeneration via delivery of MSCs, often upon varying supporting materials. In a rat unicortical tibial bone defect model, the effects of a scaffold loaded with graphene nanoparticles was analysed for their osteoconductive effects and their ability to aid in MSC differentiation. The study found that MSCs adhered to the graphene nanoparticles and when implanted into the defect resulted in improved bone regeneration and mineralisation. Results at day 45 indicated that an increase in active bone was larger in

MSC's delivered with nanoparticles but not significantly higher than MSC controls alone. However the amount of new mineralised bone was significantly higher when nanoparticles were present however this interesting result was not explored further or explained leaving a gap in the study (151). The study highlighted how MSCs have a strong osteoinductive potential alone for regeneration of bone tissue, but that inclusion of materials can have important effects on the properties of the regenerated tissue.

Other studies have weighed in on the topic of debate around MSCs and their nature, as previously discussed, and explored whether the effectiveness of MSCs comes from direct engraftment or whether the paracrine signals secreted by MSCs are responsible for the observable regenerative effects. Towards this goal Exosomes derived from MSCs, which convey proteins and generic information between cells as a form of communication, were implemented into a tricalcium phosphate scaffold. *In vivo* results in a rat calvarial defect model showed that exosome laden scaffolds outperformed control non-doped scaffolds. However additional conditions that included cell seeded scaffolds rather than scaffolds alone would allow for a more comprehensive comparison on the effectiveness of exosomes over whole cell therapies. Additionally, exosomes were derived from IPSCs induced into MSCs which is an unnecessary step from a modified cell type that could have unknown consequences. It was then established *in vitro* that internalisation of these exosomes by native MSCs aided in activating the PI3K/Akt signalling pathway that enhances osteogenic transduction (152).

As demonstrated, there are many attempts of using MSCs for bone regeneration, far more than are described here, each with varying degrees of success (28, 63, 153). The literature indicates that MSCs are effective in bone regeneration but that the key to further success lies in engineering the precise factors of the microenvironments in which the cells proliferate.

### 1.3.2 Chondral tissue

Chondrogenic tissues have a unique physical structure in that they are primarily avascular which can result in slow repair processes, scarring and difficult delivery of both drugs and cellular therapeutics alike. Cartilage is an elastic like tissue comprised

of chondrocytes, elastin, collagen fibres, proteoglycans and glycosaminoglycans (GAGs). It is similar to bone tissue but without the hard mineralised and vascular components, this makes it softer than bone and flexible but still much harder than other soft tissues such as muscle (154). Cartilage tissues are present throughout the body and have a variety of vital roles including mechanical responsibilities in load bearing joints for absorption of frictional and compressive forces protecting the underlying epiphysis of the bone (known as articular cartilage). It is present throughout the rib cage, bronchial tubes and intervertebral discs where elastic properties are required (155). Cartilage also exists somewhat externally in the case of the nose and ears.

The prevalence of cartilage pathologies is typically presented through physical trauma, osteoarthritis and intervertebral disc disease. However various rare conditions involving cartilage exist including osteochondritis dissecans (OCD)(cartilage bone interface breakdown), polychondritis (cartilage inflammation), chondrocalcinosis (calcification and hardening of cartilage), chondrosarcoma (cartilage cancer), achondroplasia dwarfism and spondyloepimetaphyseal dysplasia (SEMD)(bone growth disorder) (156). Osteoarthritis is one of the most common chronic diseases and often leads to debilitating joint pain and loss of function (157). Direct surgical transplantation of MSC populations cultured from patient bone marrow has been a methodology often used clinically for treatment of knee osteoarthritis. Orozco *et al,* following this procedure, documented the effects of MSC transplantation. The findings indicate that the minimally invasive procedure gives greater levels of tissue regeneration than other established treatments and patients indicated a significant pain relief within three months post treatment with partial functionality return. MRI analysis confirmed partial regeneration of articular cartilage over the observable period (73). However, this study only involved 12 patients and relied partially on self-assessments from the patients which reduces reliability. Despite the small sample size of the previous study this treatment procedure has been demonstrated as a viable method for cartilage regeneration in several studies with MSCs. Review studies from 2014 indicated patients that had such therapeutic effect from this procedure that they refused to undergo any further analysis or observatory surgery due to a full recovery of reported symptoms (158).

Due to the difficulties in treating this tissue there are very few strategies in which to deliver therapeutics. However, since cell-based transplants have been shown as an effective strategy, there has been further investigation into the use of MSC derived components for regenerative purposes, weighing in on the previous debate surrounding MSC function and classification. Extracellular vesicles secreted by bone marrow derived MSCs were evaluated for the therapeutic effect *in vitro* on chondrocyte monolayers stimulated by TNFα, a pro-inflammatory cytokine, in attempt to model osteoarthritic pathologies. It was shown that the extracellular vesicles negated the pro-inflammatory upregulation of COX2 signalling and inhibited TNFα related collagenase. The treatment not only reduced the inflammatory state but promoted tissue regeneration through increase of proteoglycan secretion and type two collagen deposition by the chondrocytes (159). Whilst this study demonstrates effective use of MSC derived EVs the results, while promising, still seem lacking in comparison to the beneficial effects noted by patients who underwent direct cell engraftment. Comparative studies of cell transplant, biomaterial assisted transplant and EV treatment *in vivo* would highlight how much of a contribution each approach plays in restoration of tissue function.

### 1.3.3 Musculoskeletal tissue

The capacity for regeneration of bone and cartilage tissue in many studies and clinical trials, prompts investigations into the capability to regenerate complex musculoskeletal tissue types beyond that of bone and cartilage. Injuries to complex musculoskeletal tissues such as ligaments, tendons and intervertebral discs (IVD) can cause severe and lasting pain for a variety of patients including the elderly and athletes alike (63). These complex arrangements of bone, cartilage and muscle are often difficult to access and have very little treatment options. Additionally rarer conditions related to muscle disease and development such as muscular dystrophy (muscle weakness and loss), congenital myopathy (genetic muscle weakness and loss of function), muscular atrophy (muscle wastage), Pompe disease (loss of muscle function due to abnormal build-up of sugars) and sarcopenia (loss of muscle mass) present a significant therapeutic challenge (160).

Muscle is another tissue that, like bone, appears to have an innate capability to regenerate, this makes it a prime candidate for stem cell therapies that can amplify this

naturally occurring function. Skeletal muscle is one of the three types of muscle found in the human body, the other two being cardiac and smooth muscle. This striated tissue comprises around forty percent of a typical adults' body weight and is made up from multinucleated contractile myocytes arranged in a fibrous form termed a myofiber (161). The complex arrangement of highly vascularised fibres breaks down into units called sarcomeres which comprise the actin and myosin filaments that ultimately form movement through repeated contraction and relaxation. One of the reasons for its regenerative abilities is due to the constant remodelling of its environment due to muscle turn over from general function.

An observation of muscle fibres under an electron microscope by Alexander Mauro in 1961 contemplated the relationship between mononucleated cells that lay at the periphery of myofibres (162). This observation led to the discovery of satellite cells which are skeletal muscle stem cells which aid in the high levels of tissue regeneration that characterises this tissue. Since high levels of muscle turnover and regeneration was already aided by the natural involvement of localised stem cell populations, the expansion and therapeutic delivery of these cells and other MSC types became the subject of much research to combat muscle damage and disease.

NOD/SCID mice were used in an artificial muscle damage model induced via *Naja mossambica mossambica* cardiotoxin, a snake venom which can lyse muscular tissue. The tibialis anterior muscle was damaged and then treated with local injection of labelled MSCs to track their progression. Results indicated that only 10% of transplanted cells remained after 60 days but that the number of myofibers present increased from day 10 and spread across the whole muscle length. These transplanted cells were shown to differentiate into myofibers and aid in tissue remodelling of the damage site remaining viable and in the tissue up to four months after induction. This indicated the potential of MSCs for muscle regeneration however it was shown that the myogenic potential of BM-MSCs was low in comparison to synovial membrane MSCs and adipose tissue derived MSCs (70). Despite the positive results seen the injury model methodology of inducing cell lysis is likely different from physical trauma that is often responsible for muscle damage where vasculature and surrounding area may be damaged in a more significant way. Additionally, this study does not indicate the

behaviour of MSC transplantations in disease models where certain pathologies may prevent tissue engraftment.

For aiding Duchenne's muscular dystrophy (DMD), the direct transplant of muscle stem cells into a *in vivo* DMD rat model, resulted in a significant increase in new myofibres at the site of transplantation. These grafted fibres showed the production of muscle specific proteins including the importantly absent dystrophin in the model mice. Whilst this indicates stimulation of natural tissue remodelling which is useful it does indicate that in this case direct engraftment was not significant which is contradictory of some other studies previously discussed. These transplanted cells were also capable of expanding and retaining a pool of undifferentiated cells within the host tissues (71). Further experimentation and clinical trials using the transplantation of these muscle stem cells have been met with disappointing results with little regeneration or therapeutic effect due to lack of cell survival and fusion of donor myoblasts. The current best solution to muscle regeneration has been documented via local injection of BMSC conditioned media (163).

There are currently no recorded clinical application of MSCs for skeletal muscle, however several preclinical uses in animal models discussed have highlighted a future potential if the challenges of this tissue can be overcome (164). Despite this promise the reliance on a small selection of animal models, lack of translation to human trials and overall low myogenic potential indicates that there is much more work to be done in this field.

### 1.3.4 Other tissues

The regenerative and multiple differentiation potential of MSCs has been demonstrated in a variety of vital tissue types as described above. Despite the wide ranging and importance of the tissue types described these do still not encompass the entirety of the potential of MSCs. Various other tissues have been regenerated through MSC based therapies including myocardial, hepatic, renal, nervous system, corneal, trachea, skin, lung and bladder tissues (63). An overview of these various tissues with some example studies are included in table 1.1.

| Application | Study details | Reference |
|---|---|---|
| Heart | BM-MSC transplantation in mice led to cell engraftment, myocardial differentiation and integrated tissue growth at 14 days which was still present at day 60. | (72) |
| | Phase II trial of nonischaemic cardiomyopathy in 22 patients indicated improvement to left ventricular ejection fraction and volume after intravenous administration of MSCs. | (165) |
| | BM-MSC exposure *in vitro* to 5-azacytidine and culture on a PLGA scaffolds indicated cardiac tissue formation after 14 days. | (166) |
| Nervous system | Multiple *in vitro* studies have confirmed the potential of MSCs to differentiate into neuroectodermal lineages including neurons, astrocytes and oligodendrocytes. | (167, 168) |
| | A Clinical study of 40 patients with traumatic brain injury found transplantation of MSCs via lumbar puncture improved motor function and sensation after 6 months. Patients who did not receive a transplant showed no improvement. | (169). |
| | Adipose derived MSCs cultured *in vitro* on PCL-gelatin electrospun fibre scaffolds indicated maturation of neural cells following induction. | (170). |
| | In a SCI mouse model, MSCs encapsulated in an ECM hydrogel significantly improved locomotor function with recovery of motor neurons and myelin. | (171). |
| Liver | *In vivo* studies have shown induction of BM-MSCs to functional hepatocyte like cells through conditioning with Hepatocyte growth factor (HGF) and oncostatin M. | (172, 173). |
| | Phase II clinical trials transplanted autologous MSCs for treatment of liver cirrhosis showing improvement in liver function after 3 – 6 months post infusion. | (174). |
| | Another phase II clinical trial transplanting autologous BM-MSCs was reported to promote significant liver function restoration in patients with alcoholic cirrhosis. | (175). |
| Kidney | In acute renal failure mice models, transplantation of BM-MSCs prevented tubular damage and stabilised renal function. Transplanted cells presented affinity for Lens culinaris lectin which is indicative of differentiation into tubular epithelial cells. | (74). |
| | Multiple studies have shown intracarotid injection of MSCs following induced renal ischemia in rats restored renal function and cellular death at the site of injury. | (75, 176) |
| Other tissues | MSC regenerative capacity has been demonstrated both invitro and *in vivo* in many other tissues including lung, trachea, cornea, skin, bladder, thymus, spleen, colon and pancreas. | (177-187) |

***Table 1.1:*** *Applications of MSCs in treatment of various Tissues. MSCS are capable of treating a variety of tissues including heart, nervous system, hepatic, renal, respiratory, cornea, skin, bladder, thymus, spleen, colon and pancreas. Included are short overviews of several highlighted studies involving in vitro and in vivo studies including animal models and various human clinical trials.*

# 1.4 Expansion technologies

### 1.4.1 The necessity of cell expansion

As more is known about the clinical potential of MSCs and their regenerative potential, as discussed, the next step for clinical use is to scale up and produce quantities of cells suitable for administration. In some studies the mononuclear cell fraction of fresh bone marrow aspirate, which contains a natural and significant population of MSCs, is directly delivered as a therapy. In a study of 51 patients with critical limb ischemia (CLI), Localised injection of MSCs led to a significantly higher amputation free rate in comparison to those who did not receive cell treatments after a four year follow up (188). As further trials illustrate the therapeutic potential of MSC-based therapies and this is translated into a clinical therapy, a significant increase in cell populations will be necessary for effective outcomes for increasing numbers of patients.

An analysis of 914 MSC trials from 2004-2018 was conducted and analysed for clinical procedure variations to generate an illustration of the typical MSC therapy parameters for clinical trials. Intravenous delivery was the most common means of delivery, representing 43% of all trials, and indicated an average dosage of 100 million cells per dose. Further examination showed minimal effective doses (MEDs) of 70 -190 million cells with some trials delivering as many as 1.2 billion cells per treatment (16). A schematic representation of the number of cells required per dose is in figure 1.3.

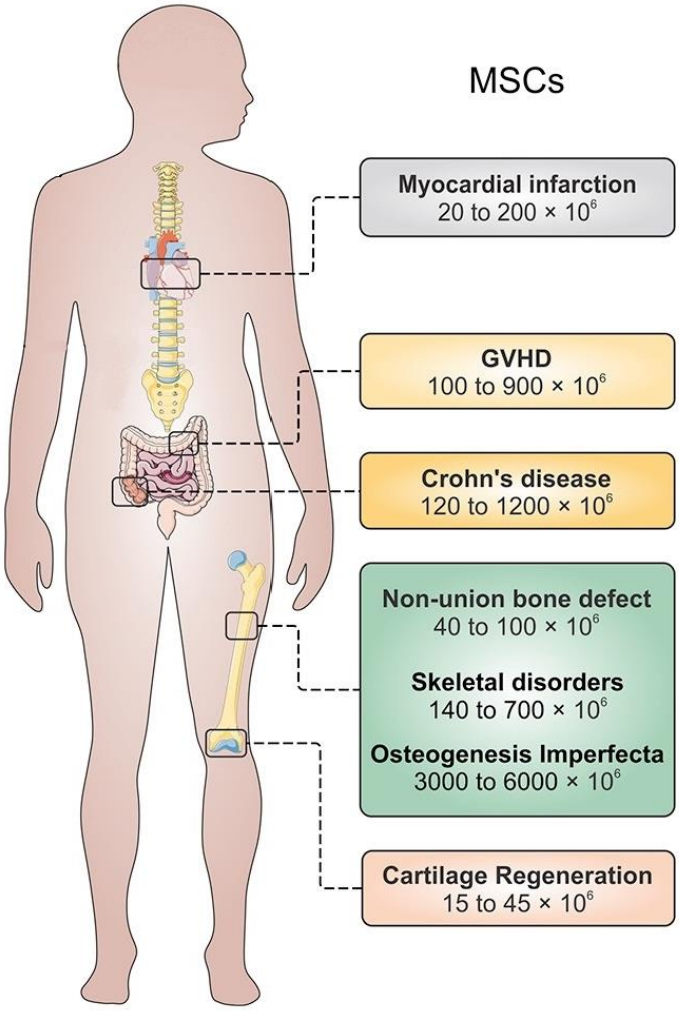


***Figure 1.3: Overview of number of MSCs needed for clinical therapies per tissue type.*** *The number of multipotent stem cells required for dosage in clinical trials for a variety of disorders including spinal cord injury, myocardial infarction and bone disorders ranging from $15x10^6$ cells - $6000x10^6$ cells. Modified with permission from Tavassoli et al (189).*

The necessity for such substantial quantities of cells becomes problematic when the number of cells that can be isolated from a patient is only a fraction of what is needed. One of the most common and reliable sources of MSCs is bone marrow. The mononuclear cell fraction of bone marrow contains only approximately 0.001% MSCs and similarly low values can be seen in other cell sources such as adipose tissue (17).

This low frequency of cells is further impacted by the inherent variability between donors, most importantly donor age. The measurement of these cells is conducted via a colony forming unit fibroblast (CFU-F) assay which estimates MSC population via the number of cells capable of forming colonies (190, 191). Newborns have a much higher frequency of MSCs with one in every 10,000 mononuclear cells, in teenagers this dips to one in 100,000 and even lower to one in 250,000 for 30 year olds, by 80 years of age this frequency is as low as one in 2,000,000 cells (192). These values also vary by cell source, adipose tissue gives the highest portion of MSCs followed closely by bone marrow and then the lowest source commonly used was umbilical cord blood. However cells from different sources displayed different behaviours, umbilical cord blood derived MSCs were isolated in lowest frequency but showed the highest proliferative capacity and lasted longest in culture as well as an absence of adipogenic differentiation in contrast to bone marrow and adipose tissue (193).

Expansion protocols for these therapeutically relevant cells therefore requires further research and development. One of the essential components for this process is a solid surface for growth given that MSCs are anchorage dependant cells, this makes expansion a more difficult process in practice than in theory as provision of significant surface area come with increased maintenance and physical limitation. Another consideration is the growth rate of MSCs. During early passages cells will grow at a consistent rate for about three weeks in 2D culture. After this initial period proliferation decreases and after around 30 passages in primary culture cells will begin to senesce and multilineage differentiation will diminish. Although cells can be used up to 40 generations in 2D culture, for the safety and efficacy of clinical treatments it is suggested that cells should be used before passage 20 which means effective expansion is required to be very rapid and avoid differentiation, if it is to be useful (18, 19).

### 1.4.2 Legacy MSC expansion techniques

Ultimately the way that expansion has been achieved to date is by providing ample surface area for cells to proliferate and grow. As discussed previously there is a limited period of time where cells can be suitably expanded before they senesce, and so

specialised expansion technologies and techniques have to be employed. In normal laboratory practice the expansion of cells in small scale is achieved by culture in fetal bovine serum (FBS) supplemented Dulbecco's modified eagle medium (DMEM) on tissue culture plastic, usually T-flasks. The near confluent cell layers are enzymatically passaged with trypsin ethylenediaminetetraacetic acid (EDTA) and a T75 flask usually produces approximately $3x10^6$ cells when passaged. Larger T-flasks of up to $225cm^2$ are available, producing $9x10^6$ cells, but ultimately the yield given by this culture method remains insufficient for generating the numbers needed for any clinical therapy.

Scale up beyond this scope becomes difficult due to the amount of space needed for incubation and the labour intensity for manual handling of so many flasks, extensive handling introduces variation and risk which may give rise to a variable product. To address this, automated robotic handling has been utilised. Robotic systems can perform actions faster, more consistently, and at a greater rate than any human with far less risk of contamination or error. These systems also often come purpose built with larger compact incubator space to aid in production, an example is the TAP biosystems device which can house 182 T-175 flasks at a time (20, 194). However, despite the strengths of this technology, it comes at significant cost, space and maintenance that may not be suitable for all purposes. Even if these issues are not a deterrent the production of cells may still struggle to meet the amount needed for many therapies as despite large storage capacities the robotic arm can still only work one or two flasks at a time and a growth period is still needed.

Multi tray systems or cell stacks are an evolution of typical culture flasks designed to streamline and condense as much flat growth surface into one structure as possible. The systems have multiple layers but can be passaged as one unit delivering a surface area of up to 25,440 $cm^2$ in a single unit, improving the yield to labour ratio. These systems deliver enough surface area as multiple T-flasks but within a much smaller footprint conserving incubator space. These methods have been used for the production of biological products such as human fibroblast interferon(21) and for clinical trials including multiple sclerosis therapies(195). Several studies investigated the feasibility of clinical MSC scale up from tissue sources exhibiting successful use of this technique (196, 197). An investigation into these structures showed that while obtaining a clinically relevant population across multiple cell stack systems, the overall growth

patterns and variability of cells was no different to those grown in T-225 flasks (21). One of the issues with this methodology is that the volume of cells it produces only just meets the threshold of most therapies but is unsuitable for those that are required to deliver a larger than average dose size (198). This technique does what standard culture methods cannot but still comes with significant costs in time, labour and materials with routine procedures such as media replacement becoming laborious and difficult due to the large size of the structures being handled. Difficulty with handling and laborious processing leads to increased likelihood of error or contamination which could be more destructive than T-flask culture as all cells will be contaminated rather than an isolated batch. Additionally, there are concerns regarding constant conditions across all surfaces regarding gaseous exchange and concentration gradients across the structure that may differ between the centre and periphery of the assembly. Since these surfaces are static with no agitation or aeration the heterogeneity of culture conditions cannot be assured which could lead to variable cell outcomes and monitoring of culture conditions such as pH, oxygen concentration and waste build up through biosensors is difficult to achieve (199).

Roller bottles are another technique for expansion of anchorage dependent cells developed originally in 1933 (22). The basis of roller bottle technology is to slowly rotate a cylindrical tissue culture plastic tube inoculated with cells and appropriate media, the media in continuous motion flows across the growing cells on the inner tube surface. A greater surface area is provided by this shape and the continuous agitation of media allows for a greater gas exchange as well as a more uniform culture environment as concentration gradients cannot be established in a moving vessel (190). These devices have notably been used in the production of vaccines and adeno-associated viral (AAV) vectors for gene therapies (200). Roller bottles are not widely used for MSC expansion although some studies have utilised this technique for MSC and hematopoietic cell expansion (201). Studies into roller bottle cultured MSCs indicated that whilst no change in cell morphology was seen due to the rotational forces of the method, the expression of IL-1 and IL-6 was reduced in comparison to those grown in T-flasks indicating potential biological variation arising from this process (190). This approach has likely not been widely adopted in MSC production due to the disadvantages it suffers such as increased labour intensity, risk of contamination, lack of real-time online monitoring systems and requirement for increased space and roller

racks within incubators. Additionally, cells in roller bottles are quite fragile and prone to cell separation due to vibrational shock from movement and so realistic use of these methods in mass production of cells within appropriate time frames is only achieved when costly automation is introduced (194).

### 1.4.3 Challenges of expanding cells

The main challenge for scale-up culture of cells destined for the clinic is that current methods struggle to meet the demand. As previously discussed engraftment levels are low due to rapid clearance of transplanted cells Although in some cases they can produce a clinically viable dose there is significant cost, time and risk associated with this. Scaling up to therapy level treatments for multiple patients at one time would exacerbate these problems and likely become unfeasible. Another challenge posed with current techniques is the loss of phenotype that can occur in planar 2D culture. Cell morphology in planar culture is altered and flattened in comparison to natural three dimensional growth in an organism, this forced flattening of the internal cytoskeleton can trigger mechanotransduction pathways leading to changes in gene expression and protein production (202). This may play a role in the reduced proliferation, loss of multipotency and increased senescence that occurs after prolonged passaging and culture (17, 203). Studies have indicated that microenvironmental changes induced by planar culture can result in a significant decrease of osteogenic and chondrogenic differentiation potential, increased adipogenic differentiation as well as impacts to migrational ability, immunomodulatory and anti-inflammatory properties (204).

Alteration of phenotype based on culture conditions can become an issue when trying to produce a standardised cell product. MSCs are impacted by even small changes in culture environment such as media composition, cell expansion technique, culture material and substrate stiffness leading to variation in outcome that is critical for large scale clinical grade therapies (205). Variation occurs naturally in cells as previously discussed so it is important to maintain good manufacturing practices (GMP) to delineate between inherent variance and introduction of variation based on handling and processing (206). A simple but often overlooked example of subtle changes between lab tests and industrial scale production is the transition to xeno-free media composition and growth supplements. In a typical laboratory setting, culture media can

include components such as fetal bovine serum (FBS) or other animal-based products. In scale up to clinical products there is apprehension about using animal products and xeno-free alternatives such as chemically defined serum or human platelet lysate must be used (207). Conversion to this method requires the need for transitioning the culture system in place and this change may result in a deviation from initial lab results (208). However, use of some xeno-free drugs can lead to enhanced cell yield, rapid growth, improved genetic stability and elimination of xenogeneic pathogens (205). The early adoption of xeno-free components in any research process should be encouraged but it is often not pursued due to increased cost of these materials in comparison to classical components.

As previously mentioned, there is natural variation in MSC qualities based on the donor and the number of cells that can be harvested is dependent upon age of the patient and tissue source. The differences in MSC phenotype is due to a range of factors. Tumour necrosis factor- stimulated gene 6 (TSG-6) is a protein heavily involved in the anti-inflammatory capabilities of MSCs, this has been demonstrated in multiple inflammation models of corneal injury, lung injury and sterile peritonitis. This protein, so crucial it is becoming thought of as a biomarker for anti-inflammatory efficacy, is secreted in higher quantities in female donor cells versus male cells due to a sexual dimorphism (209). Donor health and metabolic integrity is also becoming a widely recognised marker of MSC quality. MSCs sourced from metabolically damaged individuals such as those suffering from obesity, diabetes, atherosclerosis or other metabolic syndromes exhibit impaired function. These impairments include a reduced immunomodulatory capacity, reduced T cell interaction, reduced fibrinolytic activity and a specific loss of neuroinflammatory regulation (205, 210). Further analysis into this mechanism revealed that donor cells in a palmitate enriched environment, a saturated fatty acid rich metabolic disease model, flipped the MSCs immune suppressive characteristics to immune stimulatory states in reaction with cells of the immune system. Some donor cells also proved to be far more sensitive to palmitates than others (211). This previous work highlights the importance for cell manufacturing processes to not only maintain strict and controlled culture environments but also to screen for MSC donor quality through potency and sensitivity assays if a consistent and high-quality product is to be produced.

If the adversities already reviewed were to be overcome further issues would arise due to the simplicity and homogeneity of implanted cell populations. Nearly all tissues have a hierarchical level of complexity with multiple specific cell types accompanied by connective tissues, blood vessels, lymphatic ducts and neurons. Estimations suggest that each cell of a human body is within only a few cell lengths from a vasculature network for sufficient nutrient delivery and waste exchange, with some avascular exceptions such as cartilage and corneal tissues. Therefore, for appropriate tissue regeneration a heterogenous population of cells need to be delivered, stimulated or recruited from the host and yet most studies and trials only provide MSCs in isolation. Further examination of MSC interactions and recruitment of supporting cells is needed to be able to provide a starting population of sufficient capability to recreate the complex nature of the tissue in which it is being introduced to (76).

Once cells are expanded to appropriate levels these need to be harvested for therapies and other downstream applications, it is important that a high retrieval efficiency is achieved whilst maintaining cell viability without influence on cell phenotype or fate. The most common approach of enzymatic dissociation is achieved with trypsin or occasionally collagenase. These are usually supplied with EDTA as a metal ion chelating agent to enhance detachment through calcium and magnesium ion binding and therefore obstructing cadherin mediated attachment. This method is reliant on free diffusion of the enzyme and so is easy to achieve in 2D culture(212). The mechanics of the enzymatic disruption of cell surface proteins used for cell-to-cell contacts and substrate attachment is achieved by protease activity on the cell surface leading to focal adhesion cleavage, however exposure to such agents for long times may damage the cell. Non-enzymatic dissociation products have been approved such as versene and some of these products have been shown to maintain higher levels of immunomodulatory function, cytokine secretion and migratory ability in MSCs (213).

One novel approach gaining traction that relies on expansion but without delivery of cells as the product is the application of conditioned media. This approach takes advantage of the secretome and secreted molecules of MSCs used in inflammatory suppression as the basis of the product without the strict and sometimes uncertain nature of direct stem cell transplantation. MSC conditioned media overcomes fear of tumorigenicity, immune tolerance and infection whilst being more economical and far

more applicable to mass production of product (76). Whilst this approach may not have the same capacity as a direct stem cell therapy it has been shown that conditioned media can promote regeneration and improve disease symptoms in many animal models as well as support *ex vivo* tissue generation for transplant (76, 214). As discussed, there are still many challenges present for proper implementation of cell expansion for stem cell therapies for a variety of purposes and further understanding of cell mechanics and control is necessary to establish this approach as common practice in future medicine.

# 1.5 Microcarrier technology

### 1.5.1 Microcarrier concept

Microcarriers are a support matrix that provides surface area for the attachment and growth of adherent cell populations. This space is often presented in the form of spherical beads that are frequently cultured in spinner flasks or bioreactors to provide optimal culture environments (215). Typically, microcarriers are in the range of 100-300 µm in diameter and each bead supports several cells on its surface (216). Whilst many microcarriers commercially available are purely spheres of varying materials there are several porous or uniquely shaped microcarriers available (217). There is, however, much greater variation in experimental microcarriers within the literature (25, 204, 216, 218)

Spherical microcarriers show a lot of physical similarity with microparticles but differ not in form but in function. Microcarriers are typically designed to act only as a cell growth surface and are used as a tool for *in vitro* expansion of cells prior to harvesting and use. Microparticles are a much wider range of structures and have uses in a variety of applications such as microparticle based scaffolds. Whilst these terms isolate these structures based on function there is nothing to stop a degradable spherical microcarrier from performing the role of a microparticle if it meets the requirements.

Growth of cells on microcarrier surfaces are influenced by the biophysical and biochemical makeup of the microcarrier design and as such changes to carrier design can alter cellular outcome (219). Microcarriers provide a high surface area to volume

ratio to enable increased cell growth in comparison to flat surfaces, enabling a far denser and compact presentation of surface area within a much smaller volume. Studies have illustrated that as much as 1g of solid spherical microcarriers can easily present the same surface area and therefore support the growth of a cell population equivalent to fifteen T75 culture flasks (220).

The first microcarriers were produced in 1967 by Van Wezel who used DEAE-dextran Sephadex microcarrier beads with a positive charge to culture and expand both fibroblast-like rabbit embryonic skin cells and human embryonic lung cells *in vitro* (221). Initial popularity arose from the role of microcarriers in vaccine development where secreted cell products could be easily extracted en masse throughout a continuous culture but the method grew to encompass expansion of the cells themselves as the product of interest. As a result of Van Wezel's and others success with microcarrier culture over the following decades, many commercially produced microcarriers became available each utilising different materials, coatings and shapes exploring strategies for the most efficient cell expansion yield (189).

Due to the large variety of microcarriers that have become available several studies have compared the capabilities of commercial carriers available in order to pinpoint the most useful characteristics. Chen *et al* compared 10 popular microcarriers for the long-term cultivation and propagation of human embryonic stem cells (hESCs). Commercial examples included Cytopore, Cultispher, Cytodex and Tosoh microcarriers with several different surface coatings relating to typical ECM components such as fibronectin or laminin as well as ECM derived product Matrigel. The results of this study indicated the highest expansion efficiency in spherical or cylindrical microcarriers which carried a positive charge to attract the natural negative charge of the lipid component of cell membranes. Laminin or Matrigel surface coatings had significant roles in maintaining cell phenotypes over the duration of the culture period (222). Interestingly similar studies on commercial microcarriers, specifically pertaining to hMSC adherence, found highest expansion yield with cytodex1 carriers made from dextran that whilst spherical and positively charged had no surface coating and had a greater expansion yield than their cytodex 3 counterpart which is identical except for the addition of a thin collagen surface coating (223). A systematic analysis of thirteen microcarriers used for the expansion of BM-MSCs was conducted focusing on expansion yield as well as

harvesting difficulty and suitability to xeno-free systems. The study declared SoloHill Plastic microcarriers, a neutral charge, non-porous, spherical polystyrene based microcarrier, as the optimum choice for MSC expansion due to highest expansion yield and cell health. This microcarrier outperformed its plasticplus counterpart that is a positively charged equivalent, indicating positive charge as detrimental to expansion in this case. Additionally, SoloHill Collagen coated polystyrene carriers performed at near identical levels of cell expansion to plastic microcarriers but were not deemed optimum due to their non-xeno-free nature (224). During this analysis the study identified that, whilst agitated bioreactor culture consistently provided a significantly higher level of expansion, static microwell screening results did agree with further analysis indicating a potential route suitable for high throughput screening of microcarrier types at smaller scales (224).

### 1.5.2 Microcarrier design features

Many microcarriers are often designed to be hollow or porous in nature. This is important as it allows infiltration of cells enabling a larger surface area of growth whilst also simultaneously protecting them from shear and other surface stress. The configuration of these particles gives a highly interconnected structure which promotes cell attachment and multidirectional cell to cell interactions (23). The surface topography of microcarriers typically tend to be either smooth, microporous or macroporous, each with its benefits and challenges. Whilst smooth particles are suitable for cells not affected by shear stress they have typically less surface area, whilst porous structures provide protection, higher surface area and cell anchorage whilst promoting cell infiltration (189). To add to this, carriers may also fall along a particle or capsule type that surrounds cells or more niche methodologies such as liquid interfaces or foldable structures (225).

Commercial microcarriers are available in a range of shapes such as spherical, cylindrical, disc and hexagonal shapes. Despite the variety of microcarrier shapes highlighted the overwhelming majority of microcarriers are spherical within the 100–300 μm diameter range, this is likely due to the simplicity, cost and ease of producing particles of this size and shape by polymerising droplets rather than advanced additive manufacturing techniques to integrate topography (13). A table of various popular

commercially available microcarriers is summarised below in table 1.2. Given the wide ranging mechano-sensitivity of stem cells to mechanical forces and substrate design incorporation of topographical features for cell control is rarely attempted, likely due technological limits and cost to manufacture. Nanoscale levels of architecture integrated in microcarriers is another factor to consider, this has been utilised successfully in microcarriers designed for neurodegenerative disease treatment (226), pulmonary disorders (227) and other particle drug delivery systems (228). Enhancing cell carrier attachment and interaction has been demonstrated to be improved by incorporation of nanofibres into microspheres to give nanoscale features and signals. This has been described and applied in a novel technique by Liu *et al*, where nanofibrous microspheres were fabricated and used as an injectable cell carrier for successful knee joint regeneration in a rabbit model (229).

| Microcarrier | Manufacturer | Diameter (µm) | Shape | Type | Material | Coating | charge |
|---|---|---|---|---|---|---|---|
| Cytodex 1 | GE Healthcare /Amersham Biosciences | 190 ± 58 | spherical | solid | Dextran | DEAE | + |
| Cytodex 2 | Amersham Biosciences | 135-200 | spherical | solid | Dextran | N,N,N-trimethyl-2-hydroxyaminopropyl | none |
| Cytodex 3 | GE Healthcare | 175 ± 36 | spherical | solid | Dextran | Collagen | none |
| Cytopore1&2 | GE Healthcare | 240 ± 40 | spherical | Porous | Cellulose | DEAE | + |
| Cytoline 1 | GE Healthcare | 1700-2500 | lens | Porous | Polystyrene | none | - |
| Cytoline 2 | GE Healthcare | 1700-2500 | lens | Porous | Polyethylene /Silica | none | - |
| Hillex | SoloHill | 160-180 | spherical | solid | Polystyrene | Trimethyl ammonium | + |
| Biosilon | Nunc | 170-300 | spherical | solid | Polystyrene | None | none |
| plastic | SoloHill | 125-212 | spherical | solid | Polystyrene | None | none |
| Plastic plus | SoloHill | 125-212 | spherical | solid | Polystyrene | None | + |
| Star plus | SoloHill | 125-212 | spherical | solid | Polystyrene | None | + |
| Glass | SoloHill | 125-212 | spherical | solid | Polystyrene | silica | none |
| Collagen | SoloHill | 125-212 | spherical | solid | Polystyrene | Collagen | none |
| ProNectin | SoloHill / Thermo scientific | 169 ± 44 | spherical | solid | Polystyrene | Fibronectin | none |
| FACT III | SoloHill | 169 ± 44 | spherical | solid | Polystyrene | Gelatin | + |
| Synthemax II | Corning | 125-212 | spherical | solid | Polystyrene | Collagen and Vitronectin | none |
| Dissolvable | Corning | 200 - 300 | spherical | solid | PGA | Synthemax | none |
| Enhanced attachment | Corning | 125 - 212 | spherical | solid | Polystyrene | CellBIND | none |
| Collagen coated | Corning | 125 - 212 | spherical | solid | Polystyrene | Collagen | none |
| Untreated | Corning | 125 - 212 | spherical | solid | Polystyrene | None | none |
| SphereCol | Advanced BioMatrix | 125-212 | spherical | solid | Polystyrene | Collagen | none |
| 2D microHex | Nunc | 125 | hexagon | solid | Polystyrene | Tissue culture treated | none |
| Tosoh 65 PR | Tosoh Bioscience | 65± 25 | spherical | solid | Methacrylate | Protamine sulfate | none |
| Tosoh 10 PR | Tosoh Bioscience | 10 | spherical | solid | Methacrylate | Protamine sulfate | none |
| DE-52 | Whatman | 130 ± 60 | Cylindrical | solid | Cellulose | DEAE | + |
| DE-53 | Whatman | 130 ± 60 | Cylindrical | solid | Cellulose | DEAE | + |
| RapidCell | MP Biomedical | 150-210 | spherical | solid | Glass | none | none |
| G2767 | Sigma Aldrich | 180 ± 30 | spherical | solid | Glass | none | none |
| G2517 | Sigma Aldrich | 120 ± 30 | spherical | solid | Glass | none | none |
| Cultispher-G | Percell Biolytica | 255 ± 125 | spherical | Porous | Gelatin | none | none |
| Cultispher-GL | Percell Biolytica | 255 ± 125 | spherical | Porous | Gelatin | none | none |
| Cultispher-S | Percell Biolytica | 255 ± 125 | spherical | porous | Gelatin | none | none |
| Fibra-cel | New Brunswick | 6000 | disc | Porous | Polyester and polypropylene | none | none |
| Microsphere | Cellex | 500-600 | spherical | Porous | Collagen | none | none |
| Siran | Schott Glasswerke | 300-5000 | spherical | Porous | Glass | none | none |
| Immobasil FS | Ashby Scientific | 800 x 300 | Disc | Porous | Silicone | none | none |

***Table 1.2****: Commercially available microcarriers. Table includes product name, supplier, diameter, shape, type, material, coating and charge. DEAE – Diethylaminoethyl, PGA – Polyglycolic acid.*

In addition to the many considerations for microcarrier design there are other attributes to be considered that will affect cell behaviour, differentiation, and overall outcome. Substrate stiffness values of 34 kPa which are considered stiff or rigid enhanced the spindle-like morphology and osteogenic differentiation in MSCs. Softer and more flexible surfaces in the range of 1 kPa enhanced and promoted softer tissue differentiation such as chondrogenic, adipogenic or neuronal differentiation (230). Interestingly stiffness values in between these two extremes were far more likely to promote differentiation into a muscle lineage suggesting that the substrate stiffness presented to the cells and the subsequent influence on MSC differentiation is indicative of the stiffness of the tissue developed (231). Curvature is an important and often inescapable physical feature of microcarriers that acts as a biophysical stimulus. Schmidt *et al* demonstrated that microscale curvature of microcarriers leads to mechanotransduction through intracellular tension which in turn triggers higher likelihood of osteogenic differentiation of MSCs (232). As previously described, MSCs are influenced by environmental cues such as shape and stiffness but the chemical cues of the polymer used are also implicated in cell behaviour. Material properties including presentation of functional groups such as NH2 amine groups can enhance MSC proliferation and spreading whilst inducing osteogenic commitment. High concentrations of carboxyl (COOH) groups within the material can lead to lowered MSC spreading and enhance chondrogenesis (233).

### 1.5.3 Microcarriers with added functionality

Some groups have made attempts to incorporate responsive elements within microcarriers and produce better cell recovery. Thermoresponsive polymers such as poly N-isopropyl acrylamide (pNIPAAm) have a unique response in media where transition between soluble and insoluble behaviours is triggered at 32 °C (234). Below this trigger point the polymer exists in a hydrophilic state but sharply phase transitions to hydrophobic states above 32°C which can be manipulated for cell attachment and detachment. Cells can attach and grow above this threshold but when the temperature drops, a hydrophilic state transition is triggered which detaches cells easily from the surface, this allows for cell harvesting without the damaging effects of enzymatic interference (235). Similar results have been published by Yang *et al* (236).

Similarly, a few studies have investigated the effects of pH for responsive transitions but cell metabolism and activity involving the control of critical native enzymes is strongly pH dependent. As such, application of this stimulus even at small magnitudes can directly and negatively affect the proliferative capacity and differentiation of stem cells so is often avoided (237). Polymers have been sought and designed that are sensitive to and can respond to electromagnetic type field responses such as light, electrical fields, magnetic fields and ultrasound. These types of cues are far more amenable to remote or automated triggering and often allow spatiotemporal regulation at particular intensities and frequencies (189).

A study by, *Hong et al* (238) used TiO2 nano dot-coated quartz substrate for culture of mouse pre-osteoblastic (MC3T3-E1) cells. UV light at 365nm was found to detach more than 90% of the cultured cells whilst still maintaining high cell viability. Following the theme of UV light based responses, Griffin *et al* synthesised PEG-hydrogels for encapsulation of MSCs which upon UV irradiation, were released into suspension without any damage to cell health (239). Polymers responsive to small electrical fields have also been explored for cell harvesting applications, in this method, cells can be cultured on a thin thiol film susceptible to electrical signals. Once a signal is induced cells easily detach with no negative consequences to viability as yet another novel enzyme free method of cell harvesting (240). Liquid microcarrier systems have also been reported where cells proliferate at the interface of the culture media and a hydrophobic liquid fluorocarbon named perfluorodecalin (PFD). A study utilising this novel method successfully cultured three mammalian cell types including epithelial cells, fibroblasts and myoblasts at the media-PFD interface (241). However, most of these methods whilst well demonstrated in cell culture experiments have yet to be applied to microcarrier technology.  A commercially available microcarrier that exhibits responsive capabilities is the Global Eukaryotic Microcarrier. This paramagnetic microcarrier exhibits an alginate core combined with magnetic nanoparticles which can aid in microcarrier control both in agitation and stirring properties as well as ease of use during media replacement or washes as carrier position can be controlled (218).

Trends in recent microcarrier design includes the use of drug free methodologies for cell expansion that negate the need for enzymatic digestion for cell release, this can be

in the form of carrier degradation or through more precise and elaborate features (204). There has been increasing use of microcarriers for 3D bioprinting by integrating microcarriers as granular inks or as reinforcing particles within bioinks to aid regeneration of damaged tissues (242).

Microcarriers are traditionally used as a cell expansion technique but new products that can integrate cues to control cell differentiation or act as regulators of cell behaviour through bioinstruction are challenging this notion. Cell laden degradable microcarriers that can expand, induce differentiation and provide structural stability for cells are increasingly being used as direct injectable therapies as tissue scaffolds promoting *in situ* tissue regeneration in the form of microparticle scaffolds (243).

# 1.6 Influence of biophysical cues

The presentation of biochemical cues in biomaterials have been vastly explored in the literature. Research has investigated effects of growth factors, polymers, peptides and carbohydrates on cell behaviour and function. These biochemical cues have been demonstrated to be capable of influencing cell viability, adherence, proliferation, and differentiation (244). Whilst the effects of biophysical stimuli on cell behaviours are recognised, they are often not utilised in biomaterials design. This is due to the difficulty to manufacture and incorporate these features in comparison to biochemical cues.

The core principle of the research presented in this thesis is that microcarriers presenting various complex architectures will lead to different cellular behaviours. This will be achieved by exploring microcarrier size, geometry, topography, stiffness, and porosity which have all been shown to alter cellular outcome (23-25, 245). As such, it is vital to explore and review the literature on the molecular mechanisms by which cells respond to physical stimuli. Whilst the specific signalling mechanisms discussed are not directly quantified or characterised as part of this research, it is still imperative to understand the fundamental biology of the cellular responses that are being affected.

### 1.6.1 Mechanobiological concepts

Mechanobiology is the molecular basis of how cells sense, understand and react to physical features and forces. A cells capacity to understand and respond to physical changes is mediated by a two-step process which starts with mechanosensing of stimuli and then mechanotransduction of that signal to create an effective change in cellular behaviour (246). Mechanosensing is defined as the capability of cells to sense the mechanical features and forces of the local microenvironment. Mechanotransduction is defined as the capacity to translate those sensed stimuli into biochemical signals to produce specific molecular changes and cell responses (247, 248). The mechanisms of these responses to biophysical cues are mostly built upon observations in 2D culture but research into 3D mechanobiology is developing (26, 249).

### 1.6.2 Biophysical stimuli and their effects on Cells

Porosity has been shown to have varying effects on MSC response depending upon pore diameter and nucleus size. *In vivo* ECM porosity varies but optimal porosity in cell culture scaffolds will vary based on cell size and purpose of porosity with certain differentiation routes preferring certain pore sizes (250). A study by Lien *et al* indicated how larger pore sizes of 250 μm led to preference for chondrogenic differentiation in MSCs with increased production of GAGs and ECM components, whilst 50 μm pores lead to dedifferentiation (251) Cell migration through pores or any limiting space is mediated by cytoskeletal rearrangement and tissue ECM degradation through proteolytic enzymes such as matrix metalloproteinases (MMPs) (252). In the case of non-degradable structures, the limitation is in the degree of cytoskeletal rearrangement. Significant remodelling will require greater cellular energy expenditure, but the limitation to movement is due to the cell nucleus (252). The nucleus of the cell is the stiffest and most fragile part of the cell and requires significant effort to move through limiting architectures with nuclear shape being intrinsically linked to cellular function and health with even limited deformation potentially leading to DNA damage (253). As such the most limiting feature size is one that is of a cross sectional size similar to or smaller than the nucleus of the cell and acts as a limitation for cell migration (252, 254). Human MSCs were found to have a nucleus diameter of $10.5 \pm 2.16$ SD μm but this value can change based on a multitude of cellular factors (255). Studies of pore size in polycarbonate membranes indicated that umbilical cord MSC migration through 0.4 μm pores was not achievable, only 1.8% of cells were capable of migrating through

3 µm pores and 8% of cells were able to move through 8 µm pores indicating the gradual limiting effect of pore size on MSC migration (256)

Curvature is also shown as a mediator of cell responses. Convex surfaces increase F-actin fibre presence and osteocalcin levels in comparison to planar culture which becomes stronger with decreasing convex diameters (257, 258). The mechanism that increases osteogenesis is thought to be based on the increased cytoskeletal tension within the cell and actomyosin contraction which exerts force on the perinuclear actin cap deforming the nucleus and leading to changes in gene expression (204, 257).

The effects of micro-ridges and grooves have been demonstrated in the literature for MSC alignment and proliferation (259-261). Aligned topographies can guide cell alignment through contact guidance imposed by lateral limitation of cell spreading and focal adhesion elongation thus driving actin fibre alignment and cell elongation (261). This alignment and elongation has been shown to trigger osteogenic responses due to the stress imposed upon the nucleus by the actin stress fibres (262).

Increases in surface roughness or nanotopography also mediate MSC responses and can induce osteogenic differentiation (230, 263). Grooves as small as 350 nm were enough to induce cellular alignment of MSCs and whilst others have often reported increased expression of osteogenic markers there is also increase in neuronal markers (81). Additionally grooves at 600nm allowed modification of actin stress fibres altering morphology and proliferation in embryonic stem cells (264). Nanotopography effect is variable depending on the patterning used with nanosized holes of 120 nm diameter and 100 nm depth resulting in increased cell differentiation and bone regeneration in MSCs (265).

Other forms of mechanical stress that might be experienced include fluid shear stress which was shown to affect differentiation in osteogenic lineages due intermittent fluid flows in oscillating patterns (266). Hydrostatic pressure equivalent to that experienced in tissues (0.1 MPa – 10 MPa) was observed to enhance cartilage formation in MSCs both in planar and aggregate culture (244, 267) Mechanical strain including compression and tension are also important factor to regulate cell behaviours. Mechanical strain of 8% in BM-MSCs was shown stimulate osteogenesis by

measurement of ALP, calcium deposition, RANKL activation and mRNA expression (268)

Many of these biophysical cues induce responses through actin cytoskeletal dynamics. As such an overarching mechanism has been described to explain this called tensional integrity or tensegrity which is based on the overall cytoskeletal mechanics to explain a uniform method of biomechanical response.

### 1.6.3 Mechanosensing

Mechanosensing of the aforementioned physical features is moderated by a variety of cellular components including integrins, focal adhesions, adherens junctions, cytoskeletal and nucleus (246). Integrins are transmembrane proteins which mediate activity and signals across cell membranes. Integrins are responsible for ECM signal interpretation and bond to certain ECM components such as fibronectin, collagen, laminin and elastin and this interaction is part of the step in activating the focal adhesions complexes (269, 270).

Focal adhesions are complexes formed of multiple proteins which interface with integrins and the cytoskeleton as transducer of signals. Typical focal adhesion proteins include talin, paxillin, vinculin and focal adhesion kinase (FAK) (246). Focal adhesion formation is heavily dependent on the strength of the force transmitted by the integrin which is in turn based on strength of outside signal (271).

Adherens junctions are structures that allow signalling of mechanical stressors across multiple cells as a form of cell-to-cell communication (272). These complexes have roles in important multicellular processes such as wound healing as well as tissue growth and remodelling. Cadherins proteins act as a linking molecule to actin fibres for transmission of signals along the actin cytoskeleton (273).

Overall the largest component that acts as a common denominator is the actin cytoskeleton which is comprised of F-actin fibres and microtubules (274). The actin cytoskeleton is able to contract and change cellular responses through the interaction of actin and myosin filament (275). This cytoskeletal transmits signals to the nucleus

through attachment of the fibres to nucleus through laminins and a LINC complex which is a multi-component complex that interacts with the nucleus and can modulate nuclear protein conformation which is the driver of changes in gene expression (276). Overall external signals are sensed by outer surface proteins which convey signal through the actin cytoskeleton to the cell nucleus, this is represented in figure 1.4.

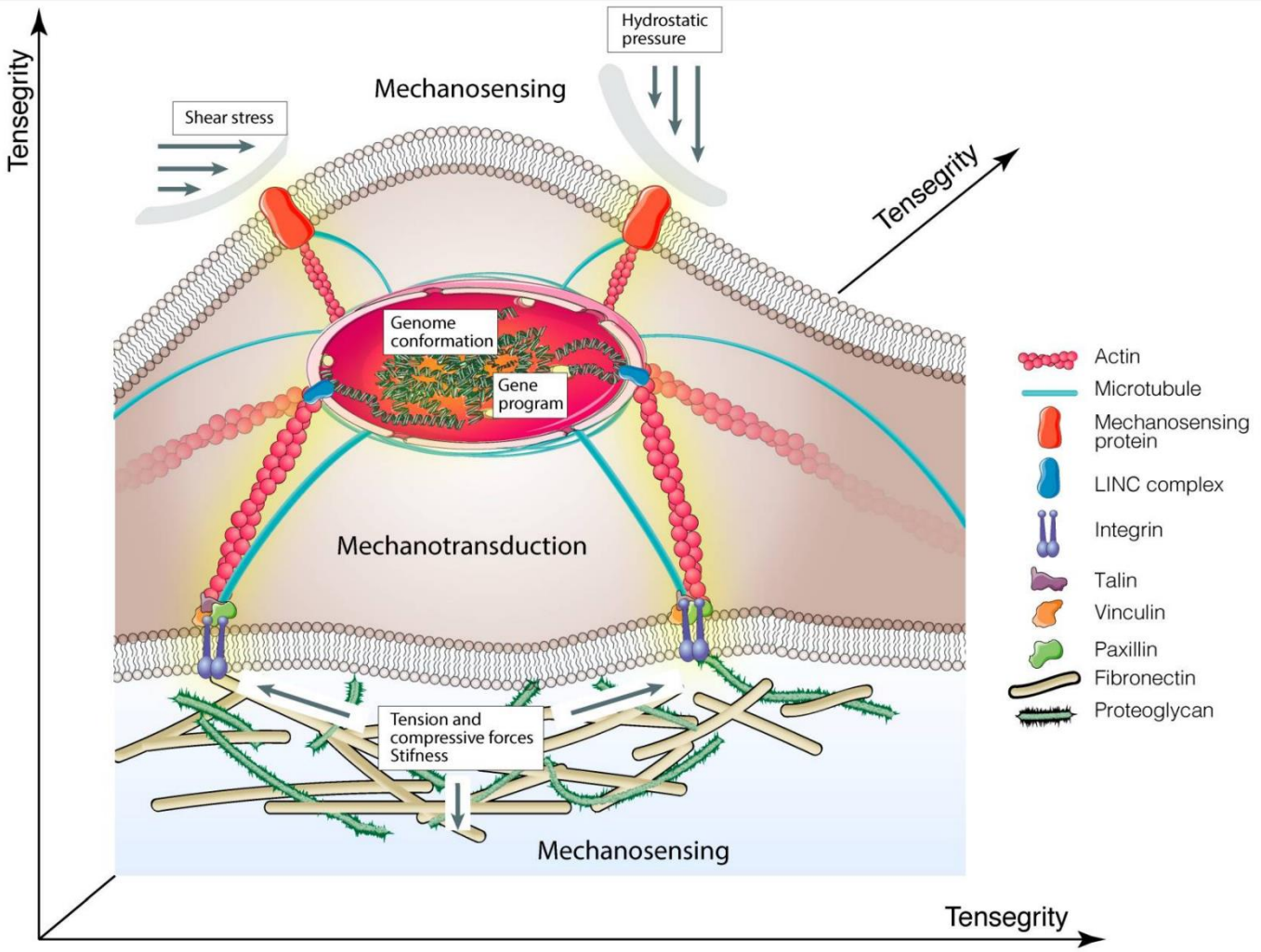


***Figure 1.4: Overview of mechanosensing and mechanotransduction pathways and components.*** *Mechanosensing components of cells including surface proteins and integrins transmit signals from outside cues through the actin skeleton to the nucleus for transduction of responses such as gene reprogramming. Reproduced from Argentati et al (246)*

### 1.6.4 Mechanotransduction signalling pathways

Sensed stimuli through mechanosensing pathways and converted to physical outcomes and behavioural changes through various mechanotransduction signalling pathways. Some of the pathways are YAP/TAZ, Rho/ROCK, FAK, mitogen-activated protein kinase (MAPK) and G-protein coupled receptors (GPCRs) (244).

YAP/TAZ signalling pathways act as a mediator and involve action of upstream signalling pathways such as MAPK, Wnt and Smad (277). YAP/TAZ has roles in cell differentiation of MSCs and accumulation in the nucleus is seen when cells experience stiff materials, this is also associated with osteogenesis (278). Unusual activity of YAP/TAZ signalling is seen in diseases such as cancer, atherosclerosis and muscular dystrophy (279).

Rho/ROCK activation is linked to actin stress fibre production and changes cell stiffness and mechanical properties (280). In apoptosis due to cell dissociation the primary causal agent is actinmyosin which is accumulated due to extreme stimulation of the Rho/ROCK pathway and when ROCK is selectively repressed cell survival increases significantly (281). Increased stiffness activates this pathway stimulating cellular contraction, this in turn activates a secondary signalling pathway called pERK which is associated with osteogenic differentiation (282).

Focal adhesion kinase (FAK), as the name suggests, is related to the focal adhesion complexes. FAK modulates differentiation through promotion of the previously discussed ROCK signalling pathway (283). Coactivation of ROCK with FAK leads to increase in ALP activity, RUNX2 and other signals of osteogenesis such as mineralisation and inhibition of this result in increased adipogenic markers and lipid production (244).

MAPK involves protein kinase enzymes which included a large number of kinases including ERK1 and JNK1 which have been demonstrated to be involved in a wide range of cellular mechanics including differentiation, proliferation, apoptosis and gene regulation (284).

GPCRs are present at cell membranes are involved in calcium signalling and was indicated to be involved in maintaining proliferation of stem cells. Stretch activated channels allow the influx of $Ca^{2+}$ which activates the MAPK pathway (244, 285).

Overall, the intricate and complex mechanisms by which cells can sense and react to a variety of physical stimuli is documented. The presented mechanisms only represent a brief overview of the main pathways and there is still much more research required to

fully understand these signals, how they apply in 3D culture and how these combine in complex environments to direct cell response. Responses of cells to topographical and physical features in the microenvironment result in changes to cell proliferation, morphology and differentiation due to activation of these pathways and as such environments can theoretically be designed to induce certain responses.

## 1.7 Project Aims and objectives

The overarching hypothesis of this work is that MSCs grown on specific geometries will exhibit a higher rate of expansion whilst still retaining stemness than those expanded through planar cell culture due to the enhanced biomechanical cues of the culture environment. This thesis focuses on employing this approach to microcarrier technology and examining the effects of such structures on cell control and enhancement of expansion yield to facilitate MSC production for therapeutic uses. The research is split into the following objectives:

1. Explore two-photon fabrication to produce complex 3D microcarrier architectures.
    a. Explore polymer suitability for fabrication at rapid speeds with high structural fidelity.
    b. Optimise fabrication for laboratory scaled microcarrier culture across a range of designs.
    c. Produce a means of suitable structural release from the fabrication surface without structural damage to the microcarriers.

2. Develop novel methodologies for the investigation of MSC growth and characteristics when grown on microcarriers.
    a. Assess biocompatibility of suitable polymers, investigate suitable surface modifications and optimise post processing techniques for enhanced cell interaction.

b. Create a technique to isolate cellular activity only to structures of interest and not to the underlying flat anchoring glass substrate.

c. Create microcarrier designs for production that have considered architectures to inspire specific biological responses for tailoring cell control.

d. Explore and optimise imaging techniques for examination of MSC-microcarrier interaction with the challenge of the natural autofluorescence of the materials used.

3. Explore microcarrier geometry on MSC response in culture.

    a. Assess and screen 3D geometry library for enhanced cellular adhesion and expansion.

    b. Quantify expansion potential of MSCs cultured on novel microcarriers and contrast to spherical (3D) and planar (2D) controls.

    c. Analyse stem cell marker panel after expansion on various microcarrier designs to determine effect on MSC phenotype.

# 2. Materials and Methods

The following materials and methods include the collection of protocols that are commonly used throughout all the performed work. Details pertaining to specifically used materials and methods can be found in their respective chapters.

## 2.1 Monomer preparation

Acylate monomers were mixed with photoinitiator Irgacure 369 (2-Benzyl-2-(dimethylamino)-4′-morpholinobutyrophenone) (Sigma) at 2% by weight. Monomers were given 24 hours at 400rpm stirring to aid diffusion of initiator. For viscous monomer an ultrasonic bath was used to aid diffusion. Acrylate monomers include pentaerythritol triacrylate (PETA), pentaerythritol tetraacrylate (PETRA), tricyclodecanedimethanol diacrylate (TCDMDA), polyethylene glycol diacrylate (PEGDA) (700Mn), Trimethylopropane ethoxylate triacrylate (TMPETA) all supplied by Sigma. Mixing and storage took place inside amber vials to shield from light and was used within two weeks of mixing. For copolymer blends each monomer was mixed with photoinitiator first then transferred to a new vial at the necessary weight ratio and mixed for a further 24 hours.

## 2.2 Two-photon polymerisation

A commercial 2PP system was used for fabrication. Monomers were loaded into a Nanoscribe photonic professional GT system (Nanoscribe GmbH & Co. KG). System specifications include a Ti:sapphire fibre-coupled diode laser of 780nm at a pulse repetition rate 80MHz equal to a pulse duration of 120 fs. Laser focusing was achieved through an oil immersion 63x, 1.4NA lens with a working distance of 180 μm. Laser power was a maximum of 50mW and typically galvo scanning was used to achieve average speeds of 10000 μm/s but this is not the system limitation. Z position was addressed by the piezo stage. 22x22mm 1.5 glass coverslips with monomer on the surface and immersion oil underneath (Zeiss Immersol) are held in place using the

system 10 space sample holder and an adhesive tape to maintain position when inverted. Fabrication took place in a UV controlled environment.

### 2.3 2PP software & 3D modelling

3D models were either obtained online within the public domain or were created through Blender open-source 3D modelling program. The majority of files were self-created through blender or generated through SCAD 3d model generators. 3D files were processed for 2PP through Nanoscribe provided DeScribe software. DeScribe software was responsible for manipulating 3D models and generating gwl code including slicing models into layers and calculating laser travel paths and coordinates. Nanowrite was responsible for 2PP operation utilising coding generated through DeScribe. Mathematical analysis of structure surface and volume was conducted through blender model analysis tools.

### 2.4 Sample development

Following laser exposure and fabrication samples were carefully removed from the stage and immersed in propylene glycol monomethyl ether acetate (PGMEA) for 20 minutes. Samples were then transferred to 2-Isopropanol for a further 10 minutes to remove any residual monomer or developer. Samples were then dried under a stream of nitrogen gas and at this point could be packaged for transfer to other facilities for post-processing and cell culture or SEM. All development was completed within a UV controlled environment.

### 2.5 Post development processing of 2PP structures

Following 2PP development (section 2.4) structures were subject to 30 mins UV post cure. Post cure was achieved using a Omnicure S2000 spot UV curing system equipped with a high pressure 200W mercury vapor short arc bulb and irradiance at 320-500nm at 40W/cm$^2$. Structures were then transferred to a Heraeus Vacutherm VT6130M Vacuum Oven at 100°C overnight. Structures were washed three times with 2-propanol followed by three washes with d$H_2O$. Structures were transferred to tissue culture and

UV sterilised for 20 minutes followed by 24 hr incubation in Dulbecco's modified eagle medium (DMEM) media supplemented with 50% fetal bovine serum (FBS) for 24hrs to promote protein adsorption. Finally, samples were washed three times with phosphate buffered saline (PBS) and seeded.

### 2.6 Mammalian cell culture

Cell culture throughout was conducted initially using NIH-3T3 fibroblasts, a well-established cell line derived from mouse embryonic cells. Minor work in confocal imaging was conducted using a genetically modified GFP containing version of the same 3T3 cell line. 3T3 Cells were provided and used throughout their $15^{th}$ - $40^{th}$ passage.

The majority of experiments and final cell analysis was conducted using immortalised human bone marrow derived mesenchymal stem cells. Cells were immortalised in house with hTERT modification. Cells were provided at $6^{th}$ passage and were used to maximum of passage 20.

Culture media for both cell lines consisted of Dulbecco's modified eagle medium DMEM (Gibco, Fisher Scientific) supplemented with 10% (v/v) FBS (Sigma), 1% (v/v) antibiotic antimycotic solution (10,000 units/mL penicillin, 10,000 µg/mL of streptomycin, and 25 µg/mL of amphotericin B) (Fisher, Gibco) and 1% (v/v) glutamine. Addition of supplements for osteogenic or other differentiation media are described in their relevant sections.

Cells were cultured at 37°C in 5% $CO_2$ as standard. Cells were primarily grown in T75 cell culture flasks until ~80% confluent with media changes every 2-3 days. For passage cells were first washed twice with PBS followed by incubation with trypsin-EDTA solution for enzymatic dissociation of cells during a 4-minute incubation period at 37°C with viewing under a microscope to ensure detachment of cells. Subsequently, 5 mL of cell culture media was then added to neutralise trypsin solution and cells were collected and centrifuged at 200g for 5 minutes. Supernatant was discarded and cells resuspended in a known volume of media of which 20 µL was mixed with the same volume of Trypan blue in an Eppendorf tube for staining of viable cells. Cells were

then added to a haemocytometer and counted under a microscope using trypan blue staining of dead cells to determine viable cell population estimates. Cells could then be seeded for experimentation or further culture at the appropriate seeding density.

For long term storage cells were cultured until confluent, passaged and $1 \times 10^6$ cells resuspended in 1 mL of freezing media which consisted of 90% v/v FBS and 10% v/v DMSO. These aliquots were transferred to cryovials and placed into a Corning Coolcell freezing container for 24 hours freezing at -80°C before transfer to -196°C liquid nitrogen storage. For cell thawing frozen cells were removed and immediately placed into a 37°C water bath for rapid thawing for around 1-2 minutes or until thawed. The 1 mL aliquot of cells were then added to 15 mL of fresh warmed cell culture media and cultured in a T75 flask. After cell adherence or 24 hours, media is replaced to remove DMSO freezing media, cells are then cultured for one passage to adjust before experimental use.

### 2.7 Alamar blue cell viability assay

Cell metabolic activity and thus visibility was conducted using Alamar blue cell viability assays (sigma) which utilise the activity of a non-toxic cell permeable dye called resazurin (7-Hydroxy-3H-phenoxazin-3-one 10-oxide). Resazurin enters metabolically active cells and is reduced to resorufin which has high fluorescence. Thus, measurement of fluorescence in a plate reader indicates degree of reduction and thus metabolic activity. The assay was performed by addition of 10% v/v Alamar blue reagent to cells growing in media, for 96 well plates with 100 µL of culture media 10 µL is added. Incubation with reagent at 37°C in the dark was maintained for 1-4 hours dependent on cell population size and desired sensitivity. Following incubation 200 µL of the reduced solution in media was transferred in triplicate to a 96-well plate. Measurement of fluorescence at excitation wavelengths between 540- 570 nm and emission wavelength between 580–610 nm with peak emission at 585 nm. Finally, remaining samples were washed with PBS to remove reagent and replaced with fresh media for continued culture.

## 2.8 Cell fixation

Cells often required fixation for imaging and staining both for fluorescence microscopy and SEM. Samples were washed with PBS three times followed by submersion in 3.7% paraformaldehyde (PFA) for 30 minutes at RT. PFA solution was then removed, and samples washed with PBS. Fixed samples were stored in PBS at 4°C.

For SEM PFA fixed cells were subject to dehydration in increasing concentrations of ethanol (ETOH). Progressive dehydration of samples was achieved by incubation for 5 minutes in graded ethanol concentration diluted in $dH_2O$ at 25%, 50%, 75%, 95% and 100% ETOH. Final 100% ETOH steps were repeated three times for full dehydration. Finally, a chemical drying agent hexamethyldisilazane (HMDS) was used. Samples were covered in HMDS and incubated for 5 minutes. Following this remaining HMDS was removed and samples were left to dry for a minimum of one hour before further SEM preparation was completed.

## 2.9 Microscopy and cell staining

Microscopy including fluorescence, phase contrast and brightfield were taken using a Leica DM IRB using QI imaging software.

Live-dead stain (Biotium) was performed on live cells without fixation. This protocol stains live cells green and dead cells red. Staining was achieved by incubation of samples with 2 µM calcein AM and 4 µM EthD-III in PBS at 37°C for 30 mins followed by washing with PBS. Following incubation with dyes cells fluoresced with appropriate dye. Dead cell controls could be conducted by incubating cells with saponin or in absence of this in ethanol.

The nuclei of fixed cells could be stained using 4', 6-diamidino-2- phenylindole dihydrochloride (DAPI). Stock solution was created at 4 mg/mL in PBS and stored at 4°C. Staining required permeabilisation and so solution with 400 ng/mL DAPI in PBS was supplemented with 0.1 vol% Triton X-100 and solution was incubated for 5 minutes. Solution was removed and washed with PBS before final suspension in PBS

and imaging. Imaging parameters for DAPI included excitation at 360 nm and emission at 460 nm.

Phalloidin staining was pursued for visualisation of F-actin. Phalloidin conjugated to fluorophores binds strongly to F-actin in cells allowing visualisation. Fixed cells are subject to permeabilisation in 0.15% Triton X for 20 minutes prior to staining then can be blocked using a 5% solution of goat serum for 30 minutes. Cells were then subject to phalloidin staining solution at 1:20 dilution of stain in PBS and incubated at 37°C in the dark for 30 mins. Solution was removed and cells washed and stored in PBS for further visualization.

### 2.10 Scanning electron microscopy

Fixed and dehydrated samples were air dried, mounted to SEM stubs affixed with carbon tabs and gold coated via a polaron E5175 sputter coater at 2.2Kv for 90 seconds. Samples were loaded into and imaged with a JEOL6490LV SEM at 5-10Kv under high vacuum. False colour in SEMs was produced using masking and colourisation of areas in Adobe Photoshop and as such was subject to author interpretation. Environmental scanning electron microscopy (ESEM) was briefly pursued for imaging of cells on structures in aqueous environments and as such cell dehydration and gold coating was not necessary. ESEM imaging was performed using an FEI Quanta 650 ESEM.

### 2.11 Confocal microscopy

Confocal images were taken using a Zeiss LSM 880C Confocal Microscope, with a 40x water immersion lens. Fixed and labelled cells on 2PP samples were already fabricated upon #1.5 coverslips which after staining were kept in $dH_2O$ until ready to mount and image. A secure seal imaging spacer sticker was added to sample coverslips and a 10-20ul drop of $dH_2O$ was added on top of the sample. This coverslip was then fixed to a microscope slide in an inverted fashion trapping the fluid within the spacer volume with excess water removed. The water objective collar was set to 0.17 and pinhole settings opened to give a larger optical slice. Generic structure imaging was performed using the 405nm laser to excite the autofluorescence from the scaffolds. After setting gain values Z-stacks were acquired.

Macroconfocal imaging was performed using a Leica TCS LSI macro confocal with super zoom capabilities and across a 16mm field of view. Sample preparation regarding staining was consistent between both methods but samples could be imaged within cell culture plates.

### 2.12 Image analysis

Image analysis of microscopy including fluorescence measurement and profiling in z-stacks along with 3D reconstruction of stacks, automated live-dead staining quantification, structure measurements from SEMs and counting was performed in Fiji-ImageJ software.

### 2.13 Statistical analysis

Statistical analysis was performed in Graphpad Prism 9. Tests used were analysis of variance (ANOVA) and Dunnett's multiple comparisons test. Significance was denoted in each figure where relevant. All graphs are presented as mean ± standard deviation (SD) unless otherwise stated and number of replicates (n) is denoted.

# 3. Two-photon fabrication of complex 3D microcarrier architectures.

## 3.1 Introduction

### 3.1.1 Additive manufacturing technologies

Additive manufacturing (AM) is generally described as a type of fabrication in which materials are joined, usually layer by layer, based on 3D model data and is often summarised as rapid prototyping or 3D-printing (286). This is in contrast to traditional manufacturing methods that are subtractive and involve removing material from a bulk stock until the desired form is achieved i.e., milling or carving.

AM breaks down into a few different categories of techniques which include vat polymerisation, binder jetting, material jetting, material extrusion, powder bed fusion, sheet lamination and directed energy deposition (287). There are many techniques within these categories and several of these are applicable to biomaterials. The key technologies used for biofabrication are largely material extrusion or fused deposition modelling (FDM), inkjet printing and various vat polymerisation lithography techniques. These lithography techniques include stereolithography (SLA), projection micro stereolithography (PμSLA) and two photon polymerisation (2PP) also known as multiphoton lithography.

The requirements for this research are to have total structure diameters of 50-300 μm and feature resolution below 2μm at maximum. This allows features that can interact with individual cells and structures that can support multiple cells at a time. Additionally, materials applicable need to be biocompatible and need to be produced relatively quickly to a level that allows laboratory scale experimentation.

Extrusion printing is a popular technique of patterning biomaterials but typical resolution range is in the range of 200-1000 μm which is several time larger than required and would not be able to fabricate structures that provide biophysical stimulation in the sensing range of individual cells (288). Typically, extrusion based

bioprinting makes its mark through the material chemistry and rheological properties of the material extruded. This technique fabricates over large distances for constructs big enough to replace whole tissues and defects in the range of millimetres to centimetres. There are many viable applications of bioprinting across a wide range of materials as recently reviewed (286, 288). However, for the purpose of this work the resolution range is not applicable to provide features at a scale small enough to interface with individual cells in a controlled and observable manner.

Inkjet printing is a jetting-based technique that produces droplets of material that can be patterned by movement of the dispersing print head. This is then followed by UV polymerisation and built layer by layer. The size of these droplets and therefore resolution is highly dependent on the material properties including viscosity and wetting behaviour as well as jetting parameters and capillary forces. Typically, resolution is in the range of 10-60 μm, which makes this technology too large for the intended purpose of features that interact at a singular cell level (289). Other disadvantages of this technique are the complexity of the printing parameters that require extensive optimisation and exhibit extreme sensitivity to slight changes in characteristics as well as lengthy fabrication times at large scale. This makes this technique not suitable to the requirements of this research.

Photopolymerisation methodologies such as various lithography techniques are commonly used for biofabrication. SLA methodologies work by compressing a thin layer of liquid resin between a build plate and LCD screen. The screen projects an image which polymerises the trapped material sticking to the plate, this can then be raised and repeated layer by layer. This methodology is fast, inexpensive and can be applied to a variety of UV-curing materials. However, the resolution size is dependent on the pixel size of the screen, which on a 4K panel is roughly 35μm. Whilst each pixel is this size, this does not necessarily correspond to minimum feature size. This is due to light bleed from the pixel into the surrounding area and the fact that a feature requires multiple pixels to form a shape other than a square. Whilst this feature size is much closer to the desired range and is suitable to all other desired parameters, the overall goal of features interacting with individual cells is not possible due to the resolution.

A recent development of SLA methodology which uses projected images rather than a screen is PμSLA which can produce a resolution as low as 2μm. This technique is far more suitable and was identified as a future mechanism for scale up, but due to novelty of this technology was not able to be applied from the start of the research. The mechanism of fabrication is dependent on the number of exposures in height, essentially ignoring the XY scale of the image. This method produces hundreds of structures as quickly as a singular one. Whilst this is advantageous for scale up, for rapid prototyping of small numbers of structures there are other more suitable and faster techniques.

Two-photon polymerisation (2PP) is a laser based technique capable of precise 3D fabrication at typical feature levels of 100 nm but in some cases as low as 50 nm (290). 2PP can vary this minimal feature size based on objective lens and power parameters allowing voxel sizes as large as several micron, making it applicable across a wide range of scales. The basic premise of 2PP is precise light induced polymerisation of photosensitive materials based on the principle of two-photon absorption (TPA). 2PP has uses in a range of areas including, photonics, microelectronics, metamaterials and biological fields as recently reviewed by Otuka *et al* (291) and Saha *et al* (292). 2PP allows rapid structuring of photopolymers at relevant scale to explore feature interaction with individual cells and overall structures than can support multiple cells at a time. This makes this technique the most appropriate fabrication methodology for this research and meets all of the necessary criteria. Whilst other smaller feature sizes can be achieved with electron, x-ray and ion beam lithography, these techniques take much longer, are difficult to scale up to laboratory scale, do not have the versatility of 2PP and require use of clean room facilities.

### 3.1.2 2PP Development

TPA was theoretically outlined and predicted in 1931 by Goeppert-Mayer (293) but not verified until shortly after the invention of the laser, critical to proving this theory, in 1961 (294). The first demonstration of 2PP was in 1965 by Pao and Rentzepis which reported polymerisation events as a chemical reaction without any structural control. It wasn't until 1997 that 2PP as a lithography technique was demonstrated, largely due to the invention of the femtosecond laser, which allowed fabrication of structures of only

a few micrometres (295). Further momentum surged in 2001 when Kawata *et al* overcame Abbe's diffraction limited resolution theory and reduced feature size from 395 nm to approximately 100 nm (296). Technological development decreased costs and inclusion of galvanometer scanning technologies have made this technology more accessible and faster. Commercialisation and dissemination of 2PP systems by companies such as Nanoscribe GmbH & Co. KG contribute to application of this technology across a range of disciplines (297).

### 3.1.3 2PP System Specifications

2PP occurs via focus and delivery of photons within a discrete region called the voxel (volumetric pixel) in which TPA initiates the photopolymerisation process. Typical 2PP setups include a solid state Ti:sapphire ($Ti:Al_2O_3$) femtosecond laser for ultrashort pulse durations of 100fs. Usually near infrared (NIR) wavelengths are utilised with a typical wavelength of 800 nm although 2PP can be achieved using wavelengths of 515 nm in the green visible light region to 1064 nm in the NIR region (298). Modern setups favour use of second harmonic fibre lasers operating at 780 nm for decreased costs and improved reliability (299). Laser power varies from a few mW to 10 W and have a pulse repetition rate between 1 KHz and 100 MHz (298). This laser source is focused through a lens of high numerical aperture onto a substrate, usually glass, upon which a monomer droplet is suspended. Irradiation within the voxel reaches exposure threshold triggering the photoinitiator (PI) and inducing photo-crosslinking.

Manufacture can occur through two methods, piezo stage movements of the sample across XYZ dimensions with a fixed static laser or by galvanometer scanning. Galvo scan-based fabrication involves use of galvanometer mirrors, one pivots across the X-axis reflecting onto a secondary mirror that pivots across the Y-axis producing XY movement of the laser travel. A Piezo stage is addressed for Z-axis movements for each layer but galvo scan travels at 10mm/s are faster than those capable by Piezo. Galvo scan modes are suitable for fast fabrication of large structures but suffer from limited focal region whereas piezo scan modes can address a larger space with potentially more accurate movements at the cost of speed (300, 301). After polymerisation uncured monomer can be dissolved and washed off leaving behind polymerised structure. A

schematical representation of a stereotypical 2PP system is demonstrated in figure 4.1. Unlike single photon polymerisation, the quadratic dependence of light intensity in TPA allows better accuracy and 3D spatial resolution of higher precision (298). Operation in the NIR region allows polymerisation of materials that are laden with living cells, given suitable biocompatibility of the uncured resist (302).

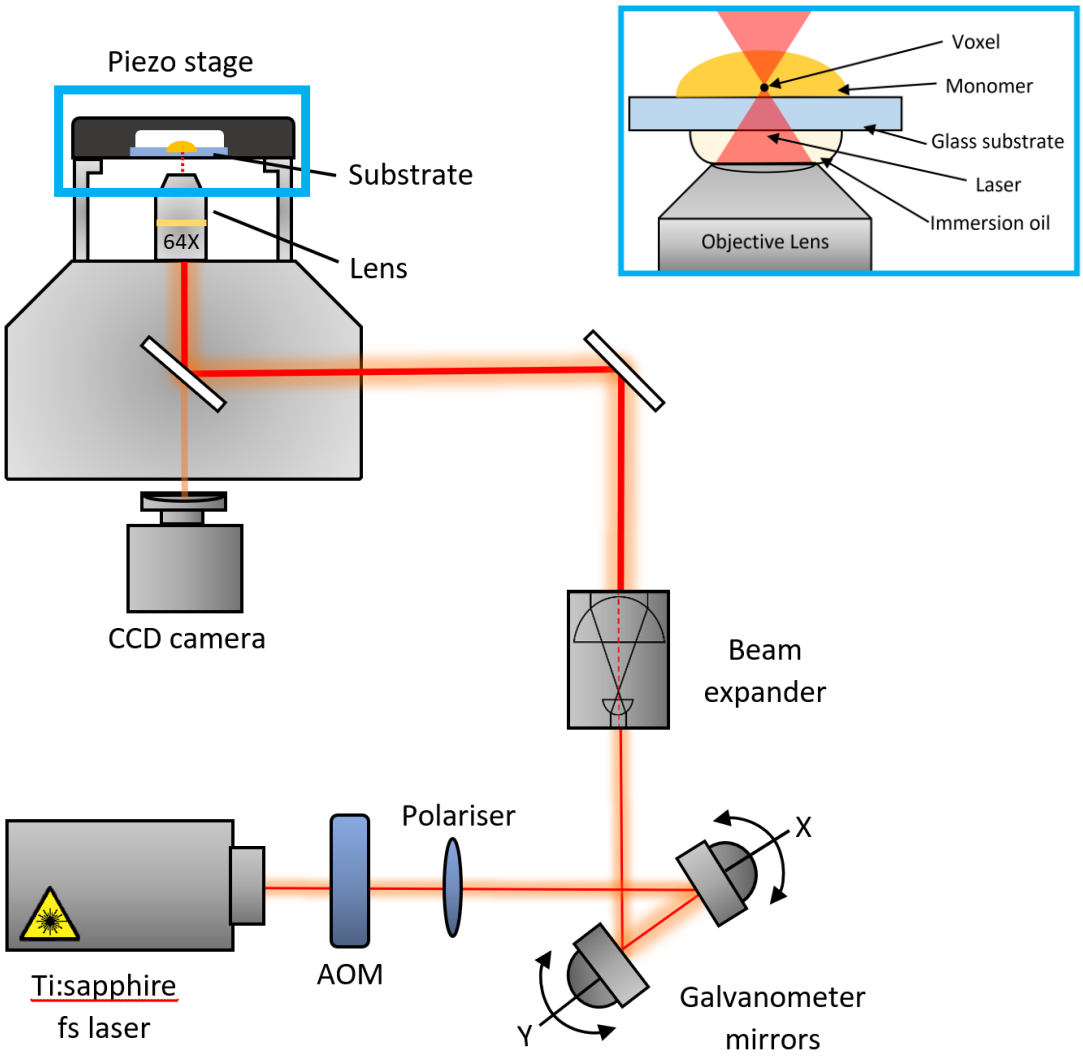


***Figure 3.1:*** *Schematical representation of a standard 2PP system (AOM: acousto-optic modulator, CCD: charged-coupled device)*

### 3.1.4 Photoinitiators

For polymerisation reactions the involvement of a photoinitiator (PI) is necessary. For 2PP PIs the two-photon absorption cross-section ($\delta_{TPA}$), which represents the probability of photon absorption, is an indicator of TPA incidence and as such PI suitability and success (303). $\delta_{TPA}$ units are given in Goeppert-Mayer (GM) in which one GM is equal to $10^{-50}$ $cm^4$ s photon $^{-1}$, commercial PIs typically have low $\delta_{TPA}$ values rarely exceeding 10GM (304). Production of PIs with high $\delta_{TPA}$ would have a high rate of TPA and initiate photopolymerisation at high efficiency making them extremely sought after (305). There are two primary polymerisation types in 2PP which are classified by the action of the PI, these are radical driven and cationic polymerisation. Cationic polymerisation is initiated through photoacid generation (PAG) for polymerisation of epoxy or vinyl ether resists and is typically less commonly used due to necessity of post-processing (304). Radical PIs can be classified as either Norrish type I or type II, type I initiators are molecules that exhibit homolytic cleavage upon exposure of appropriate wavelength light, breaking down into radical species that provide energy to initiate and propagate cross-linking. Examples include benzil dimethyl ketal (BDK) initiators such as 2-Benzyl-2-(dimethylamino)-1-[4-(morpholinyl) phenyl)]-1-butanone otherwise known as Irgacure 369. Type II initiators involve a two-step process of a light absorbing co-initiator which donates hydrogen atoms to an energised sensitiser releasing a radical for initiation and often involve tertiary amines as co-initiators (306).

### 3.1.5 TPA Mechanics

TPA in PIs is initiated via excitement through absorption of two photons, the 1$^{st}$ absorption elevates the molecule to a virtual intermediate energy state upon which second photon arrival and absorption must occur within $10^{-16}$s, based on Heisenberg's uncertainty principle, for TPA to be achieved (300) as depicted in figure 4.2. This event takes place femtoseconds apart but is often referred to as simultaneous given the short duration between states and highlights the reliance on femtosecond lasers for 2PP. TPA excitement is spatially confined dependent on light intensity and $\delta_{TPA}$, the quadratic relationship of TPA on intensity can reduce resolution by a factor $\sqrt{2}$ reaching sub-diffraction limits as first noted by Kawata *et al* (291, 296).

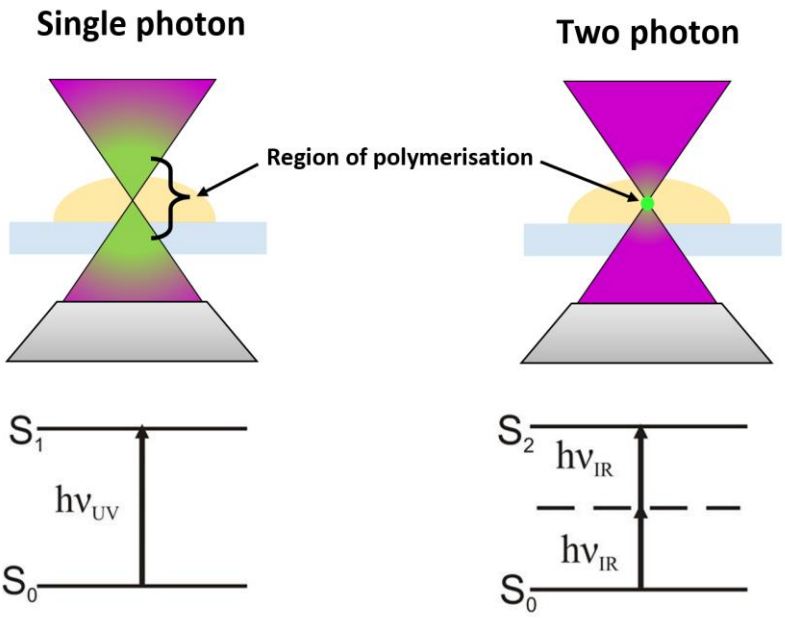


***Figure 3.2:*** *Schematical representation of single photo polymerisation vs two photon polymerisation showing changes to polymerisation region in green and corresponding simplistic Jablonski energy diagram.*

### 3.1.6 Material Suitability

Requirements for 2PP often limit material possibilities although new materials are constantly being developed and adapted for 2PP. Suitable materials are required to have transparency in visible and NIR regions, rapid curing without shrinkage, suitable refractive index and mechanical strength capable of supporting structure design. Traditionally used materials are mostly acrylates and some epoxy polymers, these have a long history of use since the inception of 2PP and contain a variety of characteristics and functionalities. Several commercial resins have been developed and deployed such as IP-series (Nanoscribe GmbH) featuring a wide range of resin characteristics, epoxy-based SU-8 (Kayaku Advanced Materials inc.) and organic-inorganic hybrid material Ormocer (Micro Resist Technology) (300, 307-309). Functionality can be added to other polymers by acrylation, such is the strategy employed by Arslan *et al* who produced acylate endcapped urethane poly-ε-caprolactone (PCL) to enable use of popular biomaterial PCL (310). Another recent interest in 2PP is the structuring of hydrogel resists for tissue engineering applications and include materials such as

PEGDA or gelatin derivatives that can be enhanced with thiol chemistries (311-313). Other interesting biomaterials being explored for 2PP include protein-based formulations such as bovine serum albumin (BSA), fibrinogen and collagen (314-316). Continued novel strategies are constantly being explored for instance the recent demonstration of 2PP of a ceramic slurry for the first time (317). The materials described are not all-inclusive and many hybrid materials are possible. Resists doped with other substances, often in the form of nanoparticles, impart additional characteristics and occasionally responsive functionality (291, 304, 318).

A literature search of commonly used materials for 2PP was conducted. Several suitably identified materials were screened for 2PP success, specifically looking for fabricability, uncompromised interface identification and processability at high speeds. Materials that did not meet these criteria or had unsuitable toxicity in the open-air system were eliminated. Five materials that met these criteria were carried forward for further use as summarised in Appendix 1. All tests were performed using Irgacure 369 as the photoinitiator and were mostly di- or tri- acrylates.

The five identified and listed materials were each chosen for their suitability in the 2PP system at high writing speeds and suitable refractive index. All materials had previously been demonstrated for 2PP fabrication in the literature (300, 319), but high-speed fabrication and suitable interface auto detection wasn't confirmed until experimental review. Acrylates have the highest level of suitability for 2PP systems with many materials used in the literature and a wide range of choices and characteristics (320). As such all five choices carried forward were acrylates, but each presented an additional useful property that could be explored. PETA was used for all around suitability, rapid polymerisation kinetics and biocompatibility with common use in the literature and acted as a baseline (300, 319). PETRA has an almost identical chemistry to PETA but with higher stiffness allowing comparison of substrate stiffness and blending to tailor this property. TMPETA has been utilised several times for functionalisation of surfaces with protein components for spatial arrangement in complex 2PP formed structures (321, 322). PEGDA allowed for hydrogel fabrication, modification of polymer wetting characteristics and a stiffness modulator (311, 312). Finally, TCDMDA was included, despite slight refractive index mismatch which impacted interface detection, for its bacterial attachment resistance which could be a

useful feature for culture or if developed into a microparticle scaffold (323, 324). TCDMDA is a chemistry rarely used in 2PP and to the authors knowledge and hasn't been demonstrated for 2PP outside of the UoN CfAM group.

### 3.1.7 Biological applications

The dissemination of 2PP technology has led to wider exploration across bioapplications. This has included the production of advanced biomedical microdevices including microneedles and smart implantable devices for drug delivery (307, 325, 326). Creation of four dimensional (4D) structures that have complex 3D architectures coupled with reactivity across a fourth dimension triggered by a stimulus creates smart reactive structures or microrobots (327). This approach was employed by Sun *et al* to create smart structures that utilise magnetic fields along with specialised corkscrew geometry for highly controlled propulsion, termed microswimmers, useful for precision medicine, biosensing and drug delivery (318). 2PP fabricated structures have also been utilised for mechanobiological studies, analysis of structure deformation by cells in constructs of known geometry and stiffness allows mathematical calculation of cellular forces exerted (328). 2PP also allows for cell spatial organisation through structural isolation and patterning this can be used in a wide range of scenarios including microfluidic based organ on chip structures (329, 330). Precise fabrication with nanoscale features can be used to replicate naturally occurring biosurfaces that have unique functional topographies (331), replication of natural ECM topography (332) or alignment and patterning of anisotropic cell types for regenerative purposes (333). Biological applications of 2PP are extensively reviewed by Otuka *et al* (291) as well as Nguyen and Narayan (334). With the vast range of implications of precise shape control in biology many potential uses are only just being conceived. Limitations to polymer suitability and biocompatibility along with fabrication speeds that hinder scalability are the major obstacles for translating 2PP to biological applications.

## 3.2 Aims and Objectives

This chapter investigates techniques for 2PP fabrication to rapidly produce particles with complex geometry for future analysis of MSC expansion potential as microcarriers. Results of this work will enable rapid and efficient structure production and novel techniques necessary for biological screening in future chapters. To achieve this the following goals were established:

1) Explore appropriate polymers capable of 2PP with suitable material characteristics for rapid microcarrier production.

2) Design strategies and optimise 2PP writing parameters for scalable production of complex structures with maintained shape fidelity and accuracy.

3) Investigate material-based methods to isolate cell activity to microcarriers via substrate modification or structural release to aid cell analysis.

## 3.3 Materials and Methods

The following methodologies are used in this chapter in addition to those presented in section two materials and methods.

### 3.3.1 IPA free Sample development

Slight modification of development protocol was necessary to fabricate upon pHEMA coated coverslips as IPA soaking stages would dissolve the coating prematurely. Sample development was continued as per section 2.3 but IPA was substituted for 3x 10 min deionised water rinses. Further rinsing, post fabrication UV curing and vacuum oven treatment was included as part of post processing to ensure no residual chemicals remained.

### 3.3.2 Manual interface finding

The Nanoscribe GT has an automatic interface finding feature, however this was not always possible as the module is calibrated to recognise a certain refractive index change between substrate and monomer. In this case, the pHEMA coatings refractive similarity to the monomer prevented this automatic operation. without this feature manual interface position can be found in person by slowly moving the focus wheel to address z position manually. If a job is running interface can be found by starting at a low z position and raising until fabrication starts through the camera. The focal plane of HEMA coating can be located without fabrication given the presence of a surface pattern that can be brought into focus as a guide. GWL code can be modified to remove automatic interface searches through removal of coding line: var $interfacePos = 0.5 in the job.gwl file coupled with removal of variable: FindInterfaceAt $interfacePos in the data.gwl file.

### 3.3.3 pHEMA coating

4g of Poly 2-hydroxyethyl methacrylate (sigma) was dissolved in 100ml (40mg/ml) of ethanol at 60°C for 6 hours with stirring until fully dissolved. 500 µL of solution was pipetted onto glass coverslips suspended by spacers and left to evaporate overnight at RT giving a 20mg covering. An even coating is left behind that can be directly used for 2PP or cell culture. After fabrication with 2PP, custom 3d printed spacers were used to support inverted samples and coat the back of the coverslip without disturbing fabricated structures. This ensured no colonisable glass space was present. Particle release could be achieved by soaking samples in IPA and filtering released structures.

### 3.3.4 Water contact angle measurement

WCA measurements were taken using a water contact angle goniometer KSV CAM200 and using 18.2MΩ de-ionised water (MilliQ water). Static measurements were recorded and analysed using the CAM200 software.

### 3.3.5 Silanization

Coverslips were subject to 10 minutes of 100% $O^2$ plasma surface etching prior to treatment. In acetone methodology coverslips were transferred to 3-methylacryloxypropyltrimethoxysilane (MAPTMS /Silane A174) dissolved in acetone at 10%. Coverslips were left in solution until use upon which removed coverslips were washed in pure acetone, IPA and then dried under nitrogen. For toluene methodology plasma etched coverslips were submerged in a 10 wt% MAPTMS in dry toluene overnight. Coverslips were washed in methanol, dried and stored under a vacuum.

### 3.3.6 Projection micro stereolithography

Projection micro stereolithography was achieved using a NanoArch S130 system (BMF Material Technology Inc., Shenzhen, China). This system uses a UV-LED light source of 405 nm with optical resolution of 2 µm and layer thickness from 5-20 µm. Structures were prototyped in BMF series supplied resins. After fabrication structures could be washed in PGMEA and IPA and removed from the build plate or directly imaged from the silicon wafer.

# 3.4 Results

### 3.4.1 Polymer Screening and calibration

Assessment of a polymer's fabrication suitability can be conducted through a woodpile sweep. A 3D woodpile structure was modelled using adjacent struts replicated on each layer perpendicular to the previous as depicted in figure 3.3A. The structure consisted of 25 evenly spaced struts per layer with 30 total layers at an overall size of 50x50x30 µm. This equated to approximate strut thickness and height of 1µm with similar spacing between repeating struts. Post-development visualisation of layer line thickness and structural integrity could be quantified via SEM. Repetition of this structure in an array varied laser power in 10% increments to deliver a power of 5mW to a maximum of 50mW across the X-axis. Writing speed was varied across the Y-axis from 1000 µm/s in 10% increments to 10000 µm/s as depicted in the coding simulation schematic in figure 3.3B. Job design in this way meant an array of structures being subject to a variety of exposure levels across an assortment of speed and power combinations. An example SEM of a woodpile sweep is shown in figure 3.3C indicating a range of structure success. This includes underexposed structures with rounded features in the left column due to insufficient laser power and overexposed and warped structures in the bottom right corner from high power being delivered at slow speeds.

Assessment of structure quality allows identification of fabrication settings that create the desired quality at the highest speed. Figure 3.3C indicates structures that are successful but fabricated at lower laser powers have more pronounced spacing between struts due to a decreased line width otherwise known as the voxel size. Woodpiles were categorised into a class system to quantify and visualise parameter success. Class one structures in green indicate a successful and accurate recreation of the 3d model with no warping or misfabrication. Class two structures in orange indicate a close similarity to the intended structure with no major structural failing but slight misfabrication or warping. Class three structures in red represent badly damaged or misfabricated structures where very little similarity to the model is achieved, in subclass 3a this is due to underexposure and in 3b this is due to overexposure. These classifications are used to produce heatmaps to visualise parameter suitability and identify trends within the exposure amounts at a glance as depicted in figure 4.3D. As this figure shows for example polymer PEGDA there is a wide range of suitable settings with great

flexibility and potential to be fabricated at speeds above 10000 µm/s. In the case of an unsuitable polymer either no fabrication or only warped fabrication would be achieved.

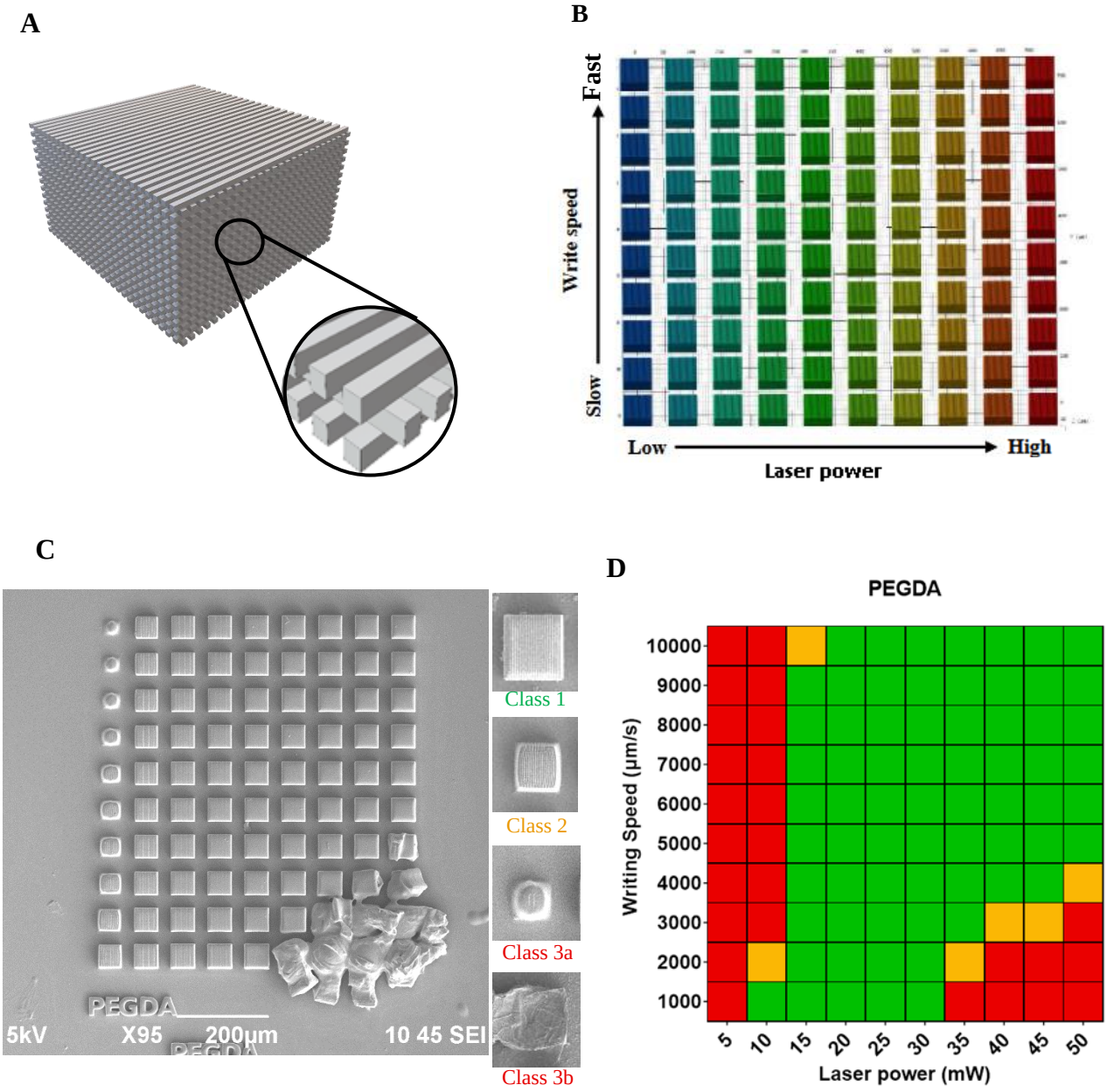


***Figure 3.3:*** *Polymer screening process schematic of woodpile sweeps. (A) 3D render of woodpile structural design used to test fabrication ability through observation of strut formation across repeating adjacent levels. (B) Graphical simulation of sweep GWL coding indicating fabrication parameters. (C) Example SEM image of succesful sweep in PEGDA indicating a wide fabrication range with example guide for classification of fabrication success. (D) results of SEM data in heatmap style graphs to visualise suitable fabrication parameter trends across writing speed and laser power which in the case of PEGDA example is quite broad.*

The process outlined in figure 3.3 was conducted for all polymers and heatmaps of processability is demonstrated in figure 3.4. Original SEM images for all polymers represented in figure 3.4 are available in appendix 2. For practicality purposes interest

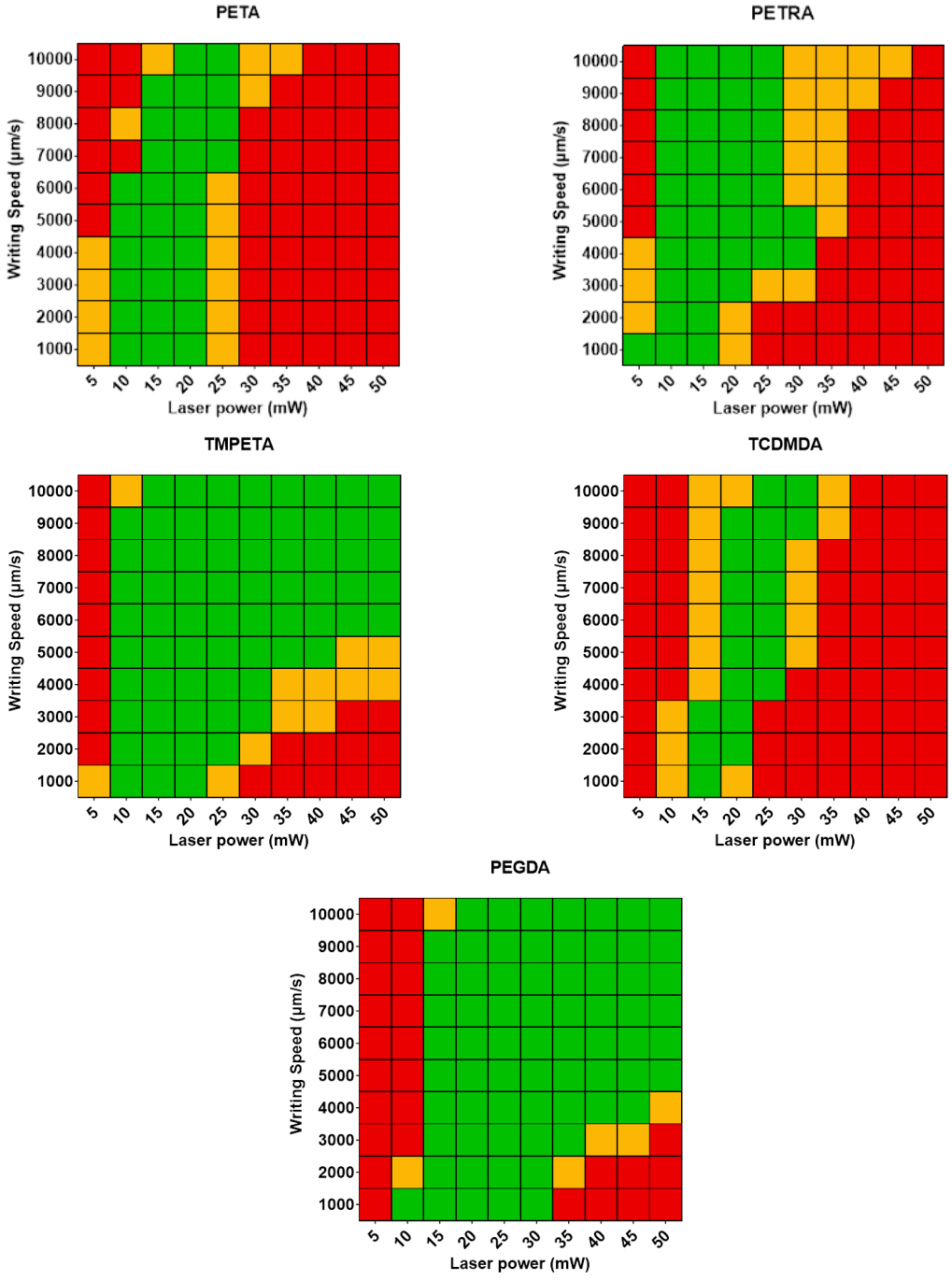


***Figure 3.4:*** *Heatmap visual representations of polymer fabrication thresholds. Woodpile sweeps were fabricated in each of the selected polymers, visual analysis of SEMs using classification system described to create heatmaps. PETA and PETRA both demonstrate moderate fabrication range. TMPETA and PEGDA demonstrate broad spectrums with a wide range of suitable settings. TCDMDA shows a very narrow range of suitable settings.*

was focused on the fastest possible speeds due to time and efficiency considerations.

PETA showed a small range of suitable fabrication settings. At the lowest writing speeds of 1000 µm/s fabrication was achieved with a laser power of 10mW and burning of polymer occurred above 20mw. Moving fabrication speeds to the fastest tested value of 10000 µm/s laser powers of 20mW produced accurate structures but values greater than 25mW began to damage structures indicating a narrow working range of only roughly 5mW at 0.1µm layer distance. PETRA, the tetraacrylated counterpart of PETA, interestingly shows similar upper exposure limits of 25mW at max speed but tolerates lower power values of 10mW with successful fabrication. Although exposure at 30mw or above lead to class two structures complete burning did not occur until 50mw values, unlike PETA where 40mW laser powers lead to complete structure destruction. TMPETA demonstrates a wide range of flexibility and suitability across a range of exposure levels with successful fabrication at 10000 µm/s at the maximum power of 50mW as well as at 15mw showing a potential to be fabricated at speeds over maximum tested which makes this an attractive candidate since fabrication can be faster. TCDMDA demonstrated the narrowest range of suitability meaning very tight control over fabrication parameters is needed to prevent structure misfabrication. At 10000 µm/s minimum power values of 25mw can be tolerated with a maximum of only 30mw showing only a 5mw working range similar to PETA. PEGDA used as an example polymer in figure 3.3 shows a similarity to TMPETA with a wide range of suitable exposure rates and possibility to use as faster speeds. The lower laser power tolerance at 10000 µm/s indicating the polymerisation threshold for each polymer is noted in table 3.2 along with their upper exposure limits before burning occurred to demonstrate their overall working range of exposure.

| Polymer | Polymerisation threshold (mW) at 10,000 µm/s | |
|---|---|---|
| | minimum | maximum |
| PETA | 20 | 25 |
| PETRA | 10 | 25 |
| TMPETA | 15 | 50 |
| TCDMDA | 25 | 30 |
| PEGDA | 20 | 50 |

***Table 3.2:*** *Summary of minimum and maximum recorded polymerisation thresholds at fastest write speed generated from heatmaps.*

### 3.4.2 Slicing distance increases speed at the cost of resolution

Slicing distance is the measure of how many cross-sectional slices are made of the model in the Z axis and how many layers are needed to complete fabrication. Whilst slicing distance is the measure of the Z axis distance, hatching distance is a comparable feature over the XY plane and measures the spacing between travel lines of the laser within one XY slice. A visual representation of this is seen in Figure 3.5A in which low slicing distances produce a cone with smooth inclines leading to a sharp point with closely knit hatching lines as depicted in the callout image visual. Whilst higher slicing distances seen in figure 3.5B produced a cone with a profile made of blockier sections that produce an uneven step by step incline with a blunt rounded tip with hatching lines being much further apart, as shown in visual callout. An experiment to determine effects of slicing and hatching distances on speed was conducted by fabricating 100 µm height cones under different slicing and hatching distances and measuring fabrication times.

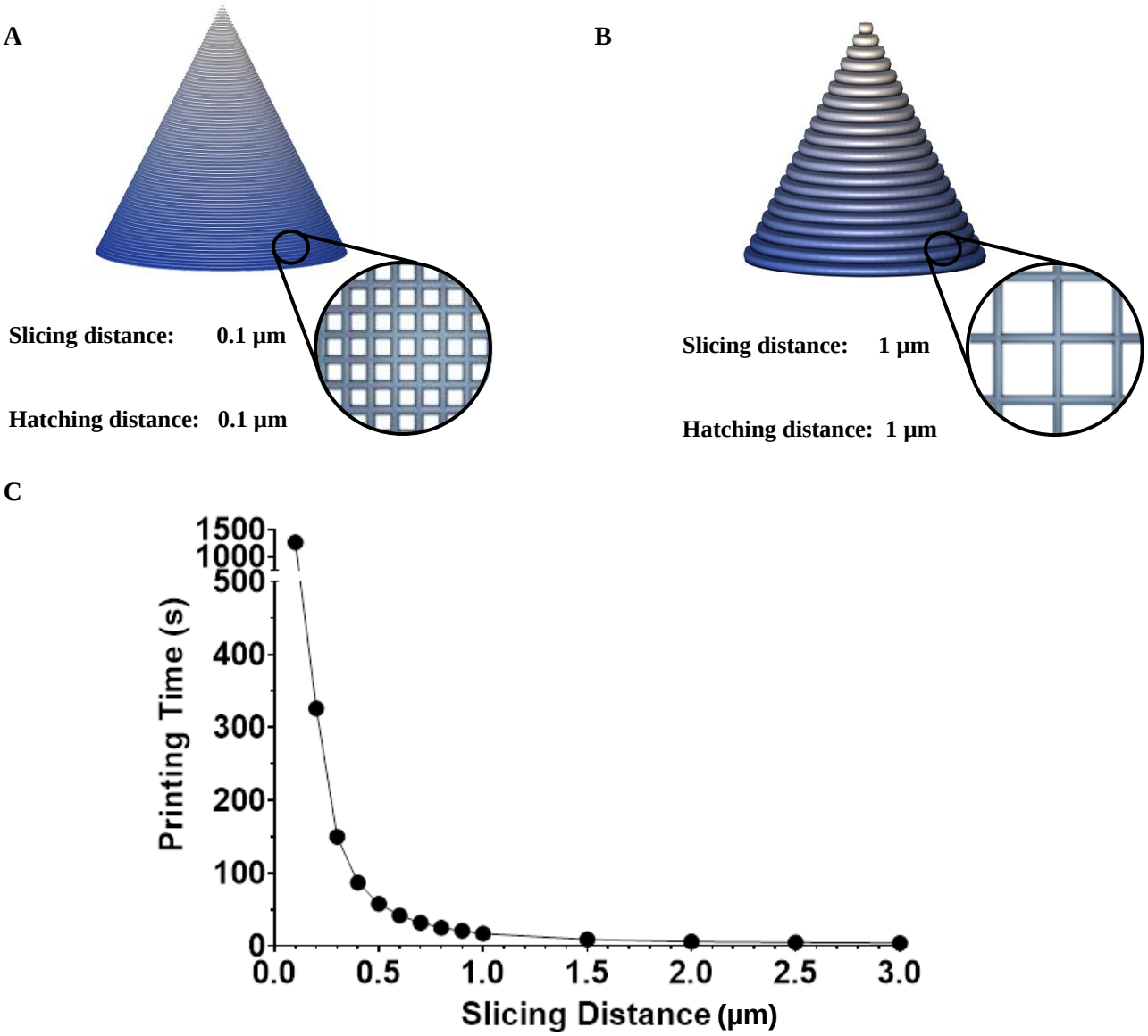


***Figure 3.5:*** *Increasing slicing and hatching distances increases fabrication speed but reduces structure quality. Cone structures fabricated with incremental variation to slicing and hatching distance. (A) Projection of structure appearance with graphical representation of hatching density at 0.1µm hatching and slicing distances. (B) Projection and visual representation under 1µm resolutions showing loss of feature detail. (C) Recorded times for cone fabrication under various layer and slicing distances indicating vastly reduced printing times at high slicing and hatching distances.*

As shown in figure 3.5C fabrication times at highest resolution, 0.1µm slicing and hatching, took just over 21 minutes. This value exponentially reduced at 0.5 µm values at which point fabrication took only 58 seconds and began to plateau reaching 17 seconds at 1 µm values and 4 seconds at extreme 3 µm values. Overall results indicate increased hatching and slicing distances leads to an exponential increase in fabrication speed at the cost of resolution.

### 3.4.3 Galvanometer acceleration reduces fabrication accuracy for a speed increase.

Exploration of galvanometer acceleration was conducted to aid in overcoming lengthy fabrication times that prevent large scale fabrication with 2PP. C180 bucky ball structures were fabricated in PETA at 0.1 slicing distance and hatching distances with all the same settings except galvo acceleration. High resolutions were used to increase number of travels and maximise the visible effect of increasing galvo acceleration. Galvo acceleration ranged from a minimum of $1ms^2$ to a maximum of 50 $ms^2$. At an acceleration value of 1 $ms^2$ it took 41 minutes to fabricate one structure. At an acceleration value of 10 $ms^2$ fabrication time was reduced by 44% down to 23 minutes. This effect continued but diminished up to maximum settings of 50 $ms^2$ which reduced fabrication down a further three minutes to a total time of approximately 20 minutes as depicted in figure 3.6B. Overall the same structure was produced at the same slicing and hatching quality twice as fast between minimum and maximum accelerations indicating how important this parameter can be in mass fabrication. SEM images in figure 3.6A depict the resulting loss in structure accuracy between minimum and maximum settings showing a minor but noticeable difference between shape accuracy. Measurement of pore sizes indicated approximately a 24% reduced pore size. Whilst shape was minorly affected, the overall structural composition was nearly identical.

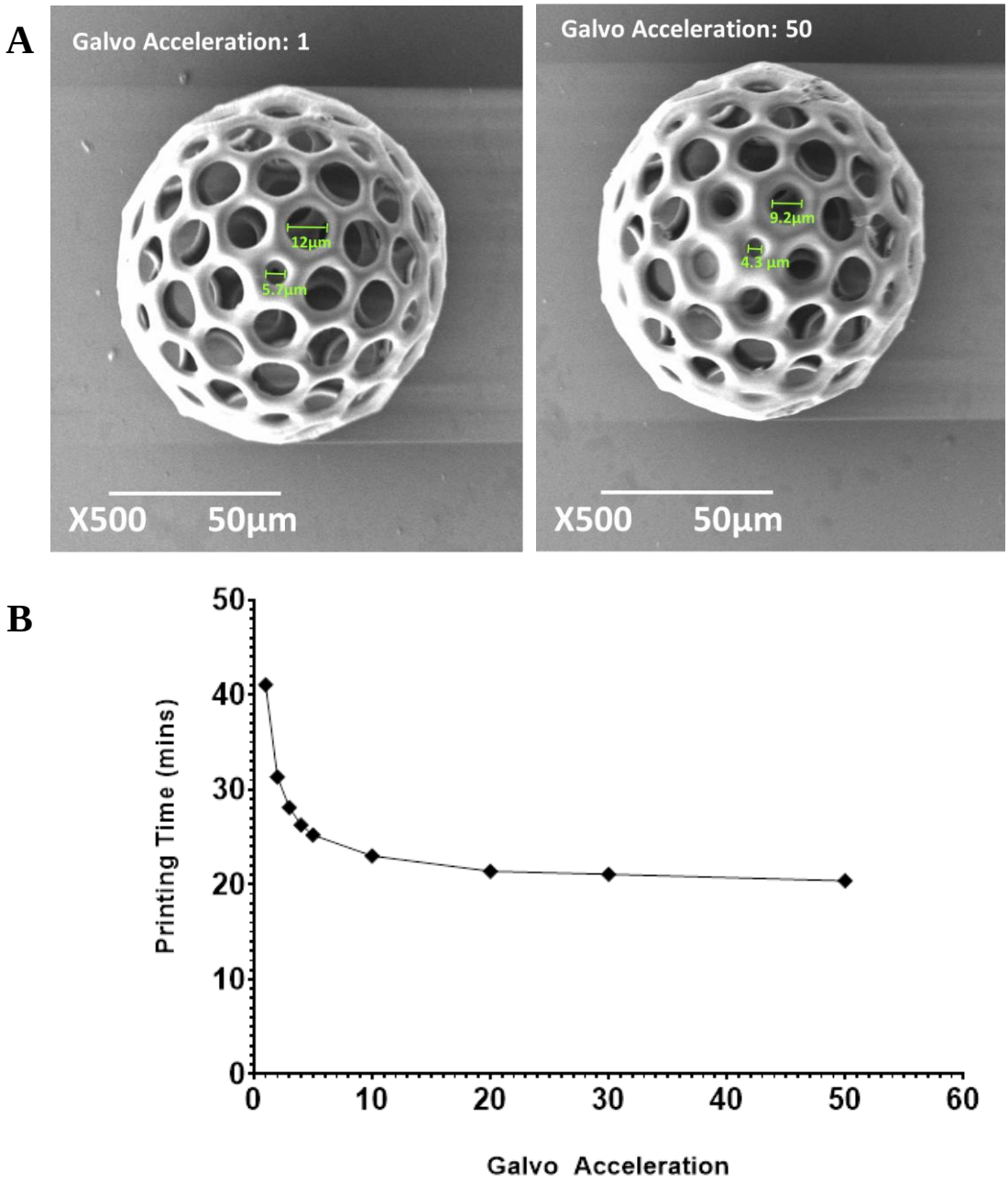


***Figure 3.6:*** *Increasing galvo acceleration decreases printing time at the cost of feature accuracy marked by a decrease in pore size by approximately 24%. (A) SEM images of c180 bucky ball structures fabricated at low galvo acceleration in comparsion to high acceleration showing overall decreased feature accuracy marked by pore size measurements annotated. (B) Graphical representation of printing time of bucky ball structures under the exact same conditions varying only galvo acceleration indicating a decrease in time with increase in acceleration.*

### 3.4.4 Fabrication errors

**Close proximity collapse**

An unusual issue appeared when trying to fabricate structures within close proximity to each other, nearby structures seemed to exhibit a regional collapse in the area facing a previously fabricated structure as seen in figure 3.7. To explore this phenomenon a series of experiments were conducted including individual structure writing vs those where the 3d model included several structures at once. This meant neighbouring structures were fabricated layer by layer across multiple particles rather than one complete particle at a time but interestingly this had no effect. This regional effect did not occur in smaller structures and still happened when internal supports were added to prevent collapse as seen in figure 3.7B. In figure 3.7C structures were fabricated one by one starting in the top left before dropping down to the next row and restarting again at the left structure. The pattern of collapse and warping is indicative of fabrication order showing how the first row had little warping either side and subsequent structures had warping in the direction facing a previously fabricated row. This issue was ultimately corrected through fine tuning of laser exposure parameters to prevent overexposure at adjacent areas in close proximity.

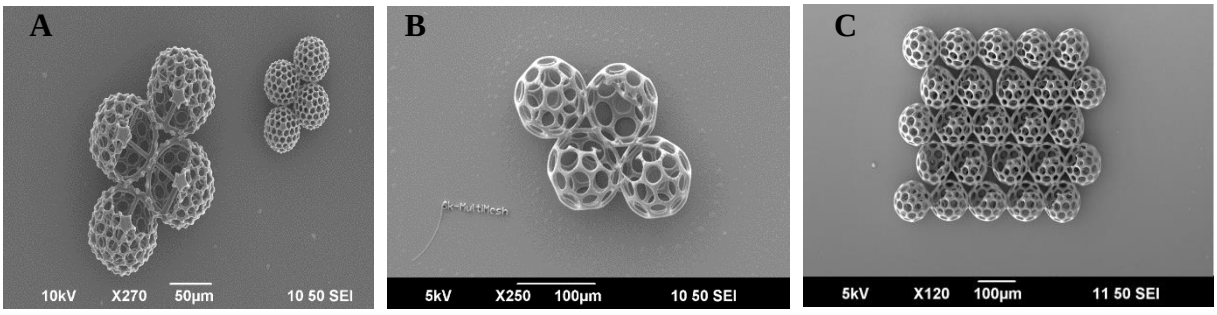


***Figure 3.7:*** *SEM images of close proximity related merging at adjacent edges. (A) initial collapsing of structures in close proximity at sections facing each other. (B) structure collapse only appears at larger structures and occurs even with internal support scaffolding. (C) lesser degree warping in a larger array of structures showing warping primarily in right bottom corners.*

**Successful fabrication**

Many issues with improper fabrication were caused by working at rapid speeds and accelerations or by using excessive power to increase line width for the purpose of achieving higher slicing and hatching distances. Fine tuning included increasing settling time before movements continued allowing rapid production of structures at high slicing and hatching with maintenance of small feature sizes as seen in figure 3.8. Initial testing and optimisations were established with woodpile and buckyball shapes. Successful fabrication was shown in figure 3.8A of a buckyball with individual discernible line widths as shown in the callout SEM at higher magnification of x15,000. Further structures of C180 buckyball hemispheres at diameters of 50, 100, 150 and 200 µm were successful and images were taken shown in figure 3.8B under maximum speed settings. Buckyball variations were also successfully printed with decreasing pore size and strut thickness as test of fabrication precision upon which fabrication was successful at all levels of complexity as shown in figure 3.8C.

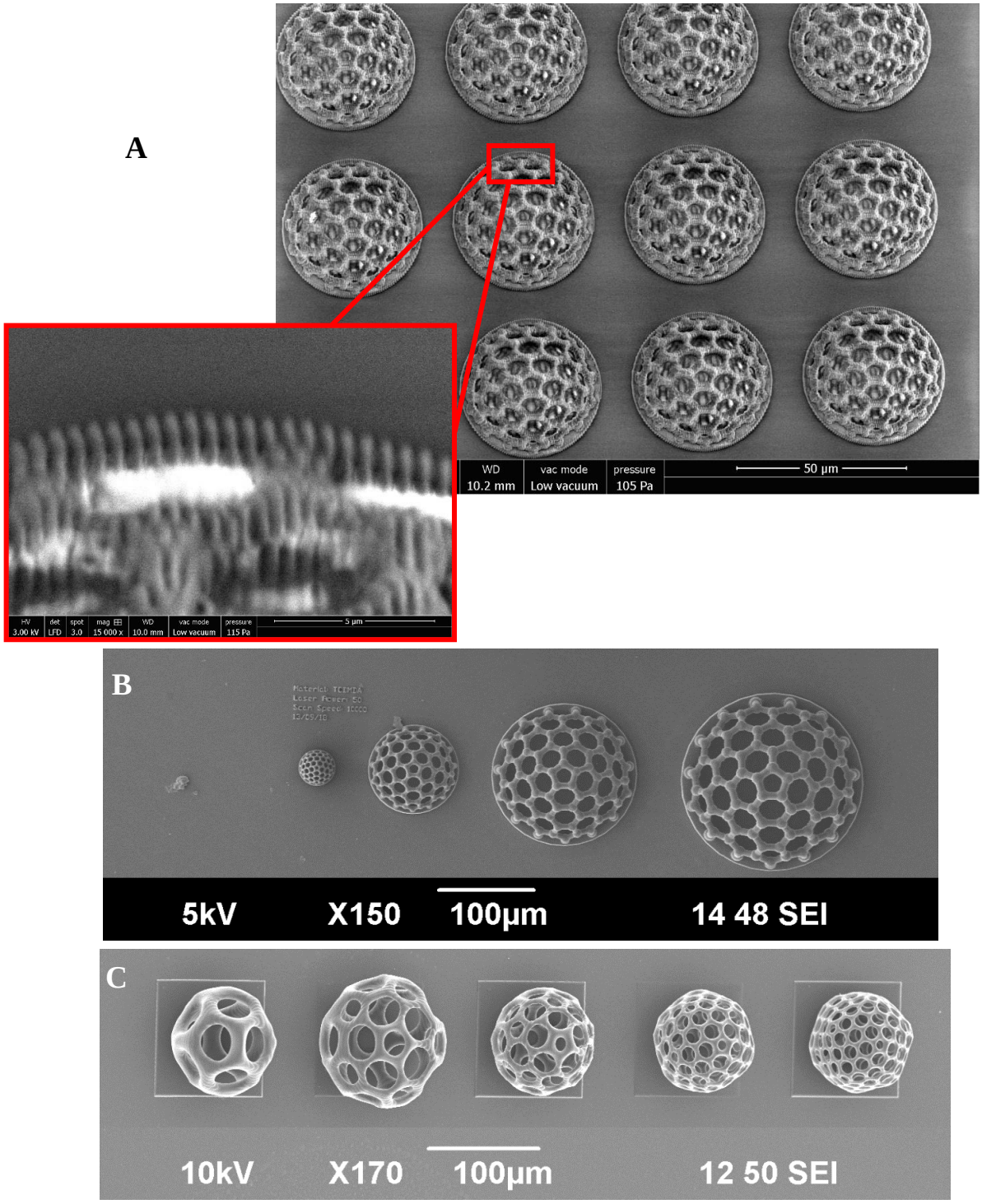


***Figure 3.8:*** *Successful fabrication of a range of buckyball sizes and porosities.* *SEM images depict (A) 50µm diameter buckyball with conservative fabrication settings to attain optimal fabrication and line width as depicted by the enhanced SEM callout indicating individual hatching lines (B) c180 buckyball domes at diameters of 50 µm, 100 µm, 150 µm and 200 µm. (C) Range of buckyball structures from C20 -C240 in which C number denotes the increase in number of pores and decrease in pore size. C numbers are derived from buckminsterfullerene nomenclature in which C refers to the number of carbon atoms.*

**Multi-layered structure designs**

Attempts to produce further 3D environments by simulating a packed scaffold or layers of dense microcarrier particles. 3D models with two layers of particles were attempted but overall particle size had to be slightly scaled down to fit within the possible writing range as shown in figure 3.9

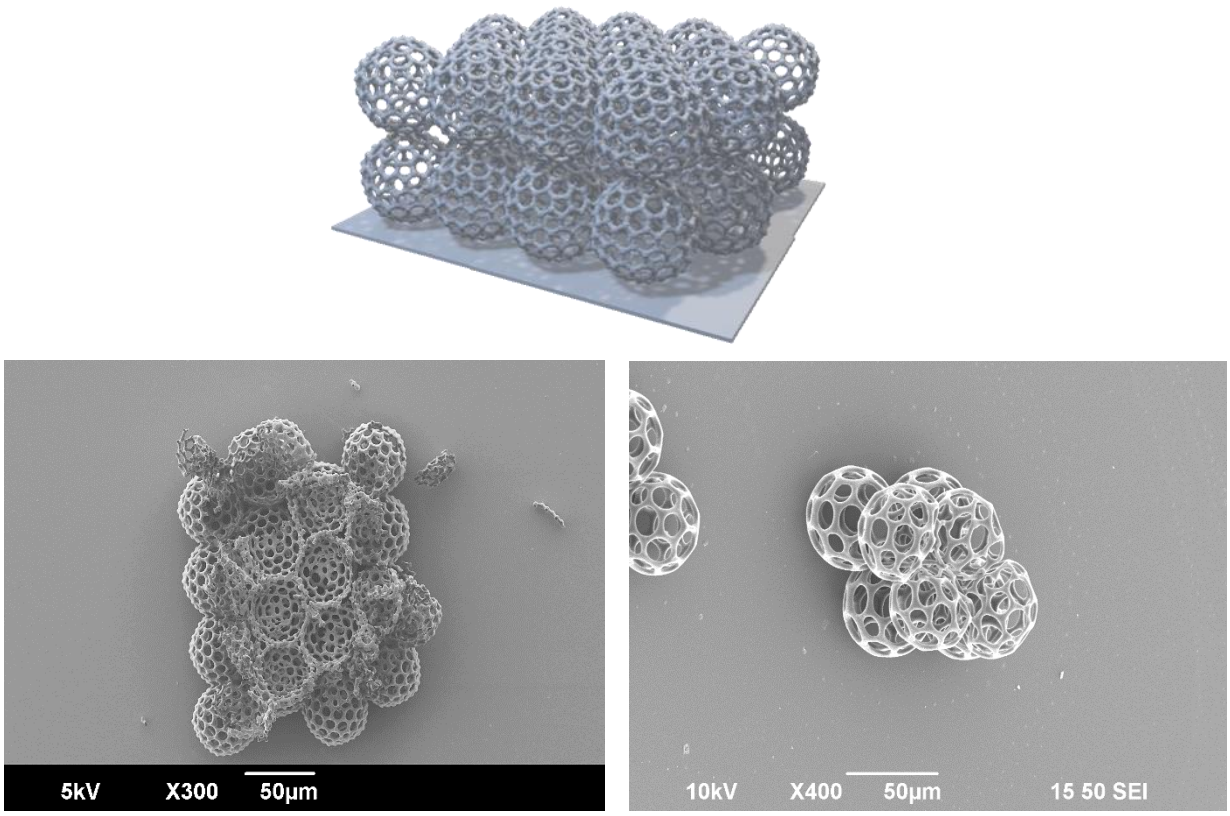


***Figure 3.9:*** *Multi-layered buckyball structure design and attempts. 3D model of 2-layer particle design with SEM of failed fabrications upon 2nd layer production, secondary smaller attempts with less particles showed better success but still could not be fabricated.*

2-layer particle structures could not be accurately fabricated. Structures of this type did not suit the microcarrier technique nor would aid in structure release and would make cell monitoring and visualisation more difficult and so were not continued forward for experimentation beyond fabrication alone.

### 3.4.5 Optimisation results

Total culmination of different explored and optimised fabrication settings were collected into a series of writing profiles, shown in table 3.3 with different levels of speed and resolution.

| Profile | LP:SS level | Slicing distance (µm) | Hatching distance (µm) | Galvanometer acceleration |
|---|---|---|---|---|
| Piezo | optimal | 0.1 | 0.1 | N/A |
| High resolution | optimal | 0.1 | 0.1 | 2 |
| Mid resolution | high | 1 | 0.8 | 40 |
| Low resolution | max | 2 | 2 | 50 |
| Extreme low resolution | max | 3 | 3 | 50 |

***Table 3.3:*** *Generic writing parameters for 2PP fabrication profiles not inclusive of shape complexity or material needs, designed for use with PETA.*

Laser Power: Scanning Speed (LP:SS) level is reflective of what level of power is used within the working range at the highest working speed possible which is important for line width and layer overlap properties. In this case optimal LP:SS represents an energy dosage equally between the minimum threshold and maximum threshold in the middle of the operating window. Max LP:SS represents a high energy dosage a few mW before burning occurs. High LP:SS represents a dosage around 85% of the maximum power before burning. These values are generalised to allow transition across multiple materials. This distinction is made as energy dosage effects voxel size and higher energy creates thicker lines. Piezo writing profile reflects all movement being produced via piezo stage movements at highest resolution giving an approximate writing speed of 25-300 µm/s. High resolution writing parameters reflects the "default" parameters often recommended by Nanoscribe using galvanometric scanning mode for X,Y coordinates, optimal LP:SS for discrete line width, 0.1 µm slicing and hatching distance for highest precision and very little acceleration. In comparison to piezo, galvo scan speeds are in the range of 1,000 and 20,000 µm/s. Mid resolution represents a combination of optimisations explored drastically reducing time at a minor loss of resolution with high lP:SS for thicker line widths allowing increased slicing distances of 1µm and 0.8 µm hatching coupled with increased galvo acceleration. This was the most common method used for future fabrication allowing rapid production of even intricate structures with small feature sizes. Low resolution writing profiles includes

max LP:SS increased slicing and hatching to 2 μm and maximal possible acceleration. This profile gained a moderate speed improvement upon mid resolution profiles for a much greater reduction in resolution resulting in visible quality loss. Extreme low resolution profile included a large 3 μm slicing and hatching distance with maximal acceleration representing the fastest possible fabrication times but extremely reduced resolution and structural integrity. Very few structures are possible in this mode with very little intricacy and this profile

An experiment producing and timing a singular C80 buckyball under the different writing profiles was conducted. Figure 3.10A indicates the time for fabrication under each profile which took 11 hours, 48 minutes and 52 seconds under traditional piezo mode. Switching to the high-resolution profile using galvo scan mode decreased this time drastically to 28 minutes and 15 seconds. The optimised mid resolution profile further reduced this fabrication time to as low as nine seconds. Low resolution reduced this time to 4 seconds and under extreme profiles as low as just one second. Mid resolution profile was used as the primary fabrication profile due to maintenance of overall shape with good structure quality in comparison to high resolution structures as seen in figure 3.10B. A speed increase of 188x in comparison to the high resolution profile was achieved. Low resolution profile gives a 423x increase over high resolution, but structure quality visibly suffers becoming rough and of low quality. SEM images of extreme low profiles was not possible due to difficulties with structure survival of the C80 buckyball hence why this profile is not practical for use except for very simplistic structures such as solid spheres. In comparison to traditional piezo 2PP at high resolution the maximum achieved increase that resulted in a viable structure is 10,633x increased speed but piezo method is not often used in favour of galvo scan modes and is not a fair comparison. These times are only for this shape under this polymer and will vary for other combinations and designs. Since profiles often balanced on the maximal power threshold before burning to produce thicker line widths and allow higher slicing capability even this low loss of power capability had significant effects if not accounted for via an increase in exposure.

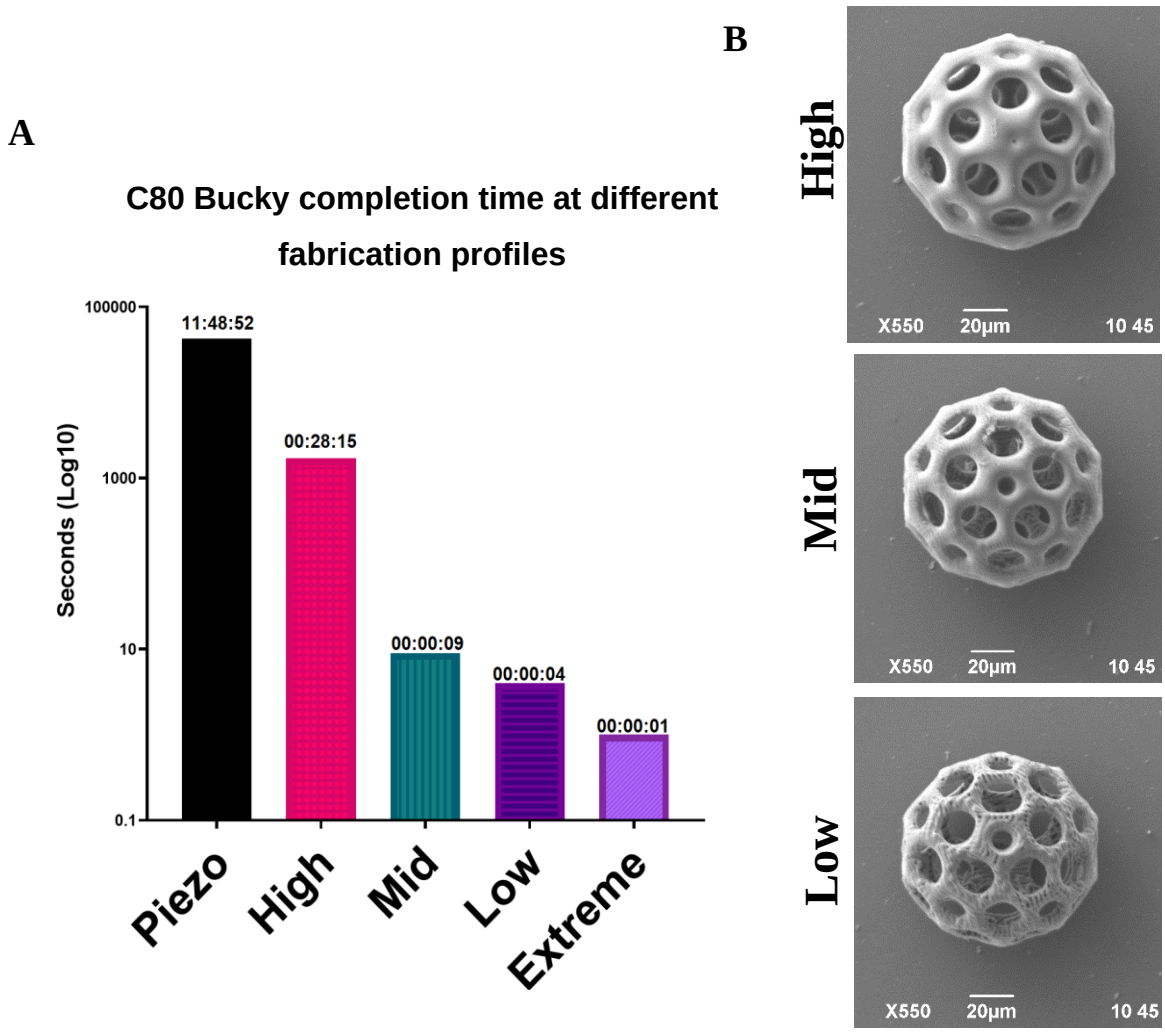


***Figure 3.10:*** *Optimisation to fabrication settings rapidly decreases fabrication times but maintains overall structure shape with minor cost to structure resolution. (A) Fabrication times of a 100 µm diameter C80 buckyball in different fabrication profiles leveraging resolution and accuracy for speed increase indicating a rapid drop from 28 minutes to 9 seconds between default unoptimized high resolution printing to optimised mid resolution printing. This is in comparison to nearly 12 hours needed by traditional piezo stage based fabrication. Further increase to speed can be achieved in low settings but structures begin to lose quality. Extreme profile write time is reduced to only one second but structures are not able to maintain layer adhesion and break apart. (B) SEM images of quality comparison between high, mid and low settings indicating a gradual loss of shape accuracy, resolution and visible hatching lines.*

### 3.4.6 Complex and experimental model production

#### Complex feature models

Structures were produced in the optimised writing profiles created to test quality of structures and benchmark capabilities. Figure 3.11A shows an Eiffel tower structure indicating capability to produce tall thin structures with small adhesion footprints and small feature sizes. 3D models of a Pikachu in figure 3.11B indicated how despite the level of precision loss, small subtle details were still present on curvature. Figure 3.11C is a benchmark structure often used in FDM 3D printing as this model contains complex features including overhangs, inclines, small features and a variety of geometries acting as an overall quality indicator. SEM's indicate faithful replication of all feature types with no issues. Figure 3.11D indicates another feature size test with a violin indicating feature levels maintained for scroll, pegs and tailpiece but individual strings or F-holes, which has submicron width, were below the possible feature size and could not be replicated by this fabrication profile. Logos for the University of Nottingham Biodiscovery institute where all cell work was conducted and for the University of Nottingham's Centre for Additive Manufacturing where all 2PP work was done were also created for public demonstration but also show level of intricacy possible. Whilst these structures acted as a measure of fabrication precision and accuracy they were also primarily used as demonstration pieces to capture attention of non-scientific audiences by recreating recognisable shapes.

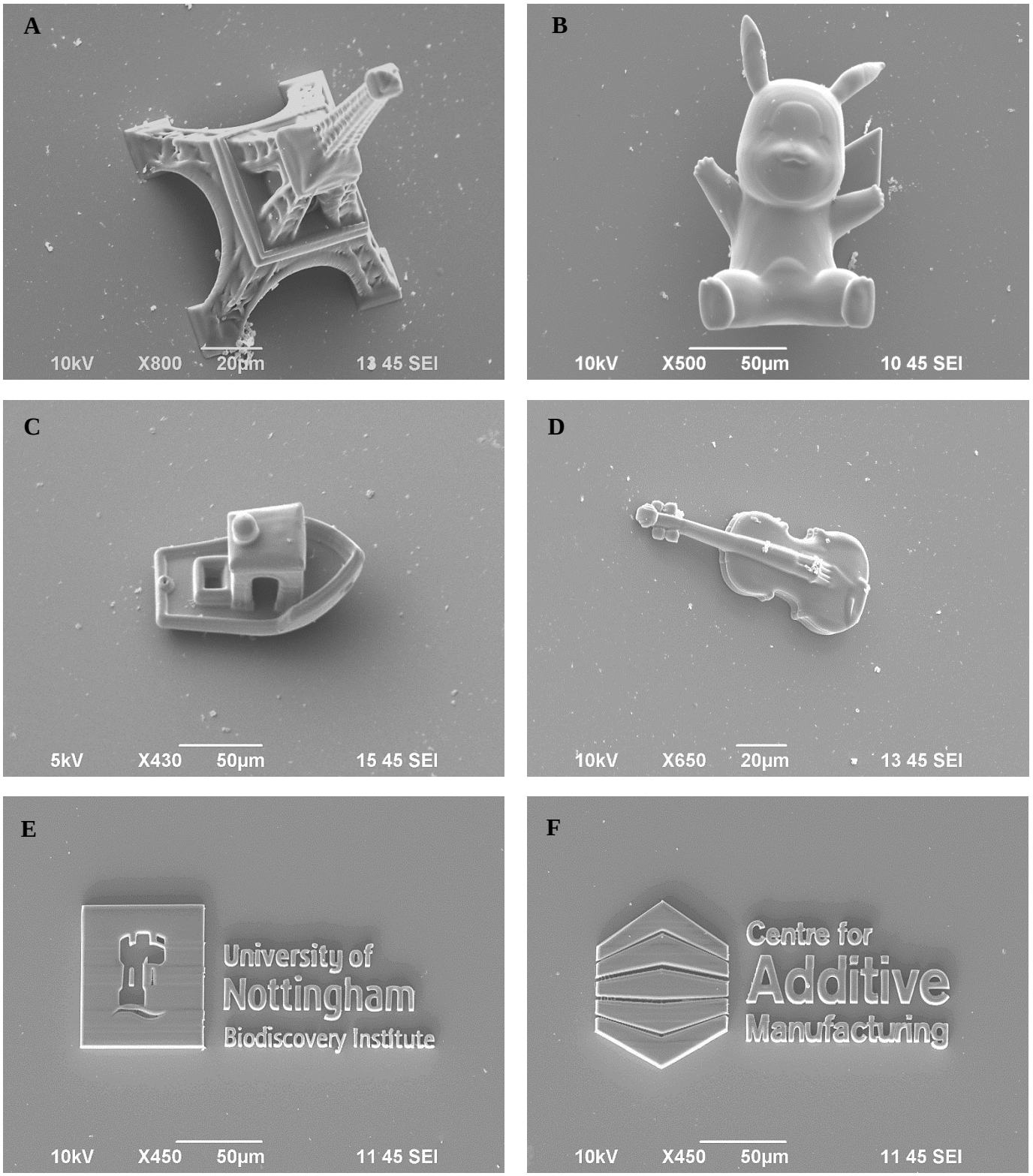


***Figure 3.11:*** *Various complex models to benchmark fabrication abilities and demonstrate capabilities of 2PP technology.* *(A) Eiffel tower structure demonstrating integrity of tall thin structures with small adhesion footprints. (B) Pikachu 3D model showing subtle. (C) Benchy tugboat testing capabilities such as overhangs. (D) fine details present on a violin model demonstrating how individual string features in model were too small to be fabricated at mid resolution profile. (E) Logo for the University of Nottingham Biodiscovery institute where all cell work was conducted. (F) Logo for the University of Nottingham's Centre for Additive Manufacturing where all 2PP work was conducted.*

**Fibre arrays**

With proper control over 2PP fabrication settings a prototype model was developed to explore whether fibre production via 2PP was possible. The advantage of this technique is that exact fibre length, thickness and distribution can be controlled to high precision with extreme reliability and reproducibility.

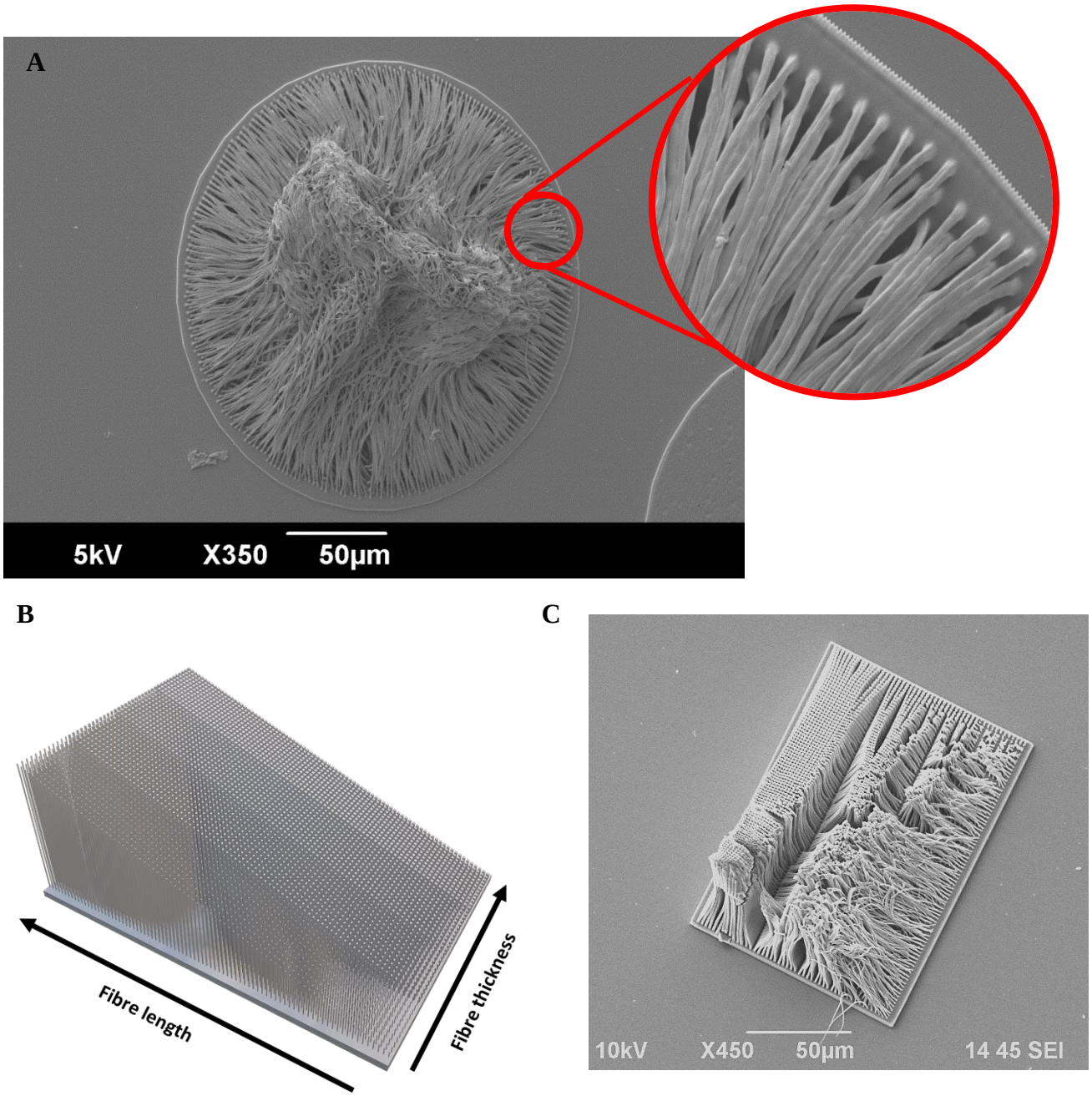


***Figure 3.12:*** *Fibre arrays demonstrating fibre production via 2PP. (A) SEM of strucutre with uniform fibre lengths and thickness of approximately 1µm all collapsed inwards. (B) 3D model of a fibre array with increasing fibre thickness in one axis and increasing fibre length in the other. (C) production of fibre array 3d model showing production is possible and that the degree of fibre flexibility is based on thickness.*

Fibres were produced in a circular uniform fashion in PETA as shown in figure 3.12A, fibre thickness was approximately 1 µm. Fibres were flexible but strong and showed no sign of snapping. Fibres collapsed due to lack of structural support and intertwined during the washing and development stage. Due to this initial finding an array was designed as seen in figure 3.12B to leverage fibre thickness against length as a fibre property screening tool. Production of this model was possible as seen in figure 3.12C but thicker fibres stood more upright and seemingly melded together requiring more spacing to prevent this. Since this model was just a proof of concept and not for continued use it was not explored further.

**Multi-material structures**

Another interesting structural possibility explored was the production of particle designs with features made from multiple different materials such as a core of one polymer chemistry and then surface features in another or multiple others. Structures were created with a 2-phase fabrication procedure where the base material and shape was fabricated and developed. Secondary polymer was added on top of previously developed structures which could then be located through the lens and manually aligned for secondary structure writing. Multiple passes of this can be done to include many polymer types not just two so complex structures with 3,4 or more different chemistries are possible. For this purpose, 3D models were designed in two phases with one base and another with floating surface features, a thin interconnected skeleton was added to the surface feature model to act as a buffer for structure misalignment, where polymer was already present the skeleton could not fabricate but where alignment was slightly off the skeleton would keep the outer structure tethered to the base. Structures produced were prototype 2-phase microcarrier designs at 100 µm diameter as seen in figure 3.13. One design featured a spherical base of TMPETA with smaller surface spheres in TCDMDA. Other structures included a spherical base in PETA with outer spikes in TMPETA and a grooved design that featured a small inner core of TCDMA and larger wedges encompassing made from PETA. False colour was added to SEM images in figure 3.13 to distinguish areas of discrete chemistry.

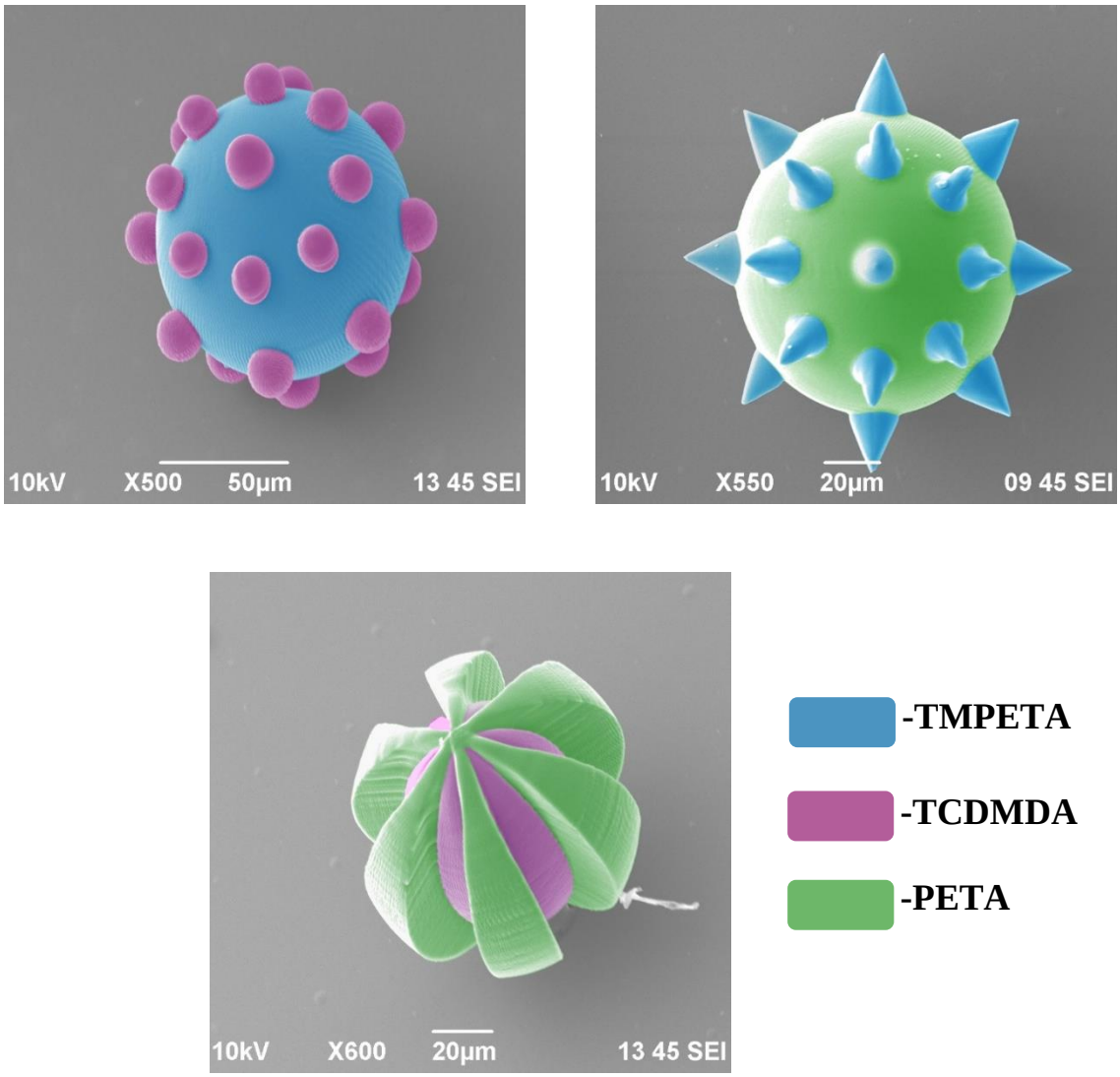


***Figure 3.13:*** *False colour SEM images of multiple materials used in particle designs. Structures produced via two stage fabrication had a base polymer and surface features in a different chemistry. Polymers represented are TMPETA in blue, TCDMDA in pink and PETA in green.*

### 3.4.7 Structure attachment

To explore surface attachment to glass substrates an experiment was conducted to test silanization methods vs their non-treated counterparts. Variations included control untreated glass, and glass coverslips silanized via two methods referred to as acetone and toluene. Acetone treatments involved silanization with silane A174 dissolved in acetone and soaked with plasma cleaned coverslips as detailed in and toluene refers to

the more thorough and chemically defined method of silanization also detailed in section 3.3.9. The premise of the experiment was to fabricate structures and see how many were recovered after development and then how many were dislodged by the physical forces of cell growth after five days. An array of 100 µm PETA buckyballs with large footprints was created to represent the type of jobs typically used and an array of small thin but long pillars, in PETA, with tiny attachment cross sections to maximise fragility and potential displacement to examine relationship. Untreated surfaces exhibited 10.6% particle retention post development and 2.7% after cell culture, acetone showed 99.6% particle retention before cell culture and 99% after showing the highest degree of attachment to surface. Toluene based treatments showed 97.8% retention post development and 75.5% after culture as shown in figure 3.14A. For pillar experiments 94.6% retention post development in untreated samples was seen but only 1% retention in cell culture where all structures were displaced by cell growth and bound in cell conglomerations. As figure 3.14B indicates acetone based treatments showed a 99% attachment pre culture and 97.6% after. Toluene showed a 99% retention post development but 24% retention after cell culture where once again most pillars were detached and grown over. Data indicates acetone conditions maintain structural attachment better than the toluene method despite being quicker, easier, and less chemically robust. However, what was noted in longer term culture is that acetone methods showed a gradual loss of adhesion over long culture periods whereas toluene methods maintained retention levels throughout.

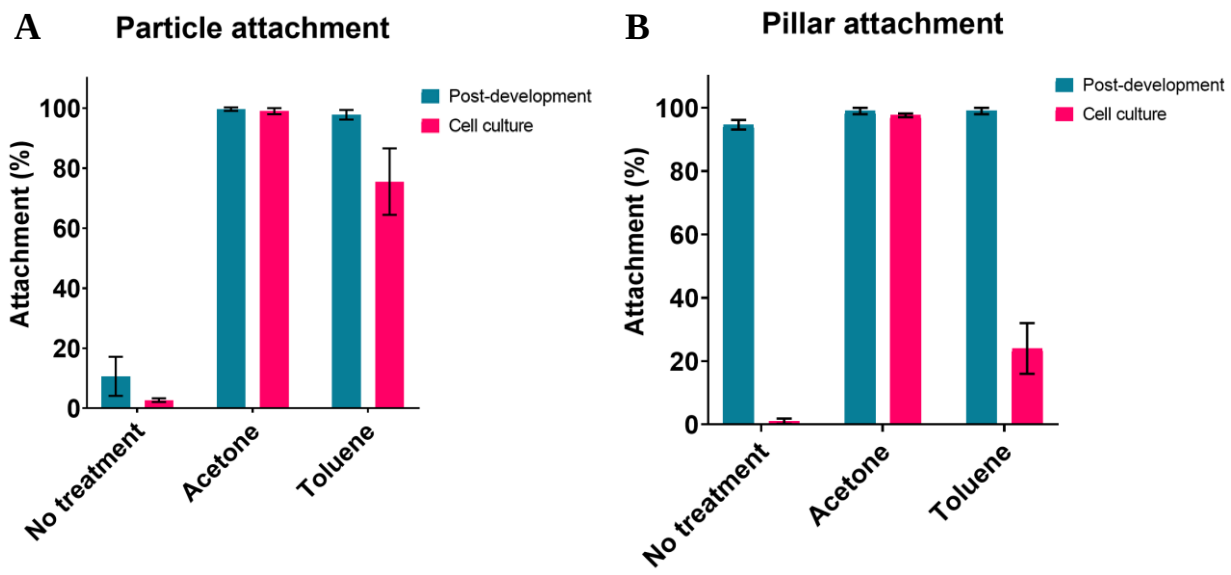


***Figure 3.14**: PETA Structure retention after development and 5-day cell culture for different silanization methodologies.* *Mean ± SD. (A) 10.6% of particles remained after development in untreated surfaces, reducing to 2.7% after cell culture. 99.6% of structures were retained and 99% post culture for acetone silanization. Toluene had 97.8% retention following development and 75.5% after cell culture. (B) for pillars, 94.6% remained following development but only 1% survival following culture on untreated surfaces. Acetone conditions gave best results with 99% retention before culture and 97.6% post culture. Toluene showed 99% attachment after development but 24% retention post culture. (n=3).*

### 3.4.8 pHEMA coating

A novel technique of fabrication upon a pHEMA coated slip was established to isolate cell activity to structures and act as a releasing agent. Release of fabricated structures from the pHEMA surface can be achieved by dissolving the coating in ethanol. This methodology led to a loss of automatic interface finding due to refractive index mismatch. A simple method to counteract this was developed to provide greater functionality and automation as shown in the schematic in figure 3.15. At the exact centre of each coated coverslip, using a 3D printed grid to hold coverslips and provide guidance, a tiny portion of the pHEMA coating could be carefully removed via scalpel or masked prior to treatment. This leaves a zone at the centre with no coating and only the typical glass monomer interface which can be automatically detected and acted as an interface calibration area for initialising a job. Movement out of this zone with removal of interface finding steps via changes to programming code meant the structure would be written continually at this previously calibrated interface. With optimisation the pHEMA coating is thin and uniform but writing at the glass interface would not account for coating thickness and would lead to the laser trying to fabricate within the space of the pHEMA resulting in structures with a cut off lower architecture. To combat this small anchoring pegs were added to the bottom of models to raise main geometry above this level, this ensured the full structure was written and since fabrication started far lower than the real polymer interface it guaranteed surface adhesion as seen in figure 3.15B. These pegs were thin and, at optimised writing parameters, lead to very little extra fabrication time. Although interface offset could be added to raise above coating level these pegs also work as a buffer for coating thickness variation across the surface maintaining adherence. This coating technique could be applied to any other coating that allows laser passage without interference.

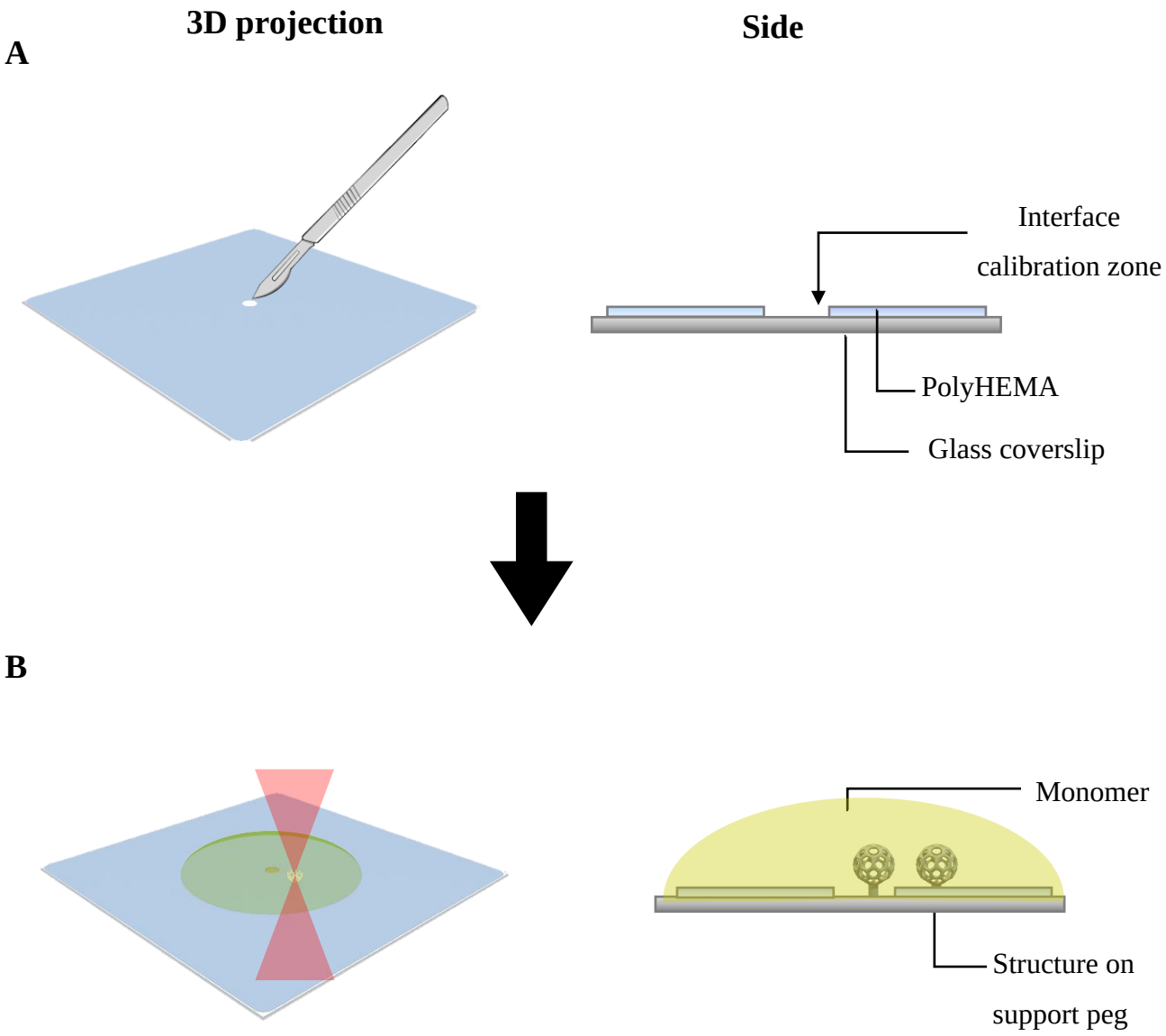


***Figure 3.15:*** *Schematical representation of methodology employed to fabricate upon polyHEMA coated substrates when interface finding isn't possible.(A) A small area at the center of the coverslip is scraped with a scalpel to remove coating and expose underlying glass which acts as a calibration zone where the glass-polymer interface can be found succesfully. (B) polymer is added and moving away from the glass zone structures can be fabricated on HEMA layer using a support peg to equate the distance for the thickness of the HEMA layer.*

Calibration to individual coverslip thickness variations could be accomplished by manually probing interface position across the surface to find what overall variation in interface and therefore coating thickness was across the writeable zone. This was done for coverslips of different pHEMA dosages and thicknesses to optimise amount of HEMA present against amount of inherent thickness variation as seen in figure 3.16. Surface profiling base on interface measurements at different points indicate the

variance of thickness across the surface. Results indicate the importance of proper manufacture on level surfaces, or the thickness profile slopes as depicted in figure 3.16A lead to substantial corrections needed to account for drift.

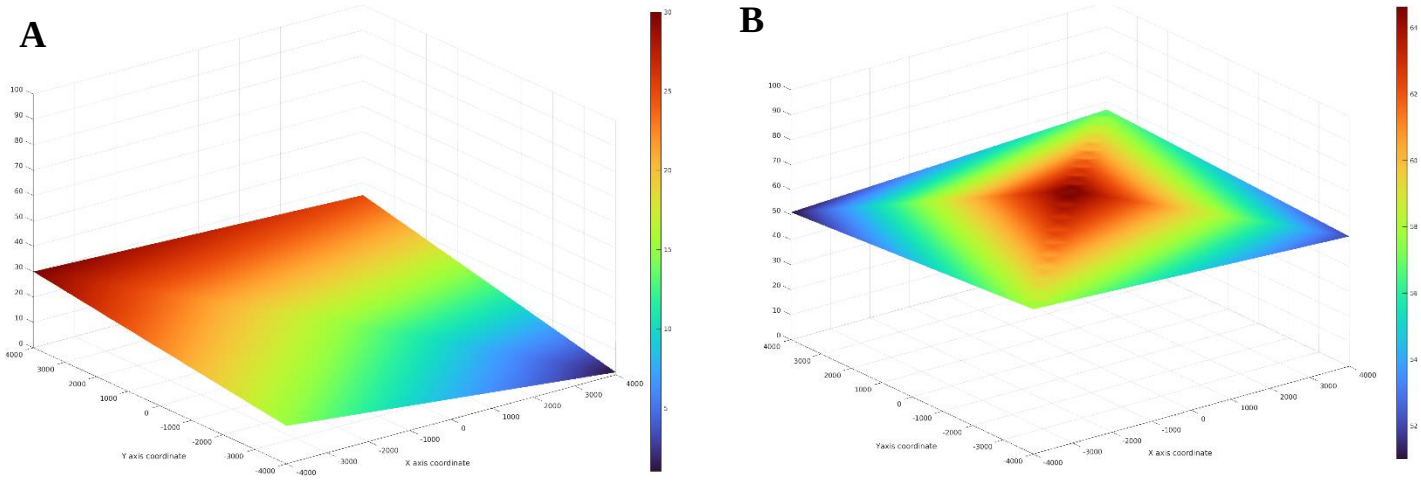


***Figure 3.16:*** *Surface thickness profiles of polyHEMA coated slips.* *(A) shows a large slope in coating due to improper production (B) typical surface profile achieved with 20mg coating showing an approximate 10µm variance across the surface with highest points at the centre.*

Different coating thicknesses were tested including 5mg, 10mg, 20mg, 40mg and 60 mg. 20mg coatings, depicted in figure 3.16B, were selected as they gave a layer thickness that was suitable in visibility, durability and cell adherence and produced a thickness with a small degree of variation. Other dosages lead to a greater thickness variation across the surface and greater swelling with no better adherence behaviour. Figure 3.17 shows structures created upon coated slips showing no issues in production associated with the coating or aberration of laser travel paths.

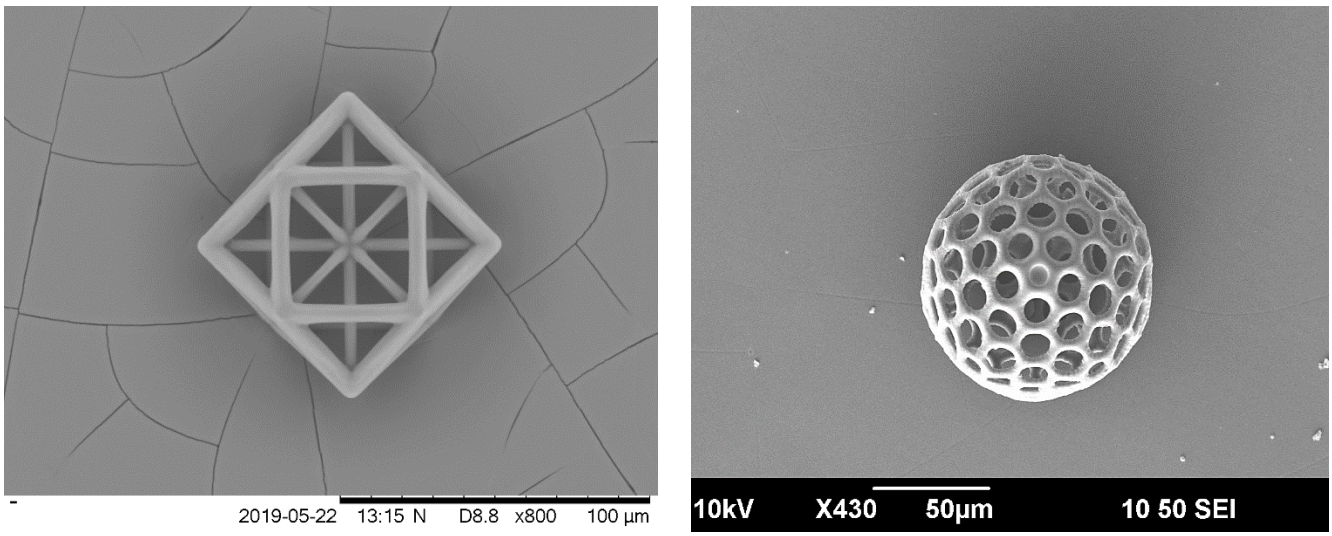


***Figure 3.17:*** *SEM images of structures fabricated on pHEMA coated coverslips successfully with no aberrations to structure shape or properties. (left image courtesy of Dr. Robert Owen)*

WCA measurements were taken to show the fundamental changes of the surface over time and quantify the presence and maintenance of this pHEMA layer. Measurements of WCA on this layer was conducted over 15 days in culture media to determine if layer properties would degrade or change over time.

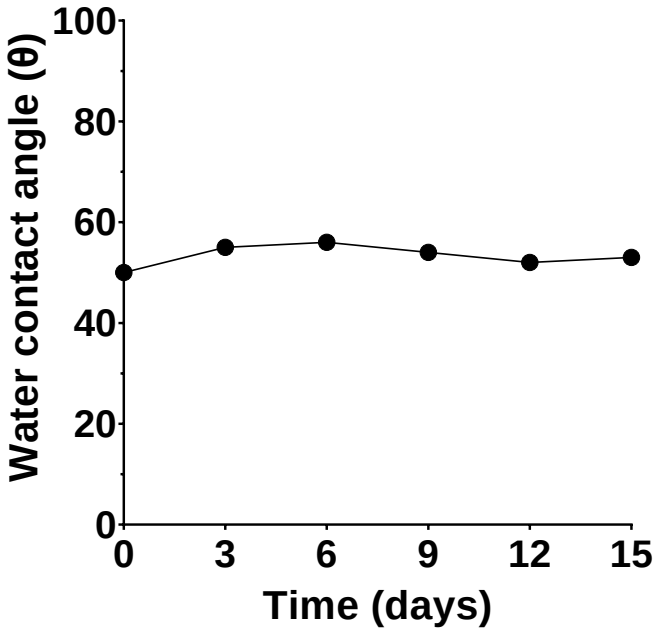


***Figure 3.18:*** *Water contact angle measurements of polyHEMA coating over 15 days in culture media showing maintenance of surface properties.*

WCA results depicted in figure 3.18 indicated an average value of 53 over the course of the experiment with a range of 6. Results indicated that surface properties or wetting behaviour is maintained over the course of the experiment.

### 3.4.9 Structure release

Structure release for free floating microcarrier culture was explored through various structure liberation methods outlined in figure 3.19. An experiment was designed to quantify the recovery rate of structures and the damage rate of structures for comparison of techniques as shown in figure 3.20. Structures were written on samples and released by the three different methods, imaging of structures was taken to quantify structure damage and quantify number of structures recovered from the fabrication surface. Percentage recovery, number of intact particles released from fabrication surface into solution, was measured via counting particles under a microscope knowing how many structures were initially written per sample.

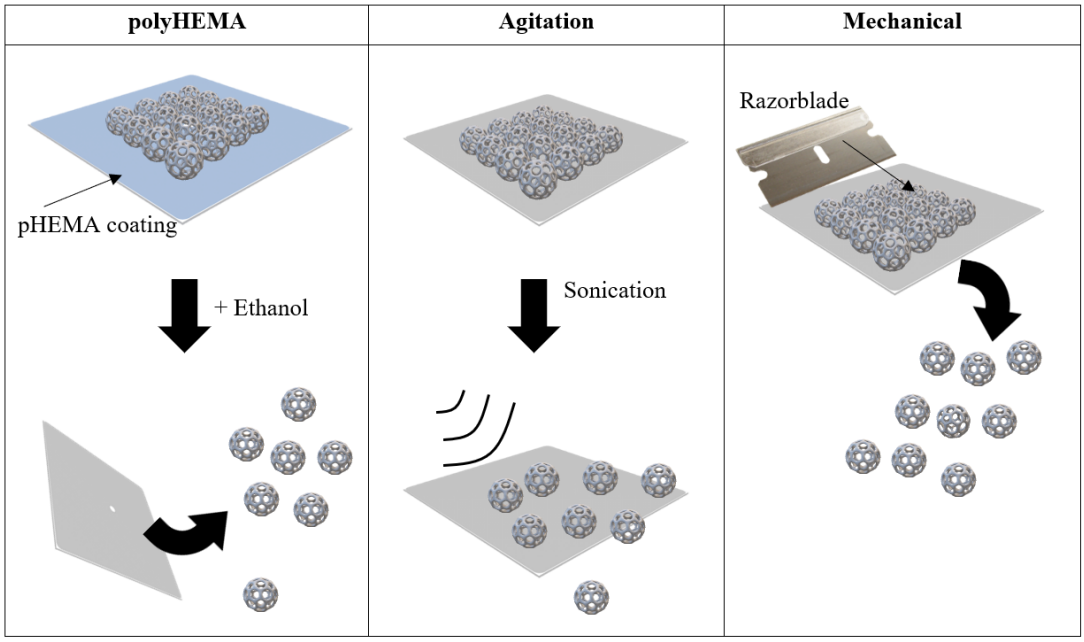


***Figure 3.19:*** *Methods of 2PP structure detachment. PolyHEMA strategies utilised ethanol to dissolve the intermediate surface coating of polyHEMA, visualised as a blue coating, that is between the glass substrate and 2PP structures thus releasing structures with no physical disruption. Agitation methods used structures written on non-silanised glass substrates and sonication or vibration over an hour to disrupt surface attachment. Mechanical disruption involved using a razorblades to scrape the glass substrate surface and physical disrupt adhesion of the structures.*

Particles mechanically dislodged had an 81.7% recovery rate but 53% of these were damaged or completely broken, this equates to an effective intact recovery of only 38.3% of fabricated structures. Particles disrupted by agitation had a 43% recovery rate as not all structures could be released by this method with 11.3% damaged and an effective intact recovery of 38.1% of fabricated structures. 98.3% of written structures were recovered under pHEMA release conditions and only 3% of those structures had physical damage equating to an effective intact recovery of 95.3%. pHEMA release was the best, easiest and most reliable structure release technique. Released structures of multiple designs via pHEMA method is pictured in figure 3.21.

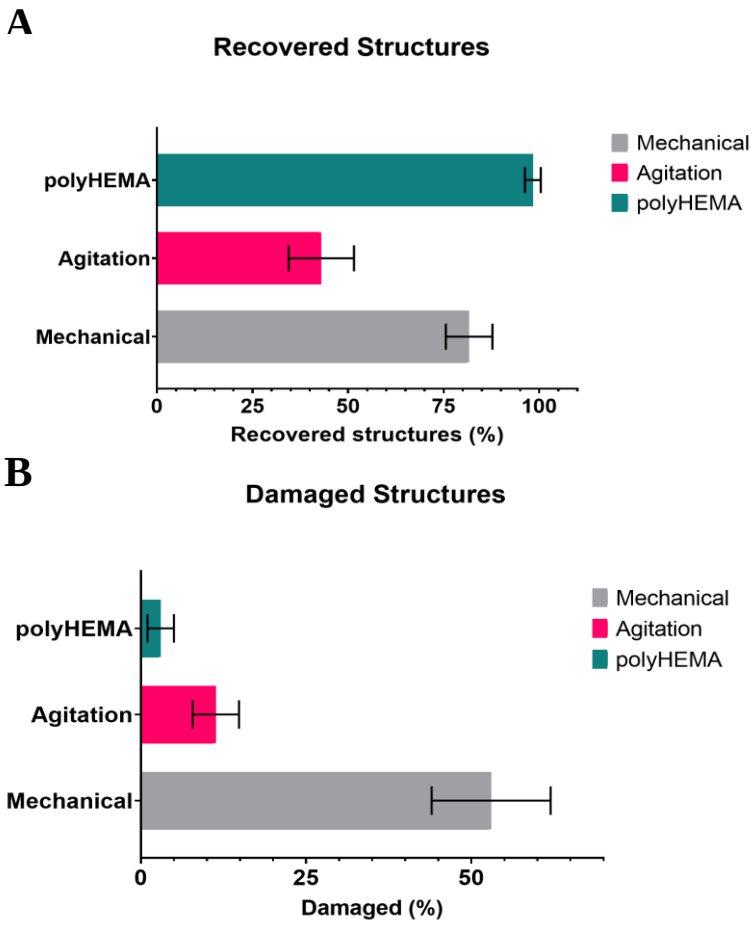


***Figure 3.20:*** *Recovery and damage to particles released by different methods Mean ± SD. (A) Percentage of structures recovered, highest recovery rates for polyHEMA and lowest for agitation based methods. (B) percentage of recovered structures that exhibited physical damaged indicating lowest damage in polyHEMA structures and highest in mechanical disruption. (n=3).*

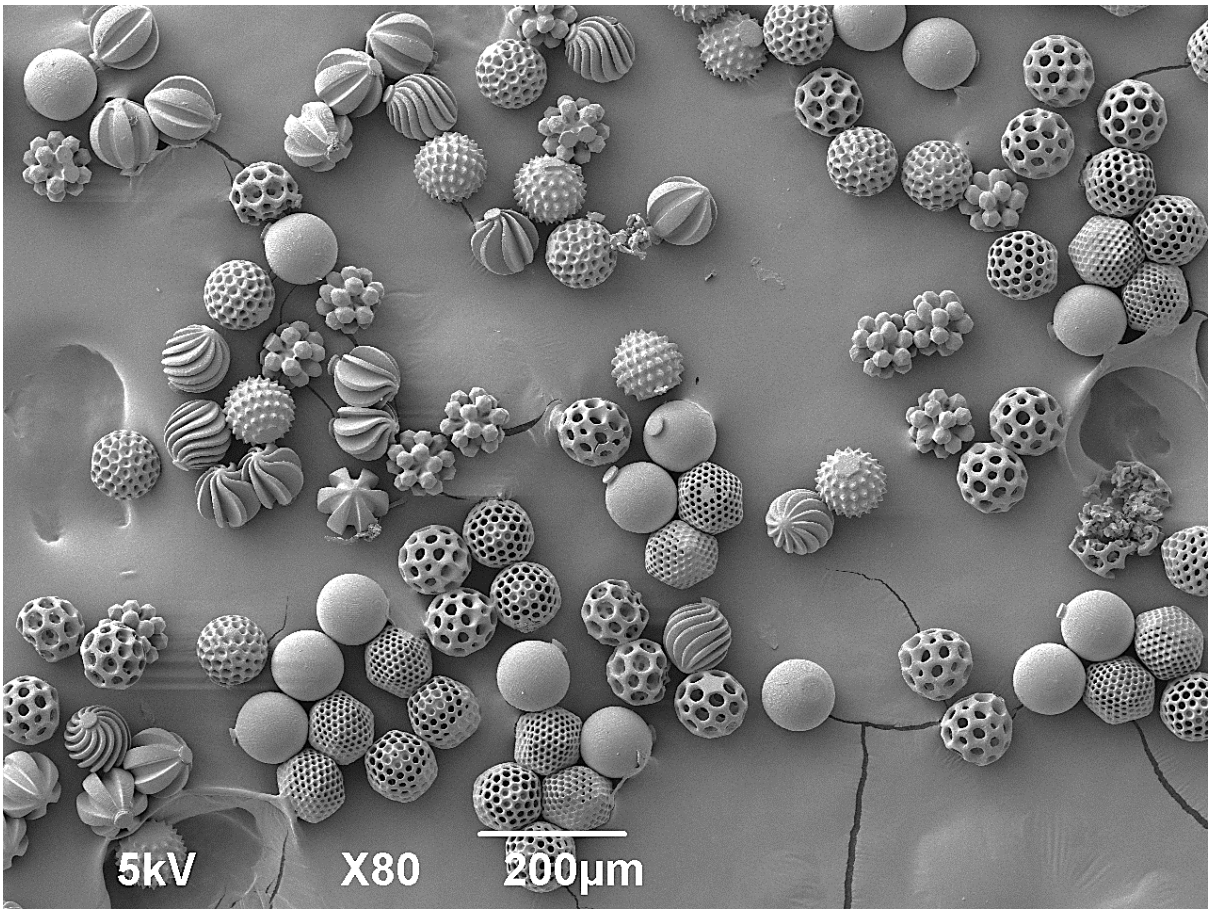


***Figure 3.21:*** *SEM of microcarriers of different architectural designs released via pHEMA method.*

## 3.5 Discussion

Often one of the most important aspects of biocompatibility is the PI used due to its reactive chemistry which can often be problematic for biological uses. Irgacure 369 was the only PI used due to common use in the literature, suitability across all polymers and reduced chemical variation across materials that could obscure results of architectural variation between replicates. Irgacure 369 has common use in 2PP for biological applications with no noted toxicity, but it has been argued that biocompatibility is not certain and other PI's may be more fitting (335, 336). Overall, these materials were taken forward for initial testing and all polymers were shown to be capable of 2PP at the high speeds necessary. Blending of polymers to vary material properties was explored, one example was co-polymers involving PEGDA with PETA that were trialled to imbue better wetting behaviours and biodegradability whilst retaining structural integrity in a similar way to Sun *et al* (318). Similarly non-suitable materials such as HEMA or DMAEMA were mixed into copolymer blends to imbue their specific qualities to a functional polymer, often severely limiting fabrication possibility due to incompatibility or radical quenching (337). Alumina chromatography to remove MEHQ inhibitor did not aid in increasing suitability (data not shown). Not all materials described were fully explored or utilised in final microcarrier designs due to focus upon mechanobiological aspects over polymer chemistry influence but were demonstrated possible as methodology to further tune structure properties.

Woodpile sweeps for assessment of fabrication suitability is a commonly practiced technique in additive manufacturing and 2PP. Although for 2PP any structure can be used as a reference for parameter sweeps, woodpiles are a structure that display thin overhanging features that upon warping or collapse form further collapse of supported layers making misfabrication very visible. Formation of thin lines are also useful in determining and visualising line width which is a property of voxel size and allow determination of resolution capabilities within the functional exposure range and not just simply a binary fabrication success or failure system. The classification of structures figure 3.3 are used to help quantify and visualise fabrication success but intermediate class two structures can exhibit degrees of success and are allocated based on authors interpretation as to amount of warping. Precise confirmation and standardisation could be achieved by geometric deviation modelling through statistical

shape analysis for consistent interpretations with mathematical degrees of deviation and possible automation (338).

Subsequent heatmaps generated from woodpile sweeps indicated the overall trends in polymerisation thresholds by identifying all working exposure levels. Variation in flexibility between polymers was wider than expected. Whilst this data presented all suitable power and speed combinations the only area of interest is in the most efficient writing parameters. The screening process could be made quicker by limiting tested parameters to only those above a threshold speed given that hits that require slow laser travels would be disregarded anyway. PETA, as previously noted, is a popular choice of material and is described as having wide ranging processability and fast reaction kinetics, although specific writing parameters are often not detailed. However, sweeps for this polymer determined a relatively small window of exposure in comparison to other materials, comparison with results determined in a similar system with the same PI matched observed values (319, 339). Interestingly PETRA has wider fabrication range than PETA despite similarity. PETRA is highly viscous and paste-like, as opposed to liquid PETA, requiring less energy to polymerise. This lower polymerisation threshold is attributed to the viscosity preventing radical diffusion away from the voxel and simultaneous prevention of oxygen diffusion into the polymer to scavenge radicals. This results in a lower energy requirement for polymerisation and a confined and subsequently larger voxel size. Despite larger line width less burning from overexposure occurs due to the confinement of energy preventing overspill and crossover of energy between lines (340). TMPETA and PEGDA showed extreme versatility allowing polymerisation at low exposure rates and a wide exposure range before burning. Power levels were increased in 5mw increments and so more precise determination of exposure levels could be attained through smaller power increments at the cost of increased fabrication time. Additionally, structures were written at high resolution with closer travels which increases exposure, as such differences in structure or resolution would shift these values.

Structures fabricated under identified settings showed structural errors when slicing distance or hatching was changed to account for model complexity and feature size. For complex designs with small intricate feature size low slicing values are needed to accurately recreate that geometry. In simple structures, such as whole spheres, much

higher slicing distances can be used without loss of features. At larger slicing distances less slices are needed increasing speed but reducing shape resolution along with total exposure amount since regions of exposure and laser travel paths are further apart. Larger hatching distances increase speed since less travels are made but comes at the cost of resolution and structural strength loss (341). Results of section 4.4.2 indicated optimum working ranges for exposure levels for a range of polymers but slicing and hatching distances reduce exposure changing the range of writing parameters that can be used. This means that structures written under 50mW laser powers and 10000µm/s speeds in PETA, which would usually burn, are tolerable at higher slicing distances. An optimal range of speed increase to resolution loss was identified at which significant speed increase can be achieved, due to its exponential relationship, with an acceptable loss of resolution. A reduction from 0.1 µm slicing and hatching to 0.4 µm results in a 14.5x speed increase whilst still maintaining sub-micron resolution. However, increased slicing can induce a nanotopography or surface roughness through layer lines (342). Li *et al* demonstrated that 200 nm features were enough to influence stem cell differentiation (343), although this feature could be deliberately induced to control cell outcomes.

Galvanometer acceleration is a fabrication variable that is often overlooked in the optimisation step. This factor is the measure of how quickly galvanometric mirrors pivot to produce X,Y laser travels. Increasing acceleration leads to faster travels at the cost of accuracy as movement precision and accuracy is hindered because of inertia. By increasing this factor to the maximum value of 50 $ms^2$ a faster fabrication speed could be achieved, realising a 44% reduction in fabrication time. This increased speed is separate to advances made through reducing slicing distance and can stack together. However, loss of laser travel accuracy does lead to a notable reduction in pore size of 24% which could limit cellular interaction. In highly intricate structures with smaller feature sizes this could lead to an inability to accurately recreate 3D model features. The speed amplification given by increasing this parameter will also be variable based on structure geometry and will depend on the prevalence of curvature vs straight lines. For the purposes of this experiment acceleration is reduced to 80% of the maximum value in mid resolution profiles to bring changes in pore size to a level that could be accounted for in the model and would not affect overall outcome. In this case increased

fabrication speed is more important than strict microscale adherence to structural accuracy.

Initial testing was performed with individual structures with large distances between replicates for the purpose of imaging. However, when combining multiple structures close to each other for arrays regional collapse at upper z limits in areas adjacent to another structure occurred. This did not happen in smaller structures and when structures were spaced apart. The reason for this is believed to be due to a combination of two issues, aberrational distortion caused by neighbouring structures particularly in the axial direction due to minor broadening of the focal spot (344). The second issue may be due to the aggressive power profiles used to achieve high speeds and slicing coupled with fast and inaccurate travels. This leads to a higher diffusion of radicals in the surrounding area so that when multiple structure passes are made within the same proximity the exposure levels in adjacent structures are too high leading to structural damage. This would explain why structures in figure 3.7C only show collapse in a direction facing a previously written structure. The broadening of focal spot due to aberrations across the z-axis explain why this only occurs in larger structures. This was remedied by increasing the settling time and reducing power slightly for closely knit structures. Once all optimisations were explored and fabrication anomalies resolved, structures of all complexities necessary could be produced at high speeds and accelerations without fabrication errors such as collapsing, skinning, or warping. Power profile adjustment within the identified working range allowed production of structures with discernible line widths when using lower power ranges.

Multi-layered scaffolds were attempted to be fabricated for two reasons. Firstly, to help entrap more cells and get a higher number of cells within the structure than those growing as a monolayer in the surrounding area, this would aid in measuring outcomes of assays. Secondly this model was a more accurate representation of a 3D environment, mimicking a packed microparticle scaffold or dense amount of microcarriers with interactions between particles not just limited to lateral dimension. However, focus is still achieved through an objective lens with a high NA and as such is subject to their limitations. The working distance of the type of objective used in this system is limited to around 180 µm, after this point the focus of the laser cannot be guaranteed and begins to dissipate losing power and resolution leading to 2PP

disruption (291, 345). This dissipation is seen in structures in figure 4.9 which coupled with aberrational distortions and scattering caused through passing through previous layers leads to structural misfabrication and collapse on the upper layer. To achieve successful fabrication within the working range the particle size would require reduction to a level at which cellular infiltration may become difficult. In conventional oil immersion mode the loss of power and resolution based on refractive index matching and objective working distance gives severe limitation in structure size over the Z-axis. However, the Nanoscribe invented DiLL working mode, which involved direct lens interaction with monomer as the immersion medium allows an inverted substrate-down fabrication approach. This method means the working distance is never exceeded and is limited only to the stage travel space; it also eliminates the necessity for exact refractive index match (346). Despite the advantages to be gained from this method it presents a technical concern given the length of jobs processed for this work and the materials used. Photosensitive materials would be in direct contact with the working lens for long periods of time, sometimes hundreds of hours continuously, and the materials do have a small chance of auto polymerising which if done in DiLL mode could lead to damage of the objective lens.

Writing profiles described in table 3.3 indicate a culmination of explored optimisations that increase fabrication speed in exchange for reduced resolution and feature size. These parameters will not be suitable or achievable with all materials and were designed for use with PETA or similar materials. Similarly, not all structures depending on complexity and smallest feature size will be possible under all these settings. Mid resolution profile could produce all structure intricacies included within this research at a rate 188 times faster than high resolution but would not be suitable for highly intricate designs or smaller structures. Mid resolution profiles also offer the greatest speed-resolution exchange as structure quality drastically decreases below these settings. As such mid resolution was the primary profile used in this work with low resolution only being employed for very simple designs such as spheres. The primary mechanism involved in this was increasing voxel size and line width by pushing exposure closer to the upper limit before the threshold of burning and is denoted as LP:SS level. This results in maximum amount of radical release and before material damage which equates to a thicker area of polymerisation (306). This allowed much higher slicing profiles to be achieved whilst still maintaining overlap and bonding of layers.

Typically the inverse of this methodology is explored, by limiting power to the threshold of polymerisation and employing radical quenchers to create smaller feature sizes (347). Low or Extreme resolution profiles could be made more viable by techniques to naturally increase voxel size such as two-photon grayscale lithography (2GL) which has controllable laser focal volume (348). Another route would be by increasing reactivity and radical release of PI (313, 339). The collection of parameters optimised and trialled throughout various experiments and writing parameters discussed collectively accumulate to a similar feature recently released by Nanoscribe as a software and product update called dynamic printing precision (DPP) (349). This functionality was not present through the research project and the work presented was developed independently before this update was released. The fastest writing mode within the DPP series allows a 10x increase in printing speed through similar optimisations discussed. However, profiles in this research present a 188-423x increase in printing speed although the level of resolution, feature size and quality retained is quite different. With optimisations in place, structure limitations were explored to see what complexity of design could be completed at a mid-resolution profile. Structures were created to demonstrate the possibilities of this machine and benchmark different feature capabilities although they serve no practical purpose other than benchmarking and public demonstration. Figure 3.11 A and D show the level of precision capable and the points at which feature sizes were not faithfully replicated such as in the Eiffel tower struts or violin details, indicating the limitation of this profile. However, tall thin structures did not warp or bend and subtle details were still present on organic curvature showing suitable stability at rapid speeds. Overhangs in both figure 3.11 B and C were easily replicated, enhanced by the speed of the writing profile reducing the time unsupported features would drift. The effects of voxel size and galvo acceleration are particularly apparent in the sharp square edges of the boat structure in figure 3.11C which are more rounded than they should be.

Whilst fibre production is far better suited to methods such as electrospinning, 2PP was explored for fibre production given that exact fibre diameters could be controlled. This isn't the first use of 2PP for fibres production, Cao *et al* produced nanofibres in a laminar flow based two photon system which allowed long continuous fibres by static laser polymerisation in a flow of monomer and was unlike the method in figure 3.12 which, to the authors knowledge, has not been demonstrated before (350). A prototype

screening tool was produced, depicted in figure 3.12B and C, varying fibre length and thickness as a structure for screening cell interaction, whilst slower than electrospinning this tool could act as a reference guide for rapid optimisation of fibre characteristics. The limitation of this tool is the material choice and fibre length however unique fibre textures, irregular shapes or fibre linked particles could be produced that would not be achievable by other fibre methodologies. Surface covering of larger structures with a surface topography of nanofibres could aid in cell adhesion and control (351).

Multi-material 2PP structures have been fabricated before but never for the purpose of free floating microcarriers (319, 321, 328). This adds another level of complexity by patterning different chemistries on the structure surface which could be used for spatial organisation on the particle. Degradable surfaces could be patterned, such as the previously described fibres, in materials such as GelMA which would aid attachment but degrade over time and reveal underlying material. In this way secondary chemical or topographical stimuli could be delivered forming a two-phase 4D structure that changes over time. The microcarrier designs in figure 3.13 were only simple two material structures to demonstrate fabrication possibility and false colour was added to demonstrate regions of different materials but without chemical analysis to prove material variability act only as an explanatory visual. Despite the potential of this technique, it was not carried on for microcarrier designs in future experiments given that the extra variables obscure differences between material stimulus and mechanical shape. Due to the fabrication technique needed to create particles in this way it requires further effort and careful monitoring, making it far more difficult for scaled production.

The mechanical process of 2PP requires an underlying surface or substrate on which written structures can attach, the surface of the substrate and point of transition to resist is called the interface. One critical function of this underlying anchoring substrate is how well structures adhere to this surface. If structures do not adhere, they will likely fall off during the washing and development process and be lost in waste materials. Whilst fabrication is possible on untreated glass the level of adherence is low and depends on the polymer chemistry. Glass surfaces are functionalised to aid in structure attachment, this is done through silanization and is considered standard procedure (319, 352). The experiment showed better adherence of all structures on glass coverslips

silanised through the acetone method. This result was unexpected given that the toluene method provided a more chemically robust treatment, however coverslips were stored in acetone mixed with silane for long periods of time unlike the toluene method that was stored in a vacuum, this prolonged exposure could account or the increased attachment. Regardless of methodology the importance of silanization is highlighted as structure attachment in untreated surfaces is very weak and a large number of structures are lost.

A novel technique developed was the premise of fabricating upon a pHEMA coated coverslip which provided multiple functions including structure release and cellular isolation. The use of pHEMA coatings for cell non-adherence has been long documented but to the authors knowledge has never been used for 2PP fabrication (353). An underlying substrate is a necessity for the methodology of 2PP, structure release has been explored before but becomes difficult with small numbers of structures. Studies have reported struggles in measuring activity of cells on 2PP structures given that the underlying glass substrate acts as a large space for monolayer growth. This means that, given the scale of 2PP fabrication, the vast majority of cells growing do not experience the material or cues of the structure and as such any assay to measure a change in cellular outcome is completely overshadowed by the surrounding growth as experienced by Ricci *et al* and Raimondi *et al* (354, 355). Demonstration and discussion of cell isolation is covered in a future chapter.

Success has been seen in both the literature and this research on writing on to materials other than glass, but these strategies still posed many problems. One difficulty presented with this pHEMA method was that it inhibited the interface finding function of the system, this is due to the polymers refractive index acting as a buffer between the glass and monomer preventing detection. The methodology outlined in figure 3.15 allowed preparation of coverslips in a way that would allow them to be used remotely and continuously without constant manual adjustment. Removal or reduction of coding for repeated interface finding had already been explored and incorporated to increase overall fabrication speed by removing the lengthy focusing times needed between movements which could sometimes take several minutes to complete. Additionally, the deliberate overlap of the peg structure ensured adhesion to the layer which at fast speeds only added a second of additional fabrication time. Work in this way allowed

programs to be automated and left unattended with movement between different samples with a high degree of success although some misalignments and failure did occasionally happen, but no more frequent than normal fabrication on glass. Measurement of interface position worked as an on-board system for screening surface profile to determine if coating thickness drift would vary beyond the buffer provided by the peg. PHEMA was applied by a bulk evaporation method as is common for biological use, this led to lack of control of layer thickness and shape but repeated trials and measurements across a variety of pHEMA amounts identified a treatment that led to a tolerable variation that mixed with the surface profiling was manageable as depicted in figure 3.16. Spin-coating could provide a better method allowing thinner and more consistent layers, a technique developed by Ingram *et al* could be of use (353). As depicted in Figure 3.17 this coating did not result in any aberration or scattering of light and did not have any effect on structure quality, but different coating thicknesses led to a patterning in the underlying surface. This surface did not appear to degrade across the measurable period with WCA data indicating consistent values within the ranges expected with slight increase in the beginning due to minor absorption of water upon initial immersion (356). A small amount of swelling was observed but did not affect structure attachment, cell adherence or attachment to underlying glass.

The secondary function of the pHEMA layer is to act as a release agent for microcarriers fabricated so that they may be dissociated from the substrate and used as free-floating particles for culture. This can be achieved by dissolving the pHEMA in IPA. However, this was not the first method tested for structure release. Structure release was first tested by mechanical disruption and agitation with inadequate results. Many 2PP studies do not seek to liberate structures and of those that do they often do not cover their release strategies. One reported method has been through agitation of structures through sonication, similar to the agitation method used in this work, the capture efficiency and damage amount is not reported only that release in this way is possible (319). Other studies have sought to use specifically designed products such as Micro Chem's LOR lift off resist for liberation of structures (357). The pHEMA method was the superior method by far as it required no physical disruption of the structure with no possibility of structure retention, structures released by this method are shown in Figure 3.20 and represent the culmination of 2PP optimisations creating

intricate designs in rapid speeds that can be easily released. Mechanical disruption was able to recover a large portion of structures but led to large amounts of damage due to the blunt physical force. Similarly, agitation was not suitable as many structures could not be released, given that silanization was needed to be able to survive the development steps. Overall, the pHEMA method developed provides suitability for all situations whether studying fixed structures or releasing them. Improvements to layer thickness by spin coating and interface detection through a dye to increase refractive index could result in a methodology that could be extremely useful for many 2PP bioapplications.

Results have shown how fast 2PP technology can be given the documented optimisations and findings however there is still limitations to manufacture at clinically relevant scale. Another technology for potential scale-up production was briefly explored and prototype structures equivalent to 2PP were created. Since PμSLA relies on an entirely different method of light processing, involving projection of UV light in a step by step layer, the feature size, materials and processing steps have some variation (358). The resolution is not as small as 2PP with feature resolution of 2 μm and slicing distances of 5 μm. However, the mechanics of this machine mean that fabrication is only measured by the number of z steps or slices and not by the lateral size of the projection. This means that many structures can be created at once in the same time it takes to make one, and whilst 2PP fabrication per individual particle may be quicker given that each PμSLA exposure takes several minutes the stage of this system allows approximately 57,600 particles to be created at once over several hours. An equivalent time to create this number of particles by 2PP under the optimised mid resolution profile, as approximated by data in figure 3.10, would be just under seven days of continuous printing. This does not consider the 10mm height of the PμSLA system. Grayscale features of this system can theoretically allow temporary sacrificial links between particles on different z layers that can hold them in place during printing and later be degraded releasing each individual particle. Using this premise to address the full 10mm height approximately 4.8 million particles could be produced in one job, although since more Z-layers are needed this would increase job time considerably. Production of 4.8 million particles by 2PP under mid resolution profile would take 1.5 years of continuous printing. As such it is easy to see why transition to this technology was pursued, although systems of these capabilities are relatively new.

PμSLA may affect the materials capable of being used in comparison to 2PP however, since the premise of this work was on shape-based influence and not polymer chemistry the findings of this research would be transferable to any technology than can create the same shapes. Another advantage of this technique is the removal of the particle diameter limit imposed by the 2PP system, many microcarriers are in the range of 200-300 μm as this has been proven most suitable for cells (189, 194) but this size particle was not possibly due to the working limit of the 2PP system in oil immersion mode. Despite the promise of this system, only initial testing presented in this chapter was possible due to acquisition of the system towards the end of the research period but showcases how clinical scale up of findings is possible.

# 3.6 Conclusion

The research identified several acrylate monomers with high suitability, unique characteristics and processability at high speeds have been selected for fabrication. Increase to slicing and hatching distance was achieved which rapidly reduces fabrication time at the cost of reduced resolution and quality. It was found that increasing galvo acceleration increases fabrication speeds but produces inaccurate laser travels leading to inaccurate 3D model recreation. Collected optimisations arranged in novel writing profiles greatly reduced fabrication times at the cost of structure quality but can be modulated per requirements. This methodology for accurate and rapid fabrication is novel and hasn't previously been collected or described in this way in the literature. Production of complex models was achieved including intricate models, fibres and multi-material structures, many of which are novel purposes of 2PP technology. Additionally, Structure attachment via silanization was explored and found necessary for structural retention throughout development process. Techniques to coat 2PP substrates with pHEMA were achieved and did not interfere with 2PP fabrication and provides useful functionality. Structural release from underlying substrates was achieved through aid of the pHEMA coating with efficient structure recovery and very little damage. The methodology described to fabricate on top of a coating to prevent cell adherence on the substrate which simultaneously acts as a releasing agent is a novel addition to the field that could revolutionise the way in which 2PP biofabrication research is conducted. Finally scale up to clinically relevant scales was identified through use of PμSLA technology.

# 4. Development of methodology for cell culture using 2PP structures.

## 4.1 Introduction

Microcarriers primarily exist for the purpose of providing surface area for cell growth in cell expansion. Recent advances in biomaterials design and understanding of cell dynamics are beginning to trigger an evolution in this technology into a much more sophisticated means of expansion. However, the core of this technology is still governed by the basic principles of any biomaterial and these considerations need to be taken into account during microcarrier design and fabrication.

Many commercial microcarriers give careful consideration to carrier design and as such a range of microcarriers have been produced out of various materials which commonly include polystyrene, glass, dextran and cellulose (194). In addition, surface coatings are sometimes added to aid in cellular adhesion and proliferation all with the premise of promoting a better cell yield (13, 189). Despite the wide range of commercial options, the vast majority are similarly spherical in shape and in the range of 100-300 μm (359). Some of the major areas for consideration in microcarrier design are biocompatibility of polymers, degradability, cell attachment and mechanical strength. Unlike implantable scaffolds considerations such as cell penetration, nutrient diffusion, waste removal and vascularisation are not necessary easing some of the difficulties seen with other cell interfacing surfaces (360).

Biocompatibility is the most essential component as surfaces will be the direct and only point of contact for cell growth, expansion can only occur efficiently within a biocompatible surface. Additionally any stress from the material may lead to different cellular outcomes (205). Another consideration in the design process is the degradability of the microcarrier. Typically, non-degradable microcarriers are used for the purpose of extend cultures and carrier reuse. However recent strategies to increase

harvest yield and processing ease have employed the use of degradable carriers which don't require potentially damaging enzymatic digestion (361, 362). Another important issue is the strategy employed to promote cell attachment to the surface. Adhesion is important not just for initial seeding but for cell microcarrier transfer during culture and addition of new microcarriers that have to be rapidly attached to during collision (359). Surface adherence has been advanced by the numerous coating strategies that can be applied such as coating with ECM derived proteins to enhance attachment or increasing positive charge of the surface (363, 364). Strategies to enhance cell attachment frequency in microcarrier suspension cultures present an ongoing challenge. Another strategy than can be applied to increase attachment efficiency is the inclusion of porosity, this factor also enhances amount of surface area and can provide shelter from surface shear stresses and collisions (204). However, the process of integrating porosity into microcarriers by lyophilisation or gas foaming means induces a loss of mechanical strength that can be difficult for culture if fragility is too high (360).

Two photon lithography (2PP) produced structures come with a unique variety of advantages and difficulties for their use in both experimental testing and scale up. The use of this technology to produce microcarriers has to address the generic requirements for any microcarrier, such as surface adherence and growth, and also overcome unique 2PP derived issues such as limited materials selection. 2PP structures greatest strength is their complete control over shape and topography at a level difficult to compete against, additionally structures produced are identical and so homogeneity is maintained unlike many microcarriers that can vary considerably in size inadvertently effecting cellular outcome (365). The form of fabrication and materials used in 2PP often favour a greater mechanical strength than highly porous structures made by processes such as foaming (28). However, limited material choices that are often not optimal for cell culture along with lengthy fabrication times are the major barriers. 2PP structures have previously been used in cell culture studies but no standardised techniques such as material post-processing or strategies to increase cellular interaction have been established (291, 303, 304, 307). In 2PP fabricated samples structures are written on an anchoring glass substrate, cell culture on such samples exposes cells to both the 3D architectures and the anchoring substrate. Exposure of cells to underlaying anchoring substrates poses difficulties in analysing cell behaviour given that most cells grow in monolayer fashion on the surrounding substrate that outweighs the active

structure. This makes measurement of cell signals come from mixed populations and environments and obscures the results of the structure. Liberation from the substrate or increased structural coverage both require much larger fabrication times to make samples large enough to handle in this fashion. Problems with underlying substrates have been noted as an issue in several 2PP papers but has not been resolved (354, 355, 366). Another problem faced when using intricate 3D structures is the method of visualisation as cells can wrap around structure features in three dimensions which, added to innate autofluorescence of 2PP derived structures, makes imaging very difficult especially when structure dimensions are greater than those measurable by typical confocal microscopy (176, 334).

Overall, production of 2PP manufactured structures for cell culture presents a variety of challenges to address for appropriate cell culturing technique and suitable measurement of cellular response without obfuscation by other cell populations. Microcarrier technology via 2PP has not been previously explored and although 2PP structure cell interactions have been briefly investigated in the literature for a variety of purposes these have always been met with obstacles that have not been resolved. As a result, no optimised or standardised methodology is available to follow or build upon.

## 4.2 Aims and Objectives

This chapter investigates the methods by which cell culture with 2PP structures can be achieved and techniques to increase and optimised cell-structure interaction. Unique strategies to combat some of the commonly encountered 2PP issues and culture limitations have been explored including limited material adherence, structure avoidance on anchoring substrate, polymer autofluorescence and 3D imaging techniques. The contents of this chapter could provide thorough and standardised methodology for cell culture on 2PP structures and details the methodology by which microcarrier assessment can be completed. To achieve this the following goals were established:

1) Explore polymer biocompatibility and cell attachment as well as ways in which to enhance this interaction.

2) Evaluate methodology to overcome unique 2PP derived issues such as autofluorescence interference in 3D imaging and cell signal dilution from surrounding monolayer growth.

3) Design unique microcarrier architectures with features capable of provoking cell bio-instruction and responses through mechanotransduction pathways for later analysis in future experiments.

# 4.3 Materials and Methods

The following methodologies are used in this chapter in addition to those presented in section two materials and methods.

### 4.3.1 Polymer leaching

Polymer leaching was achieved by incubating fabricated samples following development in DMEM complete media for 48 hours at 37°C. samples were subject to IPA washes prior to testing to ensure sterility. Media was removed and transferred to a new cell culture plate which was seeded with 3T3s under standard technique (see section 2). From this plate cell growth could be monitored and subject to further analysis.

### 4.3.2 Polymer film creation

A Pasteur pipette was used to drop two drops of monomer into the wells of a 12 well plate and lightly shaken to diffuse across the well to form a thin layer. Monomers were prepared with 2% irgacure 369 as per monomer preparation protocols in section 4.3.1. Polymer films were added in triplicate with empty (tissue culture treated polystyrene) wells as a control. After polymer spreading UV light (spectroline LW UV-A, 365 nm) was applied for 60 mins to initiate curing. Cured wells were washed following postprocessing washing protocols before addition of complete DMEM media and seeded with 3T3 cells at $0.1x10^6$ cells per well. Plates were incubated for 72 hours

before readings were taken. Argon film production was identical but within a glove box with an argon atmosphere ($O_2$ <10,000ppm).

### 4.3.3 Oxygen plasma treatment

Oxygen plasma treatment was completed using a Diener tetra 30 plasma system. Plasma was stricken using a low frequency (LF, 40 kHz) as per standardised machine programs settings. Plasma was formed using a flat static electrode. Settings all include 100% oxygen treatment for varying times leading to activation of surfaces by oxygen group deposition. Structures were used immediately following treatment and the process was integrated into post-processing procedures following vacuum oven incubation.

### 4.3.4 Poly-L-lysine coating

Coating was achieved by addition of 5mg of Poly-L-lysine (sigma) to 50ml of tissue culture water and mixed for two minutes via vortex mixing. 300 µL of Solution was pipetted on to samples taking care to cover the entirety of structures and small surrounding area within the droplet. After coating for 5 minutes the solution was aspirated and washed. Structures were allowed to dry for several hours before cell culture.

### 4.3.5 UV photobleaching

UV photobleaching was achieved using the same Omnicure S2000 spot UV curing system detailed in section 4.3.1 High intensity irradiance at 320-500 nm and 40 W/cm$^2$ was applied to structures in a secured environment. Machine auto shut off was enabled in case of overheating or bulb rupture. Structures were bleached under this system for a maximum of 35 hours during tests.

# 4.4 Results

### 4.4.1 Viability of cells in contact with structures

Structures produced and developed through 2PP lead to a notable reduction in cell viability within the immediate vicinity of fabricated structures.

The post-processing procedure, outlined in figure 4.1, was used to ensure removal of residual chemicals and maximise cell interaction. Samples were first processed via 2PP development, UV cured and stored in a vacuum oven at 100°C overnight or for a minimum of six hours. Samples could then be washed with IPA as a final check for residual monomer and initial sterilisation. Transfer to cell culture facilities and additional UV sterilisation in hood was completed to ensure sterility and as an additional safeguard given that fabrication was limited and time consuming. A final

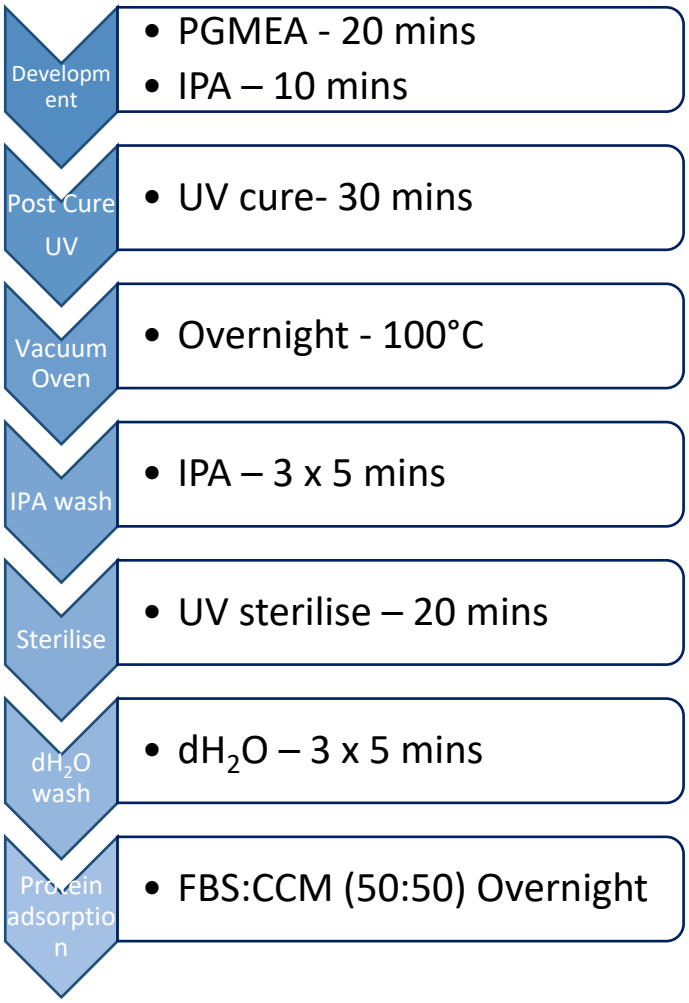


***Figure 4.1:*** *Schematic demonstrating the postprocessing steps to maximise biological interactions*

series of $dH_2O$ washes to remove any remaining IPA was conducted and finally an overnight incubation with cell culture media mixed at 50:50 ratio with FBS as a high protein conditioning media.

Cell culture media was incubated in presence of the 2PP samples for 48 hrs before media was collected and used for culture in a fresh well plate seeded with NIH-3T3 cells. Cells growing in the presence of conditioned media were subject to an Alamar blue test after 24 hours to determine if any harmful chemicals had leached out from structures. Results indicated that unwashed samples that only underwent the minimal development process prior to cell culture, necessary for sterilisation, caused a reduction of cell viability across all materials tested as seen in figure 4.2. As such, the post-fabrication washing strategy devised aided in fully removing any residual contaminants and maximised suitability for cell culture. Following post-processing procedures, media that had been in the presence of washed samples had no residual effect on cell viability as seen in figure 4.2.

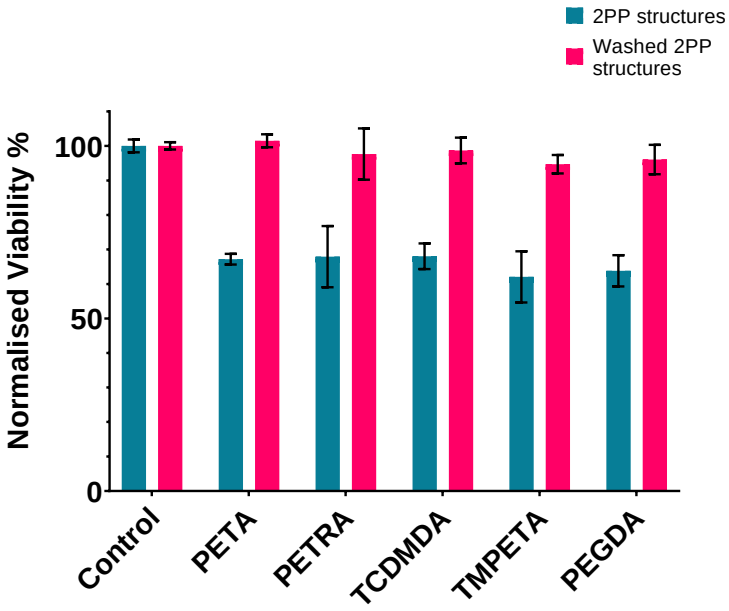


***Figure 4.2**: Viability of cells cultured in 2PP sample conditioned media before and after post-processing and washing. Control represents cells cultured on cell culture plastic with fresh media with no 2PP structure exposure Post-processing procedures improved viability in all experimental conditions. Cells seeded at $2x10^5$ cells/ml and cultured for 24 hours. Mean ± SD (n=3).*

Polymer leaching tests indicated that processing eliminated diffusion of harmful materials seeping from structures into the media. Live/dead staining of cells in the immediate vicinity of structures was used to confirm findings when cells were in direct contact with 2PP fabricated structures. Figure 4.3A depicts live/dead staining of NIH-3T3 cells in contact with unwashed structures which leads to a higher number of dead cells as marked by red ethidium homodimer III (EthD-III) staining. Figure 4.3B indicates staining in the presence of washed structures which leads to a notable increase in viable cells marked by green calcein-AM staining. Image analysis and automated counting of cells to calculate percentage of live to dead cells was pursued and is presented in figure 4.3C. In unprocessed samples there was 43% cell viability which rose to 97% after processing.

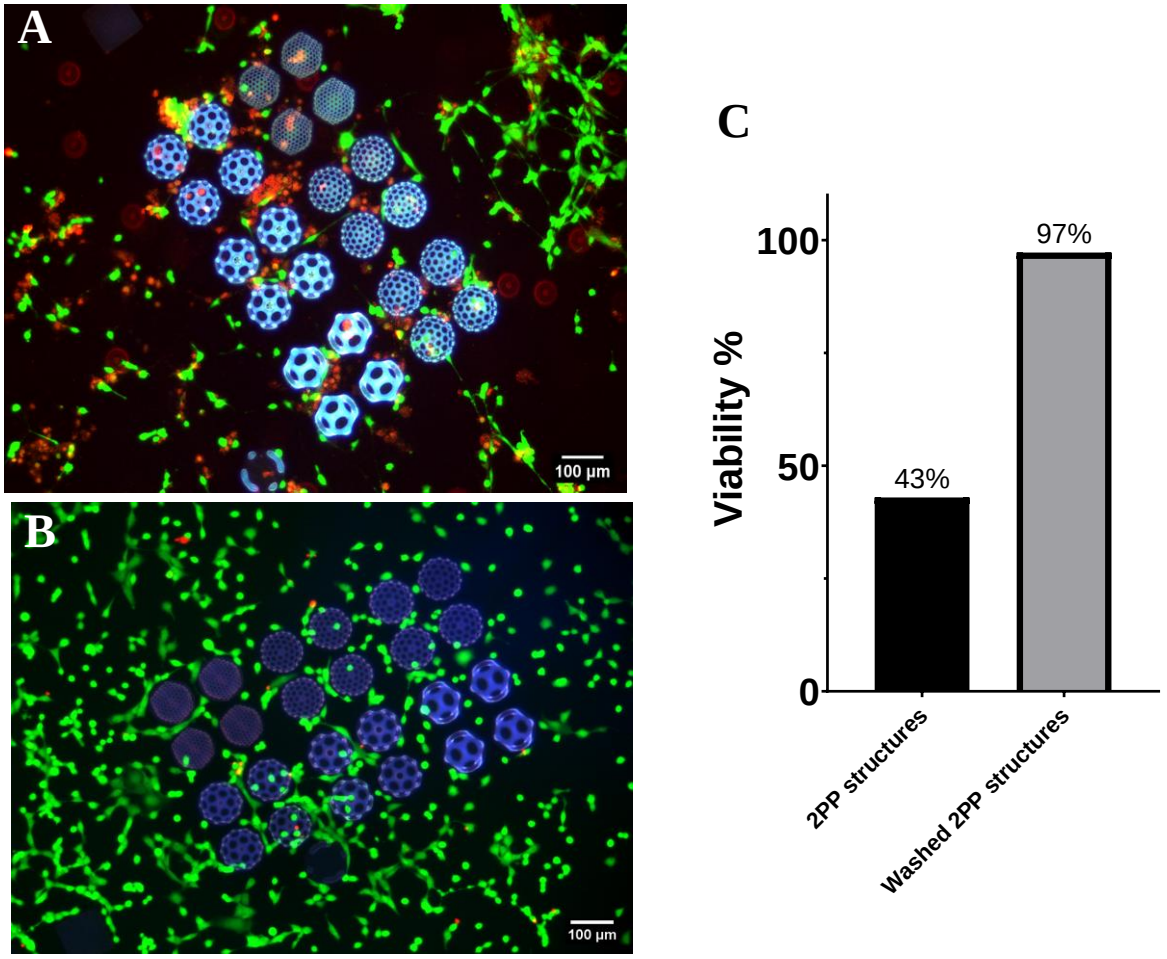


***Figure 4.3:*** *Live/dead analysis of cell in contact with PETA structures, with and without post fabrication processing. A) micrograph of unprocessed structures with a high level of dead cells. B) Microscopy after processing procedure with very few dead cells. C) Analysis of images to quantify percentage viability between conditions indicating rise in viability from 43% to 97% when including processing steps. Green is live cells, red is dead and blue is structures. Data generated from above example images (n=1). Cells seeded at $2x10^5$ cells/ml and cultured for 24 hours.*

### 4.4.2 Polymer biocompatibility

Screening of polymer films polymerised in methods other than 2PP was pursued due to the slow fabrication process in 2PP, data in figure 4.4 shows attempts to quantify three candidate materials polymerised in three ways. This was attempted so as to not be limited by 2PP fabrication time in material screening tests. PETA, PETRA and TCDMDA were initially selected for testing alternate polymerisation systems. Monomer was added to cell culture plates and polymerised under UV, then subject to the same post-processing protocol as 2PP samples. 3T3 cells were seeded on cured polymers and cultured for 72 hours upon which microscopy images were taken and Alamar blue assay was used to assess metabolic activity that could be compared to cell number for cells growing on UV polymerised films. At first materials were polymerised under a normal atmospheric oxygen environment to maintain similarity to 2PP. Materials produced in this way lead to a significantly high level of cell death and any remaining viable cells could not attach to the surface as seen in figure 4.4. Materials produced in the same way but under an argon environment led to a more complete cure of the material. PETA showed cell growth and attachment on the material surface with cell numbers comparable to control TCP. TCDMDA exhibited growth and adherence, but cells appeared less uniformly spread and more elongated, approximate cell numbers were significantly lower than the control. Cells cultured on PETRA surfaces show a significantly lower level of cell number and visibly reduced attachment on the surface in comparison to controls. Cells grown on 2PP fabricated materials showed good cell culture on PETA surfaces with cells growing and spreading all over the visible 2PP grid. PETRA surfaces showed an improved cell adhesion in comparison to their UV-argon polymerised counterparts but still a reduced level of attachment and spreading in comparison to PETA. Interestingly TCDMDA materials produced by 2PP showed a decreased cell attachment, with cells actively avoiding the material by growing around the material and in the seams between flat films. This is in opposition to those cured by UV in presence of argon which had a higher level of cell adherence.

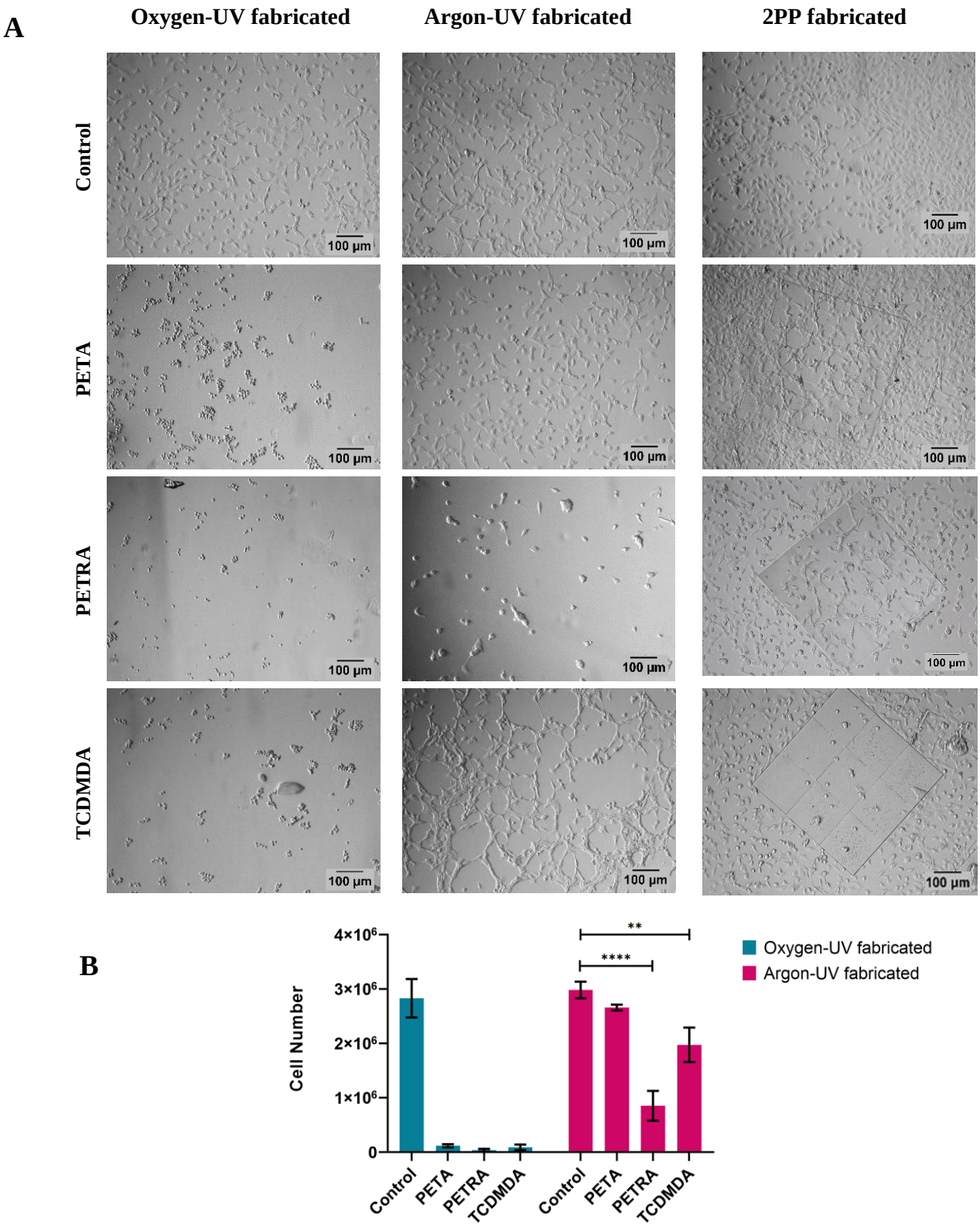


***Figure 4.4:*** *Growth of 3T3s on materials polymerised by different methods.* A*ttachment varies between methods of polymerisation for the same materials. A)* B*right field microscopy on materials polymerised under UV in the presence of oxygen and argon aswell as films fabricated through 2PP (grids visible in 2PP conditions) B) Cell number approximation grown on materials, mean ± SD, (n=3) (**= p<0.01, ****=p<0.0001). Cells seeded at 2x10$^5$ cells/ml and cultured for 24 hours.*

A reliable method of determining suitable materials without using 2PP was difficult given the slight changes in cell interactivity between polymerisation methods. The five candidate materials identified in chapter three were taken forward for biocompatibility and adherence testing with iMSCs using live/dead staining given that measurements can be isolated to the structure and surrounding area only.

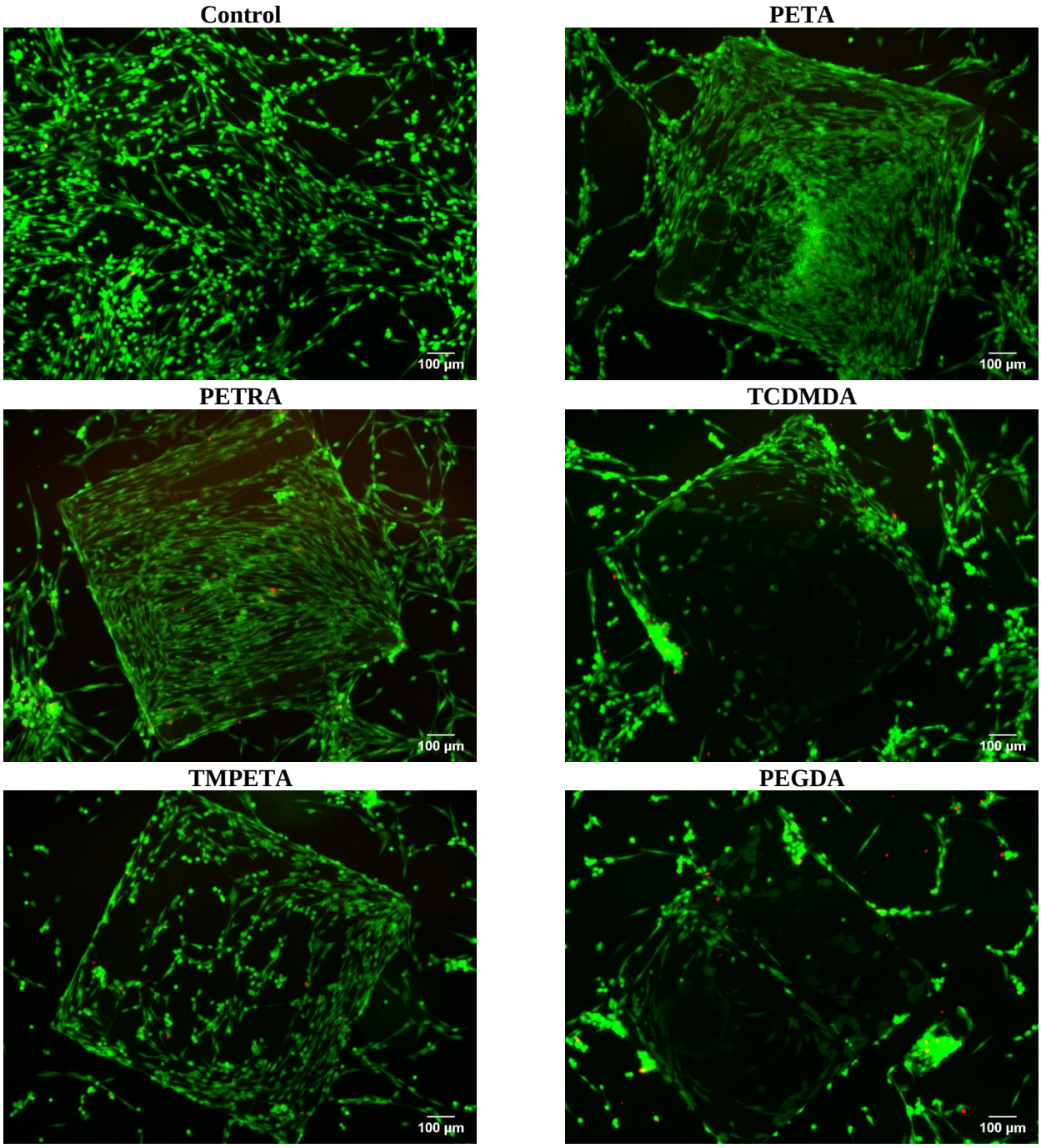


***Figure 4.5:*** *Representative live/dead microscopy of materials polymerised by 2PP. PETA, PETRA,TCDMDA, TMPETA and PEGDA films were fabricated at 1mm$^2$ and subject to culture with iMSCs then live/dead stained to assess both material biocompatibility and cell adherence. Cells seeded at 2x10$^5$ cells/ml and cultured for 24 hours*

Assays for cytotoxicity or viability were difficult to achieve in 2PP given that the written structures represented a very small portion of the available surface area and optimisations to increase fabrication speed or to isolate cell growth had yet to be achieved. Live/dead results were subject to image analysis to quantitate percentage of cells viable across the material surface and surrounding area. Images in figure 4.5 and data in figure 4.6 indicate that all materials are biocompatible with over 90% viability for all materials. For PETA films viability was 97.9%, comparable to the 98.7% viability in control samples and were not statistically significant from each other. Cells on TMPETA films showed 96.9% viability which was significantly different from controls at $p<0.05$. All other materials showed significantly less viability in comparison to controls at $p<0.0001$. Data reveals that whilst biocompatibility of materials is acceptable, the level of adherence of cells to the material varies significantly. Microcarriers require adherence of cells to the surface for expansion to be achieved and so criteria for material screening included the level of cell interactivity or adhesion. Representative images in figure 4.5 were used to calculate surface coverage and indicated that PETA and PETRA have the highest level of cell coverage which indicates increased level of cell adherence in comparison to other materials. Calculation of surface coverage in control samples as a comparison could not be determined given that these samples had no inherent autofluorescence to measure against. However, visual comparison of images in figure 4.5 indicate that coverage for PETA and PETRA materials are comparable to, or higher than, controls.

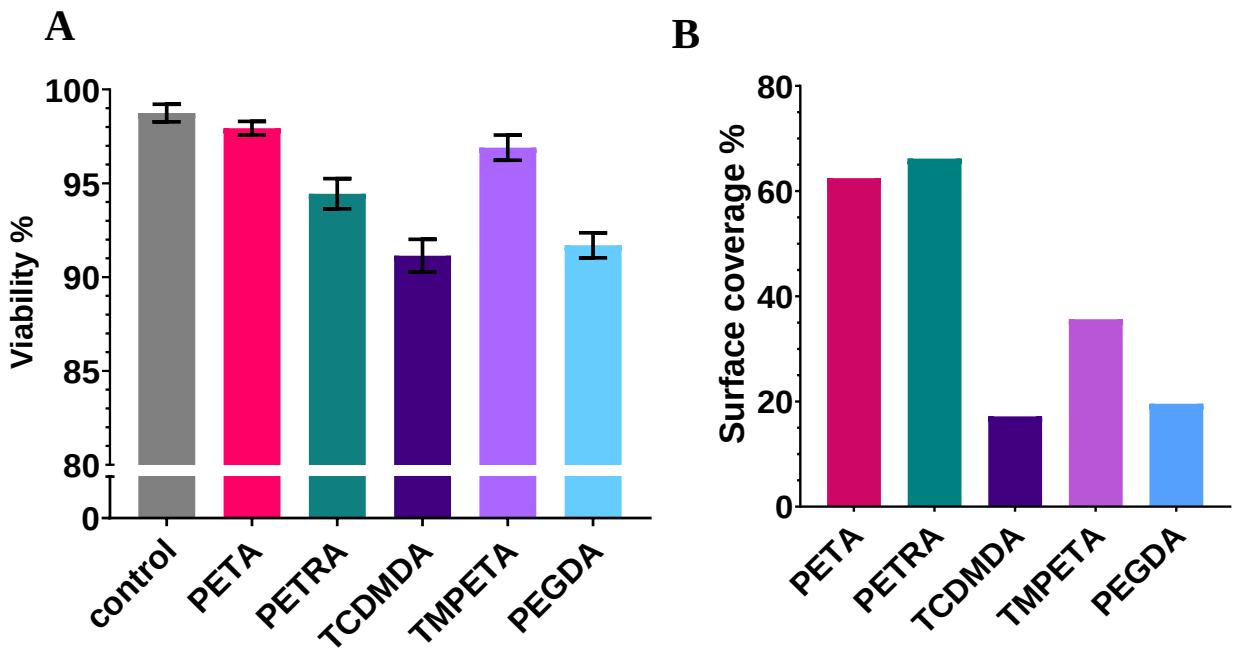


***Figure 4.6:*** *Cell viability and adherence on 2PP fabricated films derived through image analysis of live/dead microscopy. A) Percentage viability of cells grown on materials and glass control, mean ± SD (n=3, N=1). All materials except PETA were significantly different from controls (P<0.05) as determined by ANOVA tests. B) Percentage of film surface that is covered with cell growth based on example images, determined by image analysis of stain fluorescence and structure autofluorescence.*

### 4.4.3 Initial cell structure interactions

Initial cell interactions with buckyball hemispheres were investigated following development of the postprocessing strategy and analysis of polymer biocompatibility as a first trial of 3D interactions. 100 µm diameter C180 buckyball hemispheres were fabricated in PETA seeded with 3T3s and grown for seven days to ensure a high level of confluency and structure interaction. SEM images in figure 4.7 indicates that cells growing as a monolayer do grow into the structure rather than simply growing around them as was feared given the change in vertically which is an obstacle to monolayer growth. These images indicate some interesting and specific behaviours of cells growing on the buckyball hemispheres. As seen in the ESEM image in figure 4.7a cells do grow throughout structures forming a covering over the pores, cells growing on these are capable of spreading and bridging to neighbouring structures indicating that 3D cell interaction can be established. ESEM was performed to allow images within

liquids so as not to disturb any potential cell interactions although further investigation showed this level of precaution was not necessary as cell interactions were not that fragile and could be preserved through standard SEM prep such as fixation and dehydration. Another interesting feature is the emergence of singular pore hole openings in the cell growth as labelled in image A. Figure 4.7 B and C indicate standard SEM images of identical structures imaged at two different levels of confluency, this images indicated that pore overgrowth continued as confluency increased. As cell growth and ECM deposition grow thicker over the structure the underlying architecture becomes obscured given that struts are visible through the cell growth in figure 4.7B but over time become less visible in figure 4.7C. The repeated presence of a singular open pore was present in a high percentage of structures and even into extremely confluent samples. The internal growth of cells within the space within the dome was uncertain since it could not be visualised although the emergence of these pores seems to indicate a mostly hollow interior. This data was the first indication that complex structural designs and particular architectures can lead to specific and repeatable cell behaviours and growth patterns.

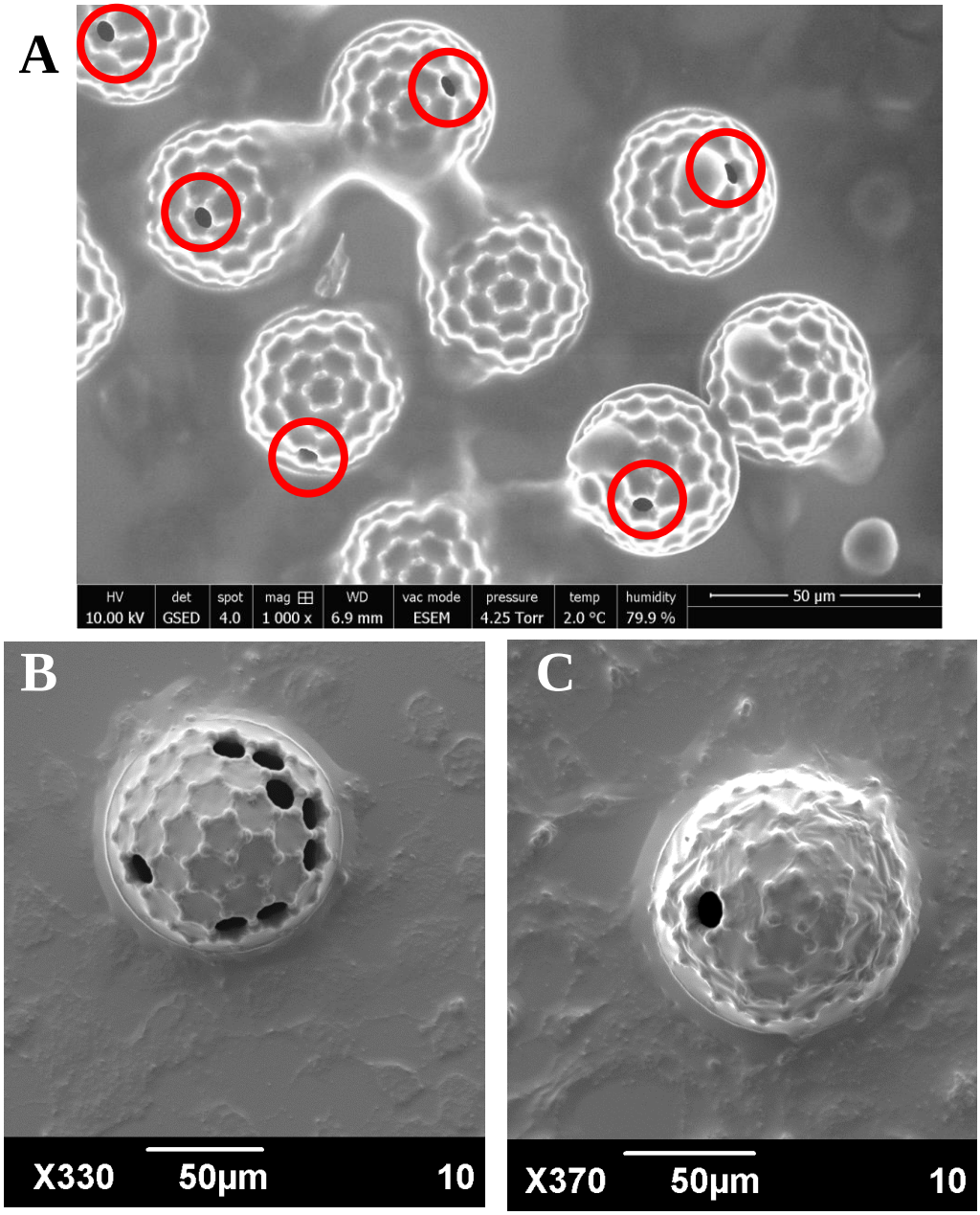


***Figure 4.7:*** *SEM images of 3T3 cell interaction with PETA C180 buckyball domes.* ***A)*** *eSEM interactions of cells with domes in close contact with red circles highlighting repeated pore opening behaviour when engulfed. B) SEM images of cells grown at structures at a low confluency. C) SEM microscopy of cells grown at structures at a high confluency.*

Next, structure interaction was probed based on overall structure size. The limitations of 2PP restricted the producible size of full particles to a maximum reliable height of 160 µm and so the other sizes chosen were 100 µm and 40 µm to give an even spread. The desired level of cell interaction is defined by the amount of structure coverage, ideally a high percentage of the structure should be covered and cellular colonisation of

struts, joints and pores. By observing interaction and coverage of these aspects without complete engulfment it was determined what size range was most suitable. Smallest structures showed a complete engulfment by monolayer growth. Largest structures showed the least level of cellular interaction with some migration of cells up and over struts but overall very little coverage. 100 µm structures showed a good level of cell interaction where structures were not completely overrun by surrounding growth but had a high level of colonisation and interaction with different features. Structures of this size had already been shown to be completely colonised when confluent in figure 4.6. The approximate measurement of structural feature sizes was obtained through 3D model measurement at the different scales used but due to resolution changes upon writing and possible shrinkage these are only approximate. The features measured include pore diameter, strut thickness, strut length and the diameter of connecting spheres within the ball-and-stick models. These dimensions are summarised in Table 4.1. This data indicates that feature sizes of approximately 5-6 µm and pore sizes of 13 µm gave the best level of cell interaction. However, despite these observations the level of interaction is based on hemisphere designs and could vary based on structure architecture and cell type used. 100 µm Particles were taken forward as the standard size to be used for two reasons, the level of cell interaction is good and overall size will not be engulfed by surrounding growth without interaction with features. Secondly, from a manufacturing point this size gives the best compromise for fabrication time in comparison to larger structures.

**A**

| Structure diameter (µm) | Pore diameter (µm) | Strut Thickness (µm) | Strut Length (µm) | Connecting ball diameter (µm) |
|---|---|---|---|---|
| 40 | 5.3 | 2.4 | 2 | 2.8 |
| 100 | 13.3 | 5.9 | 5.1 | 7.1 |
| 160 | 25 | 9.5 | 8.1 | 11.4 |

**B**

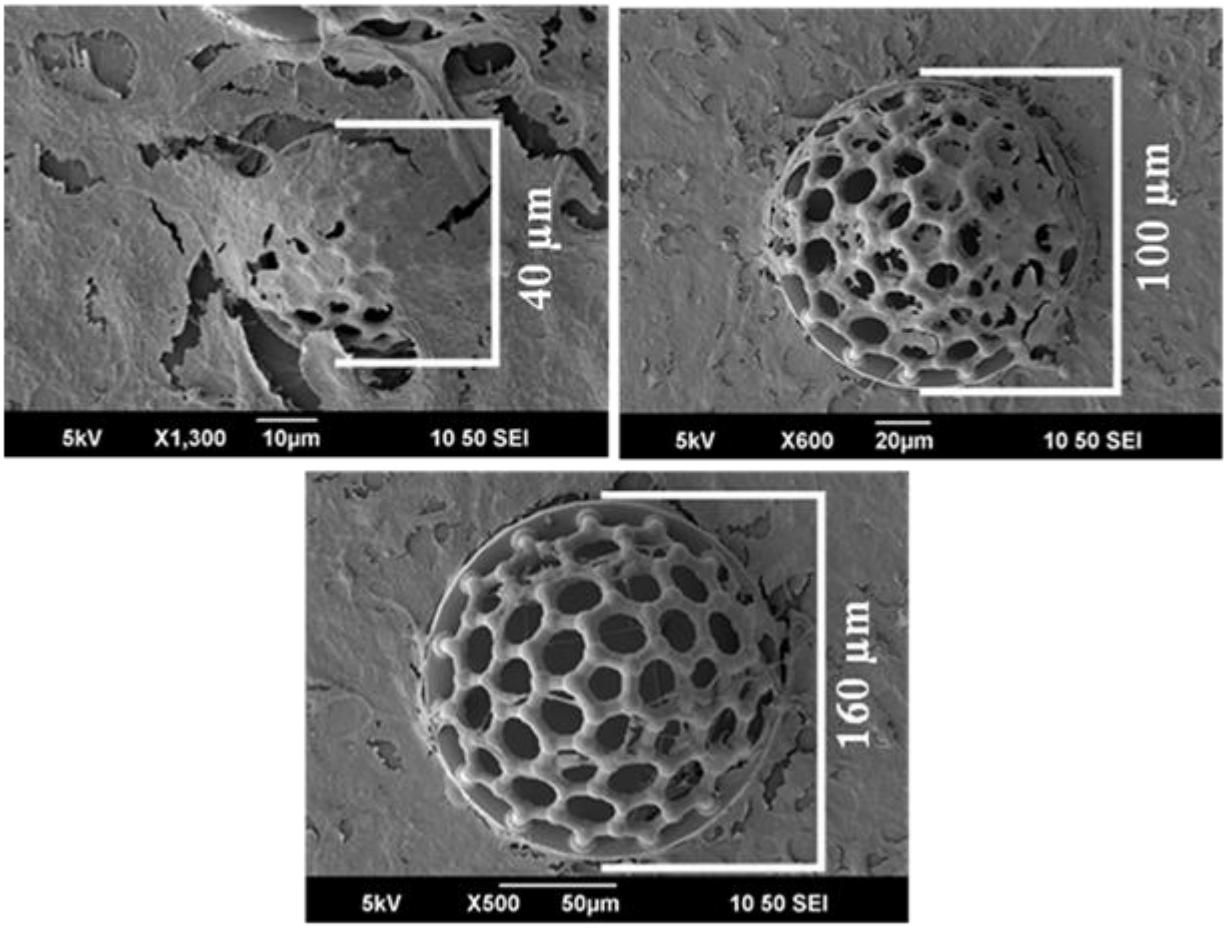


***Figure 4.8:*** *Buckyball size variations A) C180 buckyball dome approximate feature sizes at different diameters measured via 3D modelling. B) SEM images of 3T3 cells grown on PETA C180 buckyball domes of varying sizes including 40 µm, 100 µm and 160 µm diameter structures. Smallest structures were engulfed by cellular material, mid-sized structures showed good interaction with cells which grew up and across the structure whilst largest structures show the least level of cellular interaction. Cells seeded at 1x10$^5$ cells/ml and cultured for 5 days.*

### 4.4.4 Surface modification

Surface coatings were explored to increase cell adherence and interaction, this would allow fabrication with materials of a lesser natural adherence. The primary motivation behind a surface modification in this research is that by enhancing cell attachment to structures they will be guaranteed to experience the geometry of the structure and react accordingly. Initially the effects of amino acid based polylysine coating were explored to determine if enhanced cell attachment could be achieved. As such structures were produced in TCDMDA that previously exhibited the lowest level of cell interaction and seeded with 3T3s. One set of structures were untreated other than post-processing, the second set of structures were subject to polylysine treatment. Example results shown in figure 4.9 repeatedly showed enhanced colonisation of treated structures and denser cell growth in the immediate area that was covered by the droplet of poly-L-lysine solution. This indicated enhanced colonisation of materials that previously showed the lowest level of attachment and ensured cells experienced the geometry of the structure.

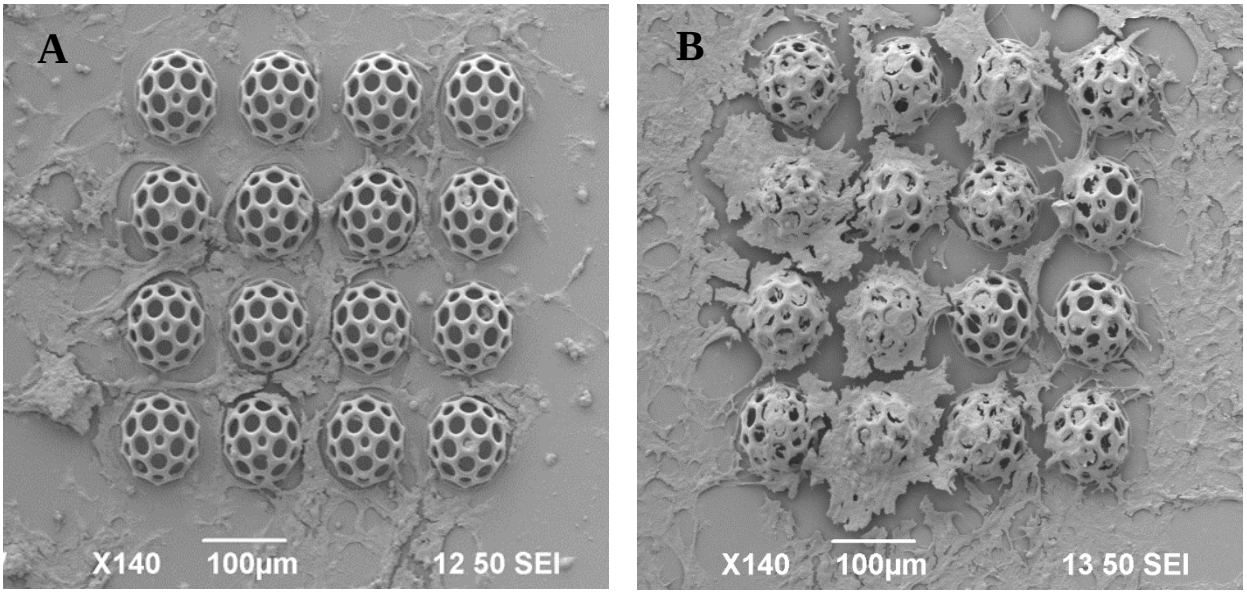


***Figure 4.9:*** *Polylysine treatment of structures enhances cell attachment. A) untreated array of bucky ball structures fabricated in TCDMDA with a low level of cell attachment. B) Poly-lysine treated buckyball array with a high level of cell attachment to structures. Cells seeded at* $1x10^5$ *cells/ml and cultured for 3 days.*

In many commercial microcarriers the only variations between competitors are the materials used or surface coatings employed. However, for the purpose of shape induced cell instruction it is important to delineate between the effect of material or coating and that of the mechanobiological cues delivered. Typically, this not an issue for most microcarriers given that shape is often not a driving factor of biological function. As such a more subtle and simpler way of enhancing the cell interaction to make it more compatible but without extreme chemical interference that could make cells bind to any shape or material. This was explored by simple oxygen plasma treatment of samples for varying time periods to determine if this could enhance material interactions. Samples were exposed to 100% O2 plasma for 1, 5 and 10 minutes and subsequent cell interaction visualised after three days of culture. Untreated structures have little cell interaction, after plasma treatment for one-minute cellular interaction is improved. Five minutes of plasma treatment resulted in a depleted cell response similar to untreated samples, but at 10 minutes of plasma treatment the cell interaction is again improved, this is depicted in Figure 4.10.

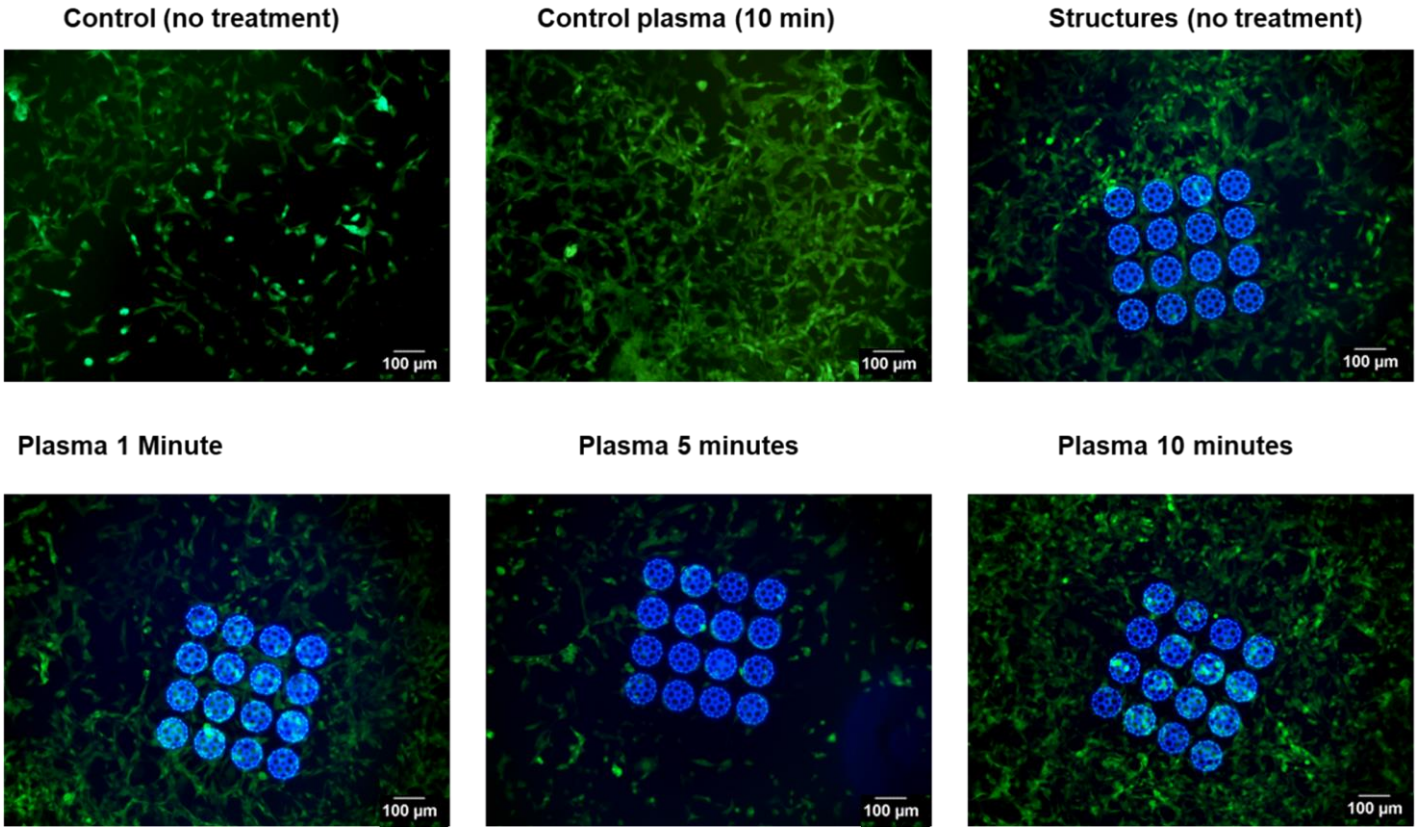


***Figure 4.10:*** *Fluorescent microscopy of iMSCs in contact with control coverslips and TCDMDA structures under varying durations of plasma treatment indicating a change in cell adhesion based on treatment duration. Cells seeded at 1x10$^5$ cells/ml and cultured for 3 days.*

### 4.4.5 Cell isolation to structures

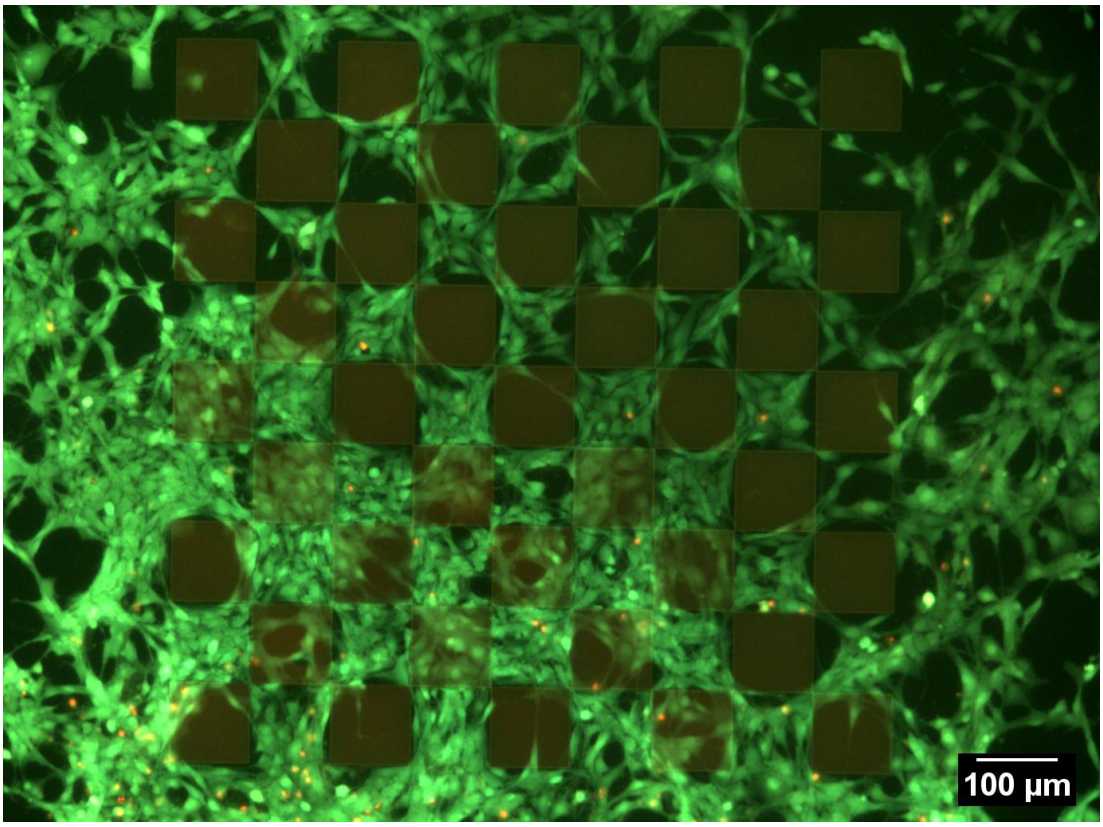


***Figure 4.11:*** *MSC avoidance and patterning due to TMPETA films in checkerboard patterns. Live/dead staining of MSCs in a gradient from the bottom left corner across films, distinguished by dark red fluorescent squares indicating level of confluency needed for films to be grown over. Cells seeded at 1x10$^5$ cells/ml and cultured for 3 days.*

As previously described, there are difficulties with experimentation imposed by the anchoring glass substrate in 2PP. This is visually demonstrated in figure 4.11 with TMPETA films in a checkerboard pattern with 100 µm x 100 µm films separated by empty underlying glass substrate. Despite the moderate attachment for TMPETA, determined in section 4.4.2, iMSCs still avoid the polymer space until higher levels of confluency as seen in the gradient of cell density from the bottom left of the image.

As such a method to isolate cells was sought and the manufacturing and 2PP aspect of this fabrication is covered in section 3.4.8. Whilst manufacture and 2PP use of this strategy has been explored in this work, the effects on cell growth and isolation have not been demonstrated. Initially the non-adherent behaviour of the coating had to be assessed, results of this experiment are demonstrated in figure 4.12. Results indicated that the deposited layer did have strong adherence prevention behaviour after

fabrication and exposure to all postprocessing steps. Cell non-adherence was maintained over three days from this initial test, but cell non-adherence and structural integrity was maintained for a much longer time as seen in section 4.4.9.

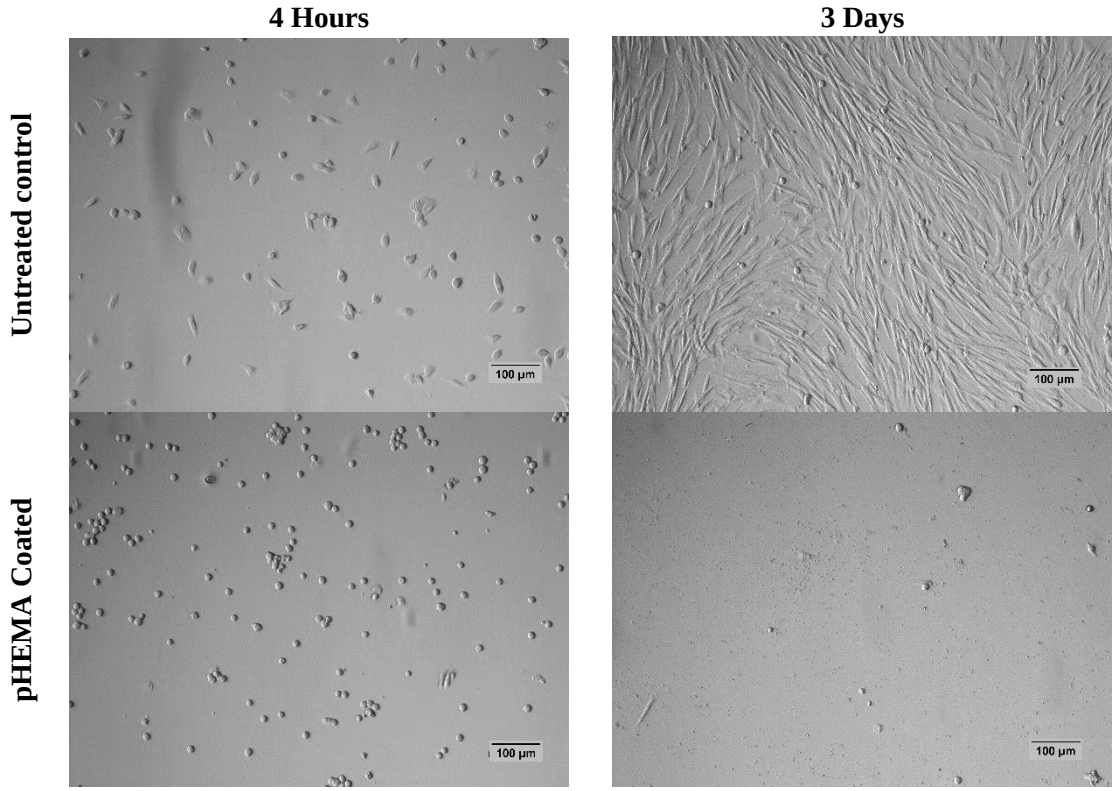


***Figure 4.12:*** *pHEMA cell adherence control testing.* *Brightfield microscopy of iMSCs grown on untreated glass control slips and on non-adherent poly-HEMA coated slips across two time points of four hours and three days indicating successful cell non-adherent behaviour on coated slips.*

Once the procedure for 2PP fabrication upon pHEMA was established and control testing had determined that the non-adherent nature was effective and maintained the next experiment sought to trial cell interaction with structures fabricated upon pHEMA coated substrates. A small 4x4 array of each buckyball variation was fabricated in PETA on pHEMA substrates as seen in figure 4.13A. Cell culture with iMSCs indicated how cells were entirely isolated to the structures only and grew within and throughout the structures. This initial test indicates how certain structure variations, which in this case is mostly indicative of pore size, can lead to different cell behaviours as the cell coverage of structures varied and interaction of cells throughout different structures was different. This preliminary trial indicates how cell interactions between structures were limited in C20 and C540 structures and heaviest in c80 structures where all four structures were linked to each other through cell growth fully bridging the gap

in between repeated structures. Figure 4.13B and C indicate the same c80 array with heavy confluence following cell growth and cell isolation is still maintained. SEM images indicates how heavily the scaffold can be colonised and live/dead fluorescence images shows how structure position can be visualised within the cell growth and that despite high confluency there is very little dead cells within the structure even within the core where necrosis usually appears first. This trial indicated the success of this technique to isolate cell growth but warranted further cell seeding optimisations given the massive reduction in colonisable surface area to prevent rapid over-confluence in experimental trials.

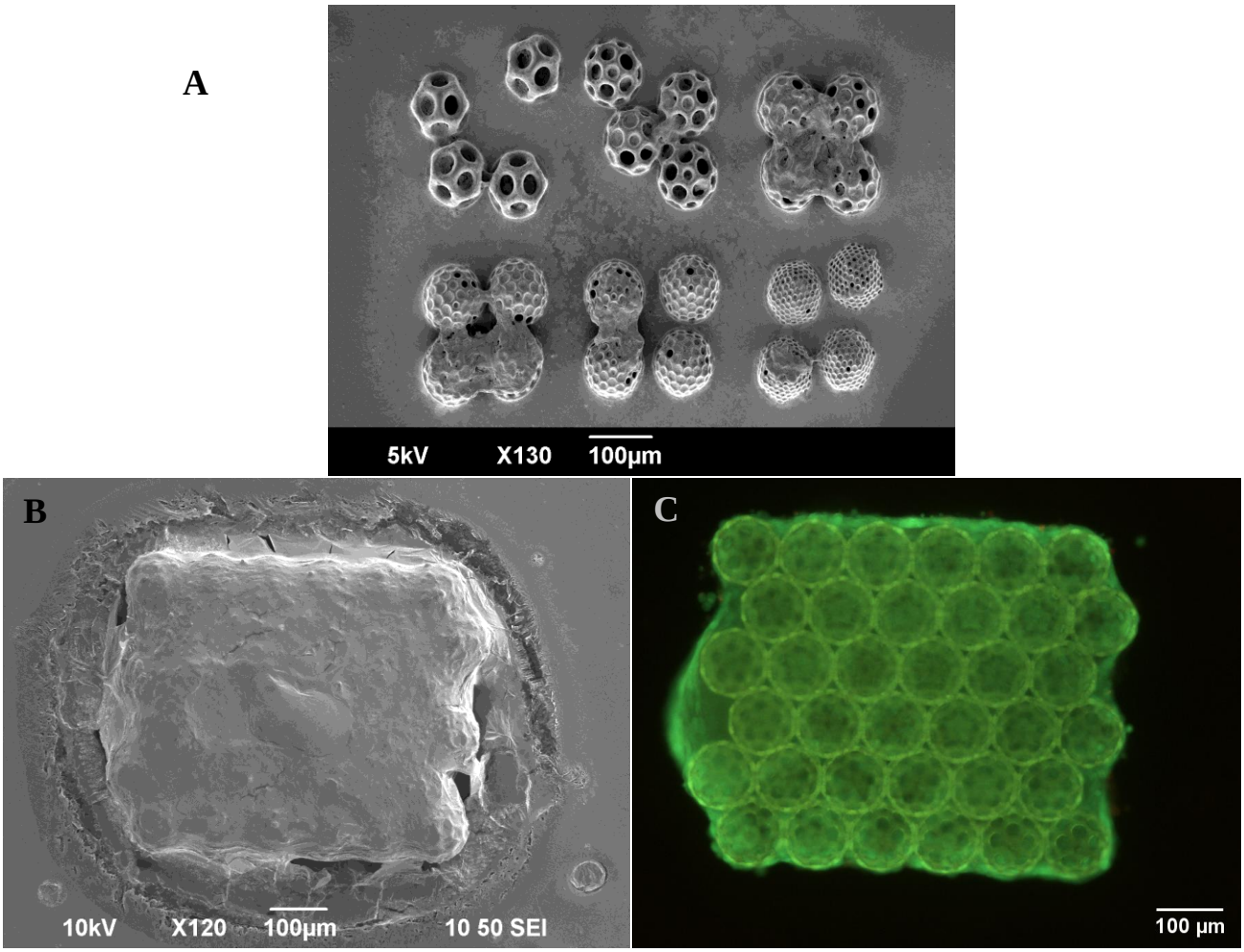


***Figure 4.13:*** *pHEMA assisted cell isolation to PETA 2PP structures. A) small array of buckyball variations on pHEMA showing cell growth within and throughout certain buckyball variations. B) Confluent array of C80 buckyball structures completely confluent with iMSCs. C) Live/dead fluorescence microscopy of the same confluent array showing viability throughout and how autofluorescence allows visualisation of structures within the cell growth. Cells seeded at* $5x10^5$ *cells/ml and cultured for 3 days.*

### 4.4.6 Autofluorescence bleaching

Structures produced via 2PP have autofluorescence in all channels under standard filter cubes, this can be seen in all fluorescence microscopy demonstrated. Autofluorescence can obscure cell signal in 3D structures, given these difficulties one strategy devised to neutralise this issue was by UV photobleaching. Arrays of buckyball structures were subject to high intensity UV exposure at 40W/cm$^2$ over 35 hours with periodic fluorescent imaging at the same exposure levels to measure the photobleaching effect. Figure 4.14 indicates the results of this process. Structures prior to treatment have a strong fluorescent signal, after six hours of exposure this signal noticeably decreases and continues to drop at a lesser rate until the final measured time point at which signal is greatly diminished but not completely eliminated. However, whilst effective for the c80 structures when applied to different designs with thicker material features such as solid spheres there is a lack of bleaching likely due to poor penetration of UV through thicker material. As such, despite the limited success of this technique it is not suitable for all designs.

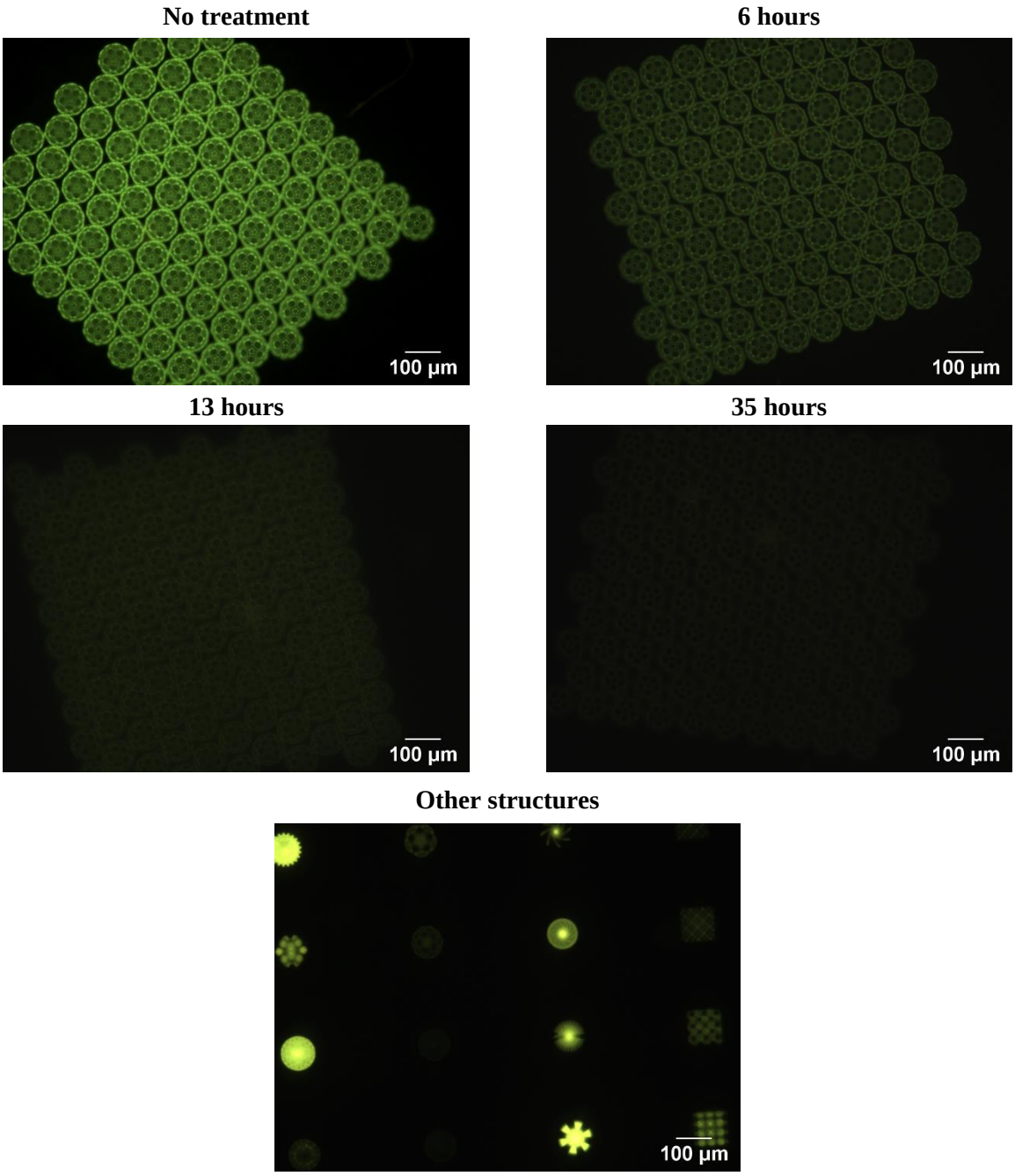


***Figure 4.14:*** *Autofluorescence photobleaching of 2PP produced structure. C80 array autofluorescence is strong prior to photobleaching and noticeably declines over the exposure period. Other structure designs that include thicker components show a lack of photobleaching after 35 hours due to lack of UV penetration.*

### 4.4.7 Confocal testing

Confocal microscopy was explored to image and analyse cellular infiltration and growth throughout structures. This was something that could not be fully achieved in traditional fluorescence microscopy as the 3D nature of these structures limited how much can be distinguished within the vertical plane. Initial confocal microscopy led to a reoccurring issue with signal cut off after a certain depth and the entirety of the structure could not be imaged when using 100 µm diameter particles. This is a common limitation in confocal without specialised components and techniques and is demonstrated in figure 4.15A with an example c80 array in blue with live/dead cell staining. As such attempts were made to maximise the depth at which the focal plane could be maintained by using a 40X water objective with collar set at 0.17 and a wider opened pinhole to give an optical section of 2.5 µm. With this method signal could be maintained to 100 µm and represents the furthest limitation of this technology. However, the trade off with this method was that signal could only be maintained through thicker optical sectioning and because of this overall resolution was lower, as seen in figure 4.15B. Individual details were still difficult to analyse and often warping and loss of signal at depth occurred meaning that as the height of the structure increased smaller details could not be seen. This limitation also applied to the structure autofluorescence meaning that whilst spheres were visible at max depth the structure designs with smaller features were practically invisible.

A

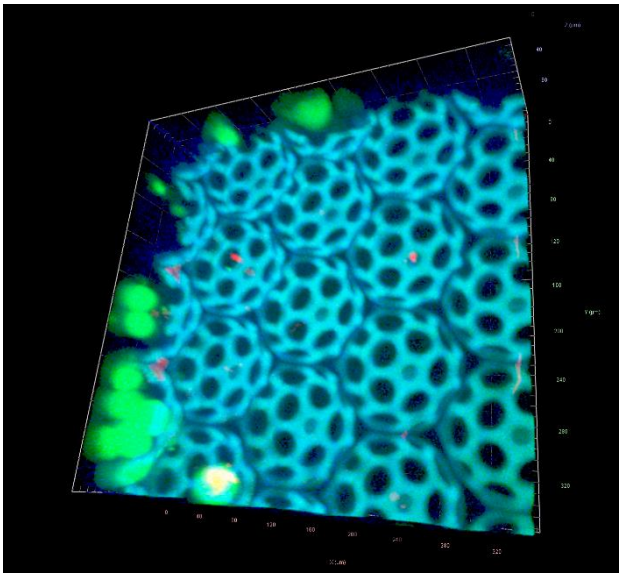

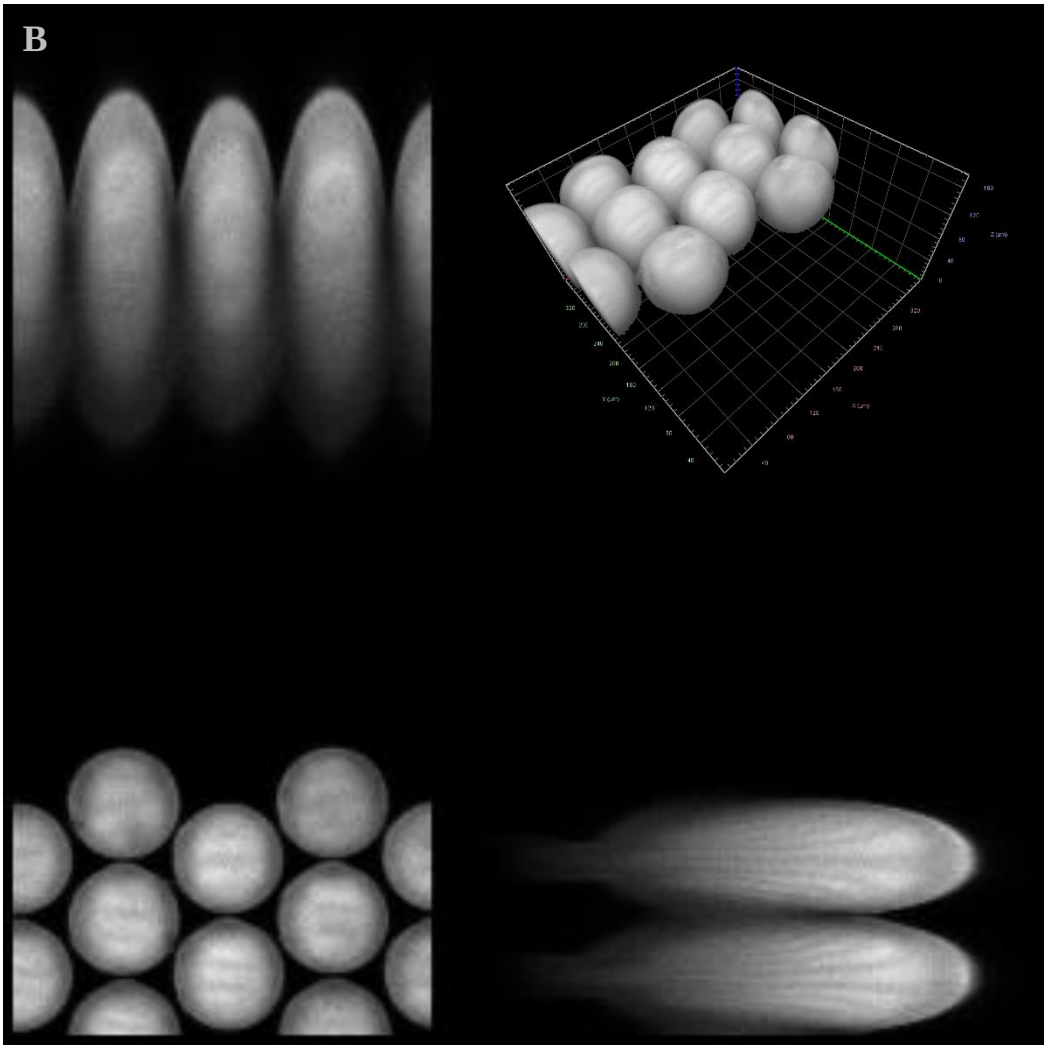


***Figure 4.15:*** *Confocal images of PETA 2PP structures. A) 3D confocal render of C80 buckyball arrays showing structure (Blue), live cells (green) and dead cells (red) at signal cut off at depth. B) optimised confocal microscopy of sphere arrays showing orthogonal projection of X, Y and Z planes with accompanying 3D render showing complete signal but warping and loss of signal at depth (Z-stack imaged with aid from Tim Self).*

Given the issue with loss of signal, technology that could image at depth was pursued. As such macroconfocal microscopy was explored for analysing cell morphology and structure colonisation. Macroconfocal would overcome issues with depth and could capture a larger field of view without stitching, although resolution capabilities may be less than typical confocal but still capable of tracking cell growth patterns. As such example images achieved with macroconfocal is demonstrated in figure 4.16. Images of iMSC monolayer growth with phalloidin based actin staining indicates resolution capable of visualising cell morphology and actin fibres as seen in figure 4.16A. Cut through Images from the middle of z-stack of a structure array with iMSC growth isolated by pHEMA shows patterns of cell growth with a colonised periphery and empty core, as demonstrated in figure 4.16B.

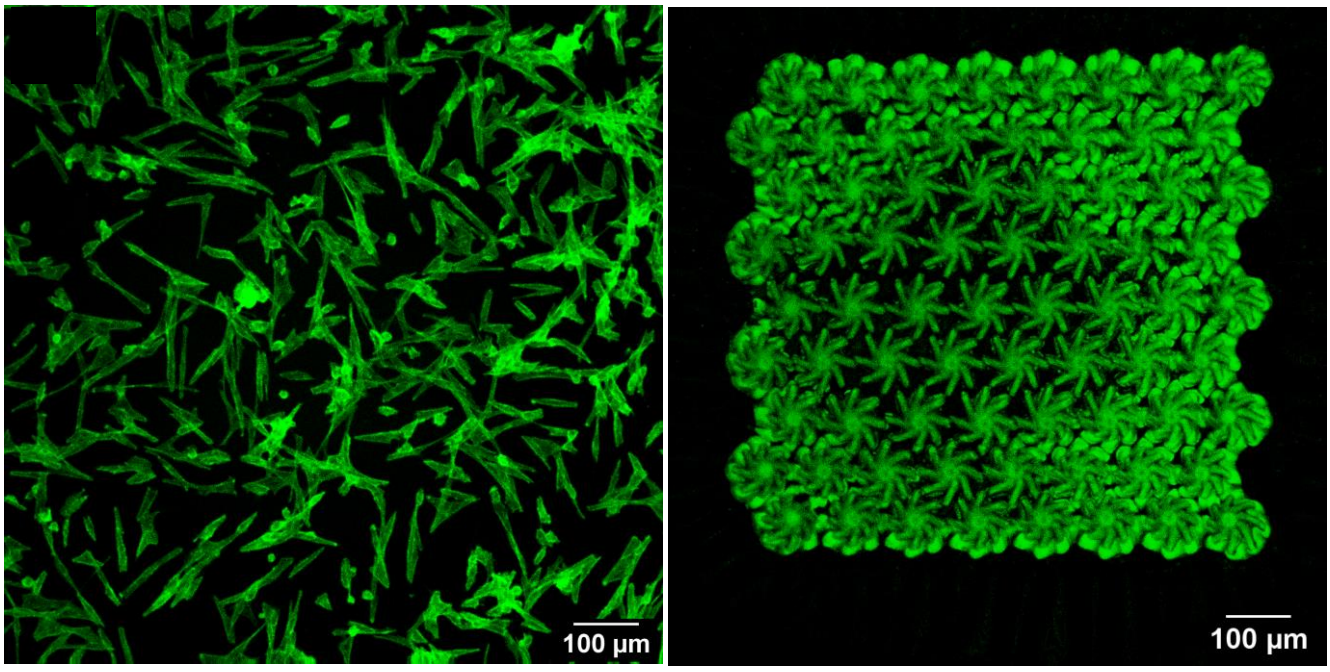


***Figure 4.16:*** *Macroconfocal of actin stained iMSCs. A) iMSCs growing as a monolayer on glass substrates. B) isolated cell growth to P*ETA *structures with a lack of infiltration into centre of the array and crossover of signal between phalloidin stain and structure autofluorescence.*

This microscopy indicates the difficulty with autofluorescence is maintained despite photobleaching in macroconfocal and although cell positions can be roughly seen they are difficult to distinguish and any attempts to measure growth amount or position through signal intensity will be marred by structure autofluorescence. However, issues

are solved with cell isolation and ability to visualise full structure height in a z-stack. Autofluorescence in conventional fluorescent microscopy is present in every channel due to the broad band of the filter cubes used, however screening of structures in macroconfocal revealed that autofluorescent signal in the 635 nm range was absent as seen in example images in figure 4.17.

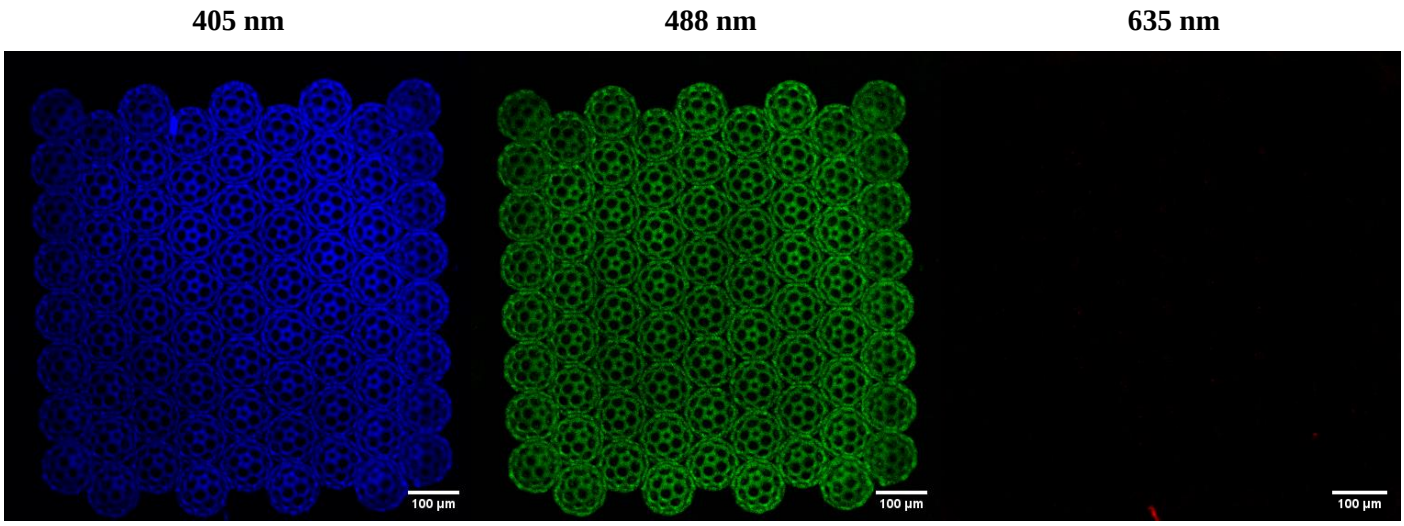


***Figure 4.17:*** *Macroconfocal imaged autofluorescence of PETA 2PP structures at 405 nm, 488 nm and 635 nm indicating a lack of autofluorescence in the 635 nm range.*

Given this autofluorescence behaviour it allows for the use of a red phalloidin stain in the 635 nm range that would allow for isolation of fluorescent signal to cellular material alone and allow full analysis of cell position throughout a scaffold with no interference from structure signal as seen in figure 4.18A. Additionally overlapping images from blue or green channels in which autofluorescence does occurs allows visualisation of cell position on structures as seen in figure 4.128 B and C. Given that fluorescence is now isolated the z-profile graphs of cell fluorescence and structure autofluorescence can be plotted to show cell growth patterns throughout the height of the structure in a 2D visual way. As figure 4.18D shows the cell growth is maximum around the 40-60 µm height region and is greater at the base of the structure and less colonised at the top. As Image analysis is possible given that these combined methods discussed allow production of z-stacks across all structure height with cell isolation to structures only and separated fluorescence signals for cells and structures.

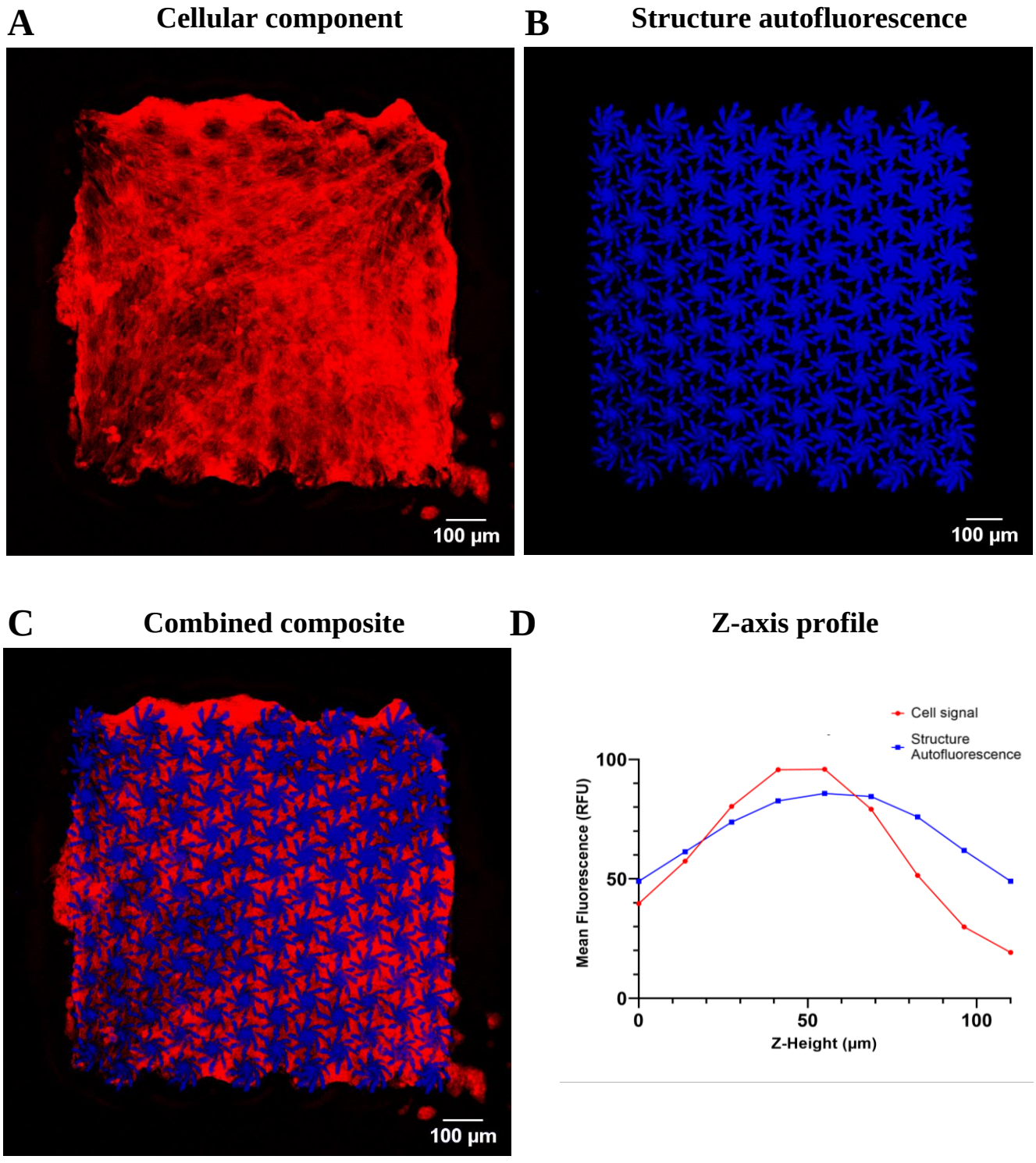


***Figure 4.18:*** *Analysis of macroconfocal z-stacks for PETA 2PP structure array with iMSC cell growth. A) Actin staining of iMSCs with red phalloidin growing over an array indicating fluorescent signal from cell growth only. B) structure autofluorescence z-stack. C) composite of combined channels to determine cell position relative to structures. D) Z-axis profile of mean fluorescence signal for red and blue channels indicating position of cell growth relative to structures in the Z-axis.*

# 4.5 Discussion

The purpose of this chapter is to explore the problems associated with cell culture on 2PP derived samples which prevent in depth analysis. As such methodology was developed to address these issues and allow full analysis of cell-structure interaction for future microcarrier design assessment.

Structures manufactured through 2PP go through a necessary development process of PGMEA and IPA soaking to remove unpolymerized monomer and residual chemicals. The 2PP standard development process may eliminate undesirable residues to an engineering standard but not a level that is suitable for cell culture. The data presented indicates that residual solvents or monomer trapped within structures are still left behind and pose problems for cell culture work without a more thorough processing strategy. This may be amplified in this research given the rapid writing profiles developed that utilise large gaps between laser travels within hatching of structures. Leaching study data indicates a reduction in viability between unprocessed and processed structures demonstrating that initial development is not sufficient in removal of residual chemicals to a level necessary for cell culture. Given that no structures are directly in contact with 2PP samples we can determine this negative effect to be due to something other than polymerised structure surface chemistry or shape. Fabricated samples present a small surface area and so the severity of this impact is reduced in leaching experiments as there is only a minute source of residual 2PP chemicals that is diluted in the media. In direct cell culture, diffusion would be emanating from structures and give a more severe localised effect. Assessment of viability was determined by an Alamar blue assay which measures metabolic activity by reduction of resazurin to resorufin and subsequent media colour change that is measured by fluorescence (367). Approximate cell number can be calculated from this metabolic data which has been proven to be equivalent to DNA based quantitation (359, 368). Alamar blue was chosen for assessment as studies have determined that is has a slight increase in sensitivity than ISO standard MTT assay and this was useful given the small amount of structures used (369).

The processing protocol devised involves multiple redundancies to ensure elimination of residual monomer or developer and attempts to ensure sterility, as such this protocol is thorough but time consuming. There is very little record of 2PP processing for cell culture in the literature, but the few documented protocols present with similar steps including washing and dual method of sterilisation with both UV and IPA (370, 371). The added steps in the devised protocol that differ from the standard regime seek to fully polymerise and remove any trapped monomer in the structure, which may be more apparent in these structures given the fast and unconventional method of fabrication. UV cure is used first as polymerisation of trapped monomer is preferred over removal so as to increase structural strength of the particle. Additionally, the overnight FBS and culture media incubation helps to better prepare the surface for cell growth with adsorbed protein that facilitates cell attachment (372). The data in figure 4.2 indicates the culmination of leaching tests and processing protocols to measure alteration to cell viability within the localised region of cell exposure to structures. Data indicates that post-fabrication processing techniques improve viability of cells in the vicinity of and in direct contact with 2PP structures and is a requirement for future cell culture.

Following development of a processing protocol that reduces interference from residual chemicals of structures appropriate biocompatibility testing of identified polymers could be explored. Initial attempts at identifying suitable polymers sought to find a system for screening of materials without need for lengthy fabrication in the 2PP system. Alamar blue assay would not be representative for 2PP derived films given that only a small area could be polymerised, due to slow fabrication speeds prior to optimisation, and surrounding cell growth on the glass substrate would obscure any result. The significant decrease in viability ($p<0.0001$) for materials polymerised under oxygen is due to incomplete polymerisation of the material. Whilst 2PP can polymerise in the presence of oxygen this is due to tight control of the focal spot and diffusion of oxygen radicals from stimulation of the PI (304). In large quantities such as films the radicals that are released upon exposure to UV light are scavenged by oxygen and as such an incomplete polymerisation occurs. To prevent this and produce a complete cure, films were produced under argon to eliminate any chance of radical scavenging. Whilst this led to a change from 2PP conditions it is essential to have a fully cured material to prevent cell death. Interestingly data appears to indicate that materials

polymerised by UV exhibit differences in behaviour and attachment of 3T3 cells in comparison to those polymerised by NIR in a 2PP system. Possibly due to the long wavelength of the Ti-sapphire NIR laser in comparison to the much shorter wavelength of UV light, as well as degrees of polymer conversion and possible patterning of the films due to laser travel lines (373). It has been documented that NIR light polymerisation offers advantages with less photodamage and less scattering than UV based curing systems which may be at play (374). It is also interesting to note with PETRA that under argon conditions cell attachment and number was much lower than that seen in 2PP samples, this may be due to the much higher viscosity of PETRA that may have hindered radical diffusion even under argon environments. However, this conclusion cannot be reliably drawn given that 2PP generated samples contain presence of two materials, the glass and the polymer, whereas in UV cured materials there is no choice for the cells. As such it was determined that for reliable polymer screening materials should be produced via 2PP.

Live/dead staining was selected as the means of viability assessment as it was the only method that could be used to isolate cell activity within the region of the polymerised film prior to production of cell isolation techniques. Data indicated acceptable biocompatibilities for all materials with viability of cells being over 90% in all cases, in comparison to glass controls PETA was the only non-significantly different material. This is in line with the literature that all these materials are biocompatible (300, 307, 323, 375). Whilst biocompatibility is essential for material use another important factor is the level of cellular attachment as structures that cannot be colonised by cells are not suitable for microcarrier production. Attachment levels were surveyed by image analysis and the measurement of surface coverage of cells in fluorescence images in figure 4.5. Results indicated the highest level of cell coverage and therefore attachment in PETA and PETRA materials and lowest for TCDMDA and PEGDA. Whilst low levels of attachment are expected for PEGDA, which has cell repellent properties, the results of TCDMDA are less understood (376). Results of TCDMDA attachment have partial disagreement with the literature as studies have reported good attachment (323, 377), similarly good attachment was seen in figure 4.4A under argon environments. Level of attachment seems to be influenced by not only the material itself but the surrounding material and what is seen may not be a lack of attachment but preference for surrounding glass substrate. Given the methods required for viability assessment the

level of attachment will inherently affect the reliability of cell viability measurements and samples with low attachment will exhibit a smaller sample of cells from which to determine viability. These difficulties may be influenced by the 2PP method but overall data has indicated an overall high level of biocompatibility and polymers that exhibit a high level of cell attachment.

Previously the only suitable cell investigations were done on 2D flat films for materials screening and the ability of cells to interact with 3d structures was uncertain given the avoidance of some structures seen previously. Initial data in figure 4.7 showed interaction of cells with the fabricated structures with growth over and within the structure. Given the nature of SEM the growth of cells internally cannot be imaged after growth over the upper surface encloses the structure. Investigation of the internal space of these structures could be probed with confocal microscopy or specialised technologies such as FIB-SEM which allows 3-dimensional SEM imaging (378). The use of 2PP for cell culture has been briefly explored before but specific geometry type explorations are limited. Of the very limited literature analysing use of buckyball like structures to culture cells have shown complete colonisation of structures similar to that seen in figure 4.7 but the phenomenon seen with repeated pore openings has not been documented (379, 380). However, geometry used in identified literature had sharper, thinner and much more angular architecture made from hexagonal and pentagonal shapes with large pore sizes, additionally the diameter of printed particles was in the range of 300 µm. This is different from the geometry employed in this study which is smaller, has more pores and struts that are much smoother and thicker relative to their size. The repeated pore opening seen in both ESEM and SEM is believed to be a naturally formed opening that is due to pressure relief within the enclosed space however examples or explanation of this cannot be found in the literature.

Probing of overall particle size was initially performed to see what size level of structure would prevent monolayer overgrowth as this would prevent geometry influence being established. Individual feature size is controllable within the determined optimum particle size but data retrieved was also initially used to determine which individual feature size would be most suitable for cell interaction. Hemispherical buckyballs were continued to be used to maximise interaction of cells with structures as with full particles only a very small portion of the structure would be able to act as an

entry route for cells growing in monolayer fashion. The data indicated that feature sizes within the 5-6 μm range and pore sizes of 13 μm gave the highest level of cell interaction. *In vivo* ECM porosity varies from 1-30 μm but optimal porosity in cell culture scaffolds will vary based on cell size and purpose of porosity with certain differentiation routes preferring certain pore sizes (250). Identified pore size fits within the range determined for optimal infiltration of fibroblasts within the literature and identifies that the controlling factor is based on nuclear deformation (252, 254).

Many commercially available microcarriers include a form of surface treatment or coating to improve cellular adhesion and proliferation often with collagen or other protein type coatings (222). Initially, coating with poly-L-lysine was conducted to act as a positive control for cell attachment and act as a forced measure to ensure cells experience the geometry of the structure. Poly-L-lysine augments cell attachment by enhancing electrostatic attraction of the ions within the negatively charged cell surface and the positive ions of the material surface (381). This technique has been seen in the literature specifically for the use of enhancing microcarrier adhesion. In a study be Shekaran *et al* coatings of both poly-L-lysine and fibronectin increased cell attachment from 69.4% to 78.3% (363). Others have used small amounts of platelet lysate to induce a greater level of attachment (382). As can be seen in the SEM images in figure 4.9. the increase in attachment here is far greater than the increase seen by Shekaran *et al*, largely due to the low level of attachment seen before. As expected, treated structures and underlying glass had a far greater level of cell attachment and proliferation than their untreated counterparts and this technique could be easily used to balance the level of attachment needed with the properties of a material that are not very prone to cell attachment. Despite the success and documented use of this technique in microcarrier design, for this study it is important to delineate the effects of microcarrier surface chemistry from the effects of microcarrier shape. Whilst surfaces should be optimised to allow better cell attachment the effects of poly-L-lysine make cell attachment possible on practically any surface and analysis to determine if enhanced cell interaction and expansion was due to shape or not would become very difficult to distinguish. As such a different and less aggressive form of surface modification was pursued.

Tissue culture plastic is oxygen plasma treated to aid in cell attachment and proliferation. In order to improve and promote cell attachment and interaction with structures, without a forced chemical attachment, the effects of plasma treatment on structures were investigated. Prior to treatment structures had a limited level of cellular interaction but interestingly whilst this increased after one minute and 10 minutes there was a decrease in effectiveness at the five-minute mark. It is theorised this phenomenon comes from the effects of surface etching, at one minute of treatment oxygen groups are deposited on the surface which improves cell adhesion. At five minutes the intensity of the etching begins to break down the surface layers of polymer exposing further polymer underneath with no deposition of oxygen groups. At 10 minutes however, this initial fragile surface layer has been etched away significantly enough that new oxygen groups are being deposited on the revealed surface, which again leads to increase in cellular attachment. This explanation seems likely based on the work of Seniutinas *et al* who specifically used oxygen plasma etching in repeated cycles on buckyballs fabricated in PETA by 2PP to etch away at the material and produce feature sizes at sub 100 nm beyond the limitation of 2PP by itself (383). Whilst cell culture reaction is not observed in the paper by Seniutinas *et al* it proves that surface material is being etched away by oxygen plasma treatment and made thinner with repeated cycles. Therefore, it is likely this is a similar reaction where at the five-minute point enough etching has occurred to break down the surface but not deposit further oxygen groups. Given that this treatment aided in cellular attachment but was still affected by structure material and shape a 10-minute oxygen plasma treatment was integrated into the postprocessing protocol and used in all future cellular experiments.

Despite efforts made to assess material biocompatibility and improve cellular interaction with structures the obstacles imposed by the 2PP method are still maintained and have limited some early experimentation methodology. The necessity of an underlying anchoring substrate, usually glass, gives two different chemistries and due to structure size surrounding monolayer growth limits measurement of cells actively experiencing the structure architecture. This issue has been raised in other 2PP based cell culture experiments with no identified solution (354, 355, 366). Ricci *et al* sought to compromise with this issue by increasing fabrication size and limiting cell culture space with a PDMS ring but could not fully eliminate interference from surrounding growth. This limited experimental testing methods to methodology that

could focus on a localised area, largely staining and microscopy, similar to how some aspects of this work has been handled (354). Maibohm *et al* imposed a different methodology by sputter coating structures and underlying substrate with gold so that surface chemistry would be maintained between surrounding monolayer growth and that of those in contact with structures. Whilst this maintained equivalent chemistries it did not account for the differences between those growing in a 3D space as oppose to those within 2D monolayers and so was still limited to localised examination (366). This issue is clearly demonstrated in figure 4.4a and figure 4.9a where most cells are seen growing around structures with little interaction, figure 4.11 stresses this polymer avoidance given the presence of glass indicating how iMSCs avoided polymer surfaces until high confluence is achieved despite optimisations and acceptable biocompatibility. As such a method to remove the interference of underlying glass and ensure any cell analysis is coming from those in contact with structures was sought. Despite the long history of pHEMA use for preventing cell adherence this has never been applied for this purpose despite the struggles documented in previous papers (353, 384). The application of pHEMA to 2PP fabrication and process of this novel technique is demonstrated in chapter 3. Figure 4.12 confirms the cell non-adherent behaviour of pHEMA with iMSCs when coated via the documented method as expected. As figure 4.13 shows this fully limits cellular growth to the fabricated structures removing much of the barriers to experimentation seen before. This method also allows for better observation of cell interaction and enables 3D culture. This image shows how cell interaction between structures differs with structure design and pore size, although future analysis will explore this aspect in more depth. This methodology could be adopted by other researchers as a more standard process to eliminate obstacles imposed on analysis methodology. Additionally, this method has dual functionality to act as a sacrificial structure releasing agent to free structures for microcarrier culture which will also be explored in a future chapter. However, despite the success of this method it does require further improvement to ease some of the added difficulties to the fabrication process and work of Ingram *et al* demonstrates how spin coating to achieve a thinner a more consistent layer could alleviate these fabrication difficulties (353). Additionally pHEMA networks have been shown to absorb and retain certain dyes (385) which could be utilised to eliminate refractive index issues in fabrication alleviating the need for manual interface calibration.

Structures produced by 2PP have a natural autofluorescence across all channels due to the photoinitiator presence in the structures. Typically, 2PP PIs are desired to have low fluorescence yield as the methods of excitation can act as a competitor for 2PP efficiency, however remnants of PI leading to autofluorescence are not uncommon (386). As such there is a large demand for PIs with high efficiency and low quantum yields and studies have identified that fluorescence can be reduced by integrating carbonyl groups that exhibit electron withdrawing effects (334). Whilst autofluorescence has been useful for measuring simple fluorescence overlap in 2D and locating structure presence through cell growth it also poses a lot of obstacles. In 3D imaging strategies to quantify amount of fluorescence or in cell morphological analysis, overlapping of signal by 3D structure autofluorescence obscures details and limits analysis. When using autofluorescence as a marker or as a template to subtract signal from other channels this limits the number of channels that can be used given that one must be maintained for this purpose. Ideally if structure autofluorescence was eliminated but fluorescence was needed to locate structure features polymers could be doped with a fluorescent molecule such as rhodamine for this purpose and limit the signal to one channel only. Of course, alternative 2PP PI's could be utilised to minimize this complication and there are many other available PI's but a lot of these also suffer with the same issue and Irgacure 369 has high reactivity which allows for rapid writing parameters as well as extremely common use in 2PP (298, 303). Other attempts to reduce this issue have sought to use NIR only fluorophores, molecular quenchers, PI free resins as well as photobleaching which was the method employed in this case (386) Photobleaching experiments demonstrated in figure 4.14 indicated successful reduction of autofluorescence in buckyball structures but when applied to structures of greater material thickness autofluorescence persisted due to lack of UV penetration at greater depths. As such full elimination of structure autofluorescence could not be achieved.

In depth high resolution confocal imaging of cells growing within structures was explored to determine cellular positions and morphology throughout the structure and assess which types of architectural features were interacted with. However, issues were found with loss of signal occurring about halfway through particle height as depicted in figure 4.15A. The issue encountered is likely just the limitation of confocal with samples used and signal loss is due spherical aberration, scattering and rapid loss of

signal at depth (387). Whilst many claim that signal is difficult to achieve at over 100 µm for any sample others claim that light penetration can go much further than this (388, 389). The use of water objectives to increase depth and tweaks to acquisition to improve depth allowed imaging of spherical carriers in figure 4.15B but whilst resolution was higher and maintained at certain depths as the orthographic view shows this level of continuity does not continue very far with the other half of the particle still struggling with maintaining signal. Overall difficulties encountered were likely due to light scattering induced by the 2PP structures. Multiphoton microscopy could be used to improve depth penetration as this method possesses twice the depth and is typically considered the best approach for imaging large samples, but this technology was not available at the given time (388).

Due to difficulties with imaging using normal confocal microscopy other methods were pursued and the option of macroconfocal became possible. Macroconfocal allows for imaging of much larger and thicker samples and as per figure 4.16 was capable of fully imaging microcarrier structures. Macroconfocal images of 2D monolayer cells in figure 4.16A showed impressive resolution and detail of cellular morphology and the example flattened z-stack image indicated how structure colonisation can be visualised with ease. Despite success with imaging over the full Z-axis of the structure now possible the issue with autofluorescence was once again made apparent. Whilst cell growth patterns in the example in figure 4.16B can be seen it is difficult to delineate in 3D as to the exact line between structure autofluorescence and cellular growth. However, testing noted that whilst standard filter cubes may exhibit fluorescence in every channel the confocal setup has a much more attuned control of measured wavelengths. As per figure 4.17 it was found that signal at 635 nm was absent with no structural autofluorescence perceived. As such a phalloidin stain within this range was used as a method to image full structure depth with signal only from cellular material which could allow better visualisation of cell growth patterns and allow measurement of cell signal via fluorescence and image analysis. An example plane from a z-stack obtained with this method, as shown in figure 4.18 indicates how cellular colonisation of microcarrier arrays can be imaged without interference and coupled with cell isolation techniques eliminates any surrounding growth. Structure autofluorescence can still be collected in separate channels and used to overlay images as seen in figure 4.18C to visualise structure position within cells. Most importantly this allows separate

measurement of fluorescence as can be seen in the graph of figure 4.18D where it can be clarified that most cellular growth is present at 40-60 μm and that growth is higher at the base of the structures rather than the top. This is in line with expectations given the force of gravity in culture.

The culmination of these experiments allows an optimised and novel methodology to fully analyse 2PP structure-cell interactions without any obstacles or limitations that are usually imposed by 2PP. 2PP structure analysis strategies have never been fully explored or set out within the literature and these techniques could be used by many other researchers to improve upon their research and gain extra freedom in experimental methodologies involving 2PP fabricated constructs.

## 4.6 Conclusion

The work presented in this chapter focused on establishing methodology for cell culture of 2PP structures without analytical limitations as well as optimisation of materials and surface. For academic and industrial purposes this research presents a framework of optimisations for culture and structure imaging as well as novel techniques for cell isolation. Overall, a lot of the obstacles imposed by 2PP structure analysis have been overcome and many authors who have been limited by these factors could be supported by the research presented. With 2PP technology becoming cheaper and more prevalent for research these issues will become more prevalent and the research presented could have great impact on methodology used in future 2PP cell studies.

A summary of key findings is outlined as follows. It was observed that optimisation to 2PP structure post-processing strategies increase cell viability in presence of structures through full removal of residual developer and trapped monomer. Additionally biocompatibility testing identified all materials used were biocompatible with greatest level of cellular adherence in PETA and PETRA materials. Surface coating identified methods to increase cell compatibility with materials and promote microcarrier attachment without forced chemical interaction. The developed pHEMA cell isolation strategies proved effective in limiting cell growth to structures allowing greater freedom of methodology and overcoming a major barrier in 2PP cell studies. It was determined that autofluorescence could be reduced in structures through

photobleaching but was not successful in thicker structural designs. Macroconfocal microscopy was shown to be an optimal and reliable method of structure imaging where other confocal techniques struggled due to structure induced light scattering. Lack of autofluorescence at 635 nm was identified and techniques to use a red phalloidin allowed imaging of stacks without interference from structure autofluorescence, overcoming another 2PP barrier. Finally, 3D models with varying architectures and feature types for microcarrier designs were produced for future microcarrier testing.

# 5. Investigating cell interactions and expansion with microcarrier designs.

## 5.1 Introduction

Cells expanded via microcarrier culture show subtle but different phenotypical traits from those that have been expanded on flat surfaces via monolayer growth (204). In MSCs these changes can include variation to cell size, morphology, viability, proliferation rate, gene expression, cell surface markers, differentiation potential and secretory profile (216, 390-392). Given these changes to MSC characteristics induced from microcarrier culture there can be variation in cell behaviour which can lead to different outcomes in therapeutic uses. Whilst many induced changes can have a positive outcome on cell behaviour the observations and experiments with planar cultures becomes less applicable to microcarrier expansion strategies (204). As such, the differences explored between planar and microcarrier culture may give indication of the type of changes that could also be seen between intricate architectures of different experimental microcarrier designs.

It has been noted by many that in microcarrier culture there is an extended lag phase in cell growth than in comparison to planar culture which indicates a greater adjustment period of cells to the culture environment (391, 393, 394). Additionally planar cultures exhibit a higher proliferation rate with a reduced cell doubling time in comparison to 3D microcarrier culture (395). Largely this disparity in proliferation rate is due to that long lag phase and when only comparing exponential growth phases microcarrier cultures compete at a level comparable or greater than planar culture (204, 395). In addition to this the exponential growth phase of cells cultured in microcarrier systems can be extended and sustained for long periods with the addition of fresh microcarriers (216, 396). Microcarrier culture can also change differentiation capacity in comparison to planar culture. Several studies have noted a far greater capacity for osteogenic and chondrogenic differentiation in microcarrier cultured cells with a decreased aptitude for

adipogenic differentiation (66, 397). In particular increased expression of early osteogenic markers such as ALP, RUNX2 and osterix have been seen in microcarrier culture indicating a greater inclination towards osteogenic lineages (363). Migration capacity is also thought to be affected by microcarrier culture with cells exhibiting smaller sizes and higher CXCR4, a chemokine receptor linked to cell mobility, than planar cultures suggesting that culture in this way favours migratory capability (395, 398). Additional changes to immunomodulatory behaviour, surface markers and DNA content has been documented in MSCs cultured via microcarriers (216, 390-392, 399). When cues experienced enable enhancement of desired aspects, such as growth rate, it is important to ensure that these do not disrupt cell quality or therapeutic potency (204).

The observed changes between culture types are derived from the 3D culture microenvironment in which cells encounter many biophysical cues that can alter cell behaviours. These biophysical cues include aspects of the microenvironment such as porosity, stiffness, curvature and surface roughness which can be sensed by cell components such as integrins, focal adhesions, adherens junctions, cytoskeleton and the nucleus triggering a variety of mechanotransduction pathways as previously reviewed in section 2.6 (26, 244). For microcarrier culture additional complexity is also introduced by shear stresses, dynamic environments and microcarrier collisions (400). All these signals are less apparent or non-existent in planar culture where cells have a flattened morphology and receive media delivered nutrients and growth factors all from one side whilst the other flattens on the substrate (401). In complex architectures there is an intricate storm of biomechanical signals with compounded stimuli and changes induced by the combination of curvature, stiffness, porosity, topography and shear stresses acting at once which leads to cell outcomes that are difficult to predict.

The final step in the methodology development was to produce 3D microcarrier designs for fabrication. These architectures were predominately designed to present features, identified in the literature, that are known to affect cell growth and differentiation with the aim of enhancing cell expansion greater than flat surfaces and modulating MSC differentiation. As such designs explored are collated in figure 5.1. These structures will be screened and analysed for cell effects within this chapter.

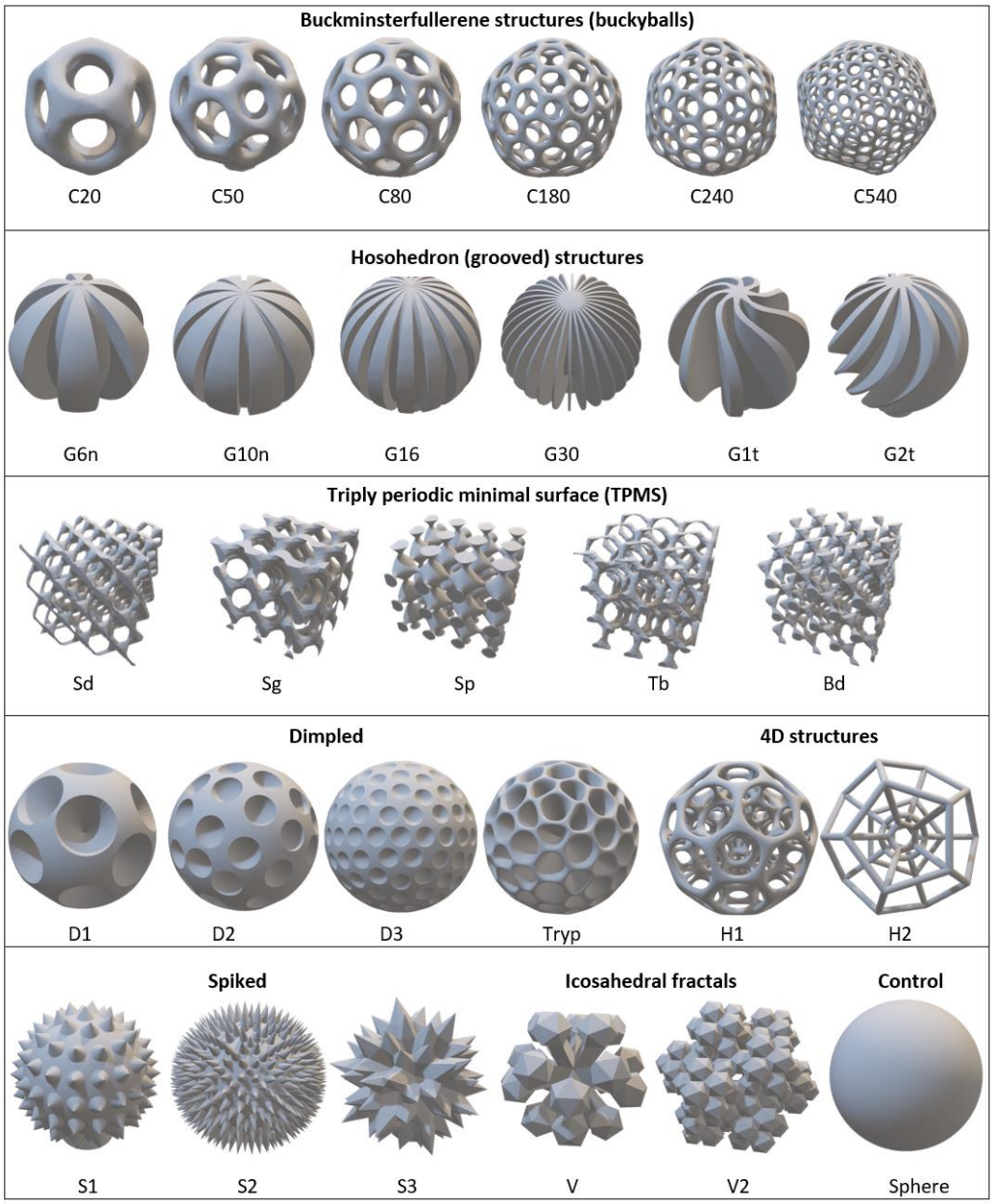


***Figure 5.1****: 3D renders of microcarrier designs with complex and specialised architectures. Model variations are grouped on geometry type and include buckyball, grooved, TPMS, dimpled, 4D, spiked and icosahedral fractal variations as well as spherical control.*

Aa set of 3D designs outlined in figure 5.1 was produced with a variety of feature types to probe interactions with cells. Given that some limitation for fabrication still exists the number of designs had to be limited and so a selection of models exploring different feature types was pursued. Buckminsterfullerene structures otherwise known as buckyballs were designed as a hollow equivalent to porous microparticles with a variation to pore size and number. Grooved structures all display a channel or groove in

which cells can align, each present with a different frequency and size of groove. The literature has repeatedly indicated that surface grooves of varying scales can direct cell growth and alignment (259-261). It has also been established that this alignment derived from channel topography can induce osteogenic commitment (402). As such grooved structures seek to test this factor in application of microcarriers. Additionally, grooves can provide surface protection from shear stress and surface collisions particularly in the case of G1t and G2t designs that, whilst designed to induce further cellular torsion in aligned cells, also work in propeller like fashion to spin and negate shear stress in free microcarrier culture. TPMS models exhibit regularity in architecture that can be extended in any direction and has zero mean curvature whilst also providing large surface area to volume ratios. These models have been explored in the literature previously for these characteristics as well as their load bearing mechanics and degree of porosity (403, 404). A selection of schwartz, tubularG and gyroid models are included with the main premise tested being the high level of surface area in comparison to other structures.

Given that microcarrier technology was initially designed to only provide increased surface area this is an important feature to test. Dimpled structures exhibit recesses of different frequency, depth and therefore curvature as well as a much deeper irregularly pocketed variant. Similar pockets or crypts are seen in natural tissues such as the intestine or corneal limbal epithelial crypts which can act as a stem cell niche (405, 406). These geometries again seek to provide surface shelter from collisions and shear stresses (217). 4D structures have limited variations and are typically included as an extension to buckyball type structures with further internal geometries for further colonisation space within the particles but may restrict cell migration. Spiked structures are lesser explored in the literature but were included to probe feature reaction as well as to investigate claims that spike structures can enhance stem cell differentiation and growth factor secretion (407). Icosahedral fractals were included for high surface area, repeated geometry delivery and as a niche to provide shelter from surface collisions. With these designs a control sphere was included as a comparison against a typical microcarrier architecture. With designs produced based on mechanobiological aspects of the literature as well as optimisation of cell culture strategies which removed experimental barriers the full exploration of microcarrier designs on MSC expansion was now possible.

## 5.2 Aims and Objectives

This chapter investigates the effect of intricate microcarrier architecture on cell behaviour by utilising designs and techniques developed in chapter 5. The overarching aim of this chapter was to identify geometries that lead to a high level of cell expansion in comparison to spherical controls and determine if these have any effect on stem cell phenotype. Initially effects of porosity on 3T3 cell structure interactions and infiltration through pores was observed before further investigation with iMSCs. Sweeps of microcarrier designs with iMSCs were conducted to find structures that lead to a high level of cell interaction which could be carried forward. Highlighted structures were produced at larger scale for morphological analysis in arrays and determination of expansion yield through DNA quantitation. Further aspects of cell behaviour over the expansion period such as protein production and osteogenic markers were reviewed before moving on to techniques for free microcarrier culture under static conditions. Finally, three designs representing a range of expansion performances were used to culture iMSCs in static microcarrier culture for analysis of stem cell markers and phenotype to determine if expansion affects the qualities of the stem cell. The contents of this chapter provides insight into the types of architecture that can result in increased cellular expansion and probes their effect on stem cell phenotypes. To achieve this the following goals were established:

1) Determine the effect of porosity on 3T3 cell interaction and structure infiltration.

2) Investigate if certain microcarrier designs lead to a higher level of cell interaction and engagement with geometry than others for further testing.

3) Explore microcarrier designs for structures that produce a higher expansion yield than spherical controls.

4) Investigate ways in which microcarriers effect cell properties such as protein production, osteogenic commitment, and stem cell surface markers.

## 5.3 Materials and Methods

The following methodologies were used in this chapter in addition to those presented in section two materials and methods.

### 5.3.1 Cell digestion

In order to analyse DNA quantitation, ALP activity and BCA cell lysates were produced through cell digestion. Media was removed from samples and cells washed three times in PBS. Cell digestion buffer was formed from sterile 1M Trizma hydrochloride solution pH8 (sigma) diluted at 15% v/v in sterile distilled $H_2O$ with addition of 1% v/v triton x-100. Solution was vortexed for several minutes to ensure mixing of triton component and was used fresh without storage or reuse. For typical microcarrier array growth in six well plates, 1ml of cell digestion buffer was added which was enough to fully cover samples and was then refrigerated overnight. Following overnight refrigeration, three cycles of freeze-thawing was achieved through repeated transfer between -80°C freezers for one hour and 37°C incubators for 15 minutes. After final thawing the structure was mechanically disrupted and scraped followed by transfer of contents to microfuge tubes and subsequently vortexed. Samples were then centrifuged at 10,000 xg for 5 minutes and supernatant transferred to a fresh tube as the cell lysate which could then be stored at -80°C.

### 5.3.2 DNA quantification

DNA quantification from cell lysates was performed using the Quant-iT high sensitivity dsDNA assay kit (Invitrogen). Working solution was produced through diluting supplied reagent at 1:200 v/v in buffer solution. 180 μL of working solution was added to each well of the 96-well plate with 20 μL of lysate to make a total volume of 200 μL. The eight supplied λ DNA standards at 0, 0.5, 1, 2, 4, 6, 8, and 10 ng/μL were loaded into wells in place of experimental lysates in order to form a standard curve. Samples were prepared in triplicate and kept shielded from prolonged exposure to light. Samples were then transferred to a plate reader with shaking function for 10 seconds to ensure thorough mixing of components. Plates were left for 10 minutes to ensure conjugation of DNA before fluorescence reading at $\lambda_{ex}$: 480 nm, $\lambda_{em}$: 530 nm.

Fluorescence values were converted to ng of DNA with a standard curve generated from the eight DNA standards. Recorded DNA values were multiplied to represent the full DNA amount extracted within the 1ml of cell digestion buffer from each sample.

### 5.3.3 Osteoinduction of MSCs

Osteoinduction of iMSCs was achieved over four weeks to match expansion period using incubation in standard osteoinductive media upon cells grown in basal media reaching 70-80% confluence. Basal DMEM media described in section two was supplemented with 5mM beta-glycerol phosphate (βGP) and 50 µg/ml ascorbic acid 2-phosphate (AA-2P) along with addition of 10 nM of corticosteroid dexamethasone. Samples were washed and media replaced every 2-3 days.

### 5.3.4 Measurement of ALP activity

Measurement of ALP was conducted by use of a Pierce pNPP Substrate Kit (Thermo Scientific) which was used according to manufacturer's instructions. The supplied 5 mg tablets of pNPP were dissolved in 5ml of diluting buffer consisting of 20% volume diethanolamine buffer and 80% volume $dH_2O$. 20 µL of cell lysate, described in section 6.3.1, was added to a clear 96 well plate with further addition of 180 µL of prepared pNPP substrate followed by incubation at room temperature until a slight colour change from colourless to yellow was observed or until 30 minutes had passed. Absorbance was measured at 405 nm every minute for 30 minutes to form activity over time. Absorbance was converted to pNP via a standard curve, yielding nmol pNP/min and normalised to DNA content.

### 5.3.5 Total protein measurement through BCA assay

Total protein was investigated using a Pierce BCA Protein Assay Kit and conducted using manufacturer instructions. 25 µL of each protein standard ranging from 0 -2000 µg/ml was added to a 96 well plate in triplicate, additionally the same volume of unknown samples were added to the well plate in triplicate. Working solution was produced through mixing supplied reagents A and B at a ratio of 1:20. 200 µL of the working solution was added to each well and mixed thoroughly on a plate shaker for 30

seconds. The plate was then incubated at 37°C for 60 minutes before cooling to room temperature. This increased incubation time from standard protocol was to increase sensitivity of assay due to the small sample size. Absorbance was then measured at 562 nm on a plate reader and values for unknown samples determined from standard curves generated from protein standards.

### 5.3.6 Mesenchymal stem cell verification by flow cytometry

Analysis of iMSC surface markers was completed on the cell line prior to expansion and then after three weeks of cell culture on microcarriers using a human mesenchymal stem cell verification multi-colour flow cytometry kit by R&D systems. The kit is based on ISCT criteria (62) and contains three conjugated antibodies CD90-APC Mouse IgG2A; Clone Thy-1A1, CD73-CFS Mouse IgG2B; Clone 606112 and CD105-PerCP Mouse IgG1; Clone 16670. The negative marker cocktail consists of CD45-PE Mouse IgG1; Clone 2D1, CD34-PE Mouse IgG1; Clone QBEnd10, CD11b-PE Mouse IgG2B; Clone 238446, CD79A-PE Mouse IgG1; Clone 706931 and HLA-DR-PE Mouse IgG1; Clone L203. Isotype controls for determining non-specific binding and a staining buffer were also supplied. Cells grown on microcarriers or monolayer controls were released through standard trypsin EDTA enzymatic digestion collected and then centrifuged at 300g for 5 minutes to collect cells. Cells were then resuspended and washed in the provided staining buffer, cells were then counted and 1 x $10^5$ transferred to a separate tube before further centrifugation at 300g for 5 minutes. Cells were then resuspended in 100 µL of staining buffer supplemented with 10 µl of each positive antibody and 10 µL of the negative marker cocktail. For isotype controls the same format is followed but with addition of isotype antibodies. All in one multicolour flow cytometry can be conducted from one combined sample as each antibody is conjugated to a different fluorophore with varying emission spectra per kit design. Samples were incubated for 45 minutes in the dark at room temperature for binding to occur. Following this cells were spun down again and resuspended in 400 µL of staining buffer and were ready for flow cytometry. Flow cytometry was conducted using an 8-color MACSQuant-10 flow cytometer from Miltenyi Biotec with compensation for spill over fluorescence from multiple fluorochrome use. Isotype controls were used to determine quadrant boundaries for non-specific binding. Data was analysed using FlowJo flow cytometry analysis software.

# 5.4 Results

### 5.4.1 Porosity investigation

Early investigations focused on the effect of pore size in buckyball structures for cell interaction and infiltration. This experiment was conducted in small arrays prior to 2PP optimisations and culture techniques in order to examine the effect of pore size on cell growth. An array of buckyball porosity variations was produced in PETA and seeded with 3T3 cells and imaged with SEM to observe cell behaviour to structures and pore sizes. Samples were fabricated as 100 µm diameter buckyball hemispheres in small arrays of each variation outlined in section 5.4.8. In each design the size of pores was increased, ranging from 6 µm up to a maximum size of 35 µm. Feature sizes and structure physical information is documented in table 5.1.

| Variant | Pore size (µm) | Approx. Strut length (µm) | Approx. Strut Diameter (µm) | Surface Area: volume ratio ($\mu m^{-1}$) |
|---|---|---|---|---|
| C20 | 35 | 25 | 12 | 26.1 |
| C50 | 28 | 20 | 9 | 40.3 |
| C80 | 21 | 15 | 7 | 53.4 |
| C180 | 15 | 11 | 5 | 81.5 |
| C240 | 11 | 8 | 3 | 93.7 |
| C540 | 6 | 5 | 2 | 141.6 |

***Table 5.1:*** *Buckyball design features sizes and Surface area to volume ratio values.*

After culture for five days 3T3 cells, presented in Figure 5.2, showed very little interaction with C20 variants with largest pore size and struts. C50, C80 and C180 variations with pore sizes of 15-28 µm seemed to allow the highest degree of infiltration from SEM analysis alone. Cells interact with other structures but grow more at the surface as is seen in structures C240 and C540 as pore sizes were in the range of only 6-11 µm. Colonisation occurs all around and in between buckyball structures, as seen in figure 5.2A, and indicates that neighbouring arrays don't prevent spreading of cells. At an individual level structures do not prevent cells spreading to the centre of the array. Substantial growth is marked by a large covering of cellular growth over the surface that interacts with multiple pores or features and not those that only have one or two individual cells on the structure surface.

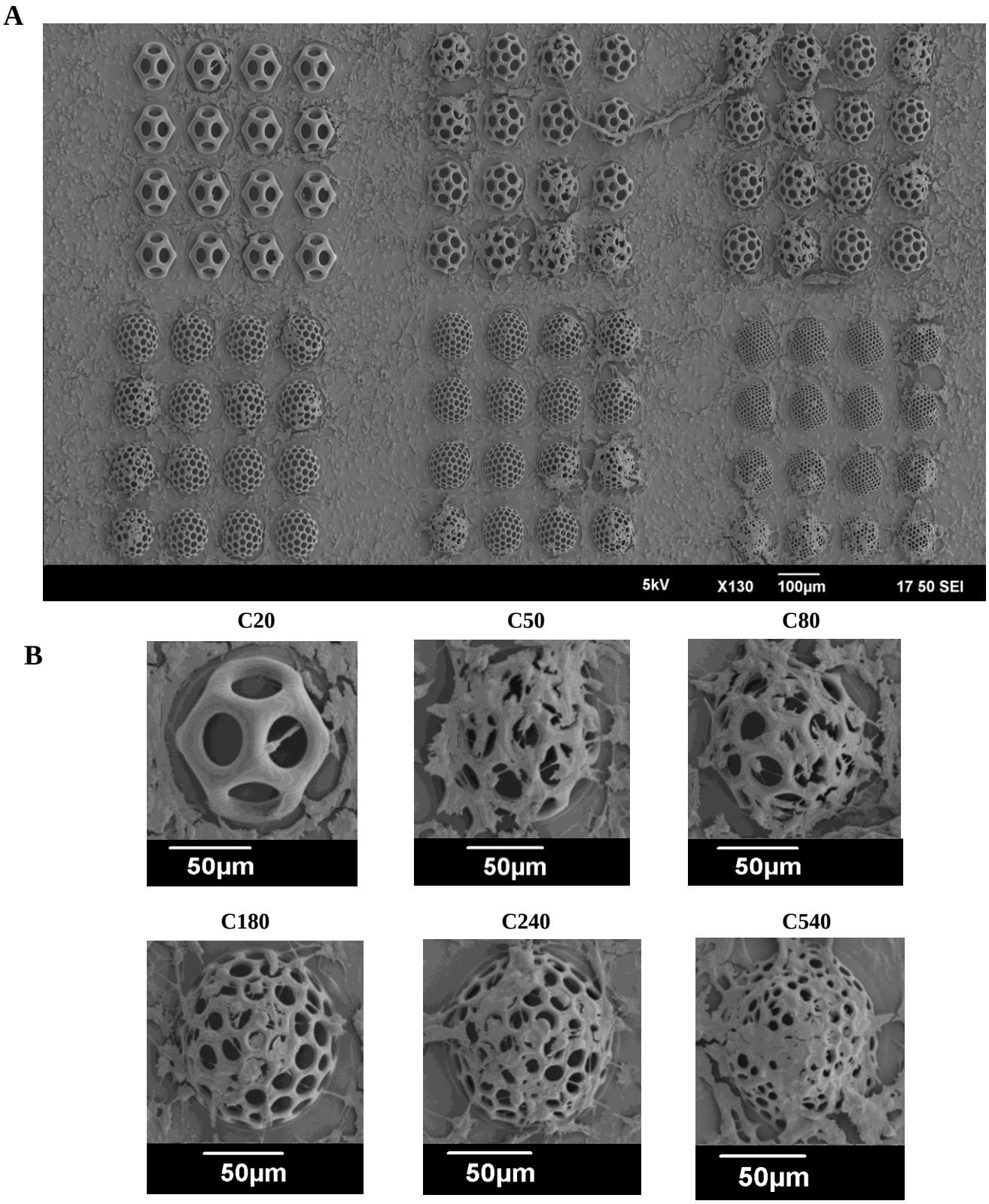


***Figure 5.2:*** *PETA Buckyball porosity 2.5D sweeps with 3T3s.* ***A)*** *Full buckyball 4x4 array SEM showing level of cellular interaction with structures indicating least interaction in C20 variations.* ***B)*** *representative higher magnification SEM of individual structures that show the highest level of confluence in each variant to visual cell morphology and positions.*

Substantial growth is seen in 0 of 16 C20 structures, 7 of 16 C50 and C80 structures, 5 of 16 C180 and C240 structures and in 8 out of 16 C540 structures. Figure 6.2B shows higher magnification SEMs of example structures that have substantial cell growth for analysing cell morphology and growth patterns. C50 and C80 structures show that single cells were unable to fully cover a pore alone and have more interaction with the perimeter of the pore. These cells often appear more angular and stretched across features. C240 and C540 structures show a more consistent growth of multiple cells spreading across the surface of features and can cover pores more easily, these cells appear more flattened and less angular than those growing on C50 or C80 structures. C180 structures exhibit qualities similar to both described cell morphologies. Cells were able to bridge across pore gaps but do not have size to fully cover them, depending on position some cells were angular whilst others have a smoother surface covering morphology. One limitation of the SEM was the inability to image the internal areas of the structure, as such growth was only seen from an outside perspective. Confocal Microscopy was pursued to visualise structure interior and level of cellular infiltration.

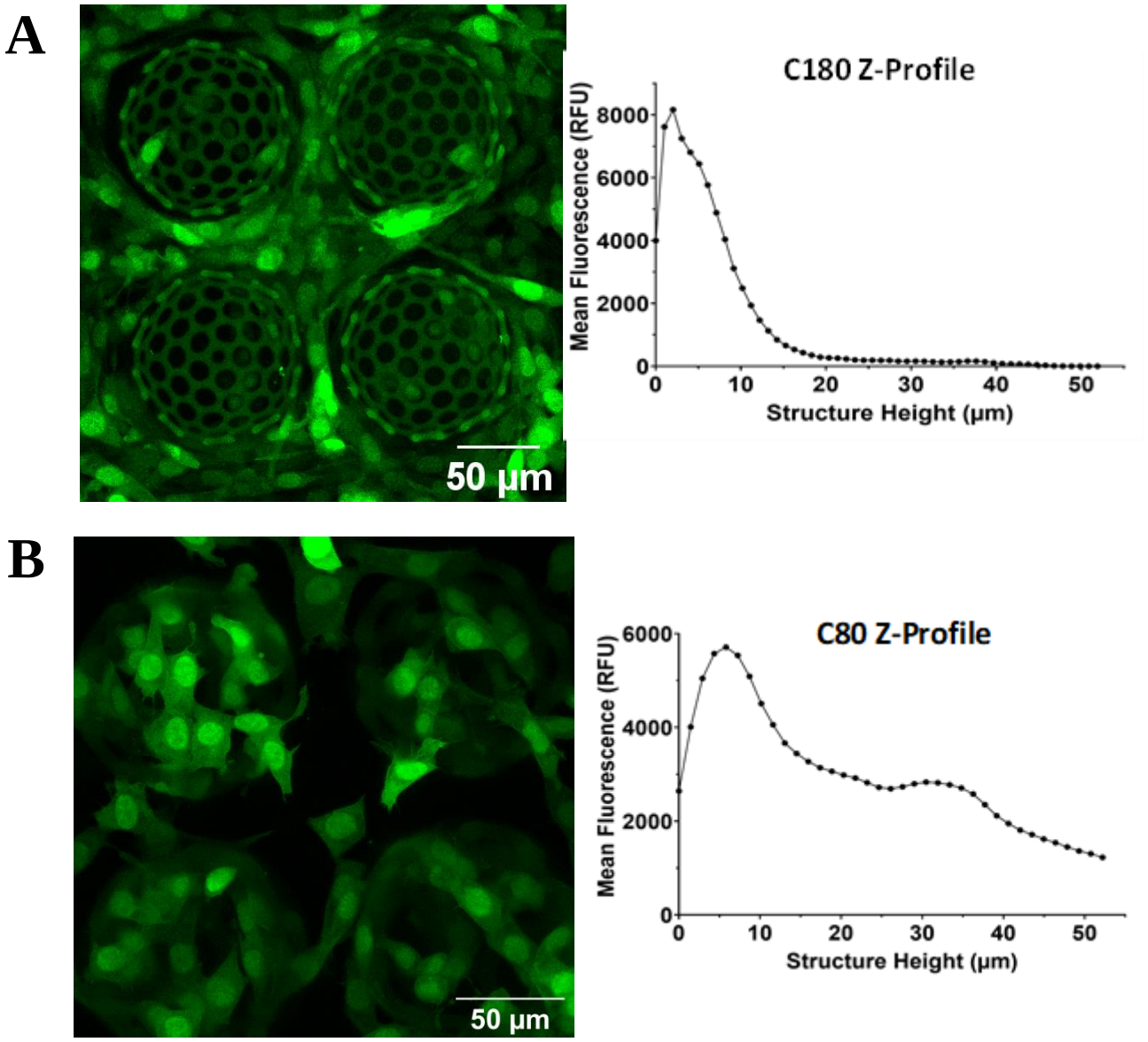


***Figure 5.3:*** *Confocal microscopy of GFP-3T3 fibroblasts seeded onto PETA C180 and C80 buckyball structures after 4 days in culture. A) Z-projection of C180 -3T3 stacks showing lack of cell infiltration. Z projection graph maps signal over height showing loss of fluorescence after the first 10 µm. B) Z-projection of C80 -3T3 stacks showing full internal colonisation of structures. Z projection graph shows the highest level of cells in the first 10 µm and then a lower but maintained level of signal over the rest of the structure*

Confocal microscopy of buckyball hemispheres at the precipice of cellular infiltration, with C80 structures and C180 structures was pursued. C180 confocal microscopy, shown in figure 5.3A, indicated little infiltration of cells into the structure interior and minor growth on the surface. Z-profile graphs represent distribution of cells over the Z axis and shows fluorescent signal only within the first 15 µm of structure height and low signal further throughout as can be seen in the images. C80 structures however, shown in figure 5.3B, indicate infiltration of cells to the interior of structures and 3D renders of stacks which were described by Z-profile graphs indicate growth of cells throughout the entirety of the height of the structure. Z profiles show an overall decline in signal throughout height, however in comparison to C180 the C80 signal is much greater even at the highest structure point still maintaining roughly 30% of the maximum signal. This analysis indicates that cellular infiltration is achieved early in culture within C80 structures with pore diameters of 21 µm but that this level of infiltration is not seen in C180 structures with a pore diameter of 15 µm.

To confirm infiltration of cells across a larger scale with movement through multiple structures a $1mm^2$ full scale C80 buckyball scaffold design was fabricated. This larger scaffold was seeded with 3T3 cells in a localised fashion to the glass substrate surrounding the scaffold and not directly on top of the scaffold, this would allow natural spreading of cells from monolayer fashion into the scaffold and prevent vertical entry during seeding. This seeding method ensured that level of migration through the scaffold could be observed. Fluorescence microscopy in figure 5.4 indicates infiltration and migration of cells through the scaffold and presence of cells towards the centre of the structure after four days, indicating level of movement through pores is not hindered by multiple structures. Overall buckyball structures were screened to confirm infiltration of 3T3 cells as an analysis of porosity influence on cells and found that infiltration is most likely in C50 and C80 designs or pore sizes around 21-28 µm.

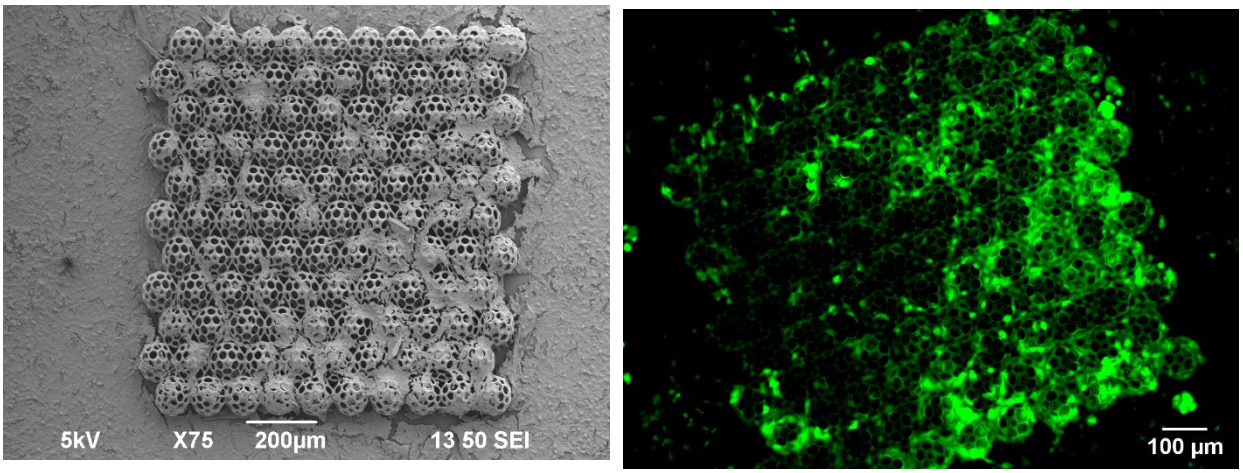


***Figure 5.4:*** *Infiltration and migration of 3T3 cells through a PETA C80 scaffold after four days of culture. Fluorescence and SEM microscopy of the same scaffold indicating level of visual infiltration and movement of cells through scaffold as between the two different methods.*

### 5.4.2 Architecture sweep

SEM analysis of the designs generated and outlined in section 5.4.8. was pursued to identify geometries that led to a high level of cell interaction with structure features. Arrays of 25 structures per each of the 29 designs with clearance of 200 µm in all directions were fabricated in PETA, postprocessed and then subject to seeding with iMSCs and cultured for five days. Fixation and SEM imaging after this culture period indicated consistently more structure interactions and cell coverage in several structure designs in comparison to others. Figure 5.5 indicated example SEM microscopy of the difference in structure interactions seen across the sweep between three example positive designs and three negative designs. Positive designs were geometries that consistently led to a high cell confluence across the majority of structures in the 25 array repeats. Not all structure types can be shown given the large number of designs screened and number of replicates, as such images in figure 5.5 were only examples of structures that exhibited different levels of cell interaction. Positive hits saw cell growth over a large percentage of surface structures and interaction with surface features. In example C80 structures the growth of cells internally can be viewed through pores. In example G1t designs the growth of cells stretches between the space of the grooves as designed. similarly in the icosahedral fractal designs cells grow within the internal

struts forming a niche between surface icosahedrons. Negative designs showed a lack of structure interaction or very little interaction in most repeats. Example negative designs in figure 5.5. show only a small amount of interaction at the base of structures as the monolayer growth met the structure base this is particularly noted in spiked examples. The example dimpled variation shows cell coverage of several of the surface pockets but only a small portion of the available spaces were colonised and most of the structure is free from cell growth. G16 structures had a small level of interaction as cells were seen growing around the circumference of the particle perpendicular to the grooves. These examples indicate the typical difference in cell interaction between different designs and cell behaviour for each design were consistent across most or all of the 25 repeats for each structure. The results of this experiment identified seven structure designs to take forward for further testing, these were largely the best performing structure or structures from each category that supported greater cell coverage but excluded dimpled and spiked variations that repeatedly showed a lack of structural interaction in all variations. The final designs taken forward were C50 and C80 from buckyball designs, G6n and G1t from grooved designs, Sg from TPMS designs, H1 from 4D structure designs and V from icosahedral fractal designs. A sphere was carried forward as a spherical comparison to a typical microcarrier morphology (3D control) and flat films were also carried forward as a 2D control. Full microscopy data across all designs is shown in appendix 3.

**Example Positive Designs**

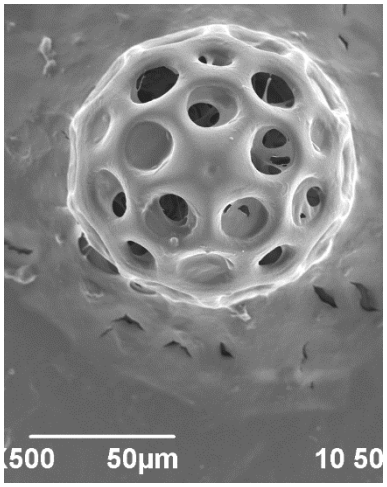


**C80 Buckyball**

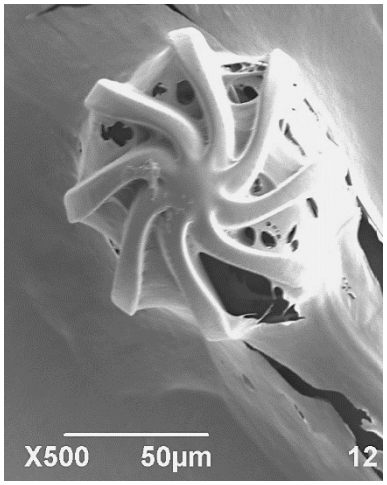


**Grooved -G1t**

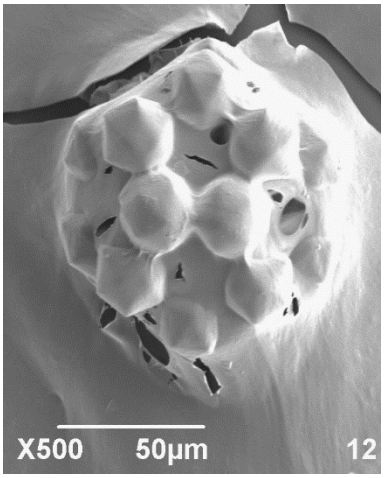


**Icosahedral fractal -V**

**Example Negative Designs**

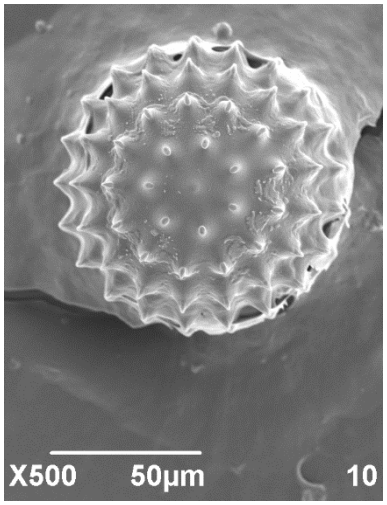


**Spiked- S1**

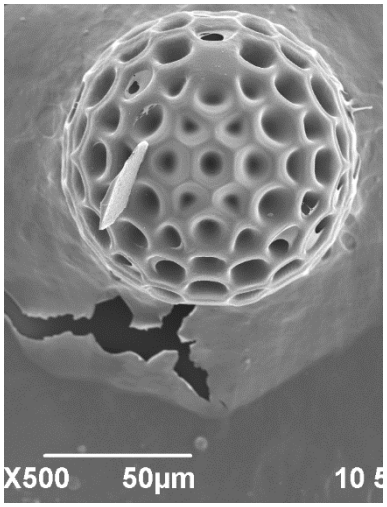


**Dimpled- Tryp**

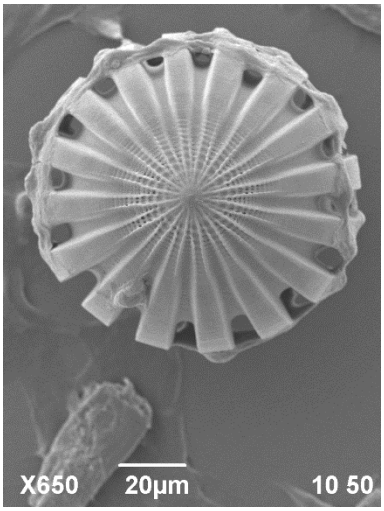


**Grooved- G16**

***Figure 5.5:*** *Example SEM microscopy of PETA structure design sweeps. Example designs that supported cell adhesion with substantial cell interaction with structure features in C80, G1t and V designs. Examples that have little cell interaction with structure features in S1, Tryp and G16 structures. (n=3,* N=1*)*

### 5.4.3 Morphological analysis of structure colonisation by macroconfocal

Following on from individual design sweeps, promising designs were scaled up for a wider assessment of cell expansion and behaviour in fixed larger multi-microcarrier arrays. This experiment used pHEMA and macroconfocal techniques previously explored in section 4. As such $1mm^2$ of 100 µm microcarriers were produced in packed arrays for cell culture. These arrays were designed in a fashion to minimise empty space and simulate a packed microcarrier environment. The seven identified experimental designs outlined in section 6.4.2 were included as well as a spherical 3D control, to simulate typical microcarrier design, and a flat 2D control. Structures were produced in PETA, post-processed by the standard set out in section 5.4.1, seeded with $5x10^3$ iMSCs and cultured at 37°C across 21 days with readings taken at day 0 ,4 ,7, 14 and 21. Day 0 readings were taken 4 hours after seeding to give time for cell attachment as an initial starting population. Cells were seeded in low quantities due to very limited surface area and growth over a long culture period. At each time point structures were washed, fixed, stained with phalloidin and mounted for macroconfocal imaging. Results for macroconfocal analysis were demonstrated in figures 5.6, 5.7 and 5.8 which display flattened stack images of phalloidin stained cells through Z-intensity projections across each design over 0, 4 and 7 days of culture. Under each image is the corresponding Z-profile graph to display fluorescence distribution through the height of the structure, with blue lines representing structure autofluorescence and red for stained actin in cells.

Day 0 images for C50 structures act as a measure of seeding efficiency and given low seeding density yield a minimal level of fluorescence as expected. This result is similar for all designs tested at day 0. As the Z-profile shows this low fluorescence signal is located only within the bottom 20 µm of structure height from the surface. By day 4, cells have significantly colonised the structure and begin to spill out of the edge of the array. These cells cannot attach given the pHEMA but have suspended growth still linked to the array edges. Z-profile shows that the majority of cells were distributed below 70 µm in structure height, but some cells were still present across full structure height indicating good interaction across all three dimensions with a peak at around 40 µm. At day seven the structure was heavily confluent and densely packed with cellular

material to the point that individual cells cannot be distinguished. Z-profiles indicate high cell presence across all the structure height but again an overall drop off in signal over 70 µm. C80 structures show a higher initial fluorescence on day 0 in comparison to C50 with a more equal distribution throughout the structure. Similar to C50 structures a high level of confluence is seen by day four with greatest concentration of cells seen below 60-70 µm. At day seven a further increase in growth is seen but distribution of cells is less uniform than C50 structures with a much larger concentration of cells in the centre of the array. Z-profiles show a typical distribution of cells with greatest localisation towards the centre of the structure height.

G1t designs show a higher initial fluorescence on day 0 than C50 or C80 structures with cells concentrated at the bottom of structures. At day four cells reach a higher level of confluency across the structure with distribution of cells throughout the structure height matching the autofluorescent signal indicating engagement across the whole structure. At day seven G1t structures show a high level of confluence but lower compared to C50 or C80 structures with visibly empty space left to colonise. A much more even distribution of cells across the structure height is seen showing good interaction and colonisation across all three dimensions. G6n structures showed the highest level of cell presence at day 0 in comparison to other structures and most cells were localised to the bottom of the structure height. However, at day four G6n structures show a lower level of confluency in comparison to C50, C80 or G1t structures with a low Z-distribution below 50 µm. At day seven cells reached a higher level of confluency but with individual cell positions still visible and further empty space left for colonisation. Structures do not reach a high cell density that prevent individual cell distinction like what is seen in previously described structures. Confluency at day seven is similar to day four results for other structures so far described. H1 structures show a low level of cell presence at day 0 with a low z distribution below 20 µm. At day four H1 structures show the lowest level of cell signal of all the designs with cells preferring to grow around the periphery of the structure as opposed to throughout the structures and again with a low Z distribution mostly below 50 µm. However, by day seven growth seems to have spread throughout the entirety of the structure and the majority of space is colonised but with further room for growth. Z-distribution still shows a tendency to congregate mostly below 50-60 µm, as is similar for many structures, and overall signal is comparable to G6n structures but less than

C50, C80 and G1t. Sg structures show a low level of cell entrapment at day 0 with majority of cells located toward array periphery and a very low z distribution. Autofluorescence of this structure is more linear given the cube like shape of each individual structure as opposed to all other designs which were spherical. Structures become more confluent by day four with an even distribution of cells throughout XY dimensions but localisation below 60 µm in Z profiles. At day 7, structures have become much more confluent than day four but a significant portion of structures is still relatively uncolonised with lots of available space to grow. Cells seem to form a more elongated morphology stretching across the structure from the top of the image downward. Z-distribution shows a better utilisation of structure space above 70 µm than previously seen but majority is still localised below this value. Day 0 results for V structure designs show a low irregularly distributed level of cell entrapment and low z distribution as is typical at day 0. More pronounced growth and uniform distribution of cells is seen by day four but the confluency is low in comparison to best performing designs. Peak Z distribution is seen at 30-40 µm with typical signal drop off after around 70 µm. At day seven a more irregular and confluent growth over the structure is seen with discrete areas of dense growth and other areas which were sparser. Cells appear more stretched across the structure in a variety of directions and Z distribution is very high below 50-60 µm with a sharp drop off over this height.

Spherical controls show a good level of cell entrapment much greater than V designs and similar to G6n. Day four growth is much more confluent with even growth throughout the structure and slight clustering of cells around array periphery. Z profile is much more distributed across the structure with peak signal around 40 µm. At day seven a low level of confluency is seen in comparison to other structures with a dense cellular cluster at the bottom right of the array possible from cells that have peeled off from structure surface. Z distribution is still evenly spread across structure height.2D controls at day 0 show a high fluorescence caused by a large number of cells scattered on the surface and around the periphery of the structure which were rounded and attached but not spread across the structure. At day four cells were beginning to spread across the surface and appear more flattened. Finally at day seven cells appear more spread and stretched across the structure surface but with greatest colonisation across structures edges.

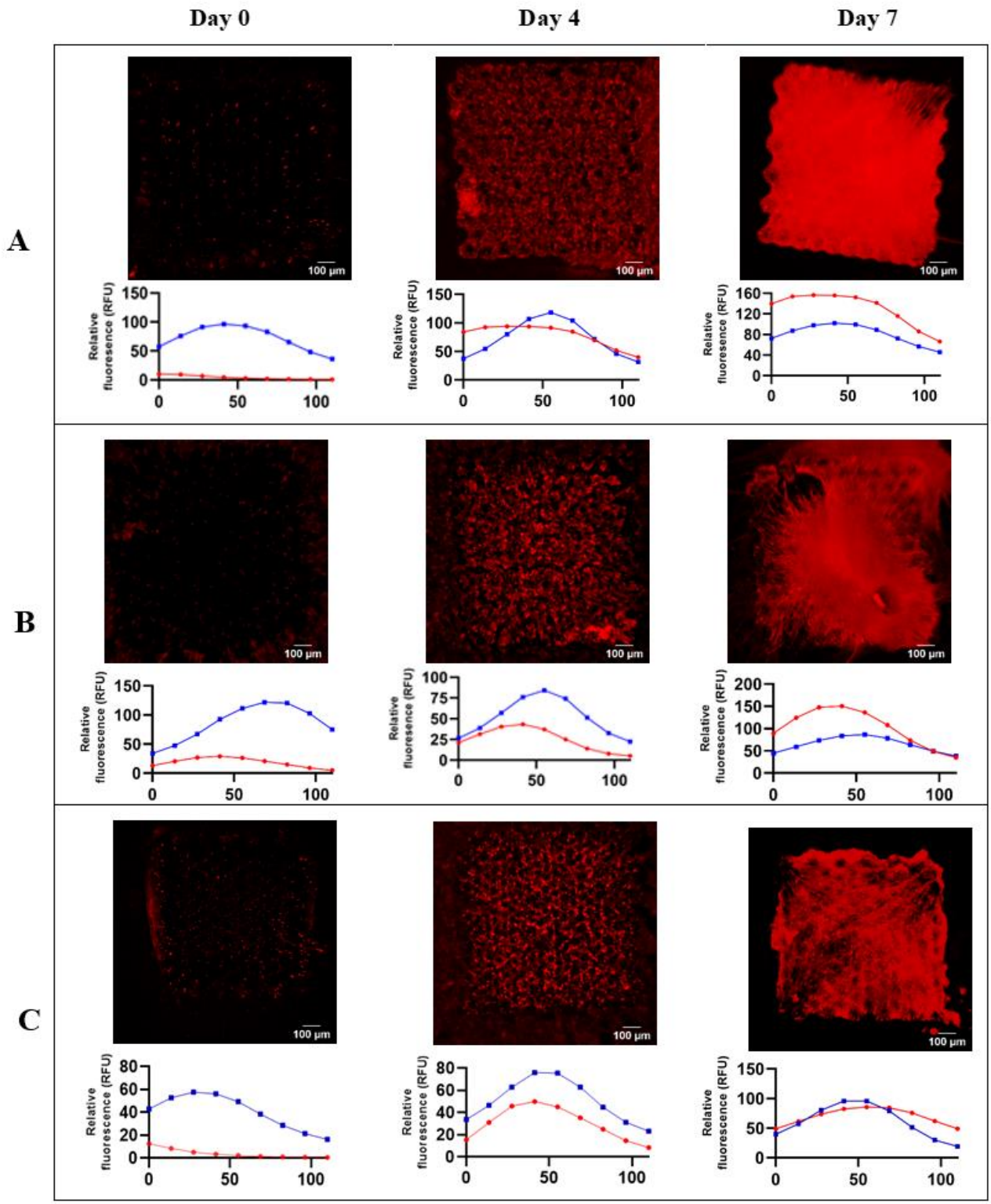


***Figure 5.6:*** *Macroconfocal morphological analysis of MSCs on microcarrier arrays 1. Intensity projections of red phalloidin stained cells across day 0, 4 and 7. Each stack accompanied below by Z-profile fluorescence with blue lines indicating PETA structure auotfluorescence and red represeting cells to indicate Z growth pattern on carrier height as marked by the x axis. A) indicates C50 structure growth. B) indicates C80 structure growth. C) indicates G1t structure growth.. (n=1,* N=1*).*

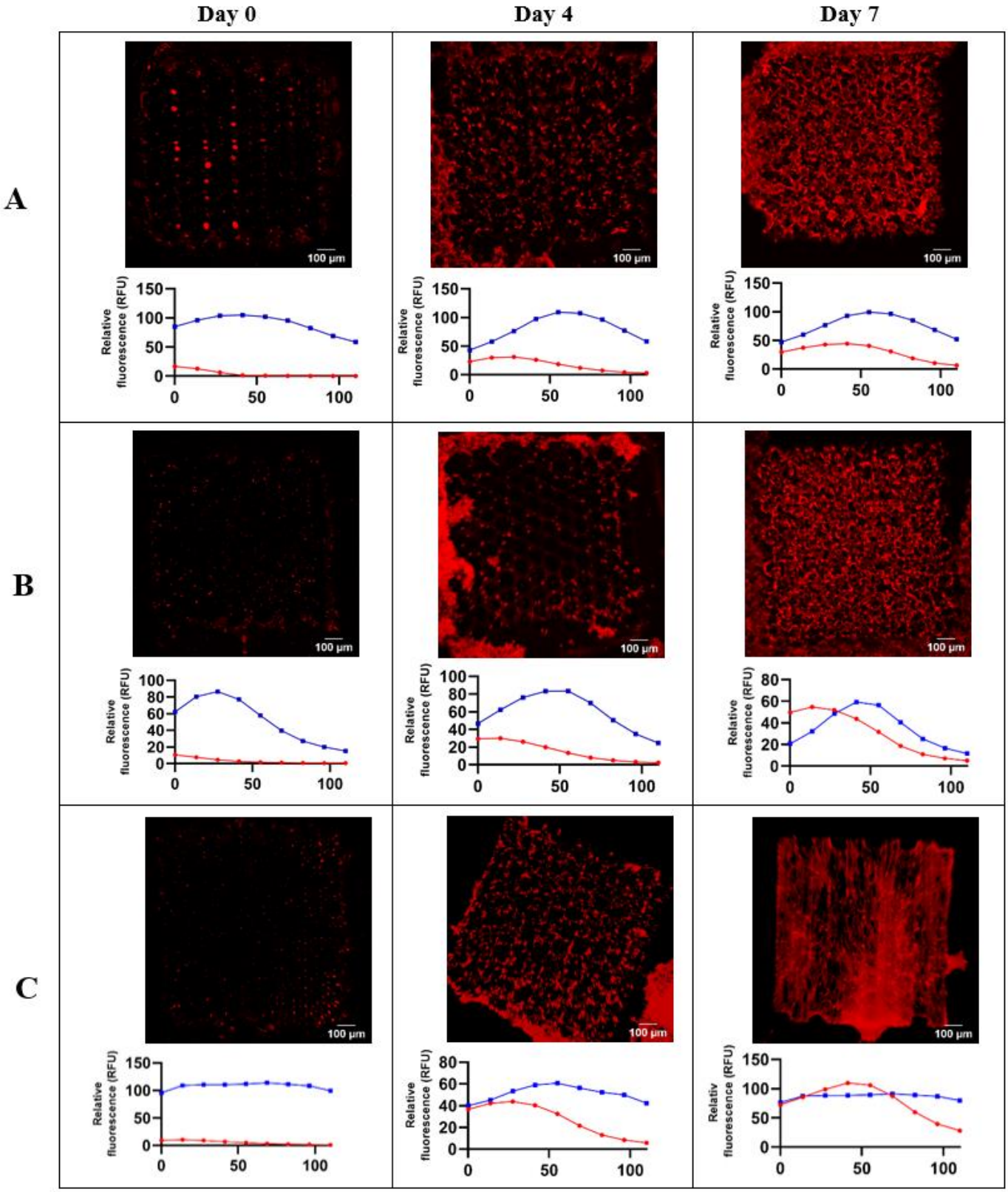


***Figure 5.7:*** *Macroconfocal morphological analysis of MSCs on microcarrier arrays2. Intensity projections of red phalloidin stained cells across day 0, 4 and 7. Each stack accompanied below by Z-profile fluorescence with blue lines indicating PETA structure auotfluorescence and red represeting cells to indicate Z growth pattern on carriers height as marked by the X-axis. A) indicates G6n structure growth. B) indicates H1 structure growth. C) indicates Sg structure growth. (n=1,* N=1*).*

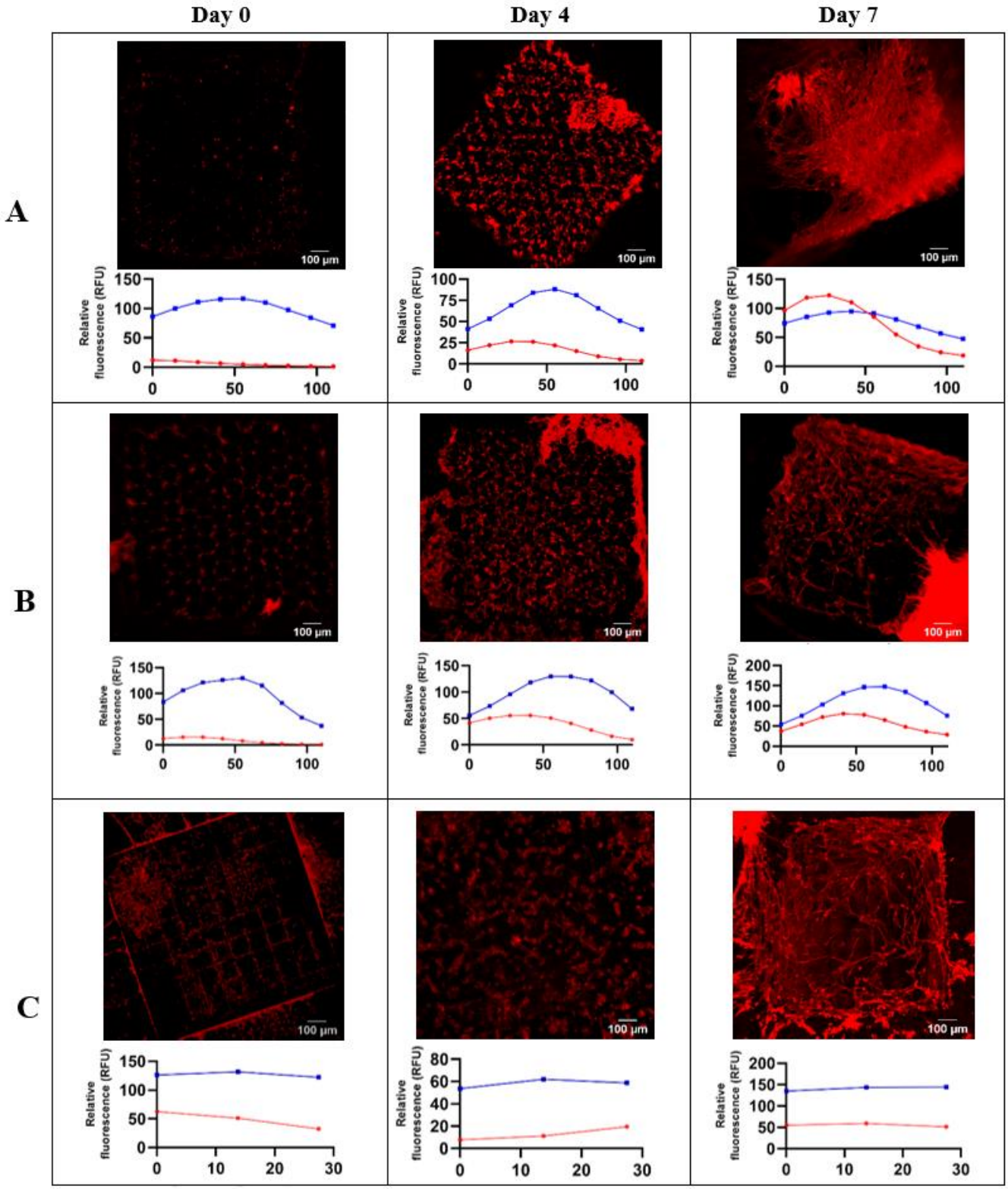


***Figure 5.8:*** *Macroconfocal morphological analysis of MSCs on microcarrier arrays3. Intensity projections of red phalloidin stained cells across day 0, 4 and 7. Each stack accompanied below by Z-profile fluorescence with blue lines indicating PETA structure auotfluorescence and red represeting cells to indicate Z growth pattern on carrier height as marked by the X-axis. A) indicates V structure growth. B) indicates Sphere structure growth as a 3D control. C) indicates Film structure growth as a 2D control. (n=1,* N=1*).*

Average fluorescence measurements of Z-intensity projections from stacks were measured per image at each time point as a single value of cell growth which over the culture period can act as a measurement of expansion yield. These values can be taken at each time point and plotted to show total growth patterns over time in comparison to other structure designs as seen in figure 5.9.

Overall results indicate that C50 structures support the most rapid cell expansion profile at all time points and reach the highest observed fluorescence at day 21. Expansion profiles of cells culture on C80 structures show a similar profile to those on C50 structures but with a slower growth rate, signal is lesser than C50 at day 4-7 but begins to catch up at days 14 and 21. C50 and C80 structures finish the experiment as the highest performing structures. G1t, V and H1 structures all show similar profiles of growth that were not as rapid as buckyball structures but greater than spherical controls at all time points except d0 with a more linear growth pattern than best performers. G6n and Sg structures appear to grow at a rate similar to spherical controls and result in a similar but slightly greater final expansion yield than spheres. 2D controls show expansion until around seven days at which point most surface area is colonised and growth begins to slow showing overall lowest signal as expected. Overall, the estimation of expansion yield though macroconfocal fluorescence measurement indicates three groups of microcarriers based on performance. One group consists of G6n, Sg and spherical controls which show the overall lowest level of expansion. C50 and C80 structures make up the best performing structures with highest estimated expansion yields and the remaining three variations all have a moderate performance greater than spherical controls but less than buckyball designs.

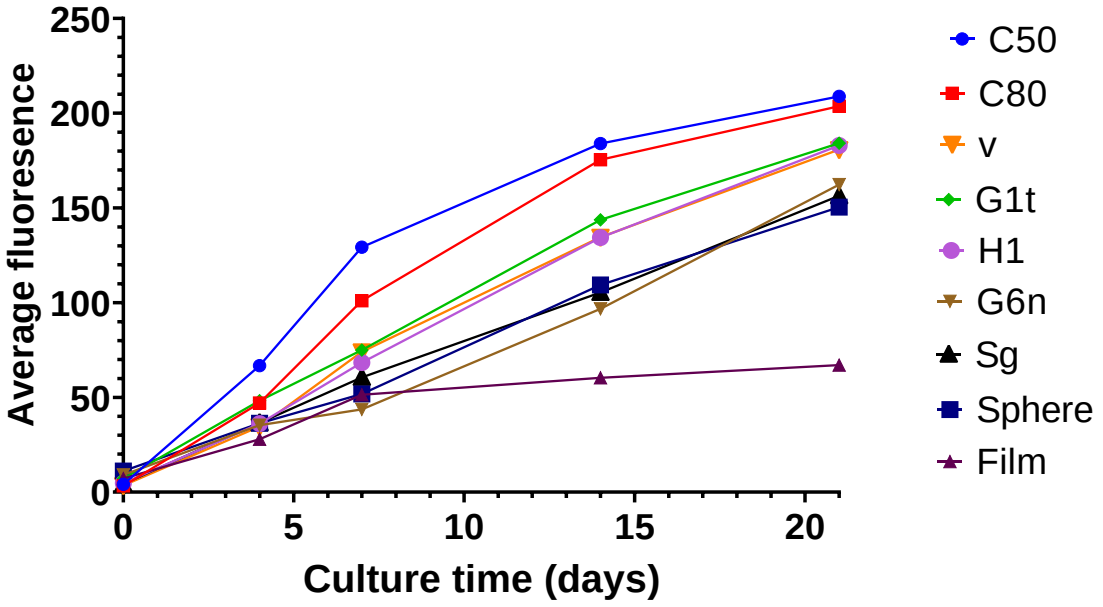


***Figure 5.9:*** *Expansion of iMSCs over 21 days across eight different PETA microcarrier variations.* *Total Average fluorescence measurements of the phaloidin portion of Z-flattened macroconfocal stacks as a measurment of total cell amount across the culture period of 21 days. At the experiment end the data indicates three resulting groups with a highest peforming group consisting of C50 and C80 structures, secondary group of G1t, H1 and V strucutres and lowest signal group with results similar to 3D control (sphere) and greater than 2D control (film). (n=1,* N=1*)*

### 5.4.4 DNA quantification expansion analysis

DNA quantification was pursued in order to accurately determine cellular expansion occurring in microcarrier designs. Experimental setup was similar to that of the macroconfocal analysis with 1mm$^2$ of seven microcarrier designs and two controls in packed arrays on pHEMA substrates for cell culture. Structures were produced in triplicate in both PETA and TMPETA, post-processed by the standard set out in section 5.4.1, seeded with 5x10$^3$ iMSCs and cultured at 37°C across 28 days. DNA measurements at days 0, 4, 7, 14, 21 and 28 were used to measure fold increase in cell population, indicating cell growth and expansion, from day 0 to normalise between designs which had different seeding efficiencies and as such starting populations. Fold

increase of designs produced in PETA were illustrated in figure 5.10. Similar to results of figure 6.9 both C50 and C80 designs led to highest fold increase at every measured time point excluding day 0. C50 performs partially greater than C80 but both support approximately an 11-fold increase in cell amount from starting populations. The third best performing design is G1t designs that show a more linear growth pattern achieving an 8-fold increase by day 28. G6n designs follow up with an approximate 6-fold increase shortly before both V and spherical 3D control designs that both produce around a 5.6- fold increase. H1 and Sg designs perform worse than spherical 3D controls but better than flat PETA films or monolayer growth on glass coverslips as positive controls. Negative controls support no growth of cells over the expansion period given absence of an adherent surface in pHEMA coverslips. The overall outcome of this experiment indicates that C50 and C80 designs lead to highest expansion yield with G1t as next best design for enhancing expansion yield.

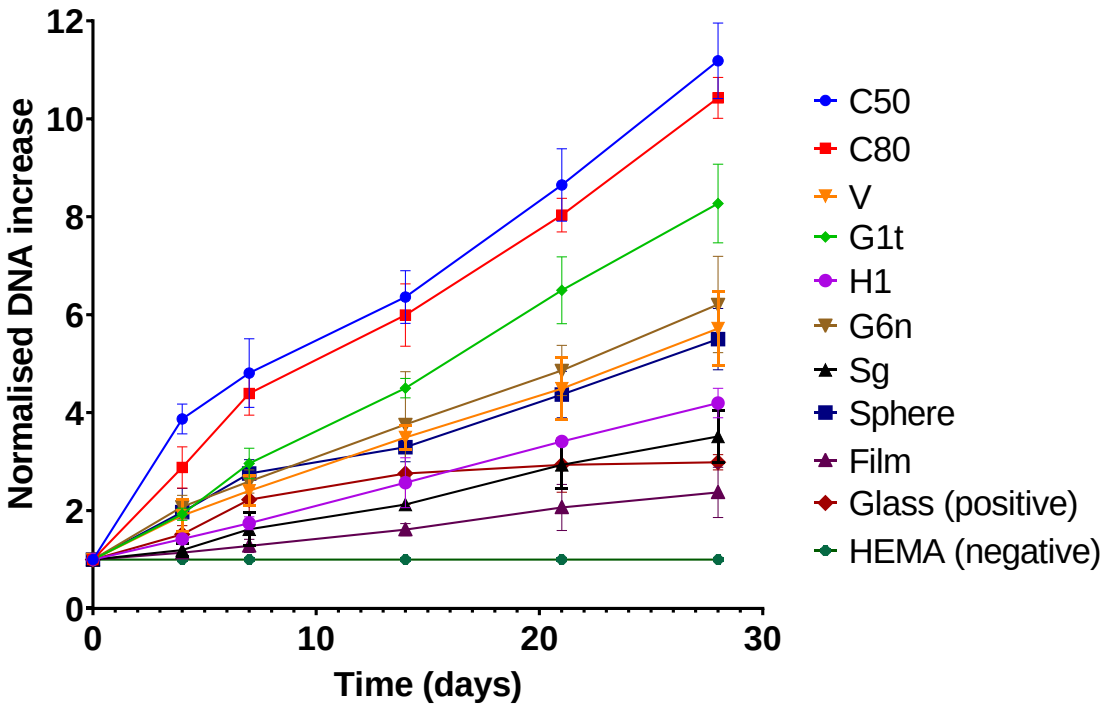


***Figure 5.10:*** *iMSC normalised DNA increase for experimental microcarrier designs in PETA. Increase of measured DNA normalised to day 0 for experimental microcarrier designs and controls fabricated in PETA across a 28-day expansion period. Results indicated highest fold increase in DNA when cells were cultured on C50 designs with a 11.2-fold increase at 28 days in comparison to a 5.5 fold increase in spherical 3D controls. Mean ± SD, (n=3,* N=1*).*

Microcarriers were also produced in TMPETA and subject to the same experimental procedure with reduced measurement points at 0, 7, 21 and 28 days to reduce fabrication time whilst still validating results in multiple materials. Results showed a reduced fold increase in all conditions in comparison to PETA but overall performance per design remained consistent. C50 and C80 designs remained best performing structures with an approximate 6-fold increase in comparison to spherical 3D controls which had a 2.8-fold increase. G1t designs showed a 4.7-fold increase and G6n had a 3.7-fold increase. All others performed similar to spherical controls and H1 and Sg designs again performed worse than spherical controls. In comparison to PETA the results from the TMPETA version of G6n pulls further away from the grouping of

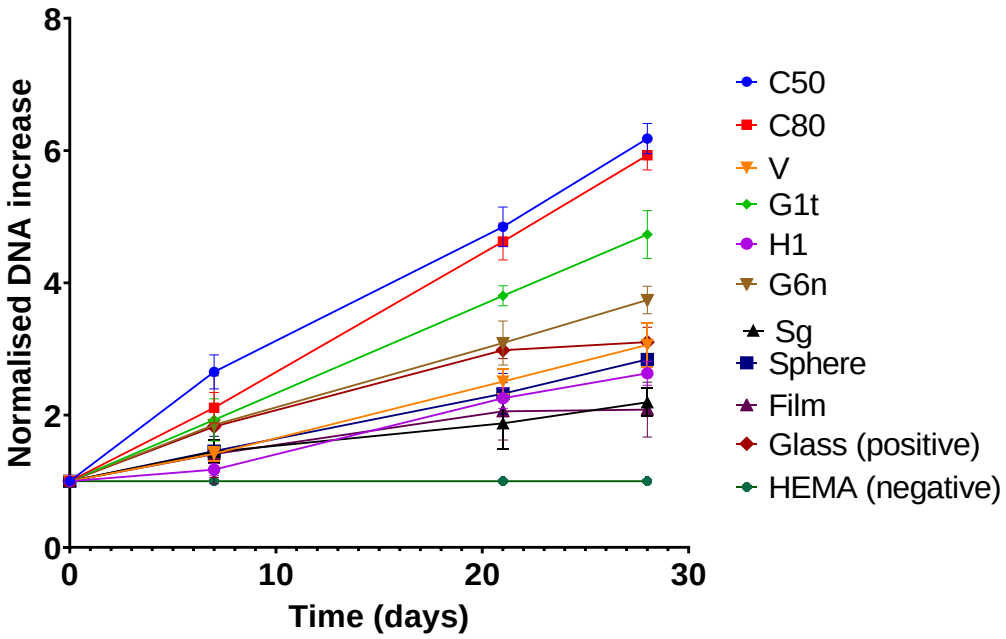


***Figure 5.11: i****MSC DNA increase over time for experimental microcarrier designs in TMPETA. Fold increase of measured DNA normalised to day 0 for experimental microcarrier designs and controls fabricated in PETA across a 28-day expansion period. Results indicated highest fold increase in C50 designs with a 6.2-fold increase at 28 days in comparison to a 2.8 fold increase in spherical 3D controls. Mean ± SD, (n=3,* N=1*).*

designs similar to spherical controls distinguishing itself as creating a better response.

These results of fold increase in DNA describe how cell expansion yield differs per microcarrier design over time and unanimously show that buckyball designs produce a greater expansion yield than other competing designs. Calculations were made from measured DNA values and the amount of surface area in each design that can be mathematically calculated from 3D models. DNA values were normalised by surface area to account for difference in microcarrier surface area and data presented in figure 5.12 indicates amount of DNA per $1mm^2$ surface area for each design. A secondary Y-axis indicates approximate cell number based on average DNA values per MSC.

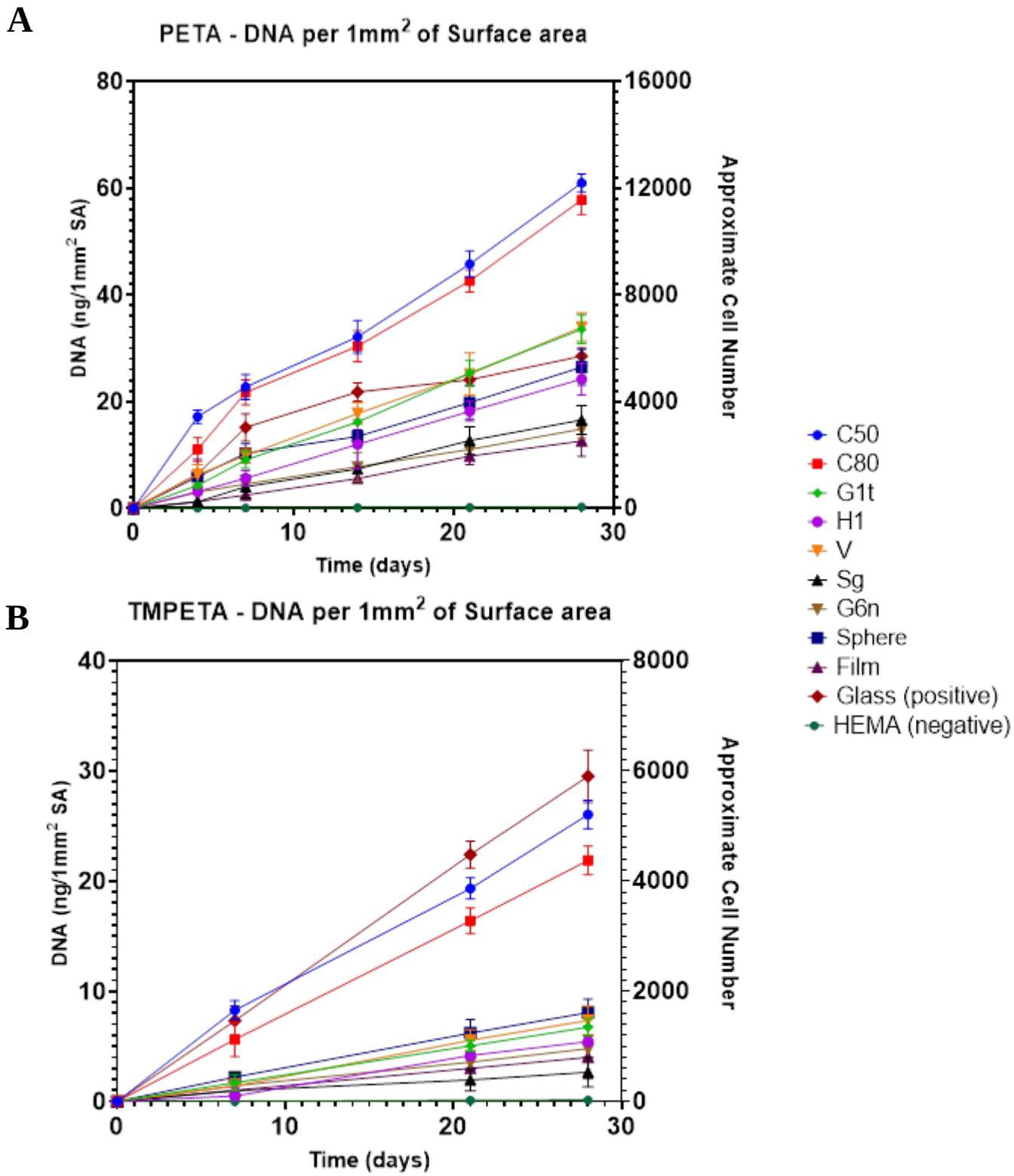


***Figure 5.12:*** *DNA per 1mm2 of surface area over time for experimental microcarrier designs.* ***DNA*** *was normalised by structure surface area for experimental microcarrier designs and controls over the 28-day expansion period. Secondary Y-axis indicates approximate cell number based on DNA values. A) Expansion results from structures fabricated in PETA indicate highest expansion in C50 designs with 61 ng of DNA per 1mm$^2$ of surface area compared to 26.5 ng in spherical comparisons. B) Expansion results from structures fabricated in TMPETA indicate highest expansion glass positive controls followed by C50 designs with 26 ng of DNA per 1mm$^2$ of surface area compared to 8 ng in spherical comparisons. Mean ± SD, (n=3,* N=1*).*

Correction by surface area indicates differences from that seen with fold increase for PETA microcarriers. C50 and C80 designs remain as most effective producing 61 ng and 57.8 ng of DNA per $1mm^2$ of surface area respectively. Both microcarriers follow a close growth pattern with C80 falling slightly short of C50 results at day 28 by 5%. However, divergence between this pattern is seen at day four where C80 structures produce an effect 35% less than their C50 competitor. C80 structures catch up by day seven measurements but this indicates an initial lag in cell expansion within the first few days in comparison to C50. With correction by surface area the performance of buckyball microcarriers were more distinguished from competitors with tied third best performance seen in both V and G1t structures with approximately 34 ng of DNA per $1mm^2$ of surface area, which is nearly half as effective as C50 designs. Glass positives provide 28.5ng of DNA per $1mm^2$ of surface area which rapidly increases performance in comparison to other designs given surface area correction and indicates better material performance. Spherical 3D controls acting as typical commercial microcarrier comparisons produce 26.5 ng of DNA per $1mm^2$ of surface area followed shortly by H1 designs with 24.2 ng. In fold increase experiments H1 designs had a considerably lower performance than spherical controls but under surface area correction have a much closer correlation. Lowest performing designs such as Sg produce only 16.5 ng of DNA per $1mm^2$ of surface area despite having one of the highest surface area values. This is followed by G6n designs with 14.8 ng of DNA per $1mm^2$ of surface area making this the lowest performing design coming in only slightly above flat controls. This is in contrast to fold increase experiments in which G6n microcarriers placed as $4^{th}$ best design for fold increase in cells.

TMPETA surface area corrected results indicate best performance at day 28 in glass positive controls which is due to difference in material adherence, although C50 designs briefly perform better at day seven measurement. C50 and C80 designs maintain best performing microcarrier designs overall with 26 and 21.8 ng of DNA per $1mm^2$ of surface area respectively. This marks a significant pull away from all other designs that produce a much less profound effect with $3^{rd}$ place spherical controls producing only 8 ng of DNA per $1mm^2$ of surface area. The least performance is seen in Sg designs, unlike PETA whose worst performer was G6n, and only produced 2.6 ng of DNA per $1mm^2$ of surface area which is less than 2D controls. The difference between PETA and TMPETA fold increase was an overall reduction in fold increase

but the majority of observed difference between designs remained relatively consistent. However, when correcting by surface area TMPETA results change significantly from previously identified trend with the only consistent finding being highest effect observed in buckyball designs.

The summary of total change in DNA per $1mm^2$ of surface area over the 28-day culture period is summarised for both materials in figure 5.13. Total change over 28 days in PETA structures indicates C50 and C80 designs as best performers which were both significantly different from spherical controls at $P < 0.0001$. G1t and V designs perform better than spherical controls but were not significantly different and Sg and G6n structures perform significantly worse than spherical controls at $P < 0.01$. Similar outcomes were seen for total change in TMPETA results with performance of C50 and C80 structures significantly different from spherical controls whilst all other microcarrier designs were non-significantly different from spheres except Sg which performed significantly worse at $P < 0.05$. Of course, these final results reflect the outcome of surface area adjusted expansion per design indicating which geometry is more effective at expansion per unit area, however fold increase results in figures 5.10 and 5.11 indicated which microcarrier performed best in overall expansion.

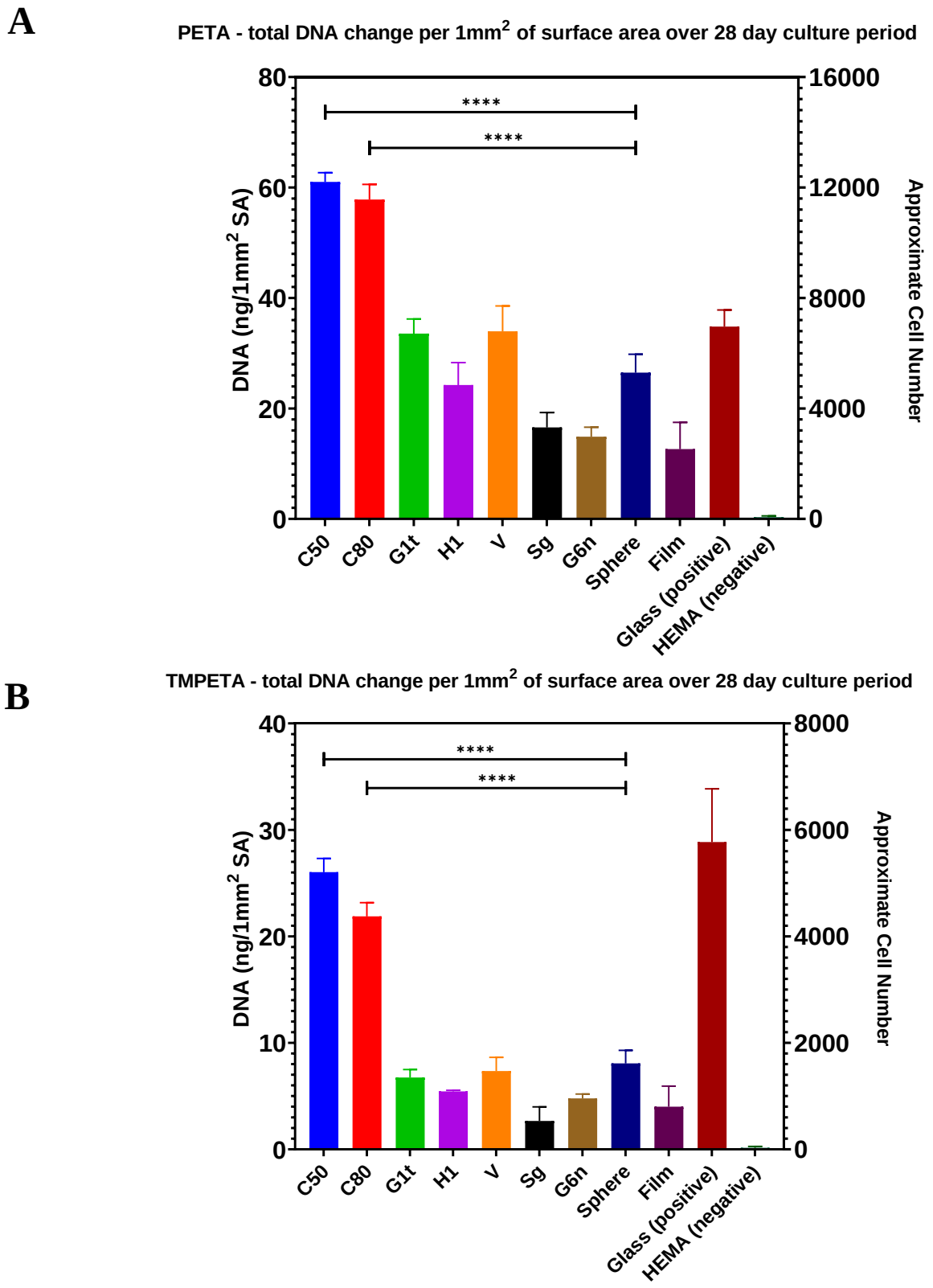


***Figure 5.13:*** *Total DNA change per 1mm2 of surface area over 28-day culture period. DNA was normalised by structure surface area for experimental microcarriers and calculated as total change from day 0 to day 28. Secondary Y-axis indicates approximate cell number. A) Expansion results from structures fabricated in PETA indicate highest DNA change per unit of surface area in C50 and C80 designs which were significantly different from spherical controls at P < 0.0001. B) Expansion results from structures fabricated in TMPETA indicates similar results with significant performance of C50 and C80 structures. Mean ± SD, (n=3,* N=1*).*

### 6.4.5 Protein production over expansion period

Cell lysates obtained from expansion experiments in section 6.4.4 were also subject to additional testing to probe further biological responses over the expansion period. Total protein production was investigated by means of a bicinchoninic acid (BCA) assay over the full 28-day period in PETA to determine any differences in protein production. Total change in protein corrected by surface area over the 28-day culture period is presented in figure 5.14.

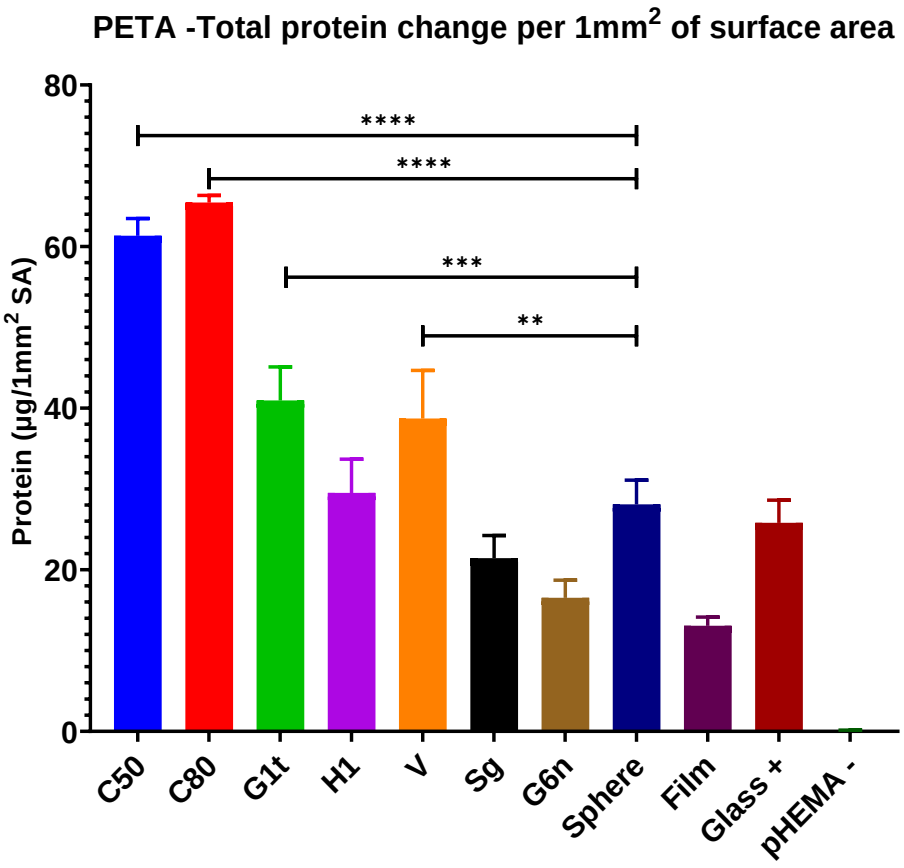


***Figure 5.14:*** *Total Protein change per 1mm2 of PETA surface area over 28-day culture period. Protein was measured via BCA assay and normalised by structure surface area for experimental microcarriers for measurement across 28 days. Results indicated highest protein in C80 designs with both buckyball designs being significantly different from spherical controls at p <0.0001. G1 structures were significant at P <0.001 and V structures at P <0.01. Mean ± SD, (n=3,* N=1*).*

The highest protein content is recorded in C80 designs followed by C50 both being significantly different from spherical 3D controls at $P < 0.0001$. Unlike DNA expansion results C80 is the highest performing design in comparison to C50 indicating a higher protein content in C80 designs despite a slightly lesser amount of DNA per unit area. G1t structures delivered the third highest recorded protein content per unit of surface area and were significantly different from spherical controls at $P < 0.001$. Additionally, V structures followed very closely to results displayed by G1t designs but were only significantly different to spherical controls at a level of $P < 0.01$. H1 structures produced an outcome that was slightly better than spherical controls but was not of a level that was significantly different. Remaining experimental microcarriers including Sg and G6n designs performed on less than spherical controls. Several of the analysed designs produced protein outcomes different from spherical controls at varying levels of significance. Whilst outcomes were similar to DNA expansion, namely with success of buckyball structures, there were some key differences indicating that level of protein is not purely based on the level of DNA or cell expansion and that some designs promote a higher level of protein production than others.

### 6.4.6 Osteogenic commitment

Secondary conducted tests with expansion derived samples from cell culture on microcarriers in basal media aimed to determine if any strong osteogenic responses were detected over the culture period by measuring alkaline phosphatase (ALP) response which is an early signal of osteoinduction. At first osteoinductive capability was tested as baseline reading for the cell line used. Osteoinductive activity was investigated by means of an ALP assay which was normalised to DNA amount across the 28-day culture period. Appendix 4 documents the osteoinduction of iMSCs with inductive media described in section 6.3. Brightfield microscopy of iMSCs taken at each measurement point and demonstrated at days 0, 14 and 28 in appendix 4 shows the change in morphology of cells over time with osteoinduction media. Cells become more elongated over time and at day 14 begin to show some dark calcium deposits that increase visibly by d28 with many calcium deposits visible throughout the cell growth. DNA normalised ALP activity over the culture period shows a low level of 0.03 nmol of pNP per minute per ng of DNA at day 0 that rapidly increases to a peak of 2.31 nmol at day 21 before reducing to 1.75 nmol at day 28. Morphological assessment and ALP activity indicates the differentiation of iMSCs into osteogenic lineages over the course of the experiment. Next ALP assessment across the 28-day expansion period from cells cultured on PETA and TMPETA experiments in basal media was conducted and compared to osteogenic controls for analysis of microcarrier growth effect on osteogenic differentiation. Data presented in figure 5.15A indicates the ALP activity levels of cells growing on PETA microcarriers. All designs show no significant difference from spherical controls with a total range over the entire experiment across all designs of 0.015 – 0.088 nmol pNP/min/ng DNA. In comparison, osteogenic controls show a value of 0.03 nmol pNP/min/ng DNA at day 0 but reach a peak of 2.3 nmol pNP/min/ng DNA at day 21. ALP activity in osteogenic controls is significantly higher than all other designs and controls at all time points except day 0, requiring a logarithmic axis to display the data visibly in the same graph. For PETA microcarriers the 21-day peak in osteogenic controls have an ALP activity 28 times greater than the highest recorded microcarrier activity. Responses for TMPETA microcarriers were similar to that of PETA with no significant difference between any designs in comparison to spherical controls and a highly significant difference, at $P < 0.0001$, to osteogenic controls which dwarf activity values from microcarrier designs.

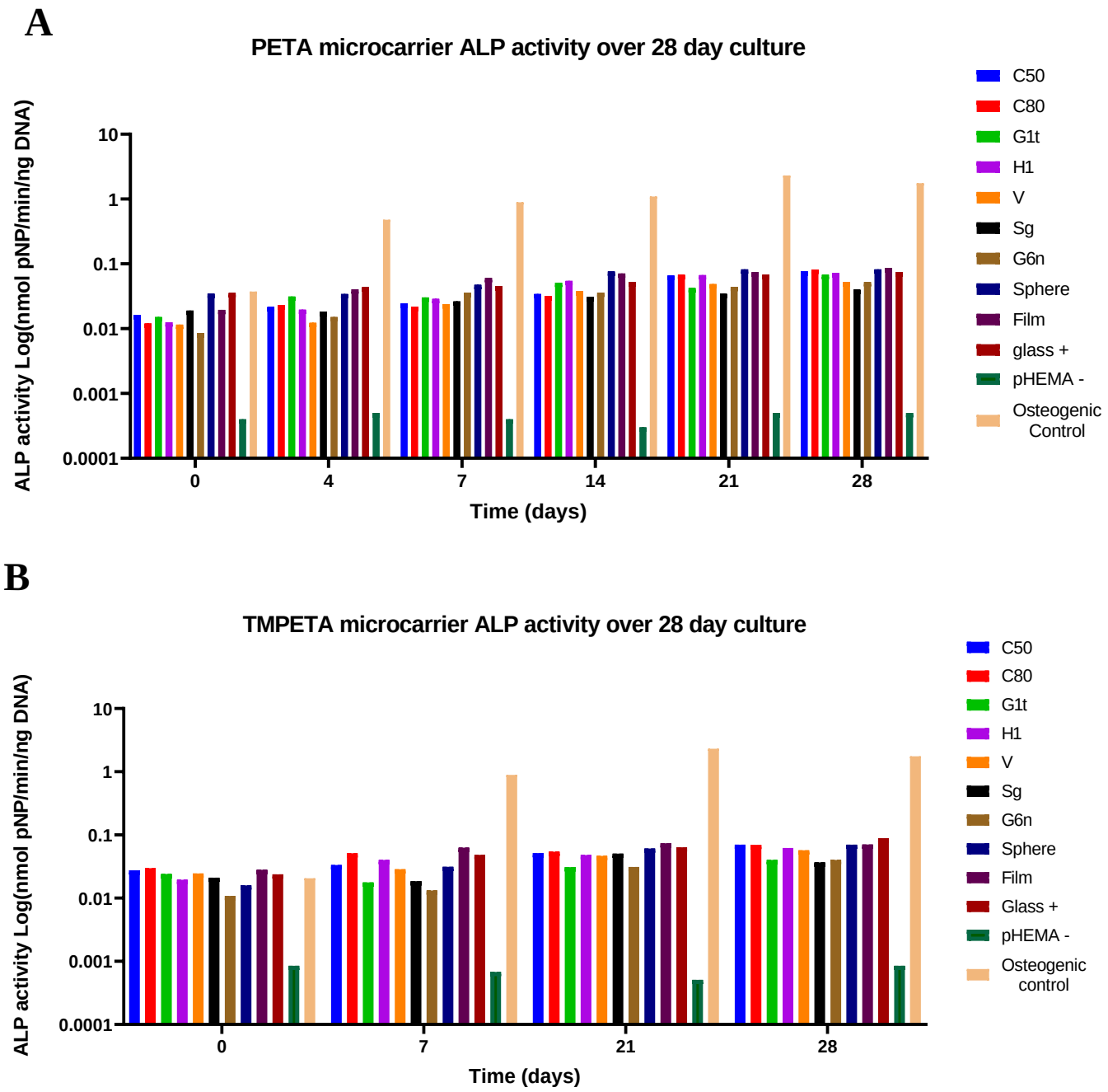


***Figure 5.15:*** *ALP activity for iMSCs expanded by PETA and TMPETA microcarrier designs in basal media. ALP activity normalised to DNA amount over 28 days of culture displayed on a logarithmic axis with differentiated controls for comparison. A) PETA microcarrier expanded cells from all designs show no significant difference from spherical controls with a total range over the entire experiment of 0.015 – 0.088 nmol pNP/min/ng DNA in comparison to osteogenic controls that show a value of 0.03 nmol pNP/min/ng DNA at day 0 but reach a peak of 2.3 nmol pNP/min/ng DNA at day 21. B) TMPETA microcarrier expanded cells from all designs show no significant difference from spherical controls similar to PETA, with osteogenic controls significantly higher at all time points except day 0. Mean, (n=3,* N=1*).*

### 6.4.7 Free microcarrier culture

To fully simulate and test microcarrier culture with experimental designs structure release from pHEMA coated substrates was pursued for free floating microcarrier culture. Carriers were prepared in the same way as previously described followed by IPA washing to dissolve pHEMA layers and release structures from the fabrication surface. Whilst the volume of carriers did not allow for scaled expansion in spinner flasks small trials of static culture in suspension culture plates were achieved using several thousand structures at a time. Initially trials to explore the feasibility of this method was pursued using c80 PETA microcarriers. Fluorescent microscopy in figure 5.16 indicated live/dead staining of iMSCs seeded onto free floating C80 microcarriers. The experiment indicated that cells do attach and grow on free floating structures, however due to the static methodology used microcarrier growth tended to form large clusters due to confluency on particles being reached causing binding across multiple structures. Whilst not all microcarriers formed clusters it was an issue that became more apparent as the culture period continued. These results were typical of microcarrier growth and expected, further optimisation to seeding strategies for culture in this way was difficult to achieve given the time needed for fabrication at this scale. Despite the large cluster of many structures these areas still maintained high viability based on localised staining seen in figure 5.16B.

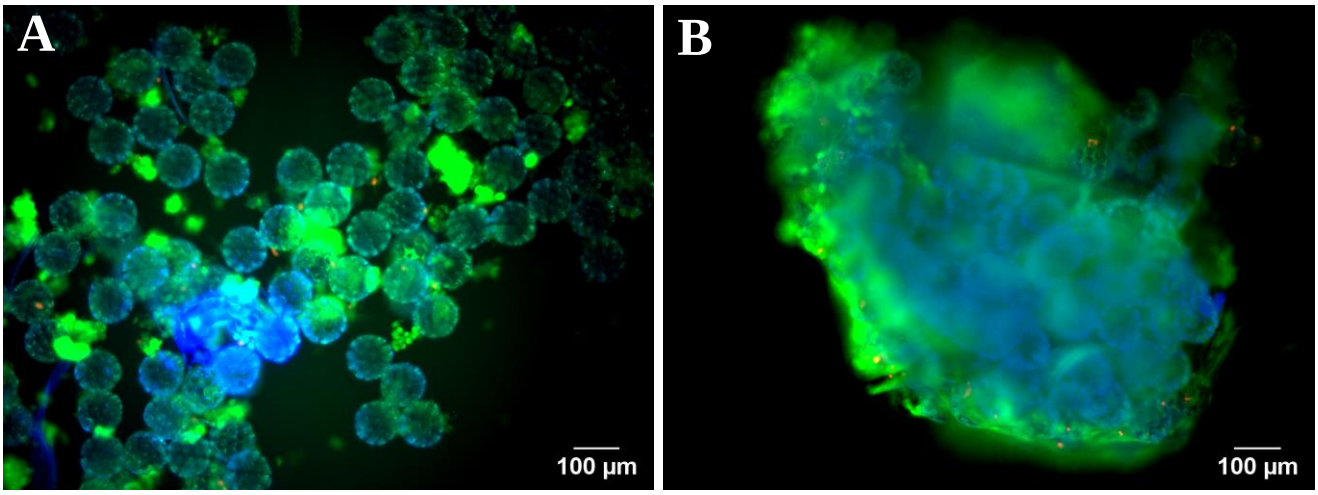


***Figure 5.16:*** *Live/Dead fluorescent microscopy of free-floating PETA microcarriers with iMSC growth. A) growth of cells throughout free floating microcarriers with little observable cell death. B) cluster formation that occurs after 6 days as confluency is reached on microcarriers.*

After trials runs of static microcarrier culture attempts at retrieving cells from microcarriers was pursued. Removal of cells was completed with trypsinisation in the same method as standard cell culture and the vast majority released from the microcarriers. The highest incidence of remaining cellular adherence to microcarriers after trypsinisation occurred in those growing in clustered formations as seen in figure 5.16B. Expanded cells retrieved were cultured for two days in tissue culture plates in a monolayer fashion to examine if there were any morphological changes to cells or changes to growth behaviour. Figure 5.17 shows growth of expanded cells from microcarriers and display typical cellular morphology expected of iMSCs that have not undergone any differentiation protocol. This is an initial sign that growth on these microcarriers did not lead to differentiation based on cell morphology. As such this experiment was only a trial of methodology and expansion potential and differentiation will be further analysed in future experiments

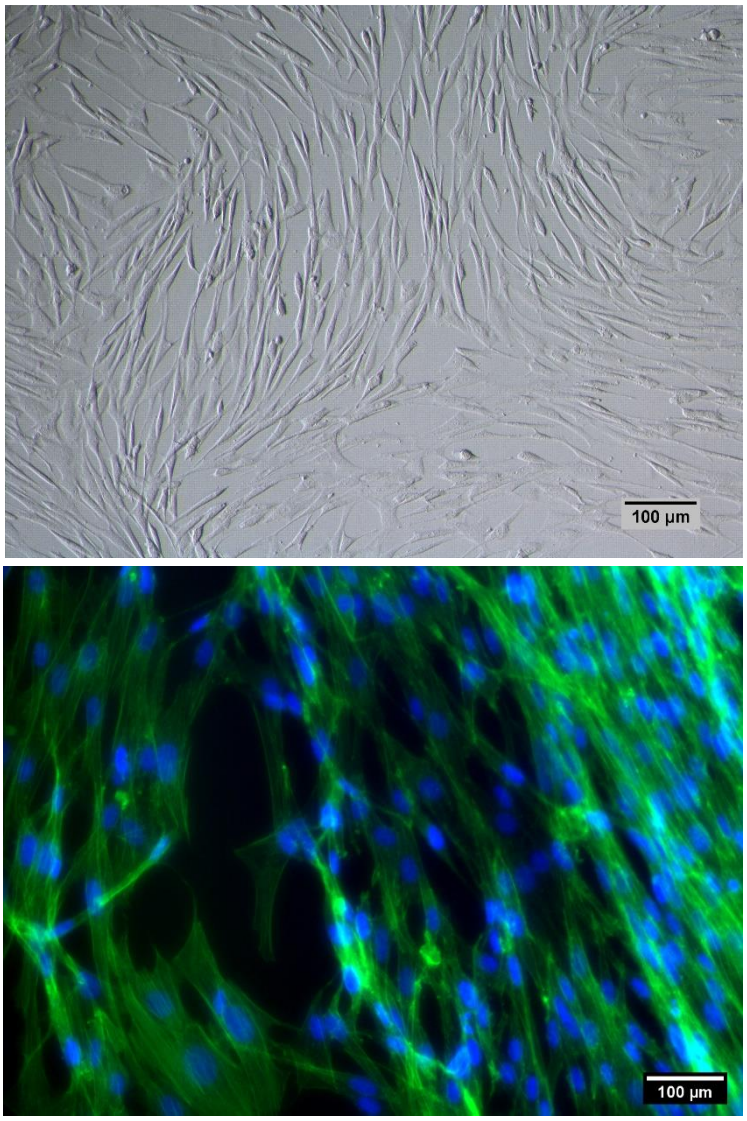


***Figure 5.17:*** *Microscopy of iMSCs expanded via C80 microcarrier culture. Brightfield microscopy of iMSCs and fluorescence microscopy with actin staining and DAPI nuclei staining.*

### 6.4.8 Stem cell marker analysis

Following on from previous microcarrier characterisation, such as expansion yield, stem cell phenotype maintenance was explored. Three microcarrier variations were included representing different expansion capabilities and iMSCs were expanded for three weeks on C50, G1t and spherical microcarriers fabricated in PETA. All expanded cells in this experiment were derived from free microcarrier culture with no underlying anchoring substrate, except control monolayer cultures. Cells were then analysed for ISCT criteria stem cell markers which include the positive expression of CD73, CD105 and CD90 along with a negative marker cocktail consisting of five markers that should not be expressed. Data from this experiment is illustrated in figure 5.18. Graphs indicate number of cells expressing each of the three positive markers on the graph Y-axis followed by number of cells positive for the negative marker cocktail presence on the X-axis. As such, expression of positive markers and lack of the negative marker cocktail should cluster cells within the top left quadrant of the graph. Isotype controls show negative expression of all markers due to inability to bind and were used to setup quadrants for limits of marker expression that were used to quantify expression on other experimental results. Overall, all variations including monolayer expanded cells show a positive shift for CD73 and CD90 in comparison to isotype controls indicating presence of these markers in the majority of the cell population. However, despite a change in pattern for CD105 there is no positive expression of this marker in a large number of cells for all variations. All results show a minor shift for the negative marker cocktail indicating presence of markers that should not be present in MSCs, whilst these represent a minority of cells there is still a stronger response than those seen in isotype controls. There were minor changes between experimental conditions with C50 leading to the highest expression of CD73 and CD90 in comparison to monolayer growth and spherical controls but none were significantly different. Summary of these results were presented in figure 5.19.

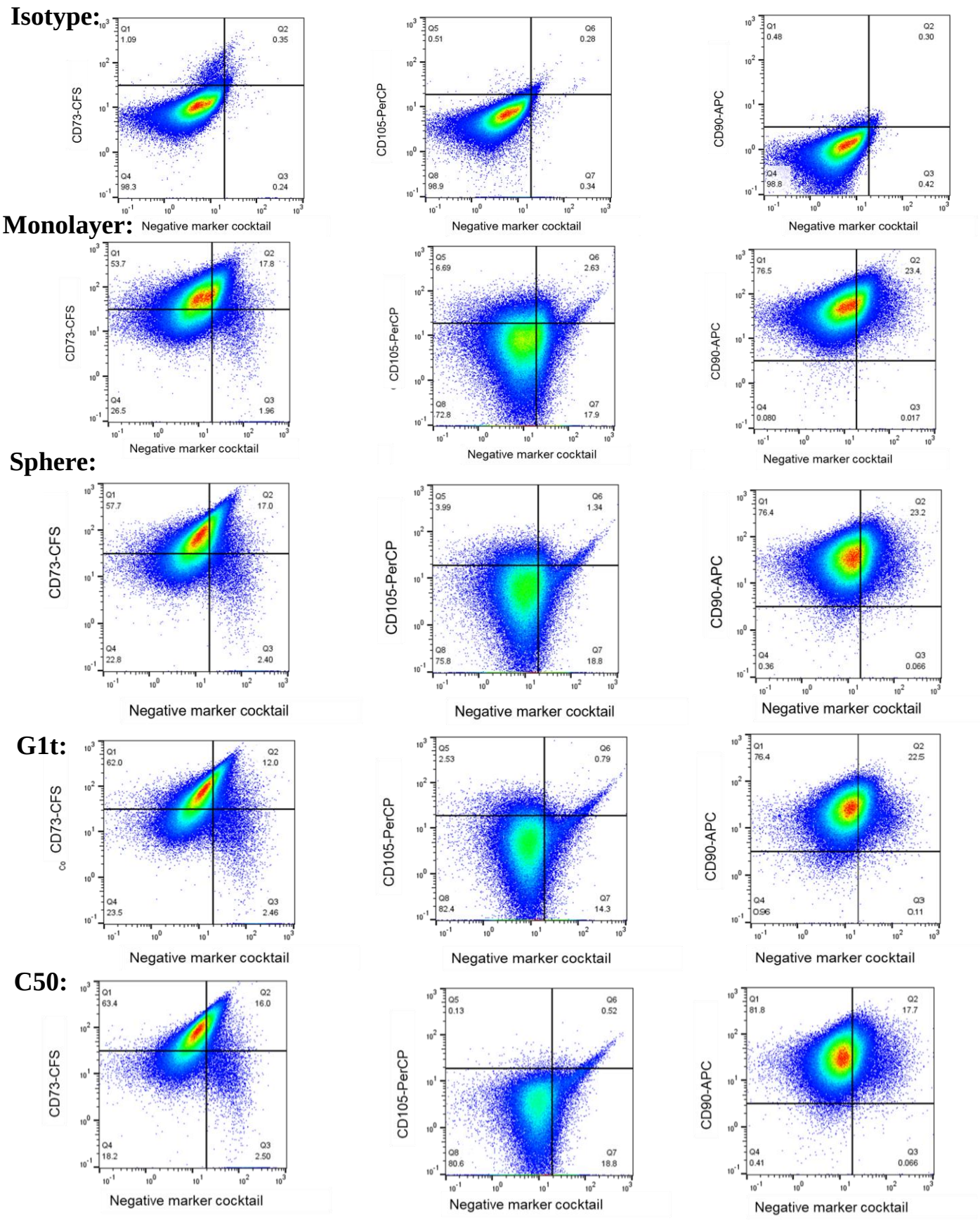


***Figure 5.18:*** *Flow cytometry of MSC marker panel on cells expanded by different PETA microcarriers.* ***Analysis*** *of three positive markers in isotype controls to monolayer, sphere, G1t and C50 expanded cells. All results indicate a shift from isotype controls to confirm presence of markers with the majority positive for CD73 and CD90 but only very small populations positive for CD105.*

Data indicates that prior to expansion 87.4% of the cell population showed expression of CD73 but 24.1% of these hits showed expression of negative marker cocktail, which included CD45, CD34, CD11b, CD79A and HLA-DR, and as such only 63.3% of cells met the ISCT criteria for CD73. After monolayer growth expansion this value dropped to 53.7% whilst spherical controls resulted in a 57.7% positive indicating an overall loss of expression but better preservation in spheres. For G1t designs 62% of cells were positive which is marginally less than prior to expansion but better than both spherical designs and monolayer growth. C50 designs produced the best result with marginal increase in positive cells to 63.4% showing maintenance of markers similar to before expanding, unlike both monolayer and spherical expansion. For CD105, positive expression is seen in 28.2% of cells prior to expansion which following monolayer growth drops drastically to 6.7% within three weeks of culture. All microcarrier designs produce a further drop in expression with spheres resulting in 4% positive expression, G1t designs with 2.5% and C50 structures resulting in only 0.1% positive expression of CD105. This indicates a loss of CD105 expression across growth that is accelerated by microcarrier expansion and most rapidly by C50 designs. For CD90 69.9% expression is seen prior to expansion which improves to 76.5% with monolayer expansion. Both spherical microcarriers and G1t microcarriers produce 76.4% positive expression almost identical to that seen in monolayer expansion. In comparison C50 designs result in an 81.8% positive expression indicating an increase in marker expression in comparison to both before expansion and other microcarrier designs. Despite these results the differences between performances of microcarrier designs and their spherical comparison were statistically non-significant. Additionally, for positive identification of MSCs marker expression is expected to be over 90% for all markers which was not observed in the cell line prior to expansion at early passages.

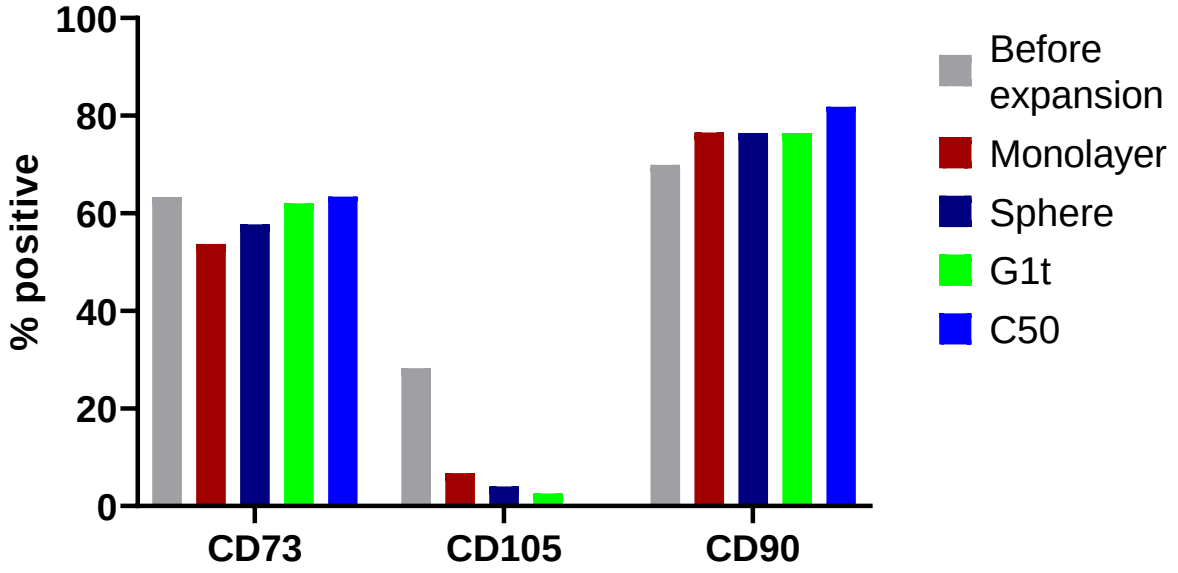


***Figure 5.19:*** *An overview of positive marker expression from flow cytometry data. Summary of percentage of cells positively expressing selected marker with absence of negative markers for monolayer grown, microcarrier grown and non-expanded cells. CD73 expression is higher when cells are cultured on microcarriers in comparison to monolayer expansion with G1t and C50 designs maintaining expression equivalent to pre-expanded values. CD105 expression negatively correlates with expansion capability of each growth variation. CD90 expression is maintained in all samples with increased expression only in c50 designs. (N=1, n=3)*

## 5.5 Discussion

Initial testing whilst optimisations and techniques were in development focused on the influence of porosity on cellular interaction and infiltration. The intent was to quantify the optimal porosity to be used in simplistic arrays as an analysis for microcarrier design concepts. Cells grown in this way exhibit a monolayer growth around structures on the anchoring substrate which can then grow into and interact with structure geometry. This differs from 3D culture induced by pHEMA coating techniques where cells were isolated to space in which they can grow in all three dimensions simultaneously without monolayer growth. Designs were initially produced as hemispheres to reduce fabrication time and provide an easier entry point for cells growing in monolayer onto structure features. In full particles designs only a small area of the particle is exposed to cell monolayer growth and could act as a bottleneck to structure colonisation. The buckyball structures used were a geometrically smoothed version of previous stick-and-ball style structures to reduce angular joints and allow for a smoother continuous surface and reduce complexity of stimuli provided in order to clarify the source of any attained effect. Given shape and structure design in buckyball structures the strut length and thickness is intrinsically linked with pore size and as such as one increases so does the other as documented in table 6.1. As such this means that the possible different effects of pore diameter and the length and thickness of struts cannot be delineated.

SEM analysis in figure 5.1 indicated a distinct lack of engagement of cells with C20 structures with a pore size of 35 µm, strut length of 25 µm and strut thickness of 12 µm. similarly, in arrays there was significant cell colonisation in 0 out of 16 structures whilst a good level of cell interaction is seen in all other structures. This may be due to the scope of architecture that cells were capable of sensing as focal adhesions which bind to surfaces creating cellular tension and signalling were only in the range 500 nm (408). It is understood that cells have the capability to sense nanoscale topographical features which affect cell adhesion, proliferation and differentiation based on features of only 15-100 nm (409). However, the effects of microscale architectures that involve the action of multiple focal adhesions, cytoskeletal rearrangement and a host of other

cellular mechanisms and signalling cascades across the whole cell were far more unknown and difficult to predict (26). What is understood is that whilst nanostructures can influence cell function, alignment and differentiation micro structures have more of an effect on overall cell morphology and cytoskeletal arrangement (410). In micro-ridged surfaces with 4-24 µm pitch grooves a level of cell alignment in 50-80% of cells whilst many others have confirmed that microscale grooves can affect cellular morphology, alignment, migration, and differentiation (411-414). Micropatterning in grids which provide anchoring in variable directions has been shown to increase multi-directional cell migration and spreading leading to a change in cell behaviours and intracellular signals (410). Whilst these effects have been observed in controlled array formats the compounding effects of complex 3D structures may limit translation of findings. In environments with constricted space, cells will migrate through obstacles by cellular deformation and cytoskeletal rearrangement but repeated restriction will impede movement (254, 415).

Results in figure 5.2 indicate interaction with all structures other than C20 with the angular morphology and positioning of cells in C50 and C80 seemingly indicative of movement through pore. This is in comparison to other structures which show growth over pore holes between connecting struts. The cellular reaction to microscale features recorded in the literature along with the typical ECM features present within tissue may indicate that the scope of architecture presented by C20 structures may not be appropriate for cells to sense or may not be suitable to prompt a response. Architecture may only be perceived as bulk material or empty space and may not present a stimulus great enough to initiate migration from the steady growing monolayer in which growth is already comfortably occurring. The behaviour of perceived infiltration around 20-30 µm pore size is comparable to similar studies on pore size in the literature, although smaller pores may still enable migration they require a greater level of cellular activity and energy to enable these movements (263). Much larger pores are capable of cell migration and often more desired in scaffolds where vascularisation and nutrient diffusion are critical. One issue encountered was the variability and gradient of cell growth across arrays. Despite movement of monolayer cell growth throughout the arrays, which can be seen in SEM images, not all structures exhibit a high level of confluence. Outer structures in arrays are more frequently colonised however, given array design there are simply more structures on the perimeter than at the centre. In

successful designs the internal four structures often show colonisation in arrays and so gradient of cell growth is likely not due structure interference or seeding method. Further cell growth over different time periods could show how colonisation and infiltration changes as confluency occurs and less surface area becomes available. Additionally larger sample sizes could aid in reliability of results but was not possible due to speed of 2PP fabrication at this time as optimisations described in section three were still being pursued.

Confocal microscopy in figure 5.3 observes the point of infiltration that appeared to be visible in SEM images but could not be confirmed since internal spacing was impossible to visualise. The Images confirms the infiltration of cells in C80 structures and lack of cellular infiltration seen in C180 designs and as previously discussed this pore size range falls within that identified by the literature that allows easy passage without significant investment by the cell. In C180 Z-profiles the small level of signal over 15-20 μm height is likely only the autofluorescent signal of the structure as 3D renders of confocal stacks show no cells within the upper parts of the structure. In C80 structures the strength of fluorescence signal is seen throughout indicate infiltration of structure interior and limits visualisation of the weaker autofluorescent signal surrounding. C80 Z profiles show an overall decline in signal throughout height which is expected given the hemispherical shape which has less surface area as structure height increases. Despite this significant fluorescent signal is still observed at peak structure height indicating full utilisation of cells across the structure which is seen in 3D reconstructions and only expressed as Z-profiles to allow reporting of three-dimensional data by 2D means. The reason for the decline in cell infiltration and limiting factor in pore size is largely due to nuclear rigidity. Cell migration through pores or any limiting space is mediated by cytoskeletal rearrangement and tissue ECM degradation through proteolytic enzymes such as matrix metalloproteinases (MMPs) (252). In the case of non-degradable structures, the limitation is in the degree of cytoskeletal rearrangement. Significant remodelling will require greater cellular energy expenditure, but the limitation to movement is due to the cell nucleus (252). The nucleus of the cell is the stiffest and most fragile part of the cell and requires significant effort to move through limiting architectures with nuclear shape being intrinsically linked to cellular function and health with even limited deformation potentially leading to DNA damage (253). As such the most limiting feature size is one that is of a cross

sectional size similar to or smaller than the nucleus of the cell and acts as a limitation for cell migration (252, 254). Human MSCs were found to have a nucleus diameter of 10.5 ± 2.16 SD μm but this value can change based on a multitude of cellular factors (255). The cells used in this initial experiment are 3T3s and as such will have a slightly smaller nucleus than the size discussed for MSCs. Measurements of the visible cell nucleus in confocal microscopy of GFP-3T3s growing within the scaffold in figure 5.3B estimate nucleus diameters of approximately 10 μm indicating similar nuclear size to the reported value of MSCs. This value for 3T3 nuclei size is consistent with the size demonstrated in the literature as 3T3 have a large nucleus in comparison to their overall form (416). This similarity in nucleus size allows expectation of similar results in MSCs. Given nucleus size in comparison to C180 pore sizes of 15 μm it is clear that pore size may limit cell travel and will be difficult for cellular infiltration. This may explain the morphology of cells seen in C180 SEMs that are capable but not likely to infiltrate until necessary due to high confluency. These initial studies only explored infiltration of structures with singular and spaced apart structures in a hemispherical fashion and would not be a true indication of a full 3D environment in a dense microcarrier culture or densely packed microparticle scaffold. Fluorescent microscopy in figure 5.4 confirms migration of cells across the array but appears to show a gradient of cell infiltration from the bottom left corner. Despite this gradient SEM images shows equal levels of cell growth on all sides surrounding the structure as such the reason for this gradient is unknown.  Gradients may simply form from the first structures to become colonised spreading more actively to surrounding areas leading to a denser growth spanning from colonised structures.

Given success of the 2.5D experiments indicating optimal porosity, which was further supported by confocal microscopy, this method was taken forward with iMSCs to analyse interactions with the variety of structures produced and detailed in section 5.4.8. As such these initial experiments could be used as sweeps for structure design to determine which architecture led to a higher level of cell interactions and analyse cell morphologies on those structures. This screening was used to find designs with a high level of cell interaction and reduce number of variations down to a level more manageable by the speed of 2PP fabrication. Positive designs are judged on SEM images across the 25 structures in each of the 29 arrays and included consistent interaction with structure features such as alignment along grooves, colonisation of

surface pits and infiltration to interiors of structures where applicable. Since microcarrier designs are intended to amplify expansion then structures with expansion enhancing qualities should exhibit visibly greater levels of confluence.

In example images in figure 5.5 closeup magnification of single structures are shown to indicate the variation in cell confluency and feature interaction between those that are considered positive hits and those that are negative. C80 structures indicate a high level of cellular infiltration and growth as can be seen through he pores confirming similar results seen in porosity analysis. iMSCs showed more structure interaction across all three dimensions and greater likelihood of infiltration than fibroblast growth. G1t structures indicate colonisation between protrusions as expected based on literature supporting the growth of cells in microscale grooves that promote cellular alignment (259-261). Additionally, growth within this niche may prevent shear stress in free culture based on structure design which would prevent cellular damage or stress response (217). However, this level of growth between grooves cannot be observed for the negative example G16 structure in which cells grow over the direction of the groove which would present a response very similar to spherical structures. This response is due to the stiffness of the cell over a groove to narrow and shallow to produce a cellular response (409). Icosahedral fractals indicate growth of cells in the predicted manner within the core of the structure which will allow surface features to prevent damage in particle collisions.

In spiked examples very little cell growth is seen within only a small perimeter at the bottom of the particle which indicates that the spiked geometry is not conducive no cell growth. Similarly in the negative dimpled example it can be seen that on several surface pores within the upper half of the particle that some pores have slight growth of cellular material. This indicates that cells have travelled within the upper portion of the structure and yet there is overall very little confluency indicating that the architecture must not be conducive to cellular growth. Whilst growth could be hidden within dimples it would be expected that much more of these would have visible covering. Many of the negative designs which have low confluency are typically more spherical block polymer shapes such as dimpled or spiked particles with less intricate features. As such this raises the question of whether growth from a surrounding monolayer is limited simply because smoother larger spherical structures present more of a challenge

in migrating over. However, despite this observation several intricate designs such as G30, C20 and several TPMS designs show little interaction despite the presence of intricate geometry indicating that the differences between designs is not solely based on access of cells from monolayer growth.

The seven final designs taken forward were C50 and C80 from buckyball designs, G6n and G1t from grooved designs, Sg from TPMS designs, H1 from 4D structure designs and V from icosahedral fractal designs. Not all chosen structures had comparable levels of cell interaction and similarly not all rejected designs were always completely devoid of cell growth. To encompass different geometries a selection across all the different design types were carried forward if significant growth was seen, in dimpled and spiked designs there was repeatedly a lack of interaction in all design variations hence the exclusion of these in further work. Whilst these designs were rejected in this simplistic experiment this does not mean that at further confluency in true 3D cultures would these designs continue to perform poorly as dimpled or surface porous structures have been shown in the literature to be effective in modulating MSC responses (204, 250, 417).

Following individual design sweeps which identified seven geometries for continued analysis, promising designs could be scaled up for a wider assessment of cell expansion and behaviour in fixed larger multi-microcarrier arrays of $1mm^2$. Using pHEMA and macroconfocal techniques previously explored in section four fluorescence could be used as a measurement of cell growth in red phalloidin stained cells along with visualisation of array colonisation. As a result of these techniques, gathered data could build upon singular particle analysis and take steps to quantify expansion potential as well as cell morphology patterns, cell migration and distribution across particle Z-axis over time. Z- axis profiles use structure autofluorescence in the blue channel to measure cell growth against structure over Z- axis. It is expected that cell growth signal will have a similar distribution to structure autofluorescence given the surface area distribution across the shape of the particle. Structure autofluorescence will be different based on structure design and as such it is not a direct comparison against cell growth and cellular values greater than autofluorescence are not necessarily a signal of extensive cell growth. However, the peaks of growth determine position of cell localisation across the structure height. The experiment lasted 28 days however day 28

results showed extremely dense growth in some structure designs that blocked fluorescence measurement leading to inaccurate measurement and so these images were not included in final analysis. In figure 5.6-5.8 only seven days of images are shown as these exhibit the greatest morphological change and observable cell patterns which become too dense after this point to visualise cell patterns. The flattened stacks and accompanying Z-profiles at day zero represent cells attached four hours post seeding and all indicate a low cell presence expected due to low seeding amount. This initial value gives a measure of seeding efficiency which is highest in spheres and lowest in Sg designs. Whilst this could lead to difference in cell growth at later time points with more visible growth in those with a higher seeding efficiency this is not seen as all have similar values and C50 structures, which are consistently best performing, start with one of the lowest seeding efficiencies. This agrees with the literature which has determined that initial cell attachment is not indicative of efficiency of cell expansion in microcarrier culture (418).

Overall arrays show growth of cellular material and cell migration throughout the array increasing over time with high confluence reached in all structures by day 7. Despite this there is still variation in cellular growth with some designs such as C50, C80 and G1t structures having confluence on day four equivalent to some structures at day seven due to difference in expansion potential. Z-profiles all show engagement of cells growing over the seven-day period and colonising more of the structure height over time and typically have a slightly lowered peak to structure autofluorescence and higher cell presence in the lower half of the particle. This continual pattern, except for films, is simply due to the effect of gravity pushing cells down towards the bottom of the structure for initial growth coupled with highest surface area at the middle of the structure (204, 249). A key difference in morphology is seen between C50 and C80 at day seven in figure 5.6 despite both leading to a similarly high level of fluorescence at day 21 and having a very similar structure layout. In C50 day seven images show heavy confluence with a densely packed array of cellular material to the point that individual cells cannot be distinguished. However, in comparison to C80 structures, which have a reduction in pore size by 7 µm down to 21 µm diameter, there is an overall less dense packing of cells with localisation to the centre with some overspill of cells around the periphery of the array. This behaviour indicates that cells may be encountering difficulty in migration through pores of C80 structures in comparison to C50 in which

they can freely migrate through. Whilst C80 pores do not fully impede cell migration they may require a slightly greater investment of cellular energy for cytoskeletal rearrangement as pore size is at the precipice of restricting free movement. Once greater confluency is established after seven days there is more necessity to move through these pores as surface area becomes limited which is why overall results catch up by experiment end. Whilst this explanation for differences aligns with the understood mechanisms of cell movement through pores it is still only theoretical as exact cell migratory mechanisms in complex microenvironments are not understood to this level of intricacy (252, 254, 415).

Other morphological analysis of stacks indicates different cellular morphologies induced from certain geometries such as Sg structures which appear to lead to cell stretching and elongation of cells. In comparison this is not seen in other structures such as H1 where cells are very small and contained. The effects of this will be determined in further experiments, such as section 6.4.6, to determine if stretching of cells seen in Sg leads to greater osteogenic commitment as the literature would suggest (414). Other events seen include day seven microscopy for spheres which appear to show a section of cell growth that may have peeled from array surface to the bottom right. This occurrence reduces reliability of measurements but is not apparent in any other samples even at higher confluence. This finding is consistent with the fact that smooth spheres will have less surface adherence for cells in comparison to structures with porosity or smaller surface feature sizes and this may have consequences in microcarrier culture if cells cannot remain adhered (410). Overall highest fluorescence is seen in C50 and C80 with highest estimated expansion yields whilst G1t, V and H1 designs have a moderate performance greater than spherical controls but less than buckyball designs. Finally lowest performing designs are G6n, Sg and spherical controls. However, these measurements are based on fluorescence measurement from phalloidin stains and as such the only guaranteed measurement is between the difference in F-actin. Whilst greater number of cells will lead to more of this staining the exact correlation between cell number and staining cannot be guaranteed. F-actin amount changes based on a variety of cellular conditions and is not a continually static amount that is even between all cells in a population(419). Additionally, data shows that the earliest response in differentiation is the reorganisation of actin filaments in the cytoskeleton that precede morphological changes, as such any physical cue that induce

differentiation may lead to a different staining amount (419). Furthermore 3D culture changes cell volume and it has been shown that this volume change can include an increase in actin fibres however this volume increase is still variable based on morphological restriction by the microenvironment (26). Given each design is different there is also varying levels of cellular restriction, this is obvious by comparing C50 structures that have a lot of empty space in comparison to spheres in which close packing reduces the area in which cells can occupy and spread. In addition, the physical measurement of multiple fluorescent signals over several overlapping cells in structures may not have the accuracy to reliably measure the combination of fluorescence without distortion from various coinciding signals. The only way to fully identify success of this method is by comparison to DNA quantitation in section 6.4.4 and by comparing fold increase we can determine that fluorescence estimation is moderately accurate. Results of fluorescence estimation identify top performing designs as well as Sg and spheres as lesser performing designs but the results at final day are not an exact match to DNA results. Results also confirm some trends seen in 6.4.2 with early structure sweeps that identified less cellular interaction with bulk spherical type designs. However, in this case the pHEMA technique eliminates the doubt that lesser interaction was seen only due to difficulties with cell accessibility from monolayer growth.

Macroconfocal analysis focused on growth patterns throughout structures but also utilised fluorescence to measure expansion potential given that information was already available through the extracted data set. However, a more accurate method of expansion analysis was pursued using DNA quantitation. The literature indicates that DNA quantitation is the most accurate and reliable way for determining cell populations growing on microcarriers and is the standard used in many studies where cell removal and microcarrier degradation is not desired (216, 420, 421). The overall outcome of this experiment indicates that C50 and C80 designs lead to highest expansion with approximately an 11-fold increase in cell amount from starting populations which is almost twice as much as spherical controls. The third best performing design is G1t that shows an 8-fold increase in comparison to spherical 3D control designs that produce around a 5.6- fold increase. H1 and Sg designs perform worse than spherical 3D controls. Unlike the results of fluorescence measured expansion, there is a greater divergence between results at later days indicating that fluorescence-based measurement of expansion at high confluence may be unreliable.

The fluorescence-based measurements still highlighted C50 and C80 designs as best performing designs but other designs such as H1 or Sg that appeared to perform better than spherical controls in fluorescence measurement are determined by DNA results to perform worse than controls. Buckyball designs are consistently best indicating the importance of porosity which is backed up by the literature which describes porosity as critical to increasing cell proliferation (263, 410). However the form of porosity in buckyball designs is different from the sort of random, interconnected porosity throughout structures that is expected in particles formed with techniques such as phase separation, solvent casting particle leaching (SCPL), gas foaming or lyophilization (422). The effectiveness of this design may come more from its hollow interior and porous frame which would not be possible to fabricate without additive manufacturing techniques. Similar designs of H1 structures, which are truncated buckyballs with reducing internal architecture do not show as favourable results but reducing internal pores may limit cell movement as previously discussed. Interestingly G1t designs show impressive expansion despite lack of porosity which indicates that this is not the only type of geometry that is important in increasing cell expansion. The effectiveness of grooves has been demonstrated in the literature for cell alignment and proliferation (259-261). However, the types of grooves represented here are not comparable with established literature as they exhibit a change in both width and curvature in a unique way. Another observable trait is that both sg and H1 designs, which both have intricate internal networks, are worst performing. Macroconfocal analysis shows that cells have access to this space and can migrate through structures but intricate internal networks of small pore size could possibly reduce expansion through physical space restriction, as previously discussed.

An identical experiment for DNA quantitation was performed in a secondary material. Inclusion of TMPETA replicates acted as a material comparison to assess whether the relationship between shape and expansion yield was consistent among multiple materials. In TMPETA replicates C50 and C80 designs remained best performing structures with an approximate 6-fold increase in comparison to spherical 3D controls which had a 2.8-fold increase. In comparison to PETA the results from the TMPETA version of G6n produce a result comparatively greater than its spherical controls. The lower ranking designs all cluster closer to each other in TMPETA versions than PETA. For example, PETA spheres produce a 5.5-fold increase and worst performing

experimental design Sg has a 3.5-fold increase, or only 63% as effective as spheres. However, in TMPETA spheres produce a 2.8-fold increase and lowest performing Sg designs produce a 2.2-fold increase which is 78.5% as effective as spheres. This indicates that despite overall similar ranking of design effectiveness the exact trends between designs are slightly changed between materials. The main reason for overall reduction in TMPETA is due to the material being less adherent to cells as concluded in section 5.4.2. This can be demonstrated by comparison of material films with glass positives which have the same space and flat geometry with the only difference being material. Films see a 2-fold increase in comparison to glass controls which show a 3.1-fold increase, which determines that TMPETA has an effect only 64% effective in comparison to glass. Glass positives also performed better than several designs when produced in TMPETA which is again due to level of adherence to glass materials in comparison to the polymer.

However, this method does not account for the innate differences in colonisable surface area between the different design variations. Surface area is variable between designs meaning that some microcarriers simply have more space for cells to grow than others. This is critical given that the classical goal of microcarriers and any expansion technology is to provide maximum surface area and in the past an expansion technologies measure of success is based purely on presentation of surface area (189, 194). This is demonstrated in flat and film controls which have $1mm^2$ of surface area, which is much smaller than any microcarrier design. This means that films reach full confluence earlier than any other design limiting the fold expansion that can be achieved by the final time point as there is no space left for colonisation. The key difference between these two interpretations of the data is that fold increase determines which microcarrier design is best for cell expansion whereas adjustment by surface area answers a more intricate question of which geometrical design delivers the greatest mechanobiological signal to increase expansion. Correction by surface area only broadens the gap in performance of buckyball structures relative to other designs as these designs don’t have a large amount of surface area in comparison to other structures. Lowest performing designs such as Sg and G6n do not lead to significant expansion despite having one of the highest surface area values. This is in contrast to fold increase experiments in which G6n microcarriers placed as 4th best design for fold increase in cells. Data suggests that contrary to the literature that provision of surface

area is not the only factor effecting expansion. With TMPETA a greater difference is seen between buckyballs and all other designs as also seen in fold increase experiments. The difference in material adherence is made evident with highest amount of DNA being achieved on glass controls following surface area correction. In surface area corrected TMPETA spherical controls the overall expansion performance is better than G1t and V structures which is not evident in PETA variations which indicates that design performance changes based on material adherence. Summary data in figure 5.14 indicates that when corrected by surface area buckyball designs are the only variations that have significantly increased expansion in comparison to spherical controls.

Protein production over the expansion period was pursued to determine if any designs lead to a different cell behaviour than others. The highest protein content is recorded in buckyball designs following the trend set by DNA quantitation. Interestingly C80 produces more protein than C50 despite highest expansion in C50. This indicates that the reduction in pore size between C50 and C80 structures somehow leads to higher protein production. G1t structures delivered the third highest recorded protein content per unit of surface area and V structures followed very closely which is similar to DNA results. However, unlike DNA results these increases in in G1t and V designs were statistically different from spherical controls. Remaining experimental microcarriers including Sg and G6n designs performed less than spherical controls still correlated with cell number determined by DNA quantitation. The reasons for these changes in protein production may be due to the interaction of cells in the differing 3d environments. Studies have demonstrated that increase in cell area and volume can lead to increases in actin cytoskeleton, additionally the morphology that cells take can result in cellular torsion which again increases protein production and stress fibres (26). Small, rounded cells, which could be due to confined physical environments, lead to a lower stress fibre and protein amount in comparison to stretched cells (423, 424). Interestingly the greatest decrease in protein in comparison to cell number was seen in glass controls. This would suggest that the glass material leads to less protein than polymer given that films showed little difference compared to cell number. This would correlate with the formation of actin stress fibres that may result from the increased adherence difficulty seen between PETA and glass. Additionally, whilst glass 2D controls will exhibit smooth surfaces the films are still 2PP produced with a nanoscale

surface topography or roughness from laser travel paths that could change the ways in which cells adhere and react to the surface. It is known that nanoscale topographies lead to a greater increase in cell adherence and induce greater cytoskeletal stress which in turn leads to further actin stress fibres (409, 425). Whilst outcomes were similar to DNA expansion, namely with success of buckyball structures, there are some key differences indicating that level of protein is not purely based on the level of DNA or cell expansion and that some designs promote an increased level of protein production than others, although the exact reasons and mechanisms for this are not fully understood. Future work could seek to investigate ECM protein expression to identify this change.

Samples were analysed for differentiation into osteogenic lineages throughout the course of the experiment with specific focus on if certain designs lead to a higher differentiation rate than others. General culture with microcarriers has been reported by many groups to increase osteogenic activity and improve the MSC aptitude for osteogenic and chondrogenic differentiation in comparison to planar culture with microcarrier culture being reported to sometimes lead to spontaneous osteogenesis in basal media (242, 258, 399, 426). Analysis of early osteogenic and chondrogenic markers in microcarrier culture indicated enhancement to RUNX2, ALPL, COL1, SOX9 and osterix expression as well as some late markers of osteogenesis such as IBSP (258, 363). In contrast microcarrier culture has been reported to lower expression of adipogenic related genes such as PPARγ2 (204). In general, this phenomenon is related to a number of physical cues that are present in microcarrier culture that are not present in planar culture. One inescapable factor in microcarrier culture is surface curvature. Convex surfaces increase F-actin fibre presence and osteocalcin levels in comparison to planar culture which becomes stronger with decreasing convex diameters (257, 258). The mechanism that increases osteogenesis is thought to be based on the increased cytoskeletal tension within the cell and actomyosin contraction which exerts force on the perinuclear actin cap deforming the nucleus and leading to changes in gene expression (204, 257). This mechanism is applicable to a range of different physical cues that lead to changes in cellular cytoskeletal elements and are often present in intricate architectures. Spreading of cells across topographical features that increase cellular area and volume is shown to lead to osteogenic induction such as microscale ridges and other micropatterns along with microscale pores (414, 427-429).

In addition, increases in surface roughness caused by nanotopography and material stiffness or elasticity can induce osteogenic differentiation (230, 263). These physical factors are often present in microcarriers at variable levels, depending on specific microcarrier material and design, and even more abundant in the 2PP microcarriers investigated in this work. As such, osteogenic differentiation is a relatively likely outcome if MSC phenotype cannot be maintained and would not be suitable for expansion where osteogenic priming is not desired. Given this information the measurement of ALP activity, which is an early marker of osteogenesis, was conducted to ensure the stability of the stem cell phenotype over culture period and observe if certain architectures lead to a higher likelihood of osteogenic differentiation than others. Baseline levels were first tested in the iMSCs when subject to an osteoinduction protocol as a comparison. Microscopy indicates the change in cell morphology along with expected results with cell elongation and calcium deposits. ALP activity rapidly increases and peaks at 21 days before activity reduces which is consistent with the transition of cells into more mature osteogenic tissues as detailed in the literature (430, 431).

ALP activity detected from cells cultured on the various microcarrier designs show that after normalisation to DNA amounts there is no significant difference between any of the designs and that all structures show activity levels to be a fraction of positive induced controls cultured in osteogenic media. This data indicates that no osteogenic response is seen although full maintenance of stem cell phenotype cannot be confirmed until further testing.  If induction of osteogenic response was desired incorporation of hydroxyapatite nanoparticles could be incorporated into 2PP resins to produce structures that actively increase osteogenic responses and this approach has been used before in other biomaterials designs (432). Whilst 2PP fabricated complex microcarrier designs such as those presented in this research have not been investigated previously other particles with surface topographical features have been demonstrated to have osteoinductive effects. Surface textured PLA microparticles of dimpled and angular varieties produced through emulsion-based techniques indicated increased ALP activity in dimpled particles in comparison to smooth controls. Additionally, osteocalcin levels indicated significant difference between both dimpled and angular particles in comparison to smooth controls but yet ALP levels of angular particles did not differ

from smooth controls (417). This data indicates that additional tests might be necessary to confirm absence of osteoinduction.

Free microcarrier culture was pursued for scale up experiments and use of microcarriers 3D suspension culture and not as fixed arrays. Despite this the volume of carriers that could be produced limited culture to static methods only. So far measurement of microcarrier effectiveness and cellular effects are indicative only of static fixed culture which would not necessarily indicate their performance in agitated free microcarrier culture. Studies have suggested that growth of MSCs between static culture and agitated culture in spinner flasks are not comparable with agitated cultures leading to enhanced growth (222, 418). Despite this static culture is still a viable and commonly used method of growth and does not lead to cell necrosis or cell death above normal rates (222). Other studies have found that statically cultured aggregates showed no cellular membrane damage and that cells harvested from these clusters had high viability after dissociation (222). This would agree with Live/dead staining in which indicates that both on early culture and in high confluency clusters there is still a low level of cell death. Whether the observed difference between designs would remain in agitated culture is uncertain as there is no precedent for microcarriers of this type in different culture techniques. Microcarriers can sometimes lead to a similar level of proliferation as planar culture, depending on the microcarrier used, and increase in expansion is achieved only through additional surface area. However even when proliferation rates are similar there is increased cell volume and morphology changes when grown in 3D (433). Retrieval of iMSCs from microcarriers and replating of these in planar culture indicated typical morphologies as seen in figure 5.17 with no retained differences to cell volume or area. This indicates that cells remain largely unchanged throughout expansion despite changes to morphology that might occur during microcarrier interaction. This is important as static microcarrier culture can potentially expose cells growing on microcarriers to increased levels of shear stress and surface collisions that may not have occurred in fixed arrays. Increased shear stress, typically those experienced in agitated structures, can result in reduced MSC quality, viability and therapeutic potential and increase osteogenic differentiation (434, 435). Live/dead staining does not indicate any reduced viability in static microcarrier culture and microscopy of expanded cells do not exhibit morphologies or markers of osteogenesis. Transition to free microcarrier culture, even in static forms, still increases the chances

of particle collisions which can result in cell damage along with aggregation and clustering (436). Whilst clustering is seen in static growth this only formed after high confluency was achieved and is more attributed to the static method of growth. Live/dead microscopy of clusters can determine that if collisions were the cause of clusters they did not lead to any notable cell death. As such the liberation of particles from pHEMA substrates and subsequent static microcarrier culture was successful without any visible signs of cell damages and removal of cells from carriers was achieved with simple enzymatic digestion even in clustered growth. As such this technique was taken forward to stem cell marker analysis to ensure microcarrier based growth was more akin to normal microcarrier culture methods but ultimately were still limited based on fabrication capability.

Following on from identification of structures that lead to a high expansion yield the effects on stem cell phenotype were explored. Expansion of stem cell for therapies or experimentation need to maintain stem cell phenotypes, quality and therapeutic capability in order to be useful. With enhanced expansion based on architecture there could be a strong chance of phenotypical change as well. Utilising the free microcarrier culture method described in section 6.4.7 and scaling up microcarrier production from small structure arrays the stem cell phenotypes of iMSCs cultured on three microcarrier variations was pursued. iMSCs were expanded for three weeks on C50, G1t and spherical microcarriers fabricated in PETA. These structures represented the best performing design, moderate expansion design and spherical 3D control as a typical microcarrier comparison. The ranking of these designs is based on data presented in figure 5.9 with microcarrier performance being rated on fold increase of cells. Cells were then analysed for ISCT criteria stem cell markers along with monolayer grown cells to determine if expansion led to any changes in stem cell markers or phenotype both between microcarriers and in comparison to planar culture. ISCT criteria outlines specific standards to classify as an MSC. These include the positive expression of surface markers CD73, CD90 and CD105 and the absence of CD34, CD45, HLA-DR, CD14 or CD11B, CD79α or CD19 expression (62). The two other standards include adherence to tissue culture plastic and the capability of *in vitro* trilineage differentiation to adipogenic, chondrogenic and osteogenic lineages (62). However, it is still reported that cells falling under these criteria can still exhibit variance in biological features based on donor variation, source material, culture materials and conditions (63, 204).

The expected expression of these markers should be ≥95% expression for positive markers and ≤2% expression for any of the negative markers. Data indicated unexpected results with marker expression not reaching this standard in all positive markers and presence of negative markers higher than permitted. This finding occurred with freshly thawed cells at low passage number and presented in this way even prior to any expansion. The iMSCs were prepared and immortalised in house and were at passage number 7, the lowest number at which they were received after immortalisation. The analysis was conducted with multiple similarly immortalised cells used by many groups and was always the same. The literature shows how surface markers and differentiation potential of MSCs can be extremely variable even within young populations with other positive markers such as Stro-1 can be expressed at less than 10% by P3. Further to this, most positive markers assessed had around 96% expression only just crossing the permissible threshold. CD73 was seen to be maintained through P3-P8 however CD90 saw a low but non-significant drop at P8 whilst CD105 saw a drop in expression starting from P5 and reaching lowest expression by P7. Additional loss of surface markers CD106 and CD146 were seen to significantly change and deplete from P3 -P8 (437). This indicates how variable expression of these specific markers can be even in primary MSCs extracted from bone marrow.

The literature does not agree on the exact effects of immortalisation to MSCs relative to their surface marker profile with some studies suggesting that hTERT modified MSCs maintain expression of markers at rates similar to unmodified cells (438). However other studies have indicated that this can significantly effect expression with the modification leading to 88% expression in CD73, 93% expression in CD90 and a larger reduction of CD105 positive cells down to as low as 25% (439). These values are much closer to the observed values seen in experiments particularly with highest expression in CD90, moderate expression of CD73 and low presentation of CD105. Given stem cell marker variability in comparison to ISCT criteria the experiment progressed to determine how those levels of marker expression were maintained across the expansion period. CD73 correlates to the NT5E gene which codes for the enzyme ecto-5′-nucleotidase which is involved in adenosine conversion from AMP and is associated with immune regulation and interpretation of paracrine signals in mediation of anti-inflammatory activity (440). Presence of this surface marker which would correlate

with MSCs strong immunomodulatory capacity reduced in monolayer expansion but was better maintained in 3D culture with preservation seemingly linked to expansion capability with C50 maintaining phenotype prior to expansion. This correlates with the literature which suggests that 3D culture increases paracrine immunomodulatory potential of MSCs in comparison to planar culture (441). CD90, also known as Thy-1, is a glycosylphosphatidylinositol (GPI) anchored glycoprotein that is involved in numerous cell functions, notably high CD90 expression in MSCS is associated with maintaining undifferentiated phenotypes with reduction in expression marking lineage commitment (442). Data indicates an increase in this surface marker across all conditions with equal presence across monolayer grown cells across those expanded on Spheres and G1t designs and a greater increase in cells expanded on C50 structures. This would seemingly indicate that C50 enhanced the undifferentiated state of MSCs cultured and overall this disagrees with the expected outcome of general loss of phenotype over time (437). CD105 also known as endoglin is a type I transmembrane protein which is implicated as a receptor in TGFβ signalling and recognised as a marker for endothelial cell growth and angiogenesis (443).

Interestingly a far decreased value of CD105 was seen in all expansion methods with the lowest value correlating expansion efficiency achieved in C50 structures that had practically no expression of this marker. This decrease in CD105 is observed to different degrees in various other studies indicating that despite ISCT criteria is often variable in MSC population(437, 439). Studies have identified that MSC populations that show negative CD105 markers are consistent with a far increased immunomodulatory profile in comparison to those that are CD105 positive and may be due to autocrine production of TGFβ1 in CD105 negative cells (444) . Despite this no change in MSC stemness or differentiation potential was seen between the two populations which challenges the accuracy or necessity of criteria set out by ISCT since CD105 expression is not necessary for MSC function which should perhaps be revisited given the increase in information over the past 16 years from the implementation of the criteria in 2006 (62, 444). Investigation of immunomodulatory profiles of MSCs expanded on different microcarriers could give an indication of another aspect that could vary between carrier designs. Despite findings the experiment should be repeated with primary MSCs that do pass the criteria prior to expansion in order to fully understand the effects of microcarrier expansion on stem cell phenotype.

## 5.6 Conclusion

Early work analysed 3T3 interaction with buckyball structures indicating an appropriate pore size diameter that leads to cellular infiltration. Arrays of the 29 designs were screened to identify geometries with high levels of cell interaction highlighting seven positive designs. Growth analysis results estimated cell expansion yield through measurement of total fluorescence and later confirmed with DNA quantitation that buckyball designs led to an expansion yield two times greater than spherical controls. G1t designs produced a moderate expansion response greater than spherical controls but less than buckyball designs. Structure geometry impact was investigated by surface area correction indicating a significant expansion effect triggered by buckyball designs that was not due to presence of surface area alone. Total protein content of cells over the expansion period indicated that whilst protein was correlated to expansion yield that some designs led to a higher protein production than others which may be due to cytoskeletal stress. Early osteogenesis marker ALP was explored but none of the designs led to a significantly high ALP activity indicating lack of osteogenic differentiation over expansion period. Free static microcarrier culture indicated healthy expansion of cells that were retrievable by normal enzymatic digestion methods. Stem cell marker analysis concluded that expression of markers was not as expected but was not significantly different between microcarrier types. Overall, the investigation concluded by identifying cell morphologies, expansion profiles and other characteristics attributed to microcarrier designs with highlight of buckyball designs in leading to far increased expansion profiles in comparison to typical spherical profile of most commercial microcarriers. Further work to investigate change in expression of surface markers is required to draw reliable conclusions.

# 6. General discussion and future work

Suitability of materials in 2PP is limited to mostly acrylates and some epoxy polymers although new materials are constantly being developed and adapted for 2PP (310, 314, 317). As such materials used in initial work are all acrylate types that have previously been demonstrated for 2PP fabrication in the literature (300, 319). Biocompatibility testing was first attempted without using 2PP to save time on lengthy fabrication, but results yielded results with TCDMDA and PETRA that did not translate to their 2PP produced counterparts. In PETRA the viscosity may have hindered radical diffusion when exposed in large quantities which prevented a full cure thus affecting biocompatibility. The addition of the underlying glass substrate in 2PP samples provided cells on 2PP samples with choice of two materials as such what might be observed is preference for surrounding glass given relatively small size of films as opposed to inability to adhere to 2PP fabricated films. For future work both issues encountered could be remedied by spin coating as used in other polymer coating studies (353). This technique wasn't pursued initially as only a few polymers were required for testing given choice to pursue microcarrier shape over materials but presents an opportunity for future work. Further analysis with 2PP fabricated samples indicated high biocompatibility of all materials, this is in line with the literature that all these materials are biocompatible (300, 307, 323, 375). Further exploration of available materials could be a future step that could provide better cell adherence and fabricability which could enhance microcarrier effect even further. This is also an interesting area for future exploration as expansion yield appeared to be affected by differences between the PETA and TMPETA materials despite identical geometry. Future materials work could be expanded to use of modified versions of popular biomaterials such as PCL or PLA that are made 2PP accessible through chemical modification such as urethane end capping (310, 445-447). These materials would not only be more suitable for cells, have potential degradability and be more characterised in the literature but they would also serve as a better comparison to commercial microcarriers.

Fabrication speed limits were addressed by a series of writing optimisations intended to increase fabrication speed at the cost of resolution. A reduction from 0.1 µm slicing and hatching to 1 µm results in a 74x speed increase whilst still maintaining faithful 3D model fabrication. However, increased slicing leaves more pronounced layer lines and can induce a nanotopography or surface roughness (342). Li et al demonstrated that 200 nm features could influence stem cell differentiation (343), although this feature could be deliberately induced to control cell outcomes. Surface roughness has been shown to alter wettability, cell attachment, protein adsorption, proliferation, MSC differentiation and can alter how cells perceive substrate stiffness (11, 409). Additional speed increase can be pursued through increasing laser travel acceleration which trades laser travel accuracy for speed increase. Galvo acceleration is an aspect of fabrication not considered or mentioned in the 2PP literature outside of photonics. Further speed increases could be sought through experimentation with different polymer chemistries and photoinitiator. More reactive photoinitiators that release more radicals upon excitation could lead to a larger voxel size, this would in turn mean that higher slicing distances could be used without layer disconnect seen in extreme low resolution writing profiles (313, 339). Other ways to achieve faster fabrication include the more recently established two-photon grayscale lithography (2GL) which has controllable laser focal volume (348). Lowest resolution profiles reduced C80 particle fabrication to as low as one second but were not viable structures mostly due to layer delamination. With suggestions to combat this, stable one second particle production could be achieved which could be fast enough to allow for fabrication without an anchoring base as fabrication would be completed before the particle had time to drift. This could then be applied to a continuous flow lithography system for high throughput microcarrier fabrication similar to systems that have achieved this with very simple shapes (448).

The 2PP process was shown in this work to also be suitable for fibre production in a controlled fashion initially explored as a potential surface coating or architectural feature on structures. 2PP has been used to produce fibres before but in a way that involves a fixed voxel point with polymer flowing continually to create a long continuous fibre which appear impractical in comparison to techniques such as electrospinning (350). Future work could focus on continuing exploration of potential uses such as fibre screening tools or production of unique fibre textures, irregular shapes or fibre linked particles that would not be achievable by other fibre

methodologies. Multi material structures were another 2PP possibility explored but not taken further and present an opportunity for future work. Whilst production of such 2PP structures has been demonstrated in the literature it has never been translated to microcarrier production (321, 328). Future exploration of this area could focus on production of microcarriers with outer coating materials for initial adherence that degrade to reveal secondary chemical or topographical stimuli forming a two or more phase 4D structure.

The optimisations made to increase 2PP speed had a dramatic impact on scalability for laboratory experiments, however for clinical scaled production 2PP still fails to meet the necessary production level. Novel and future technologies such as 2GL, multi-focal beam splitting and holographic lithography may allow for future 2PP technologies to address clinical scale (348, 449, 450). For current work scale up feasibility was explored using PμSLA which was shown to reproduce buckyball geometry with minor increase in size due to loss of resolution in comparison 2PP. Production in this methodology could address scale-up theoretically being able to produce millions of microcarriers within the space of a few days which could take years by 2PP even with current optimisations. Optimisations of this technology represents steps planned to be pursued within this research that was not possible due to effects of the COVID-19 pandemic.

Novel techniques for 2PP production and cell structure isolation were identified in this research with fabrication of 2PP structures on cell repellent polymer coatings for isolation of cells to structures and elimination of extraneous signals from surrounding non-relevant growth. This addresses issues found within own experimentation but also addresses difficulties note by others using 2PP structures to study cell behaviours (354, 355). However, this method is still in need of further optimisations and further work which could be achieved through methods discussed by Ingram *et al* (353). Additionally, interface detection through a dye to increase refractive index could result in a methodology that could be extremely useful for many 2PP bioapplications. Surface modification to improve cellular adhesion to carriers was pursued given that many commercially available microcarriers include a form of surface treatment or coating to improve cellular adhesion and proliferation often with collagen or other protein type coatings (222). Significantly improved adherence was seen when structures were

treated with poly-L-lysine, a technique that has been previously used in the literature for increasing microcarrier adherence (363). However, these effects were strong enough that it became difficult to delineate the effects of microcarrier surface chemistry from the effects of microcarrier shape. Surface treatment was pursued that improved surface suitability for cells without a forced attachment, given tissue culture plastic is oxygen plasma treated this was the method applied. This proved effective in increasing cell attachment but identified a phenomenon under different etching times that has been used by others to reduce feature size (383). Whilst sub 100 nm resolution is not necessary for this work this method could be applied to intricate structures than can be fabricated rapidly using increased voxel sizes and thicker lines followed by etching to reduce that thickness allowing structures with the same feature size to be produced many times faster.

One of the first architectural features explored for cell interaction was pore size diameter that was tested through a series of buckyball variations cultured with 3T3's. results showed a lack of engagement of cells with C20 structures with a pore size of 35 µm, heavy colonisation of C50 and C80 structures in which cells assumed an angular morphology and positioning across pores. Growth in C180-C540 exhibited growth but was more of an outside covering and interior growth could not be confirmed. The issue was C20 was believed to be due to the architectural sensing limits of cells since focal adhesions which bind to surfaces creating cellular tension and signalling are only in the range 500 nm (408). Cellular infiltration around 20-30 µm pore size is comparable to similar studies on pore size in the literature (254, 263). Confocal microscopy examines the point of infiltration confirming the infiltration of cells in C80 structures and lack of cellular infiltration seen in C180 designs. The reason for the decline in cell infiltration and limiting factor in pore size is largely due to nuclear rigidity. Cell migration through pores is mediated by cytoskeletal rearrangement and significant remodelling will require greater cellular energy expenditure, but the limitation to movement is due to the cell nucleus (252). The nucleus of the cell is the stiffest and most fragile part of the cell and requires significant effort to move through limiting architectures with nuclear shape being intrinsically linked to cellular function and health with even limited deformation potentially leading to DNA damage (253). This migratory function through identified pore sizes was further confirmed in larger arrays. Future work could seek to explore the differences seen in iMSCs vs the 3T3s initially used as well as

utilisation of pHEMA techniques and greater number of designs with smaller pores size changes to fully explore this movement in greater detail.

Whilst initial testing focused on buckyball designs as controlled measures of porosity the greatest strength of this technology was yet to be employed and so a variety of 3D models were designed for production as microcarriers. These architectures were designed to present features, identified in the literature, which are known to affect cell growth and differentiation with the aim of enhancing cell expansion greater than flat surfaces and modulating MSC differentiation. Whilst buckyballs addressed porosity grooved structures explored the effect of directed cell growth and alignment that has been show in the literature to effect proliferation and differentiation (259, 261, 402). Several designs including icosahedral fractals are designed to provide protection from shear stress and surface collisions which can damage cells (217). TPMS models exhibit large surface area to volume ratios along with high load bearing mechanics and porosity, microcarrier technology was initially designed to only provide increased surface area and as such this is an important feature to test (404). Dimpled structures exhibit recesses of different frequency, depth and therefore curvature and similar pockets are seen in natural tissues which provide further degrees of curvature as well as surface shelter from collisions and shear stresses (405, 406). 4D structures include internal geometries for further colonisation space and further 3d integration of tissues with anchorage in all directions. Spiked structures are lesser explored in the literature but were included to probe feature reaction as well as to investigate claims that spike structures can enhance stem cell differentiation and growth factor secretion (407). With these designs a control sphere was included as a comparison against a typical microcarrier architecture given that the vast majority of commercial microcarriers are spherical in nature owed largely due to the manufacturing methods. With varying designs manufactured in arrays testing was pursued with iMSCs to determine effects of structures on cell growth and interaction using the same methodology employed in porosity investigations, Results of this investigation identified seven structures that had visibly high confluency and structure interaction across several of design types.

Strategies for imaging were often complicated by the autofluorescence of the structures due to the photoinitiator presence which is not uncommon in 2PP structures (386). In cell morphological analysis overlapping signal due to autofluorescence obscures details

and limits analysis. Irgacure 369 was the initiator used which has high reactivity and allows for rapid writing parameters as well as extremely common use in 2PP (298, 303). Alternative strategies could be utilised such as NIR only fluorophores, molecular quenchers, PI free resins as well as photobleaching which was the method employed in this case (386). Photobleaching reduced autofluorescence but was not successful in structures of greater material thickness due to lack of UV penetration. Despite this issue, confocal images was pursued but issues with loss of signal due spherical aberration, scattering and rapid loss of signal at depth limited success (387). Multiphoton microscopy could be used to improve depth penetration as this method possesses twice the depth and is typically considered the best approach for imaging large samples (388). In the absence of this, macroconfocal was used which showed impressive resolution and detail of cellular morphology but still retained autofluorescence. No autofluorescence was seen at 635 nm as such a phalloidin stain within this range was used allowing full structure depth with signal from cellular material and structure autofluorescence independent of each other.

Following individual design sweeps scale up was pursued for a wider assessment of cell expansion and behaviour in fixed larger multi-microcarrier arrays. Day zero results represent cells attached four hours post seeding and act as a measure of seeding efficiency which is highest in spheres and lowest in Sg designs. Whilst seeding efficiency does not vary significantly the observations indicates that seeding efficiency is not indicative of microcarrier performance as C50 structures have low seeding efficiency despite overall highest expansion yield. This agrees with the literature which has determined that initial cell attachment is not indicative of efficiency of cell expansion in microcarrier culture (418). There was observed variation in cellular growth in C50, C80 and G1t structures having confluence on day four equivalent to some structures at day 7. Z-profiles indicate greater growth in the lower half of all designs which is believed to be because of gravity (204, 249). C50 and C80 designs show variation in early growth patterns at day seven believed to be due to difficulty in migration through pores which are slightly smaller in C80 designs although exact cell migratory mechanisms in complex microenvironments are not understood to this level of intricacy (252, 254, 415). Overall highest fluorescence is seen in C50 and C80 with highest estimated expansion yields whilst G1t, V and H1 designs have a moderate performance greater than spherical controls but less than buckyball designs.

DNA quantification was pursued in order to accurately determine the amount of cellular expansion occurring in microcarrier designs. DNA quantitation is the most accurate and reliable way for measuring cell populations and is the standard used in many studies with alternatives being counting of detached cells and metabolic assays (216, 420, 421). The overall outcome indicates that C50 and C80 designs lead to highest expansion with approximately twice as much as spherical controls whilst G1t shows nearly 1.5 times the expansion of spheres. All others produce less or equivalent to spherical controls. Buckyball designs are consistently best indicating the importance of porosity which is backed up by the literature which describes porosity as critical to increasing cell proliferation (263, 410). G1t designs show impressive expansion despite lack of porosity which indicates that this is not the only type of geometry that is important in increasing cell expansion. Correction by surface area indicated which geometries have a greater expansive effect for future design and proved buckyball structures as most effective despite having a lower surface area than many other designs. This shows that maximum surface area is not the most important factor in microcarrier design (189, 194). Overall both sg and H1 designs which have intricate internal networks and are worst performing which may be due to the limiting space preventing cell spreading which is reported increase proliferation (410). Future work could use advanced microscopy techniques such as multiphoton microscopy to observe cell volumes in greater detail and determine total cell volume and aspect ratio in best performing designs. With known cell volumes analysis of gene expression relating to regulatory genes associated with cytoskeletal organisation and morphology such FAM40A, FAM40B or FMNL3 among others could be pursued to understand this mechanism (451). Additional proteomic analysis of cell cytoskeletal elements could also be probed but for a system as large and complex as the cytoskeleton would present a significant challenge despite being recently demonstrated in plant cells (452). This would also aid understanding of protein production during expansion which indicated higher protein production in some designs that did not correlate to cell amount.

Samples were analysed for differentiation into osteogenic lineages as general culture with microcarriers has been reported by many groups to increase osteogenic activity (399, 426). This tendency is due to a number of physical cues that are present in microcarrier culture including surface curvature, surface roughness, substrate stiffness, cytoskeletal tension and increased cell spreading (204, 230, 257, 414, 429).

Microcarriers showed no significant difference between any of the designs and had very low activity in comparison to positive controls thus indicating that no osteogenic response is seen. Other studies have demonstrated that in textured particles ALP levels do not always correlate with other osteogenic marker presentation such as osteocalcin (417). This could indicate further testing is needed with other markers or ideally analysis of gene expression related to differentiation. RNA was extracted from scaffolds for this purpose but was not analysed due to limitation to the experimental period and would represent one of the immediate tests that could be pursued in further work. Further tot his future work could include incorporation of hydroxyapatite into 2PP resins to produce structures that actively increase osteogenic responses and this approach has been used before in other biomaterials designs (432).

Whilst ALP activity may aid in to determining osteogenic differentiation it doesn't count for overall stemness and as such flow cytometry of stem cell surface markers was performed. Cells were first tested for free microcarrier culture under static conditions and cell retrieval from confluent microcarriers which was achieved with no issues. Following this, iMSCs were expanded for three weeks on C50, G1t and spherical microcarriers fabricated in PETA. These structures represented the best performing design, moderate expansion design and spherical 3D control as a typical microcarrier comparison. Data indicated unexpected results with marker expression not reaching this standard in all positive markers and presence of negative markers higher than permitted. Interestingly a far decreased value of CD105 was seen in all expansion methods and practically no expression of this marker in best performing designs. This decrease in CD105 specifically is seen in other studies indicating that despite ISCT criteria is often variable in MSC populations and indicates an enhanced immunomodulatory capacity without loss of stemness (437, 439, 444). Investigation of immunomodulatory profiles of MSCs expanded on different microcarriers could give an indication of another aspect that could vary between carrier designs. One of the most immediate future goals would be repetition of this experiment with MSCs that fit the ISCT criteria in order to fully understand the effects of microcarrier expansion on stem cell phenotype. This was not pursued only due to time limitations and the need for multiple donors which was difficult to achieve as large numbers of microcarriers were needed for static microcarrier culture.

An additional limitation to the conducted research is the use of immortalised MSC lines for experimentation. The limited culture period of primary cells dues to cell senescence is a major challenge for experimental investigation and therapeutic use, with cell lines only being experimentally viable for a short period of time. In practice this leads to the thawing of cryopreserved cells of an earlier passage in order to continue experimentation, not only does this become a time-consuming practice but integrates further issues due to sensitivity and possible variation of the thawing process. As such, immortalised cells with longer viable culture life spans but with intact phenotypic expression is often used as a tool in research do reduce variation and maintain reliability of experimental results (453). The iMSCs used in this research were immortalised via lentiviral transfection of E6/E7 and hTERT genes as previously described (454). This methodology has been shown to work effectively whilst maintaining overall phenotype including cell morphology, stem cell marker expression, differentiation, and cell adhesion. Similar cell lines have been used previously for characterisation of immunomodulatory and osteoinductive proficiency within biomaterials research (455, 456). This method of immortalisation has also been extended to other stem cell types with similar retention of stem cell features and capabilities (453).

Critically, evaluation of this immortalisation technique has been shown to maintain mechano-responsive pathways in transformed cells with intact mechanosensing and transduction pathways ensuring that cells exhibit the same morphological responses to mechanical stimuli as their unmodified counterparts (457). As such, the use of these immortalised cells which maintain stem cell characteristics and mechanosensitivity do not reduce the validity or reliability of the conducted research. Despite the advantages of these immortalised cell lines there are still some disadvantages that have been recognised. Notably, risk of tumorigenic potential, genetic instability, reduction in adipogenic potential and changes to hormonal sensitivity have been discussed. Studies have indicated that MSCs immortalisation processes which involve the hTERT mechanism can lead to impaired insulin-dependent and cAMP-dependent signalling which affects the adipogenic differentiation potential of these cells (458, 459).

Towards this goal, recent advances have sought to produce conditional immortalised cell populations that can deliver the experimental and scalability advantages of an

immortalised cell line with the capacity to selectively switch off this ability and revert back to their natural growth characteristics to ensure safety of transplanted cell populations (460). This future tool may address the issues encountered and provide a more useful approach for future research.

The benefits of these immortalised cells for this research far outweigh their limitations given that *in-vitro* experiments that do not involve adipogenesis are the pursuit. However, to ensure validity and reliability of experimentation continued research from this point would seek to employ primary MSCs for all future experiments. This step is to ensure that this technology is not benefitting from the modified growth profiles of the cells and delineate this as a possible variable in the expansion outcome. As such, iMSCs would only be used in early mass architectural screenings to identify useful designs.

Several future experiments have been already outlined which would form immediate tasks for continuation of this work. These include exploring spin coating to improve pHEMA coating, testing of PμSLA for scale up, repetition of flow cytometry work, analysis of gene expression and comparison to commercial carriers. All of these experiments were originally planned for completion but were not accomplished due to disturbances caused by the COVID-19 pandemic. Further identified routes for broader experimentation include multiphoton microscopy for better morphological analysis of single cells, added complexity with multi-material microcarriers and further work to materials including pursuit of polymers with better adherence and degradability. The next steps in experimentation along with possible future application are highlighted in figure 6.1.

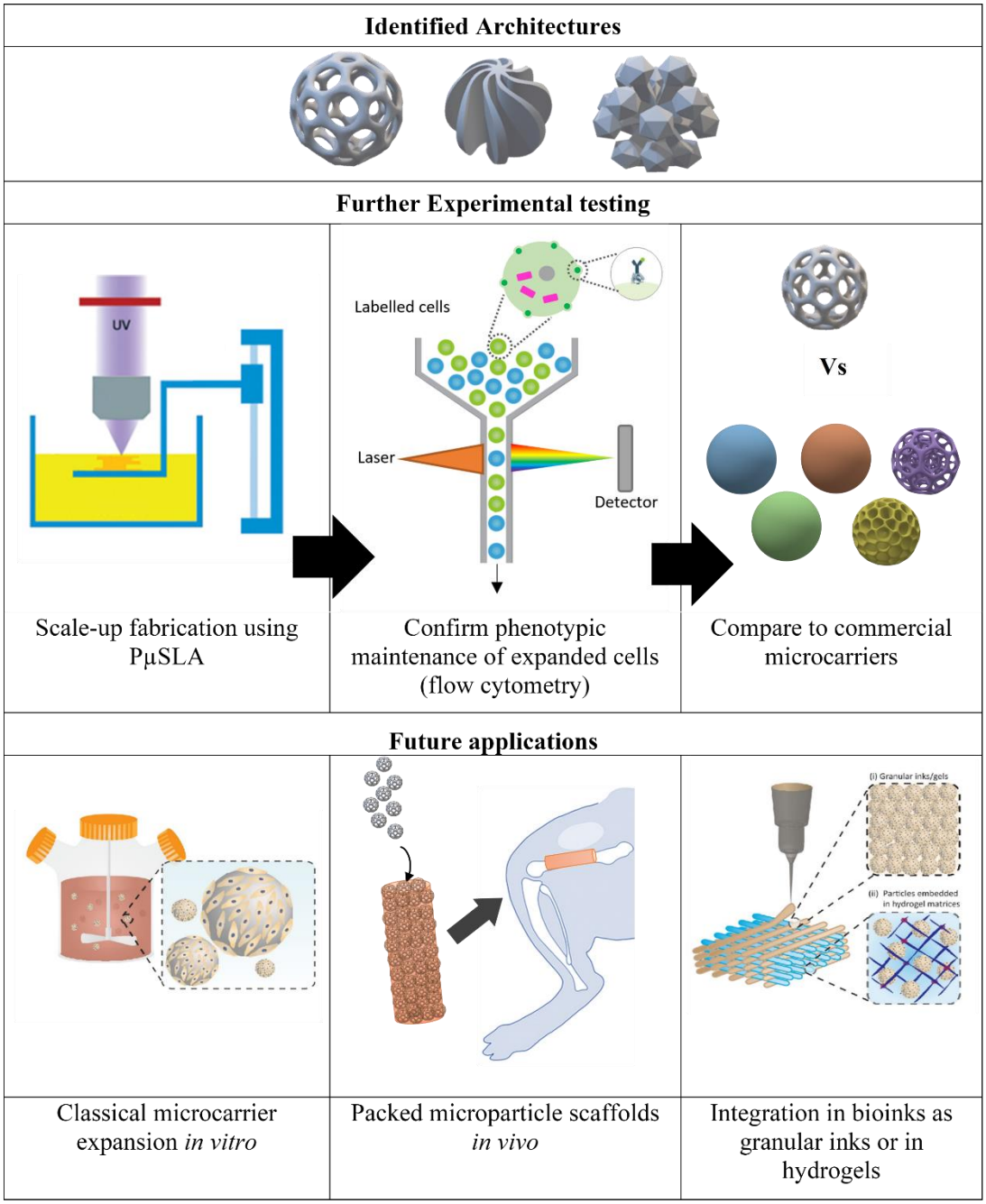


***Figure 6.1:*** *Future experimentation and applications of next generation microcarriers. Identified architectures can be fabricated at scale using PμSLA with repetition of flow cytometry to evaluate MSC marker expression leading to comparison to commercial products to evaluate expansion potential. Future applications include intended expansion as well as microparticle based scaffolds and as bioinks. Adapted from Neto et al (23).*

The work presented in this thesis establishes novel methodologies as part of a toolkit for mechanobiological testing of MSC expansion using two photon lithography as its source of mechanical stimulation. Novel fabrication techniques to enhance scalability, creation of microcarrier designs that impact proliferative capacity, and techniques by which to isolate cell growth to zones of mechanical stimulation all contribute to this methodology. This toolkit, which is the first of its kind, can be used to screen any

conceivable design within this scale and ascertain its effect on MSC expansion and phenotype and as such brings the field forward.

Despite these advancements, the work discussed does have several limitations and improvements which should be considered. Many of these have gone unaddressed experimentally due to the length of the fabrication process and delays due to the pandemic. One limitation, as previously discussed, is the reliance on immortalised stem cell lines for testing. These cell lines, whilst useful as a cell culture tool, can have minor impact upon phenotypic outcome and growth profiles and as such future work should be conducted with primary MSCs to overcome this limitation and validate effects on expansion capacity. Whilst mechanosensitivity is maintained in immortalised cell lines and enhanced expansion is seen prior to confluency it is still useful to ensure the effects persist in non-modified cells.

An additional weakness of this research is the limited analysis of phenotypic outcome of cells and mixed results with marker expression that does not meet the ISCT criteria. Without further testing with primary MSCs that meet the established criteria and analysis through marker expression and PCR, as outlined in future experimentation, the assessment of effect on MSC phenotype cannot be verified. Despite the uncertainty of phenotypic outcome, technologies that either expand and maintain stem cell phenotypes or those that drive differentiation can still be useful tools.

Another weakness of this research is the lack of a comprehensive and controlled expression of mechanical stimuli. Limitations in fabrication efficiency, especially prior to optimisation, limited the number of geometries that could be screened. Smaller controlled geometrical variation of isolated features such as vertex angle, dihedral angle or feature size that change in small increments could aid in isolating and understanding the key geometrical cues that enhance proliferation. The final geometries tested in this research vary considerably and each design constitutes a variety of geometrical cues leading to difficulty in understanding why some designs are effective and others are not. Further high throughput screening utilising the optimisations outlined in this research coupled with image analysis and machine learning could aid in identification of geometrical cues that enhance proliferation and influence differentiation. Establishing what geometric features have a positive outcome could

shape future designs and allow for experimentation that examines how these features induce their effects on the cell. Work of this type was not possible within the scope of this research and could constitute a future project.

Whilst fabrication optimisations have allowed scale up to laboratory relevant scales and perhaps to small animal models, the translation to large scale clinical use is still a barrier. This work briefly outlines a future methodology to address this scale up issue, but it is not fully demonstrated within this research. Included experimentation only demonstrates that replication of designs are possible and only theoretical calculations of fabrication time frames are included. Full scale up fabrication should ideally be pursued to ensure that this technology can be effectively used as a therapy or else the findings, while promising, will be difficult to realise. The outlined novel fabrication methodology to address scale up was not available at the beginning of this research and hence was not the initial starting point. Despite this, for small scale architecture screening 2PP still remains the most viable candidate due to the differences in fabrication technique at scale i.e. with SLA techniques it would take longer to produce a singular particle or small numbers of particles then it would be with 2PP. Combination of these two methodologies should be used for future research as the key factor in this work is physical design which can be translated across any fabrication technology that can work at a similar level of scale and resolution.

Finally, the initial aim of this research was to create a microcarrier technology which improved upon its current state by utilising mechanobiological influence. However, in this research it was not possible to compare experimental designs to commercial competitors and only to the typical spherical design utilised by most products. In order to meet this aim comparison to commercial competitors is needed and evaluation of the effectiveness of geometries when more appealing material chemistries are present needs to be verified. The understanding of the hierarchy of influence on cells is limited and in the presence of more suitable materials will geometrical influence be as effective as seen in this research. These questions would be difficult to address given the limited suitability of materials to 2PP but comparison to commercial competitors should be the first step.

Despite the need for future work to fully explore and establish this approach, the work provided takes that first critical step towards achieving this goal. The influence of biophysical environmental cues such as geometry or topography have limited use in the field at large and this work seeks to highlight the importance of this and integrate this approach into the microcarrier field. If the discussed future limitations are solved with favourable outcomes, then the application to other fields outside of microcarrier design might be realised. Such outputs include application to microparticle scaffolds or in other materials as granular bioinks and are briefly outlined in figure 6.1.

One final missing element in the scope of this research has been the application to cell types beyond MSCs. This restriction was necessary to allow consistent testing and ease fabrication scale issues by focusing on only one cell type for initial development and optimisation of techniques. MSCs are a therapeutically useful and relevant cell type with potential across a range of tissues and regenerative medicine approaches as previously discussed and reviewed (63). However, there are many other cell types that have similar potential in regenerative medicine. Other important cell types to expand include pluripotent stem cells (PSCs) such as IPSCs, which have been previously discussed. These cells have potential given their pluripotent nature and overcoming ethical concerns with the use of other PSCs such as embryonic stem cells (ESCs). In addition to this other adult stem cells (ASCs) such as hematopoietic stem cells (HSCs) or neural stem cells (NSCs) provide therapeutic potential for more specific groups of tissues (461).

Another cell type that expansion could be useful for is cancer stem cells (CSCs), which can be expanded for the purpose of disease modelling and drug testing. CSCs have recently been re-examined for their role in cancer and are thought to initiate tumours, maintain tumour environments, and be the basis of cancer recurrence and metastasis (462, 463). With immortal self-renewing capabilities and differentiation into a variety of cancerous cell types these cells are beginning to be implicated in the failure of so many previous cancer therapies (464). CSCs are present in almost all solid tumours but only exist in very discrete populations representing less than 0.04% of the tumour mass (465). The scarcity of these cells along with no standardised techniques for expansion makes them difficult to identify and investigate leading to slow progress in the maturity of cancer stem cell directed treatments.

It is also important to consider the expansion of various cell types where products of the cell are required rather than the cell population themselves. This has been previously discussed in production of extracellular vesicles, conditioned media, antibodies and proteins. As such, there are many different types of cells that could be expanded for many different reasons. However, the scope of this research only focuses on MSCs directly, which limits its current potential. Many microcarriers are considered as universal tools between cell types with products being sold for any application. With the introduction of mechanobiology approaches this statement may be less true given the varying and specific biomechanical properties of different tissues. Appropriate testing among a variety of popular cell types could be a future route to fully explore the potential of this technology at a greater scale. This work forms the basis of this approach and allows future experimentation bringing the field forward.

# 7. Conclusion

This thesis has demonstrated the use of two-photon lithography for production of unique microcarriers that leverage their complex architectures to influence cell proliferation and differentiation through biophysical stimuli. Optimisations to fabrication techniques have allowed for rapid production of intricate designs in several materials with different characteristics. Novel techniques developed ways to isolate cell growth to fixed 2PP substrates eliminating extraneous signals in cell assays and increasing the way in which cells growing on structures can be analysed. Experimental observation indicated C50 and C80 buckyballs increase expansion yield in comparison to spherical controls which represent typical microcarrier design. This response was believed to be due to changes to cellular morphology as a result of the structure architecture that influences cytoskeletal mechanics and subsequently gene expression. Stem cell phenotype variation was explored but yielded unexpected results and requires further work to reliably quantify the effect of microcarriers on stem cell markers.

The findings of this work and techniques developed contribute to development of next generation microcarrier technology and takes the field forward. Most importantly this work has demonstrated that biomechanical cues are integral to enhancing cell expansion and that provision of surface area is not the only factor to consider. Further study with transfer of experimental results to a technology capable of higher throughput would be necessary for translation to clinical scale production. Microcarriers that intelligently shape cellular proliferation and differentiation can act both *in vitro* and *in vivo* as tissue modulators evolving beyond their primary function to address multiple purposes in regenerative medicine and beyond.

# References


1. Wu R, Hu X, Wang JA. Concise Review: Optimized Strategies for Stem Cell-Based Therapy in Myocardial Repair: Clinical Translatability and Potential Limitation. STEM CELLS. 2018;36(4):482-500.

2. Andersson-Rolf A, Zilbauer M, Koo B-K, Clevers H. Stem Cells in Repair of Gastrointestinal Epithelia. Physiology. 2017;32(4):278-89.

3. Peired AJ, Sisti A, Romagnani P. Mesenchymal Stem Cell-Based Therapy for Kidney Disease: A Review of Clinical Evidence. 2016;2016:1-22.

4. Zhao L, Chen S, Shi X, Cao H, Li L. A pooled analysis of mesenchymal stem cell-based therapy for liver disease. Stem Cell Res Ther. 2018;9(1):72.

5. Liu X, Zheng P, Wang X, Dai G, Cheng H, Zhang Z, et al. A preliminary evaluation of efficacy and safety of Wharton's jelly mesenchymal stem cell transplantation in patients with type 2 diabetes mellitus. Stem Cell Research & Therapy. 2014;5(2):57.

6. Hernigou P, Guissou I, Homma Y, Poignard A, Chevallier N, Rouard H, et al. Percutaneous injection of bone marrow mesenchymal stem cells for ankle non-unions decreases complications in patients with diabetes. International Orthopaedics. 2015;39(8):1639-43.

7. Barker RA, Parmar M, Studer L, Takahashi J. Human Trials of Stem Cell-Derived Dopamine Neurons for Parkinson's Disease: Dawn of a New Era. Cell Stem Cell. 2017;21(5):569-73.

8. Duru LN, Quan Z, Qazi TJ, Qing H. Stem cells technology: a powerful tool behind new brain treatments. Drug Delivery and Translational Research. 2018;8(5):1564-91.

9. Zhao Q, Ren H, Han Z. Mesenchymal stem cells: Immunomodulatory capability and clinical potential in immune diseases. Journal of Cellular Immunotherapy. 2016;2(1):3-20.

10. Robinson PG, Murray IR, West CC, Goudie EB, Yong LY, White TO, et al. Reporting of Mesenchymal Stem Cell Preparation Protocols and Composition: A Systematic Review of the Clinical Orthopaedic Literature. The American Journal of Sports Medicine. 2019;47(4):991-1000.

11. Tavassoli H, Javadpour J, Taheri M, Mehrjou M, Koushki N, Arianpour F, et al. Incorporation of Nanoalumina Improves Mechanical Properties and Osteogenesis of Hydroxyapatite Bioceramics. ACS Biomaterials Science & Engineering. 2018;4(4):1324-36.

12. Mittwede PN, Gottardi R, Alexander PG, Tarkin IS, Tuan RS. Clinical Applications of Bone Tissue Engineering in Orthopedic Trauma. Current Pathobiology Reports. 2018;6(2):99-108.

13. Chen AK-L, Reuveny S, Oh SKW. Application of human mesenchymal and pluripotent stem cell microcarrier cultures in cellular therapy: Achievements and future direction. Biotechnology Advances. 2013;31(7):1032-46.

14. Scotti C, Gobbi A, Nakamura N, Peretti GM. Stem Cells for Cartilage Regeneration: A Roadmap to the Clinic. Stem Cells International. 2018;2018:7348560.

15. Kalamegam G, Memic A, Budd E, Abbas M, Mobasheri A. A Comprehensive Review of Stem Cells for Cartilage Regeneration in Osteoarthritis. In: Turksen K, editor. Cell Biology and Translational Medicine, Volume 2: Approaches for Diverse Diseases and Conditions. Cham: Springer International Publishing; 2018. p. 23-36.

16. Kabat M, Bobkov I, Kumar S, Grumet M. Trends in mesenchymal stem cell clinical trials 2004-2018: Is efficacy optimal in a narrow dose range? STEM CELLS Translational Medicine. 2020;9(1):17-27.

17. Wong KU, Zhang A, Akhavan B, Bilek MM, Yeo GC. Biomimetic Culture Strategies for the Clinical Expansion of Mesenchymal Stromal Cells. ACS Biomaterials Science & Engineering. 2021.

18. Prockop DJ, Brenner M, Fibbe WE, Horwitz E, Le Blanc K, Phinney DG, et al. Defining the risks of mesenchymal stromal cell therapy. Cytotherapy. 2010;12(5):576-8.

19. Sensebé L, Bourin P, Tarte K. Good manufacturing practices production of mesenchymal stem/stromal cells. Hum Gene Ther. 2011;22(1):19-26.

20. Thomas RJ, Anderson D, Chandra A, Smith NM, Young LE, Williams D, et al. Automated, scalable culture of human embryonic stem cells in feeder-free conditions. Biotechnology and Bioengineering. 2009;102(6):1636-44.

21. Pakos V, Johansson A. Large scale production of human fibroblast interferon in multitray battery systems. Dev Biol Stand. 1985;60:317-20.

22. Gey GO. An Improved Technic for Massive Tissue Culture. The American Journal of Cancer. 1933;17(3):752-6.

23. Neto MD, Oliveira MB, Mano JF. Microparticles in Contact with Cells: From Carriers to Multifunctional Tissue Modulators. Trends in Biotechnology. 2019;37(9):1011-28.

24. He Y, Park K. Effects of the Microparticle Shape on Cellular Uptake. Molecular Pharmaceutics. 2016;13(7):2164-71.

25. Li M, Joung D, Hughes B, Waldman SD, Kozinski JA, Hwang DK. Wrinkling Non-Spherical Particles and Its Application in Cell Attachment Promotion. Scientific Reports. 2016;6(1):30463.

26. Zonderland J, Moroni L. Steering cell behavior through mechanobiology in 3D: A regenerative medicine perspective. Biomaterials. 2021;268:120572.

27. Mason C, Dunnill P. A brief definition of regenerative medicine. Regenerative Medicine. 2008;3(1):1-5.

28. Chocholata P, Kulda V, Babuska V. Fabrication of Scaffolds for Bone-Tissue Regeneration. Materials. 2019;12(4):568.

29. Langer R, Vacanti J. Tissue engineering. Science. 1993;260(5110):920-6.

30. Khademhosseini A, Langer R, Borenstein J, Vacanti JP. Microscale technologies for tissue engineering and biology. Proceedings of the National Academy of Sciences. 2006;103(8):2480-7.

31. Peppas N, Langer R. New challenges in biomaterials. Science. 1994;263(5154):1715-20.

32. Huebsch N, Mooney DJ. Inspiration and application in the evolution of biomaterials. Nature. 2009;462(7272):426-32.

33. Webber MJ, Appel EA, Meijer EW, Langer R. Supramolecular biomaterials. Nat Mater. 2016;15(1):13-26.

34. Mandrycky C, Wang Z, Kim K, Kim D-H. 3D bioprinting for engineering complex tissues. Biotechnology Advances. 2016;34(4):422-34.

35. Muir K, Kalladka D. Brain repair: cell therapy in stroke. Stem Cells and Cloning: Advances and Applications. 2014:31.

36. Haeckel E. Natürliche Schöpfungsgeschichte von Dr. Ernst Häckel, Professor in Jena. Berlin bei Georg Reimer. 1868 S. 568. Archiv der Pharmazie. 1868;189(3):282-3.

37. Ramalho-Santos M, Willenbring H. On the Origin of the Term “Stem Cell”. Cell Stem Cell. 2007;1(1):35-8.

38. Till JE, McCulloch EA. A Direct Measurement of the Radiation Sensitivity of Normal Mouse Bone Marrow Cells. Radiation Research. 1961;14(2):213.

39. Becker AJ, McCulloch EA, Till JE. Cytological Demonstration of the Clonal Nature of Spleen Colonies Derived from Transplanted Mouse Marrow Cells. Nature. 1963;197(4866):452-4.

40. Thomas ED, Lochte HL, Lu WC, Ferrebee JW. Intravenous Infusion of Bone Marrow in Patients Receiving Radiation and Chemotherapy. New England Journal of Medicine. 1957;257(11):491-6.

41. Little M-T, Storb R. History of haematopoietic stem-cell transplantation. 2002;2(3):231-8.

42. Condic ML. Totipotency: What It Is and What It Is Not. Stem Cells and Development. 2014;23(8):796-812.

43. Evans MJ, Kaufman MH. Establishment in culture of pluripotential cells from mouse embryos. Nature. 1981;292(5819):154-6.

44. Levi B, Glotzbach JP, Wong VW, Nelson ER, Hyun J, Wan DC, et al. Stem Cells. Journal of Craniofacial Surgery. 2012;23(1):319-23.

45. Dushnik-Levinson M, Benvenisty N. Embryogenesis in vitro: Study of Differentiation of Embryonic Stem Cells. Neonatology. 1995;67(2):77-83.

46. Moroni F, Mirabella T. Decellularized matrices for cardiovascular tissue engineering. Am J Stem Cells. 2014;3(1):1-20.

47. Neirinckx V, Coste C, Rogister B, Wislet-Gendebien S. Concise Review: Adult Mesenchymal Stem Cells, Adult Neural Crest Stem Cells, and Therapy of Neurological Pathologies: A State of Play. STEM CELLS Translational Medicine. 2013;2(4):284-96.

48. Carlson AL, Bennett NK, Francis NL, Halikere A, Clarke S, Moore JC, et al. Generation and transplantation of reprogrammed human neurons in the brain using 3D microtopographic scaffolds. 2016;7:10862.

49. Zhong C, Liu M, Pan X, Zhu H. Tumorigenicity risk of iPSCs in vivo: nip it in the bud. Precision Clinical Medicine. 2022;5(1).

50. Koch JM, D'Souza SS, Schwahn DJ, Dixon I, Hacker TA. Mesenchymoangioblast-derived mesenchymal stromal cells inhibit cell damage, tissue damage and improve peripheral blood flow following hindlimb ischemic injury in mice. Cytotherapy. 2016;18(2):219-28.

51. Caplan AI. Mesenchymal stem cells. Journal of Orthopaedic Research. 1991;9(5):641-50.

52. Friedenstein A, Heersche J, Kanis J. Bone and mineral research. Amsterdam: Elsevier; 1990.

53. Pittenger MF. Multilineage Potential of Adult Human Mesenchymal Stem Cells. Science. 1999;284(5411):143-7.

54. Zhu H, Guo Z-K, Jiang X-X, Li H, Wang X-Y, Yao H-Y, et al. A protocol for isolation and culture of mesenchymal stem cells from mouse compact bone. Nature Protocols. 2010;5(3):550-60.

55. Toma JG, Akhavan M, Fernandes KJL, Barnabé-Heider F, Sadikot A, Kaplan DR, et al. Isolation of multipotent adult stem cells from the dermis of mammalian skin. Nature Cell Biology. 2001;3(9):778-84.

56. Zuk PA, Zhu M, Ashjian P, De Ugarte DA, Huang JI, Mizuno H, et al. Human Adipose Tissue Is a Source of Multipotent Stem Cells. Molecular Biology of the Cell. 2002;13(12):4279-95.

57. Ausems CRM, Raaijmakers RHL, Van Den Broek WJAA, Willemse M, Van Engelen BGM, Wansink DG, et al. Intrinsic Myogenic Potential of Skeletal Muscle-Derived Pericytes from Patients with Myotonic Dystrophy Type 1. Molecular Therapy - Methods & Clinical Development. 2019;15:120-32.

58. Gronthos S, Mankani M, Brahim J, Robey PG, Shi S. Postnatal human dental pulp stem cells (DPSCs) in vitro and invivo. Proceedings of the National Academy of Sciences. 2000;97(25):13625-30.

59. Sipp D, Robey PG, Turner L. Clear up this stem-cell mess. Nature. 2018;561(7724):455-7.

60. Horwitz EM, Le Blanc K, Dominici M, Mueller I, Slaper-Cortenbach I, Marini FC, et al. Clarification of the nomenclature for MSC: The International Society for Cellular Therapy position statement. Cytotherapy. 2005;7(5):393-5.

61. Crisan M, Yap S, Casteilla L, Chen C-W, Corselli M, Park TS, et al. A Perivascular Origin for Mesenchymal Stem Cells in Multiple Human Organs. Cell Stem Cell. 2008;3(3):301-13.

62. Dominici M, Le Blanc K, Mueller I, Slaper-Cortenbach I, Marini F, Krause D, et al. Minimal criteria for defining multipotent mesenchymal stromal cells. The International Society for Cellular Therapy position statement. Cytotherapy. 2006;8(4):315-7.

63. Han Y, Li X, Zhang Y, Han Y, Chang F, Ding J. Mesenchymal Stem Cells for Regenerative Medicine. Cells. 2019;8(8):886.

64. Caplan AI. Mesenchymal Stem Cells: Time to Change the Name! Stem Cells Translational Medicine. 2017;6(6):1445-51.

65. Caplan AI. What's in a Name? Tissue Engineering Part A. 2010;16(8):2415-7.

66. Aggarwal S, Pittenger MF. Human mesenchymal stem cells modulate allogeneic immune cell responses. Blood. 2005;105(4):1815-22.

67. Gao F, Chiu SM, Motan DAL, Zhang Z, Chen L, Ji HL, et al. Mesenchymal stem cells and immunomodulation: current status and future prospects. Cell Death & Disease. 2016;7(1):e2062-e.

68. Lee C-W, Chen Y-F, Wu H-H, Lee OK. Historical Perspectives and Advances in Mesenchymal Stem Cell Research for the Treatment of Liver Diseases. Gastroenterology. 2018;154(1):46-56.

69. Fan X-L, Zhang Y, Li X, Fu Q-L. Mechanisms underlying the protective effects of mesenchymal stem cell-based therapy. Cellular and Molecular Life Sciences. 2020;77(14):2771-94.

70. De La Garza-Rodea AS, Van Der Velde I, Boersma H, Gonçalves MAFV, Van Bekkum DW, De Vries AAF, et al. Long-Term Contribution of Human Bone Marrow Mesenchymal Stromal Cells to Skeletal Muscle Regeneration in Mice. Cell Transplantation. 2011;20(2):217-32.

71. Cerletti M, Jurga S, Witczak CA, Hirshman MF, Shadrach JL, Goodyear LJ, et al. Highly Efficient, Functional Engraftment of Skeletal Muscle Stem Cells in Dystrophic Muscles. 2008;134(1):37-47.

72. Toma C, Pittenger MF, Cahill KS, Byrne BJ, Kessler PD. Human Mesenchymal Stem Cells Differentiate to a Cardiomyocyte Phenotype in the Adult Murine Heart. Circulation. 2002;105(1):93-8.

73. Orozco L, Munar A, Soler R, Alberca M, Soler F, Huguet M, et al. Treatment of Knee Osteoarthritis With Autologous Mesenchymal Stem Cells. Transplantation Journal. 2013;95(12):1535-41.

74. Morigi M. Mesenchymal Stem Cells Are Renotropic, Helping to Repair the Kidney and Improve Function in Acute Renal Failure. Journal of the American Society of Nephrology. 2004;15(7):1794-804.

75. Lange C, Tögel F, Ittrich H, Clayton F, Nolte-Ernsting C, Zander AR, et al. Administered mesenchymal stem cells enhance recovery from ischemia/reperfusion-induced acute renal failure in rats. Kidney International. 2005;68(4):1613-7.

76. Pittenger MF, Discher DE, Péault BM, Phinney DG, Hare JM, Caplan AI. Mesenchymal stem cell perspective: cell biology to clinical progress. npj Regenerative Medicine. 2019;4(1).

77. Pezzi A, Amorin B, Laureano Á, Valim V, Dahmer A, Zambonato B, et al. Effects Of Hypoxia in Long-Term In Vitro Expansion of Human Bone Marrow Derived Mesenchymal Stem Cells. J Cell Biochem. 2017;118(10):3072-9.

78. Rossetti T, Nicholls F, Modo M. Intracerebral Cell Implantation: Preparation and Characterization of Cell Suspensions. Cell Transplantation. 2016;25(4):645-64.

79. Amer MH, Rose FRAJ, Shakesheff KM, White LJ. A biomaterials approach to influence stem cell fate in injectable cell-based therapies. Stem Cell Research & Therapy. 2018;9(1).

80. Teng CJ, Luo J, Chiu RC, Shum-Tim D. Massive mechanical loss of microspheres with direct intramyocardial injection in the beating heart: implications for cellular cardiomyoplasty. J Thorac Cardiovasc Surg. 2006;132(3):628-32.

81. Guilak F, Cohen DM, Estes BT, Gimble JM, Liedtke W, Chen CS. Control of Stem Cell Fate by Physical Interactions with the Extracellular Matrix. Cell Stem Cell. 2009;5(1):17-26.

82. Higuchi A, Ling QD, Kumar SS, Chang Y, Alarfaj AA, Munusamy MA, et al. Physical cues of cell culture materials lead the direction of differentiation lineages of pluripotent stem cells. J Mater Chem B. 2015;3(41):8032-58.

83. Ullah M, Liu DD, Thakor AS. Mesenchymal Stromal Cell Homing: Mechanisms and Strategies for Improvement. iScience. 2019;15:421-38.

84. Bayo J, Real A, Fiore EJ, Malvicini M, Sganga L, Bolontrade M, et al. IL-8, GRO and MCP-1 produced by hepatocellular carcinoma microenvironment determine the migratory capacity of human bone marrow-derived mesenchymal stromal cells without affecting tumor aggressiveness. Oncotarget. 2016;8(46).

85. Kean TJ, Lin P, Caplan AI, Dennis JE. MSCs: Delivery Routes and Engraftment, Cell-Targeting Strategies, and Immune Modulation. Stem Cells Int. 2013;2013:732742.

86. Levy O, Mortensen LJ, Boquet G, Tong Z, Perrault C, Benhamou B, et al. A small-molecule screen for enhanced homing of systemically infused cells. Cell Rep. 2015;10(8):1261-8.

87. Molnar V, Pavelić E, Vrdoljak K, Čemerin M, Klarić E, Matišić V, et al. Mesenchymal Stem Cell Mechanisms of Action and Clinical Effects in Osteoarthritis: A Narrative Review. Genes. 2022;13(6):949.

88. Liu H, Li R, Liu T, Yang L, Yin G, Xie Q. Immunomodulatory Effects of Mesenchymal Stem Cells and Mesenchymal Stem Cell-Derived Extracellular Vesicles in Rheumatoid Arthritis. Front Immunol. 2020;11:1912.

89. Ciccocioppo R, Bernardo ME, Sgarella A, Maccario R, Avanzini MA, Ubezio C, et al. Autologous bone marrow-derived mesenchymal stromal cells in the treatment of fistulising Crohn's disease. Gut. 2011;60(6):788-98.

90. Nojehdehi S, Soudi S, Hesampour A, Rasouli S, Soleimani M, Hashemi SM. Immunomodulatory effects of mesenchymal stem cell-derived exosomes on experimental type-1 autoimmune diabetes. J Cell Biochem. 2018;119(11):9433-43.

91. Németh K, Leelahavanichkul A, Yuen PS, Mayer B, Parmelee A, Doi K, et al. Bone marrow stromal cells attenuate sepsis via prostaglandin E(2)-dependent reprogramming of host macrophages to increase their interleukin-10 production. Nat Med. 2009;15(1):42-9.

92. Weiss ARR, Dahlke MH. Immunomodulation by Mesenchymal Stem Cells (MSCs): Mechanisms of Action of Living, Apoptotic, and Dead MSCs. Frontiers in Immunology. 2019;10(1191).

93. Luz-Crawford P, Djouad F, Toupet K, Bony C, Franquesa M, Hoogduijn MJ, et al. Mesenchymal Stem Cell-Derived Interleukin 1 Receptor Antagonist Promotes Macrophage Polarization and Inhibits B Cell Differentiation. Stem Cells. 2016;34(2):483-92.

94. Melief SM, Geutskens SB, Fibbe WE, Roelofs H. Multipotent stromal cells skew monocytes towards an anti-inflammatory interleukin-10-producing phenotype by production of interleukin-6. Haematologica. 2013;98(6):888-95.

95. Deng Y, Zhang Y, Ye L, Zhang T, Cheng J, Chen G, et al. Umbilical Cord-derived Mesenchymal Stem Cells Instruct Monocytes Towards an IL10-producing Phenotype by Secreting IL6 and HGF. Scientific Reports. 2016;6(1):37566.

96. Braza F, Dirou S, Forest V, Sauzeau V, Hassoun D, Chesné J, et al. Mesenchymal Stem Cells Induce Suppressive Macrophages Through Phagocytosis in a Mouse Model of Asthma. STEM CELLS. 2016;34(7):1836-45.

97. Eggenhofer E, Steinmann JF, Renner P, Slowik P, Piso P, Geissler EK, et al. Mesenchymal stem cells together with mycophenolate mofetil inhibit antigen presenting cell and T cell infiltration into allogeneic heart grafts. Transplant Immunology. 2011;24(3):157-63.

98. Chang C-L, Leu S, Sung H-C, Zhen Y-Y, Cho C-L, Chen A, et al. Impact of apoptotic adipose-derived mesenchymal stem cells on attenuating organ damage and reducing mortality in Rat sepsis syndrome induced by cecal puncture and ligation. Journal of Translational Medicine. 2012;10(1):244.

99. Sung P-H, Chang C-L, Tsai T-H, Chang L-T, Leu S, Chen Y-L, et al. Apoptotic adipose-derived mesenchymal stem cell therapy protects against lung and kidney injury in sepsis syndrome caused by cecal ligation puncture in rats. Stem Cell Research & Therapy. 2013;4(6):155.

100. Galleu A, Riffo-Vasquez Y, Trento C, Lomas C, Dolcetti L, Cheung TS, et al. Apoptosis in mesenchymal stromal cells induces in vivo recipient-mediated immunomodulation. Science Translational Medicine. 2017;9(416):eaam7828.

101. Pang SHM, D'Rozario J, Mendonca S, Bhuvan T, Payne NL, Zheng D, et al. Mesenchymal stromal cell apoptosis is required for their therapeutic function. Nature Communications. 2021;12(1):6495.

102. Ratushnyy A, Ezdakova M, Yakubets D, Buravkova L. Angiogenic Activity of Human Adipose-Derived Mesenchymal Stem Cells Under Simulated Microgravity. Stem Cells and Development. 2018;27(12):831-7.

103. Sanz L, Santos-Valle P, Alonso-Camino V, Salas C, Serrano A, Vicario JL, et al. Long-term in vivo imaging of human angiogenesis: Critical role of bone marrow-derived mesenchymal stem cells for the generation of durable blood vessels. Microvascular Research. 2008;75(3):308-14.

104. Meier RP, Mahou R, Morel P, Meyer J, Montanari E, Muller YD, et al. Microencapsulated human mesenchymal stem cells decrease liver fibrosis in mice. J Hepatol. 2015;62(3):634-41.

105. Ono M, Ohkouchi S, Kanehira M, Tode N, Kobayashi M, Ebina M, et al. Mesenchymal stem cells correct inappropriate epithelial-mesenchyme relation in pulmonary fibrosis using stanniocalcin-1. Mol Ther. 2015;23(3):549-60.

106. Xu X, Xu Z, Xu Y, Cui G. Effects of mesenchymal stem cell transplantation on extracellular matrix after myocardial infarction in rats. Coron Artery Dis. 2005;16(4):245-55.

107. Zhuang W-Z, Lin Y-H, Su L-J, Wu M-S, Jeng H-Y, Chang H-C, et al. Mesenchymal stem/stromal cell-based therapy: mechanism, systemic safety and biodistribution for precision clinical applications. Journal of Biomedical Science. 2021;28(1):28.

108. Kamarajan P, Bunek J, Lin Y, Nunez G, Kapila YL. Receptor-interacting Protein Shuttles between Cell Death and Survival Signaling Pathways. Molecular Biology of the Cell. 2010;21(3):481-8.

109. Pan G-z, Yang Y, Zhang J, Liu W, Wang G-y, Zhang Y-c, et al. Bone marrow mesenchymal stem cells ameliorate hepatic ischemia/reperfusion injuries via inactivation of the MEK/ERK signaling pathway in rats. Journal of Surgical Research. 2012;178(2):935-48.

110. Feng Y, Zhu R, Shen J, Wu J, Lu W, Zhang J, et al. Human Bone Marrow Mesenchymal Stem Cells Rescue Endothelial Cells Experiencing Chemotherapy Stress by Mitochondrial Transfer Via Tunneling Nanotubes. Stem Cells and Development. 2019;28(10):674-82.

111. Babenko VA, Silachev DN, Popkov VA, Zorova LD, Pevzner IB, Plotnikov EY, et al. Miro1 Enhances Mitochondria Transfer from Multipotent Mesenchymal Stem Cells (MMSC) to Neural Cells and Improves the Efficacy of Cell Recovery. Molecules. 2018;23(3):687.

112. Ahmad T, Mukherjee S, Pattnaik BR, Kumar M, Singh S, Rehman R, et al. Miro 1 Knockdown in Stem Cells Inhibits Mitochondrial Donation Mediated Rescue of Bronchial Epithelial Injury. Biophysical Journal. 2013;104(2):659a.

113. Jiang D, Gao F, Zhang Y, Wong DSH, Li Q, Tse H-f, et al. Mitochondrial transfer of mesenchymal stem cells effectively protects corneal epithelial cells from mitochondrial damage. Cell Death & Disease. 2016;7(11):e2467-e.

114. Gonçalves FDC, Luk F, Korevaar SS, Bouzid R, Paz AH, López-Iglesias C, et al. Membrane particles generated from mesenchymal stromal cells modulate immune responses by selective targeting of pro-inflammatory monocytes. Scientific Reports. 2017;7(1).

115. Raposo G, Stahl PD. Extracellular vesicles: a new communication paradigm? Nat Rev Mol Cell Biol. 2019;20(9):509-10.

116. Tamura R, Uemoto S, Tabata Y. Immunosuppressive effect of mesenchymal stem cell-derived exosomes on a concanavalin A-induced liver injury model. Inflamm Regen. 2016;36:26.

117. Dalirfardouei R, Jamialahmadi K, Jafarian AH, Mahdipour E. Promising effects of exosomes isolated from menstrual blood-derived mesenchymal stem cell on wound-healing process in diabetic mouse model. J Tissue Eng Regen Med. 2019;13(4):555-68.

118. Zhang B, Wu X, Zhang X, Sun Y, Yan Y, Shi H, et al. Human umbilical cord mesenchymal stem cell exosomes enhance angiogenesis through the Wnt4/β-catenin pathway. Stem Cells Transl Med. 2015;4(5):513-22.

119. Liu D, Kou X, Chen C, Liu S, Liu Y, Yu W, et al. Circulating apoptotic bodies maintain mesenchymal stem cell homeostasis and ameliorate osteopenia via transferring multiple cellular factors. Cell Res. 2018;28(9):918-33.

120. Liu H, Liu S, Qiu X, Yang X, Bao L, Pu F, et al. Donor MSCs release apoptotic bodies to improve myocardial infarction via autophagy regulation in recipient cells. Autophagy. 2020;16(12):2140-55.

121. Krasnodembskaya A, Song Y, Fang X, Gupta N, Serikov V, Lee JW, et al. Antibacterial Effect of Human Mesenchymal Stem Cells Is Mediated in Part from Secretion of the Antimicrobial Peptide LL-37. STEM CELLS. 2010;28(12):2229-38.

122. Mei SHJ, Haitsma JJ, Dos Santos CC, Deng Y, Lai PFH, Slutsky AS, et al. Mesenchymal Stem Cells Reduce Inflammation while Enhancing Bacterial Clearance and Improving Survival in Sepsis. American Journal of Respiratory and Critical Care Medicine. 2010;182(8):1047-57.

123. Bermudez MA, Sendon-Lago J, Eiro N, Trevino M, Gonzalez F, Yebra-Pimentel E, et al. Corneal Epithelial Wound Healing and Bactericidal Effect of Conditioned Medium From Human Uterine Cervical Stem Cells. Investigative Ophthalmology & Visual Science. 2015;56(2):983-92.

124. Vizoso F, Eiro N, Cid S, Schneider J, Perez-Fernandez R. Mesenchymal Stem Cell Secretome: Toward Cell-Free Therapeutic Strategies in Regenerative Medicine. International Journal of Molecular Sciences. 2017;18(9):1852.

125. Yang D, Chen Q, Hoover DM, Staley P, Tucker KD, Lubkowski J, et al. Many chemokines including CCL20/MIP-3α display antimicrobial activity. Journal of Leukocyte Biology. 2003;74(3):448-55.

126. Shi L, Wang L, Xu R, Zhang C, Xie Y, Liu K, et al. Mesenchymal stem cell therapy for severe COVID-19. Signal Transduction and Targeted Therapy. 2021;6(1).

127. Golchin A, Seyedjafari E, Ardeshirylajimi A. Mesenchymal Stem Cell Therapy for COVID-19: Present or Future. Stem Cell Reviews and Reports. 2020;16(3):427-33.

128. COVID-19 Stem cell search query [Internet]. 2021 [cited 24/11/2021]. Available from: https://clinicaltrials.gov/ct2/results?term=stem+cell&cond=COVID-19&age_v=&gndr=&type=&rslt=&Search=Apply.

129. Leng Z, Zhu R, Hou W, Feng Y, Yang Y, Han Q, et al. Transplantation of ACE2- Mesenchymal Stem Cells Improves the Outcome of Patients with COVID-19 Pneumonia. Aging and disease. 2020;11(2):216-28.

130. Meng F, Xu R, Wang S, Xu Z, Zhang C, Li Y, et al. Human umbilical cord-derived mesenchymal stem cell therapy in patients with COVID-19: a phase 1 clinical trial. Signal Transduction and Targeted Therapy. 2020;5(1).

131. Sengupta V, Sengupta S, Lazo A, Woods P, Nolan A, Bremer N. Exosomes Derived from Bone Marrow Mesenchymal Stem Cells as Treatment for Severe COVID-19. Stem Cells and Development. 2020;29(12):747-54.

132. Liang B, Chen J, Li T, Wu H, Yang W, Li Y, et al. Clinical remission of a critically ill COVID-19 patient treated by human umbilical cord mesenchymal stem cells: A case report. Medicine (Baltimore). 2020;99(31):e21429-e.

133. Lin PP, Wang Y, Lozano G. Mesenchymal Stem Cells and the Origin of Ewing's Sarcoma. Sarcoma. 2011;2011:1-8.

134. Amariglio N, Hirshberg A, Scheithauer BW, Cohen Y, Loewenthal R, Trakhtenbrot L, et al. Donor-Derived Brain Tumor Following Neural Stem Cell Transplantation in an Ataxia Telangiectasia Patient. PLoS Medicine. 2009;6(2):e1000029.

135. Uccelli A, Moretta L, Pistoia V. Mesenchymal stem cells in health and disease. Nature Reviews Immunology. 2008;8(9):726-36.

136. Karnoub AE, Dash AB, Vo AP, Sullivan A, Brooks MW, Bell GW, et al. Mesenchymal stem cells within tumour stroma promote breast cancer metastasis. Nature. 2007;449(7162):557-63.

137. Weis SM, Cheresh DA. Tumor angiogenesis: molecular pathways and therapeutic targets. Nature Medicine. 2011;17(11):1359-70.

138. Chen G, Yue A, Ruan Z, Yin Y, Wang R, Ren Y, et al. Human Umbilical Cord-Derived Mesenchymal Stem Cells Do Not Undergo Malignant Transformation during Long-Term Culturing in Serum-Free Medium. PLoS ONE. 2014;9(6):e98565.

139. Wang Y, Fan H, Zhou B, Ju Z, Yu L, Guo L, et al. Fusion of human umbilical cord mesenchymal stem cells with esophageal carcinoma cells inhibits the tumorigenicity of esophageal carcinoma cells. Int J Oncol. 2012;40(2):370-7.

140. Melzer C, Von Der Ohe J, Hass R. MSC stimulate ovarian tumor growth during intercellular communication but reduce tumorigenicity after fusion with ovarian cancer cells. Cell Communication and Signaling. 2018;16(1).

141. Li W, Ren G, Huang Y, Su J, Han Y, Li J, et al. Mesenchymal stem cells: a double-edged sword in regulating immune responses. Cell Death & Differentiation. 2012;19(9):1505-13.

142. García-Bernal D, García-Arranz M, Yáñez RM, Hervás-Salcedo R, Cortés A, Fernández-García M, et al. The Current Status of Mesenchymal Stromal Cells: Controversies, Unresolved Issues and Some Promising Solutions to Improve Their Therapeutic Efficacy. Frontiers in Cell and Developmental Biology. 2021;9(609).

143. ClinicalTrials.gov. Stem cell studies index 2022 [Available from: https://clinicaltrials.gov/ct2/results?cond=&term=stem+cell&cntry=&state=&city=&dist=.

144. ClinicalTrials.gov. Mesenchymal stem cell studies index 2022 [Available from: https://clinicaltrials.gov/ct2/results?cond=&term=Mesenchymal+stem+cell&cntry=&state=&city=&dist=.

145. Kazanci M, Roschger P, Paschalis EP, Klaushofer K, Fratzl P. Bone osteonal tissues by Raman spectral mapping: Orientation–composition. Journal of Structural Biology. 2006;156(3):489-96.

146. Kanczler JM, Oreffo ROC. Osteogenesis and angiogenesis: The potential for engineering bone. Eur Cells Mater. 2008;15:100-14.

147. Office of the Surgeon G. Reports of the Surgeon General. Bone Health and Osteoporosis: A Report of the Surgeon General. Rockville (MD): Office of the Surgeon General (US); 2004.

148. Calori GM, Colombo M, Mazza E, Ripamonti C, Mazzola S, Marelli N, et al. Monotherapy vs. polytherapy in the treatment of forearm non-unions and bone defects. Injury. 2013;44:S63-S9.

149. Calori GM, D'Avino M, Tagliabue L, Albisetti W, D'Imporzano M, Peretti G. An ongoing research for evaluation of treatment with BMPs or AGFs in long bone non-union: Protocol description and preliminary results. Injury. 2006;37(3):S43-S50.

150. Giannoudis PV, Einhorn TA, Marsh D. Fracture healing: The diamond concept. Injury. 2007;38:S3-S6.

151. Elkhenany H, Bourdo S, Hecht S, Donnell R, Gerard D, Abdelwahed R, et al. Graphene nanoparticles as osteoinductive and osteoconductive platform for stem cell and bone regeneration. Nanomedicine: Nanotechnology, Biology and Medicine. 2017;13(7):2117-26.

152. Zhang J, Liu X, Li H, Chen C, Hu B, Niu X, et al. Exosomes/tricalcium phosphate combination scaffolds can enhance bone regeneration by activating the PI3K/Akt signaling pathway. Stem Cell Research & Therapy. 2016;7(1).

153. Fu, Liu, Halim, Ju, Luo, Song. Mesenchymal Stem Cell Migration and Tissue Repair. Cells. 2019;8(8):784.

154. Asanbaeva A, Masuda K, Thonar EJMA, Klisch SM, Sah RL. Cartilage growth and remodeling: modulation of balance between proteoglycan and collagen network in vitro with β-aminopropionitrile. Osteoarthritis and Cartilage. 2008;16(1):1-11.

155. Richardson SM, Kalamegam G, Pushparaj PN, Matta C, Memic A, Khademhosseini A, et al. Mesenchymal stem cells in regenerative medicine: Focus on articular cartilage and intervertebral disc regeneration. Methods. 2016;99:69-80.

156. Krishnan Y, Grodzinsky AJ. Cartilage diseases. Matrix Biology. 2018;71-72:51-69.

157. Arden N, Nevitt MC. Osteoarthritis: Epidemiology. Best Practice & Research Clinical Rheumatology. 2006;20(1):3-25.

158. Pak J, Lee JH, Lee SH. Regenerative Repair of Damaged Meniscus with Autologous Adipose Tissue-Derived Stem Cells. BioMed Research International. 2014;2014:1-10.

159. Vonk LA, Van Dooremalen SFJ, Liv N, Klumperman J, Coffer PJ, Saris DBF, et al. Mesenchymal Stromal/stem Cell-derived Extracellular Vesicles Promote Human Cartilage Regeneration In Vitro. Theranostics. 2018;8(4):906-20.

160. Shadrach JL, Wagers AJ. Stem cells for skeletal muscle repair. Philosophical Transactions of the Royal Society B: Biological Sciences. 2011;366(1575):2297-306.

161. Yin H, Price F, Rudnicki MA. Satellite Cells and the Muscle Stem Cell Niche. Physiological Reviews. 2013;93(1):23-67.

162. Mauro A. SATELLITE CELL OF SKELETAL MUSCLE FIBERS. The Journal of Biophysical and Biochemical Cytology. 1961;9(2):493-5.

163. Świerczek-Lasek B, Tolak L, Bijoch L, Stefaniuk M, Szpak P, Kalaszczynska I, et al. Comparison of Muscle Regeneration after BMSC-Conditioned Medium, Syngeneic, or Allogeneic BMSC Injection. Cells. 2022;11(18):2843.

164. Salemi S, Prange JA, Baumgartner V, Mohr-Haralampieva D, Eberli D. Adult stem cell sources for skeletal and smooth muscle tissue engineering. Stem Cell Research & Therapy. 2022;13(1):156.

165. Butler J, Epstein SE, Greene SJ, Quyyumi AA, Sikora S, Kim RJ, et al. Intravenous Allogeneic Mesenchymal Stem Cells for Nonischemic Cardiomyopathy. Circulation Research. 2017;120(2):332-40.

166. Xing Y, Shi S, Zhang Y, Liu F, Zhu L, Shi B, et al. Construction of engineered myocardial tissues in vitro with cardiomyocyte-like cells and a polylactic-co-glycolic acid polymer. Mol Med Rep. 2019;20(3):2403-9.

167. Hernández R, Jiménez-Luna C, Perales-Adán J, Perazzoli G, Melguizo C, Prados J. Differentiation of Human Mesenchymal Stem Cells towards Neuronal Lineage: Clinical Trials in Nervous System Disorders. Biomol Ther (Seoul). 2020;28(1):34-44.

168. Zhang H, Huang Z, Xu Y, Zhang S. Differentiation and neurological benefit of the mesenchymal stem cells transplanted into the rat brain following intracerebral hemorrhage. Neurol Res. 2006;28(1):104-12.

169. Wang S, Cheng H, Dai G, Wang X, Hua R, Liu X, et al. Umbilical cord mesenchymal stem cell transplantation significantly improves neurological function in patients with sequelae of traumatic brain injury. 2013;1532:76-84.

170. Fesharaki M, Razavi S, Ghasemi-Mobarakeh L, Behjati M, Yarahmadian R, Kazemi M, et al. Differentiation of Human Scalp Adipose-Derived Mesenchymal Stem Cells into Mature Neural Cells on Electrospun Nanofibrous Scaffolds for Nerve Tissue Engineering Applications. Cell J. 2018;20(2):168-76.

171. Papa S, Vismara I, Mariani A, Barilani M, Rimondo S, De Paola M, et al. Mesenchymal stem cells encapsulated into biomimetic hydrogel scaffold gradually release CCL2 chemokine in situ preserving cytoarchitecture and promoting functional recovery in spinal cord injury. Journal of Controlled Release. 2018;278:49-56.

172. Lee K-D, Kuo TK-C, Whang-Peng J, Chung Y-F, Lin C-T, Chou S-H, et al. In vitro hepatic differentiation of human mesenchymal stem cells. Hepatology. 2004;40(6):1275-84.

173. Schwartz RE, Reyes M, Koodie L, Jiang Y, Blackstad M, Lund T, et al. Multipotent adult progenitor cells from bone marrow differentiate into functional hepatocyte-like cells. 2002;109(10):1291-302.

174. El-Ansary M, Abdel-Aziz I, Mogawer S, Abdel-Hamid S, Hammam O, Teaema S, et al. Phase II Trial: Undifferentiated Versus Differentiated Autologous Mesenchymal Stem Cells Transplantation in Egyptian Patients with HCV Induced Liver Cirrhosis. Stem Cell Reviews and Reports. 2012;8(3):972-81.

175. Suk KT, Yoon J-H, Kim MY, Kim CW, Kim JK, Park H, et al. Transplantation with autologous bone marrow-derived mesenchymal stem cells for alcoholic cirrhosis: Phase 2 trial. Hepatology. 2016;64(6):2185-97.

176. Tögel F, Hu Z, Weiss K, Isaac J, Lange C, Westenfelder C. Administered mesenchymal stem cells protect against ischemic acute renal failure through differentiation-independent mechanisms. American Journal of Physiology-Renal Physiology. 2005;289(1):F31-F42.

177. Collins A. Stem-cell therapy for bronchopulmonary dysplasia. Curr Opin Pediatr. 2020;32(2):210-5.

178. Xu T, Zhang Y, Chang P, Gong S, Shao L, Dong L. Mesenchymal stem cell-based therapy for radiation-induced lung injury. Stem Cell Research & Therapy. 2018;9(1).

179. Sun Z, Wang Y, Gong X, Su H, Han X. Secretion of rat tracheal epithelial cells induces mesenchymal stem cells to differentiate into epithelial cells. Cell Biology International. 2012;36(2):169-75.

180. Pan S, Zhong Y, Shan Y, Liu X, Xiao Y, Shi H. Selection of the optimum 3D-printed pore and the surface modification techniques for tissue engineering tracheal scaffold in vivo reconstruction. Journal of Biomedical Materials Research Part A. 2019;107(2):360-70.

181. Navas A, Magaña-Guerrero FS, Domínguez-López A, Chávez-García C, Partido G, Graue-Hernández EO, et al. Anti-Inflammatory and Anti-Fibrotic Effects of Human Amniotic Membrane Mesenchymal Stem Cells and Their Potential in Corneal Repair. STEM CELLS Translational Medicine. 2018;7(12):906-17.

182. Lohan P, Murphy N, Treacy O, Lynch K, Morcos M, Chen B, et al. Third-Party Allogeneic Mesenchymal Stromal Cells Prevent Rejection in a Pre-sensitized High-Risk Model of Corneal Transplantation. Frontiers in Immunology. 2018;9(2666).

183. Qi C, Xu L, Deng Y, Wang G, Wang Z, Wang L. Sericin hydrogels promote skin wound healing with effective regeneration of hair follicles and sebaceous glands after complete loss of epidermis and dermis. Biomater Sci. 2018;6(11):2859-70.

184. Zhou Z, Yan H, Liu Y, Xiao D, Li W, Wang Q, et al. Adipose-derived stem-cell-implanted poly(ϵ-caprolactone)/chitosan scaffold improves bladder regeneration in a rat model. Regen Med. 2018;13(3):331-42.

185. Wang Z, Lin Y, Jin S, Wei T, Zheng Z, Chen W. Bone marrow mesenchymal stem cells improve thymus and spleen function of aging rats through affecting P21/PCNA and suppressing oxidative stress. Aging. 2020;12(12):11386-97.

186. Xu J, Wang X, Chen J, Chen S, Li Z, Liu H, et al. Embryonic stem cell-derived mesenchymal stem cells promote colon epithelial integrity and regeneration by elevating circulating IGF-1 in colitis mice. Theranostics. 2020;10(26):12204-22.

187. Khatri R, Mazurek S, Petry SF, Linn T. Mesenchymal stem cells promote pancreatic β-cell regeneration through downregulation of FoxO1 pathway. Stem Cell Research & Therapy. 2020;11(1).

188. Idei N, Soga J, Hata T, Fujii Y, Fujimura N, Mikami S, et al. Autologous Bone-Marrow Mononuclear Cell Implantation Reduces Long-Term Major Amputation Risk in Patients With Critical Limb Ischemia. Circulation: Cardiovascular Interventions. 2011;4(1):15-25.

189. Tavassoli H, Alhosseini SN, Tay A, Chan PPY, Weng Oh SK, Warkiani ME. Large-scale production of stem cells utilizing microcarriers: A biomaterials engineering perspective from academic research to commercialized products. Biomaterials. 2018;181:333-46.

190. Jung S, Panchalingam KM, Wuerth RD, Rosenberg L, Behie LA. Large-scale production of human mesenchymal stem cells for clinical applications. Biotechnology and Applied Biochemistry. 2012;59(2):106-20.

191. Castro-Malaspina H, Ebell W, Wang S. Human bone marrow fibroblast colony-forming units (CFU-F). Prog Clin Biol Res. 1984;154:209-36.

192. Caplan AI. Adult mesenchymal stem cells for tissue engineering versus regenerative medicine. Journal of Cellular Physiology. 2007;213(2):341-7.

193. Kern S, Eichler H, Stoeve J, Klüter H, Bieback K. Comparative Analysis of Mesenchymal Stem Cells from Bone Marrow, Umbilical Cord Blood, or Adipose Tissue. STEM CELLS. 2006;24(5):1294-301.

194. Rafiq QA, Coopman K, Hewitt CJ. Scale-up of human mesenchymal stem cell culture: current technologies and future challenges. Current Opinion in Chemical Engineering. 2013;2(1):8-16.

195. Connick P, Kolappan M, Patani R, Scott MA, Crawley C, He X-L, et al. The mesenchymal stem cells in multiple sclerosis (MSCIMS) trial protocol and baseline cohort characteristics: an open-label pre-test: post-test study with blinded outcome assessments. Trials. 2011;12(1):62.

196. Mareschi K, Rustichelli D, Calabrese R, Gunetti M, Sanavio F, Castiglia S, et al. Multipotent Mesenchymal Stromal Stem Cell Expansion by Plating Whole Bone Marrow at a Low Cellular Density: A More Advantageous Method for Clinical Use. Stem Cells International. 2012;2012:1-10.

197. Reinisch A, Bartmann C, Rohde E, Schallmoser K, Bjelic-Radisic V, Lanzer G, et al. Humanized system to propagate cord blood-derived multipotent mesenchymal stromal cells for clinical application. Regen Med. 2007;2(4):371-82.

198. Rowley JA, Abraham E, Campbell AM, Brandwein HJ, Oh SK, editors. Meeting Lot-Size Challenges of Manufacturing Adherent Cells for Therapy2012.

199. Randers-Eichhorn L, Bartlett R, Sipior J, Frey D, Carter G, Lakowicz J, et al. Fluorescence-lifetime-based sensors: oxygen sensing and other biomedical applications: SPIE; 1996.

200. Liu YL, Wagner K, Robinson N, Sabatino D, Margaritis P, Xiao W, et al. Optimized Production of High-Titer Recombinant Adeno-Associated Virus in Roller Bottles. BioTechniques. 2003;34(1):184-9.

201. Andrade-Zaldívar H, Kalixto-Sánchez MA, de la Rosa APB, De León-Rodríguez A. Expansion of Human Hematopoietic Cells from Umbilical Cord Blood Using Roller Bottles in CO2 and CO2-Free Atmosphere. Stem Cells and Development. 2010;20(4):593-8.

202. Thomas CH, Collier JH, Sfeir CS, Healy KE. Engineering gene expression and protein synthesis by modulation of nuclear shape. Proceedings of the National Academy of Sciences. 2002;99(4):1972-7.

203. Bara JJ, Richards RG, Alini M, Stoddart MJ. Concise Review: Bone Marrow-Derived Mesenchymal Stem Cells Change Phenotype Following In Vitro Culture: Implications for Basic Research and the Clinic. STEM CELLS. 2014;32(7):1713-23.

204. Tsai A-C, Jeske R, Chen X, Yuan X, Li Y. Influence of Microenvironment on Mesenchymal Stem Cell Therapeutic Potency: From Planar Culture to Microcarriers. Frontiers in bioengineering and biotechnology. 2020;8:640-.

205. Boland LK, Burand AJ, Boyt DT, Dobroski H, Di L, Liszewski JN, et al. Nature vs. Nurture: Defining the Effects of Mesenchymal Stromal Cell Isolation and Culture Conditions on Resiliency to Palmitate Challenge. Frontiers in Immunology. 2019;10(1080).

206. Yin JQ, Zhu J, Ankrum JA. Manufacturing of primed mesenchymal stromal cells for therapy. Nature Biomedical Engineering. 2019;3(2):90-104.

207. Karnieli O, Friedner OM, Allickson JG, Zhang N, Jung S, Fiorentini D, et al. A consensus introduction to serum replacements and serum-free media for cellular therapies. Cytotherapy. 2017;19(2):155-69.

208. Jossen V, Van Den Bos C, Eibl R, Eibl D. Manufacturing human mesenchymal stem cells at clinical scale: process and regulatory challenges. Applied Microbiology and Biotechnology. 2018;102(9):3981-94.

209. Lee RH, Yu JM, Foskett AM, Peltier G, Reneau JC, Bazhanov N, et al. TSG-6 as a biomarker to predict efficacy of human mesenchymal stem/progenitor cells (hMSCs) in modulating sterile inflammation in vivo. Proceedings of the National Academy of Sciences. 2014;111(47):16766-71.

210. Kizilay Mancini O, Shum-Tim D, Stochaj U, Correa JA, Colmegna I. Age, atherosclerosis and type 2 diabetes reduce human mesenchymal stromal cell-mediated T-cell suppression. Stem Cell Research & Therapy. 2015;6(1).

211. Boland L, Burand AJ, Brown AJ, Boyt D, Lira VA, Ankrum JA. IFN-γ and TNF-α Pre-licensing Protects Mesenchymal Stromal Cells from the Pro-inflammatory Effects of Palmitate. Molecular Therapy. 2018;26(3):860-73.

212. Nienow AW, Rafiq QA, Coopman K, Hewitt CJ. A potentially scalable method for the harvesting of hMSCs from microcarriers. Biochemical Engineering Journal. 2014;85:79-88.

213. Garg A, Houlihan DD, Aldridge V, Suresh S, Li KK, King AL, et al. Non-enzymatic dissociation of human mesenchymal stromal cells improves chemokine-dependent migration and maintains immunosuppressive function. Cytotherapy. 2014;16(4):545-59.

214. Maguire G. Stem cell therapy without the cells. Communicative & Integrative Biology. 2013;6(6):e26631.

215. Petry F, Salzig D. Impact of Bioreactor Geometry on Mesenchymal Stem Cell Production in Stirred-Tank Bioreactors. Chemie Ingenieur Technik. 2021;93(10):1537-54.

216. Tsai AC, Pacak CA. Bioprocessing of human mesenchymal stem cells: From planar culture to microcarrier-based bioreactors. Bioengineering. 2021;8(7).

217. Li B, Wang X, Wang Y, Gou W, Yuan X, Peng J, et al. Past, present, and future of microcarrier-based tissue engineering. Journal of Orthopaedic Translation. 2015;3(2):51-7.

218. Çakmak S, Çakmak AS, Gümüşderelioğlu M. PNIPAAm-grafted thermoresponsive microcarriers: Surface-initiated ATRP synthesis and characterization. Materials Science and Engineering C. 2013;33(5):3033-40.

219. Wu C-Y, Stoecklein D, Kommajosula A, Lin J, Owsley K, Ganapathysubramanian B, et al. Shaped 3D microcarriers for adherent cell culture and analysis. Microsystems & Nanoengineering. 2018;4(1):21.

220. Malda J, Frondoza CG. Microcarriers in the engineering of cartilage and bone. Trends Biotechnol. 2006;24(7):299-304.

221. Van Wezel AL. Growth of Cell-strains and Primary Cells on Micro-carriers in Homogeneous Culture. Nature. 1967;216(5110):64-5.

222. Chen AK-L, Chen X, Choo ABH, Reuveny S, Oh SKW. Critical microcarrier properties affecting the expansion of undifferentiated human embryonic stem cells. 2011;7(2):97-111.

223. Schop D, Van Dijkhuizen-Radersma R, Borgart E, Janssen FW, Rozemuller H, Prins HJ, et al. Expansion of human mesenchymal stromal cells on microcarriers: growth and metabolism. Journal of Tissue Engineering and Regenerative Medicine. 2010;4(2):131-40.

224. Rafiq QA, Coopman K, Nienow AW, Hewitt CJ. Systematic microcarrier screening and agitated culture conditions improves human mesenchymal stem cell yield in bioreactors. Biotechnology Journal. 2016;11(4):473-86.

225. Shim TS, Kim S-H, Yang S-M. Elaborate Design Strategies Toward Novel Microcarriers for Controlled Encapsulation and Release. Particle & Particle Systems Characterization. 2013;30(1):9-45.

226. André EM, Passirani C, Seijo B, Sanchez A, Montero-Menei CN. Nano and microcarriers to improve stem cell behaviour for neuroregenerative medicine strategies: Application to Huntington's disease. Biomaterials. 2016;83:347-62.

227. El-Sherbiny IM, Smyth HDC. Biodegradable nano-micro carrier systems for sustained pulmonary drug delivery: (I) Self-assembled nanoparticles encapsulated in respirable/swellable semi-IPN microspheres. International Journal of Pharmaceutics. 2010;395(1-2):132-41.

228. Dobson J. Magnetic micro- and nano-particle-based targeting for drug and gene delivery. Nanomedicine. 2006;1(1):31-7.

229. Liu X, Jin X, Ma PX. Nanofibrous hollow microspheres self-assembled from star-shaped polymers as injectable cell carriers for knee repair. Nat Mater. 2011;10(5):398-406.

230. Engler AJ, Sen S, Sweeney HL, Discher DE. Matrix Elasticity Directs Stem Cell Lineage Specification. Cell. 2006;126(4):677-89.

231. Gilbert PM, Havenstrite KL, Magnusson KEG, Sacco A, Leonardi NA, Kraft P, et al. Substrate Elasticity Regulates Skeletal Muscle Stem Cell Self-Renewal in Culture. Science. 2010;329(5995):1078-81.

232. Schmidt JJ, Jeong J, Kong H. The Interplay Between Cell Adhesion Cues and Curvature of Cell Adherent Alginate Microgels in Multipotent Stem Cell Culture. Tissue Engineering Part A. 2011;17(21-22):2687-94.

233. Curran JM, Chen R, Hunt JA. Controlling the phenotype and function of mesenchymal stem cells in vitro by adhesion to silane-modified clean glass surfaces. Biomaterials. 2005;26(34):7057-67.

234. Tang Z, Akiyama Y, Okano T. Temperature-Responsive Polymer Modified Surface for Cell Sheet Engineering. Polymers. 2012;4(3):1478-98.

235. Lee EJ, Kim YH. Synthesis and thermo-responsive properties of chitosan-g-poly (N-isopropylacrylamide) and HTCC-g-poly(N-isopropylacrylamide) copolymers. Fibers and Polymers. 2010;11(2):164-9.

236. Yang L, Pan F, Zhao X, Yaseen M, Padia F, Coffey P, et al. Thermoresponsive Copolymer Nanofilms for Controlling Cell Adhesion, Growth, and Detachment. Langmuir. 2010;26(22):17304-14.

237. Zhang Z. Injectable biomaterials for stem cell delivery and tissue regeneration. Expert Opinion on Biological Therapy. 2017;17(1):49-62.

238. Hong Y, Yu M, Weng W, Cheng K, Wang H, Lin J. Light-induced cell detachment for cell sheet technology. Biomaterials. 2013;34(1):11-8.

239. Griffin DR, Kasko AM. Photodegradable Macromers and Hydrogels for Live Cell Encapsulation and Release. Journal of the American Chemical Society. 2012;134(42):17833-.

240. Inaba R, Khademhosseini A, Suzuki H, Fukuda J. Electrochemical desorption of self-assembled monolayers for engineering cellular tissues. Biomaterials. 2009;30(21):3573-9.

241. Pilarek M, Grabowska I, Ciemerych MA, Dąbkowska K, Szewczyk KW. Morphology and growth of mammalian cells in a liquid/liquid culture system supported with oxygenated perfluorodecalin. Biotechnology Letters. 2013;35(9):1387-94.

242. Levato R, Visser J, Planell JA, Engel E, Malda J, Mateos-Timoneda MA. Biofabrication of tissue constructs by 3D bioprinting of cell-laden microcarriers. Biofabrication. 2014;6(3):035020.

243. Wang Y, Yuan X, Yu K, Meng H, Zheng Y, Peng J, et al. Fabrication of nanofibrous microcarriers mimicking extracellular matrix for functional microtissue formation and cartilage regeneration. Biomaterials. 2018;171:118-32.

244. Naqvi SM, McNamara LM. Stem Cell Mechanobiology and the Role of Biomaterials in Governing Mechanotransduction and Matrix Production for Tissue Regeneration. Frontiers in bioengineering and biotechnology. 2020;8:597661-.

245. Zheng H, Du W, Duan Y, Geng K, Deng J, Gao C. Biodegradable Anisotropic Microparticles for Stepwise Cell Adhesion and Preparation of Janus Cell Microparticles. ACS Applied Materials & Interfaces. 2018;10(43):36776-85.

246. Argentati C, Morena F, Tortorella I, Bazzucchi M, Porcellati S, Emiliani C, et al. Insight into Mechanobiology: How Stem Cells Feel Mechanical Forces and Orchestrate Biological Functions. International Journal of Molecular Sciences. 2019;20(21):5337.

247. Jansen KA, Donato DM, Balcioglu HE, Schmidt T, Danen EHJ, Koenderink GH. A guide to mechanobiology: Where biology and physics meet. Biochimica et Biophysica Acta (BBA) - Molecular Cell Research. 2015;1853(11, Part B):3043-52.

248. Wolfenson H, Yang B, Sheetz MP. Steps in Mechanotransduction Pathways that Control Cell Morphology. Annual Review of Physiology. 2019;81(1):585-605.

249. Zayzafoon M, Gathings WE, McDonald JM. Modeled Microgravity Inhibits Osteogenic Differentiation of Human Mesenchymal Stem Cells and Increases Adipogenesis. Endocrinology. 2004;145(5):2421-32.

250. Loh QL, Choong C. Three-Dimensional Scaffolds for Tissue Engineering Applications: Role of Porosity and Pore Size. Tissue Engineering Part B: Reviews. 2013;19(6):485-502.

251. Lien SM, Ko LY, Huang TJ. Effect of pore size on ECM secretion and cell growth in gelatin scaffold for articular cartilage tissue engineering. Acta Biomater. 2009;5(2):670-9.

252. Wolf K, Te Lindert M, Krause M, Alexander S, Te Riet J, Willis AL, et al. Physical limits of cell migration: Control by ECM space and nuclear deformation and tuning by proteolysis and traction force. Journal of Cell Biology. 2013;201(7):1069-84.

253. Dahl KN, Ribeiro AJS, Lammerding J. Nuclear Shape, Mechanics, and Mechanotransduction. Circulation Research. 2008;102(11):1307-18.

254. Krause M, Yang FW, Te Lindert M, Isermann P, Schepens J, Maas RJA, et al. Cell migration through three-dimensional confining pores: speed accelerations by deformation and recoil of the nucleus. Philosophical Transactions of the Royal Society B: Biological Sciences. 2019;374(1779):20180225.

255. Lipowsky HH, Bowers DT, Banik BL, Brown JL. Mesenchymal Stem Cell Deformability and Implications for Microvascular Sequestration. Annals of Biomedical Engineering. 2018;46(4):640-54.

256. Li DJ, Chai JK, Han YF, Sun TJ, Deng HP, Zhao JY, et al. Growth and migration of umbilical cord mesenchymal stem cells on polycarbonate membrane with different pore sizes. Zhonghua Yi Xue Za Zhi. 2011;91(10):699-702.

257. Werner M, Blanquer SBG, Haimi SP, Korus G, Dunlop JWC, Duda GN, et al. Surface Curvature Differentially Regulates Stem Cell Migration and Differentiation via Altered Attachment Morphology and Nuclear Deformation. Advanced Science. 2017;4(2):1600347.

258. Tseng PC, Young TH, Wang TM, Peng HW, Hou SM, Yen ML. Spontaneous osteogenesis of MSCs cultured on 3D microcarriers through alteration of cytoskeletal tension. Biomaterials. 2012;33(2):556-64.

259. Lücker PB, Javaherian S, Soleas JP, Halverson D, Zandstra PW, McGuigan AP. A microgroove patterned multiwell cell culture plate for high-throughput studies of cell alignment. Biotechnology and Bioengineering. 2014;111(12):2537-48.

260. Anene-Nzelu CG, Peh KY, Fraiszudeen A, Kuan YH, Ng SH, Toh YC, et al. Scalable alignment of three-dimensional cellular constructs in a microfluidic chip. Lab on a Chip. 2013;13(20):4124-33.

261. Leclech C, Barakat AI. Is there a universal mechanism of cell alignment in response to substrate topography? Cytoskeleton. 2021;78(6):284-92.

262. Yang L, Gao Q, Ge L, Zhou Q, Warszawik EM, Bron R, et al. Topography induced stiffness alteration of stem cells influences osteogenic differentiation. Biomaterials Science. 2020;8(9):2638-52.

263. Bružauskaitė I, Bironaitė D, Bagdonas E, Bernotienė E. Scaffolds and cells for tissue regeneration: different scaffold pore sizes—different cell effects. Cytotechnology. 2016;68(3):355-69.

264. Gerecht S, Bettinger CJ, Zhang Z, Borenstein JT, Vunjak-Novakovic G, Langer R. The effect of actin disrupting agents on contact guidance of human embryonic stem cells. Biomaterials. 2007;28(28):4068-77.

265. Dalby MJ, Gadegaard N, Tare R, Andar A, Riehle MO, Herzyk P, et al. The control of human mesenchymal cell differentiation using nanoscale symmetry and disorder. Nat Mater. 2007;6(12):997-1003.

266. Li YJ, Batra NN, You L, Meier SC, Coe IA, Yellowley CE, et al. Oscillatory fluid flow affects human marrow stromal cell proliferation and differentiation. Journal of Orthopaedic Research. 2004;22(6):1283-9.

267. Angele P, Yoo JU, Smith C, Mansour J, Jepsen KJ, Nerlich M, et al. Cyclic hydrostatic pressure enhances the chondrogenic phenotype of human mesenchymal progenitor cells differentiated in vitro. Journal of Orthopaedic Research. 2003;21(3):451-7.

268. Zhang R, Wan J, Wang H. Mechanical strain triggers differentiation of dental mesenchymal stem cells by activating osteogenesis-specific biomarkers expression. Am J Transl Res. 2019;11(1):233-44.

269. Mohammed D, Versaevel M, Bruyère C, Alaimo L, Luciano M, Vercruysse E, et al. Innovative Tools for Mechanobiology: Unraveling Outside-In and Inside-Out Mechanotransduction. Frontiers in bioengineering and biotechnology. 2019;7:162-.

270. De Arcangelis A, Georges-Labouesse E. Integrin and ECM functions: roles in vertebrate development. Trends Genet. 2000;16(9):389-95.

271. Atherton P, Lausecker F, Carisey A, Gilmore A, Critchley D, Barsukov I, et al. Force-independent interactions of talin and vinculin govern integrin-mediated mechanotransduction. bioRxiv. 2019:629683.

272. Khalil AA, de Rooij J. Cadherin mechanotransduction in leader-follower cell specification during collective migration. Experimental Cell Research. 2019;376(1):86-91.

273. Takeichi M. Dynamic contacts: rearranging adherens junctions to drive epithelial remodelling. Nature Reviews Molecular Cell Biology. 2014;15(6):397-410.

274. Harris AR, Jreij P, Fletcher DA. Mechanotransduction by the Actin Cytoskeleton: Converting Mechanical Stimuli into Biochemical Signals. Annual Review of Biophysics. 2018;47(1):617-31.

275. Sun SX, Walcott S, Wolgemuth CW. Cytoskeletal Cross-linking and Bundling in Motor-Independent Contraction. Current Biology. 2010;20(15):R649-R54.

276. Hieda M. Signal Transduction across the Nuclear Envelope: Role of the LINC Complex in Bidirectional Signaling. Cells. 2019;8(2):124.

277. Shao Y, Sang J, Fu J. On human pluripotent stem cell control: The rise of 3D bioengineering and mechanobiology. Biomaterials. 2015;52:26-43.

278. Dupont S, Morsut L, Aragona M, Enzo E, Giulitti S, Cordenonsi M, et al. Role of YAP/TAZ in mechanotransduction. Nature. 2011;474(7350):179-83.

279. Panciera T, Azzolin L, Cordenonsi M, Piccolo S. Mechanobiology of YAP and TAZ in physiology and disease. Nat Rev Mol Cell Biol. 2017;18(12):758-70.

280. Tenney RM, Discher DE. Stem cells, microenvironment mechanics, and growth factor activation. Current Opinion in Cell Biology. 2009;21(5):630-5.

281. Zhang L, Valdez JM, Zhang B, Wei L, Chang J, Xin L. ROCK Inhibitor Y-27632 Suppresses Dissociation-Induced Apoptosis of Murine Prostate Stem/Progenitor Cells and Increases Their Cloning Efficiency. PLoS ONE. 2011;6(3):e18271.

282. Arnsdorf EJ, Tummala P, Kwon RY, Jacobs CR. Mechanically induced osteogenic differentiation – the role of RhoA, ROCKII and cytoskeletal dynamics. Journal of Cell Science. 2009;122(4):546-53.

283. Hyväri L, Ojansivu M, Juntunen M, Kartasalo K, Miettinen S, Vanhatupa S. Focal Adhesion Kinase and ROCK Signaling Are Switch-Like Regulators of Human Adipose Stem Cell Differentiation towards Osteogenic and Adipogenic Lineages. Stem Cells International. 2018;2018:2190657.

284. Cargnello M, Roux PP. Activation and function of the MAPKs and their substrates, the MAPK-activated protein kinases. Microbiol Mol Biol Rev. 2011;75(1):50-83.

285. Doze VA, Perez DM. GPCRs in stem cell function. Prog Mol Biol Transl Sci. 2013;115:175-216.

286. Germaini M-M, Belhabib S, Guessasma S, Deterre R, Corre P, Weiss P. Additive manufacturing of biomaterials for bone tissue engineering – A critical review of the state of the art and new concepts. Progress in Materials Science. 2022;130:100963.

287. Reddy K, Dufera S. ADDITIVE MANUFACTURING TECHNOLOGIES. 2019.

288. Altıparmak SC, Yardley VA, Shi Z, Lin J. Extrusion-based additive manufacturing technologies: State of the art and future perspectives. Journal of Manufacturing Processes. 2022;83:607-36.

289. Derby B. Additive Manufacture of Ceramics Components by Inkjet Printing. Engineering. 2015;1(1):113-23.

290. Emons M, Obata K, Binhammer T, Ovsianikov A, Chichkov BN, Morgner U. Two-photon polymerization technique with sub-50 nm resolution by sub-10 fs laser pulses. Optical Materials Express. 2012;2(7):942.

291. Otuka AJG, Tomazio NB, Paula KT, Mendonça CR. Two-Photon Polymerization: Functionalized Microstructures, Micro-Resonators, and Bio-Scaffolds. Polymers. 2021;13(12):1994.

292. Saha SK, Wang D, Nguyen VH, Chang Y, Oakdale JS, Chen S-C. Scalable submicrometer additive manufacturing. Science. 2019;366(6461):105-9.

293. Göppert-Mayer M. Elementary processes with two quantum transitions. Annalen der Physik. 2009;18(7-8):466-79.

294. Kaiser W, Garrett CGB. Two-Photon Excitation in CaF2:EU2+. Physical Review Letters. 1961;7(6):229-31.

295. Maruo S, Nakamura O, Kawata S. Three-dimensional microfabrication with two-photon-absorbed photopolymerization. Optics Letters. 1997;22(2):132-4.

296. Kawata S, Sun H-B, Tanaka T, Takada K. Finer features for functional microdevices. Nature. 2001;412(6848):697-8.

297. Anscombe N. Direct laser writing. Nature Photonics. 2010;4(1):22-3.

298. Harinarayana V, Shin YC. Two-photon lithography for three-dimensional fabrication in micro/nanoscale regime: A comprehensive review. Optics & Laser Technology. 2021;142:107180.

299. Yang D, Jhaveri SJ, Ober CK. Three-Dimensional Microfabrication by Two-Photon Lithography. MRS Bulletin. 2005;30(12):976-82.

300. Liao C, Wuethrich A, Trau M. A material odyssey for 3D nano/microstructures: two photon polymerization based nanolithography in bioapplications. Applied Materials Today. 2020;19:100635.

301. Jonušauskas L, Gailevičius D, Rekštytė S, Baldacchini T, Juodkazis S, Malinauskas M. Mesoscale laser 3D printing. Opt Express. 2019;27(11):15205-21.

302. Tromayer M, Dobos A, Gruber P, Ajami A, Dedic R, Ovsianikov A, et al. A biocompatible diazosulfonate initiator for direct encapsulation of human stem cells via two-photon polymerization. Polymer Chemistry. 2018;9(22):3108-17.

303. Huang Z, Chi-Pong Tsui G, Deng Y, Tang C-Y. Two-photon polymerization nanolithography technology for fabrication of stimulus-responsive micro/nano-structures for biomedical applications. Nanotechnology Reviews. 2020;9(1):1118-36.

304. Bouzin M, Zeynali A, Marini M, Sironi L, Scodellaro R, D'Alfonso L, et al. Multiphoton Laser Fabrication of Hybrid Photo-Activable Biomaterials. Sensors. 2021;21(17):5891.

305. Zhang S, Wan XY, Peng YH, Yin Q. Synthesis and properties of four new two-photon polymerization initiators with expanded conjugated structures. IOP Conference Series: Materials Science and Engineering. 2019;479:012109.

306. Ligon SC, Liska R, Stampfl J, Gurr M, Mülhaupt R. Polymers for 3D Printing and Customized Additive Manufacturing. Chemical Reviews. 2017;117(15):10212-90.

307. Liao C, Anderson W, Antaw F, Trau M. Two-Photon Nanolithography of Tailored Hollow three-dimensional Microdevices for Biosystems. ACS Omega. 2019;4(1):1401-9.

308. Seet KK, Juodkazis S, Jarutis V, Misawa H. Feature-size reduction of photopolymerized structures by femtosecond optical curing of SU-8. Applied Physics Letters. 2006;89(2):024106.

309. Doraiswamy A, Jin C, Narayan RJ, Mageswaran P, Mente P, Modi R, et al. Two photon induced polymerization of organic–inorganic hybrid biomaterials for microstructured medical devices. Acta Biomaterialia. 2006;2(3):267-75.

310. Arslan A, Steiger W, Roose P, Van den Bergen H, Gruber P, Zerobin E, et al. Polymer architecture as key to unprecedented high-resolution 3D-printing performance: The case of biodegradable hexa-functional telechelic urethane-based poly-ε-caprolactone. Materials Today. 2021;44:25-39.

311. Manghnani PN, Di Francesco V, Panella La Capria C, Schlich M, Miali ME, Moore TL, et al. Preparation of anisotropic multiscale micro-hydrogels via two-photon continuous flow lithography. Journal of Colloid and Interface Science. 2022;608:622-33.

312. Hasselmann NF, Hackmann MJ, Horn W. Two-photon fabrication of hydrogel microstructures for excitation and immobilization of cells. Biomedical Microdevices. 2018;20(1).

313. Dobos A, Van Hoorick J, Steiger W, Gruber P, Markovic M, Andriotis OG, et al. Thiol–Gelatin–Norbornene Bioink for Laser-Based High-Definition Bioprinting. Advanced Healthcare Materials. 2020;9(15):1900752.

314. Kaehr B, Shear JB. Multiphoton fabrication of chemically responsive protein hydrogels for microactuation. Proceedings of the National Academy of Sciences. 2008;105(26):8850-4.

315. Gebinoga M, Katzmann J, Fernekorn U, Hampl J, Weise F, Klett M, et al. Multi-photon structuring of native polymers: A case study for structuring natural proteins. Engineering in Life Sciences. 2013;13(4):368-75.

316. Koroleva A, Gittard S, Schlie S, Deiwick A, Jockenhoevel S, Chichkov B. Fabrication of fibrin scaffolds with controlled microscale architecture by a two-photon polymerization–micromolding technique. Biofabrication. 2012;4(1):015001.

317. Sänger JC, Pauw BR, Sturm H, Günster J. First time additively manufactured advanced ceramics by using two-photon polymerization for powder processing. Open Ceramics. 2020;4:100040.

318. Sun HCM, Liao P, Wei T, Zhang L, Sun D. Magnetically Powered Biodegradable Microswimmers. Micromachines. 2020;11(4):404.

319. Hu Q, Rance GA, Trindade GF, Pervan D, Jiang L, Foerster A, et al. The influence of printing parameters on multi-material two-photon polymerisation based micro additive manufacturing. Additive Manufacturing. 2022;51:102575.

320. Baldacchini T, LaFratta CN, Farrer RA, Teich MC, Saleh BEA, Naughton MJ, et al. Acrylic-based resin with favorable properties for three-dimensional two-photon polymerization. Journal of Applied Physics. 2004;95(11):6072-6.

321. Richter B, Hahn V, Bertels S, Claus TK, Wegener M, Delaittre G, et al. Guiding Cell Attachment in 3D Microscaffolds Selectively Functionalized with Two Distinct Adhesion Proteins. Advanced Materials. 2017;29(5):1604342.

322. Yasa IC, Tabak AF, Yasa O, Ceylan H, Sitti M. 3D-Printed Microrobotic Transporters with Recapitulated Stem Cell Niche for Programmable and Active Cell Delivery. Advanced Functional Materials. 2019;29(17):1808992.

323. He Y, Luckett J, Begines B, Dubern J-F, Hook AL, Prina E, et al. Ink-jet 3D printing as a strategy for developing bespoke non-eluting biofilm resistant medical devices. Biomaterials. 2022;281:121350.

324. Hook AL, Chang CY, Yang J, Atkinson S, Langer R, Anderson DG, et al. Discovery of Novel Materials with Broad Resistance to Bacterial Attachment Using Combinatorial Polymer Microarrays. Advanced Materials. 2013;25(18):2542-7.

325. Dabbagh SR, Sarabi MR, Rahbarghazi R, Sokullu E, Yetisen AK, Tasoglu S. 3D-printed microneedles in biomedical applications. iScience. 2021;24(1):102012.

326. Son AI, Opfermann JD, McCue C, Ziobro J, Abrahams JH, Jones K, et al. An Implantable Micro-Caged Device for Direct Local Delivery of Agents. Scientific Reports. 2017;7(1).

327. Fu P, Li H, Gong J, Fan Z, Smith AT, Shen K, et al. 4D printing of polymers: Techniques, materials, and prospects. Progress in Polymer Science. 2022;126:101506.

328. Lemma ED, Spagnolo B, De Vittorio M, Pisanello F. Studying Cell Mechanobiology in 3D: The Two-Photon Lithography Approach. Trends in Biotechnology. 2019;37(4):358-72.

329. Larramendy F, Yoshida S, Maier D, Fekete Z, Takeuchi S, Paul O. 3D arrays of microcages by two-photon lithography for spatial organization of living cells. Lab on a Chip. 2019;19(5):875-84.

330. van der Velden G, Fan D, Staufer U. Fabrication of a microfluidic device by using two-photon lithography on a positive photoresist. Micro and Nano Engineering. 2020;7:100054.

331. Maddox S, Afshar-Mohajer M, Zou M. Digitization, replication, and modification of physical surfaces using two-photon lithography. Journal of Manufacturing Processes. 2020;54:180-9.

332. Gill EL, Li X, Birch MA, Huang YYS. Multi-length scale bioprinting towards simulating microenvironmental cues. Bio-Design and Manufacturing. 2018;1(2):77-88.

333. Agrawal L, Saidani M, Guillaud L, Terenzio M. Development of 3D culture scaffolds for directional neuronal growth using 2-photon lithography. Materials Science and Engineering: C. 2021;131:112502.

334. Nguyen AK, Narayan RJ. Two-photon polymerization for biological applications. Materials Today. 2017;20(6):314-22.

335. Thompson JR, Worthington KS, Green BJ, Mullin NK, Jiao C, Kaalberg EE, et al. Two-photon polymerized poly(caprolactone) retinal cell delivery scaffolds and their systemic and retinal biocompatibility. Acta biomaterialia. 2019;94:204-18.

336. Nguyen AK, Gittard SD, Koroleva A, Schlie S, Gaidukeviciute A, Chichkov BN, et al. Two-photon polymerization of polyethylene glycol diacrylate scaffolds with riboflavin and triethanolamine used as a water-soluble photoinitiator. Regenerative Medicine. 2013;8(6):725-38.

337. Sun Q, Juodkazis S, Murazawa N, Misawa H, Mizeikis V. Freestanding and movable photonic microstructures fabricated by photopolymerization with femtosecond laser pulses. Journal of Micromechanics and Microengineering Structures, Devices and Systems. 2010;20(3):5.

338. Zhu Z, Anwer N, Mathieu L. Geometric deviation modeling with Statistical Shape Analysis in Design for Additive Manufacturing. Procedia CIRP. 2019;84:496-501.

339. Zhang F, Hu Q, Castañon A, He Y, Liu Y, Paul BT, et al. Multi-branched benzylidene ketone based photoinitiators for multiphoton fabrication. Additive Manufacturing. 2017;16:206-12.

340. Zandrini T, Liaros N, Jiang LJ, Lu YF, Fourkas JT, Osellame R, et al. Effect of the resin viscosity on the writing properties of two-photon polymerization. Optical Materials Express. 2019;9(6):2601.

341. Cordeiro AS, Tekko IA, Jomaa MH, Vora L, McAlister E, Volpe-Zanutto F, et al. Two-Photon Polymerisation 3D Printing of Microneedle Array Templates with Versatile Designs: Application in the Development of Polymeric Drug Delivery Systems. Pharmaceutical Research. 2020;37(9).

342. Schift H, Kirchner R, Chidambaram N, Altana M. Surface smoothening of the inherent roughness of micro-lenses fabricated with 2-photon lithography: SPIE; 2018.

343. Li X, Klausen LH, Zhang W, Jahed Z, Tsai C-T, Li TL, et al. Nanoscale Surface Topography Reduces Focal Adhesions and Cell Stiffness by Enhancing Integrin Endocytosis. Nano Letters. 2021;21(19):8518-26.

344. Sun H-B, Kawata S. Two-Photon Photopolymerization and 3D Lithographic Microfabrication. NMR • 3D Analysis • Photopolymerization. Berlin, Heidelberg: Springer Berlin Heidelberg; 2004. p. 169-273.

345. Obata K, El-tamer A, Koch L, Hinze U, Chichkov BN. High-aspect 3D two-photon polymerization structuring with widened objective working range (WOW-2PP). Light: Science and Applications. 2013;2(12):4.

346. Faraji Rad Z, Prewett PD, Davies GJ. High-resolution two-photon polymerization: the most versatile technique for the fabrication of microneedle arrays. Microsystems & Nanoengineering. 2021;7(1).

347. Bougdid Y, Sekkat Z. Voxels Optimization in 3D Laser Nanoprinting. Scientific Reports. 2020;10(1).

348. Aderneuer T, Fernández O, Ferrini R. Two-photon grayscale lithography for free-form micro-optical arrays. Opt Express. 2021;29(24):39511-20.

349. Nanoscribe_GmbH. Photonic Professional GT2 - dynamic printing precision 2022 [Available from: https://www.nanoscribe.com/en/products/photonic-professional-gt2.

350. Cao X, Gao Q, Li S, Hu S, Wang J, Fischer P, et al. Laminar Flow-Based Fiber Fabrication and Encoding via Two-Photon Lithography. ACS Applied Materials & Interfaces. 2020;12(48):54068-74.

351. Baker BM, Handorf AM, Ionescu LC, Li W-J, Mauck RL. New directions in nanofibrous scaffolds for soft tissue engineering and regeneration. Expert Review of Medical Devices. 2009;6(5):515-32.

352. Kurselis K, Kiyan R, Bagratashvili VN, Popov VK, Chichkov BN. 3D fabrication of all-polymer conductive microstructures by two photon polymerization. Opt Express. 2013;21(25):31029.

353. Ingram PN, Chen YC, Yoon E, editors. PolyHEMA soft lithograpy for selective cell seeding, migration blocking, and high-throughput suspension cell culture. 17th International Conference on Miniaturized Systems for Chemistry and Life Sciences, MicroTAS 2013; 2013.

354. Ricci D, Nava M, Zandrini T, Cerullo G, Raimondi M, Osellame R. Scaling-Up Techniques for the Nanofabrication of Cell Culture Substrates via Two-Photon Polymerization for Industrial-Scale Expansion of Stem Cells. Materials. 2017;10(1):66.

355. Raimondi MT, Eaton SM, Laganà M, Aprile V, Nava MM, Cerullo G, et al. Three-dimensional structural niches engineered via two-photon laser polymerization promote stem cell homing. Acta Biomaterialia. 2013;9(1):4579-84.

356. De Giglio E, Cafagna D, Giangregorio M, Domingos M, Mattioli-Belmonte M, Cometa S. PHEMA-based thin hydrogel films for biomedical applications. Journal of Bioactive and Compatible Polymers. 2011;26(4):420-34.

357. Stein O, Liu Y, Streit J, Campbell JH, Lu YF, Aglitskiy Y, et al. Fabrication of Low-Density Shock-Propagation Targets Using Two-Photon Polymerization. Fusion Science and Technology. 2018;73(2):153-65.

358. Ge Q, Li Z, Wang Z, Kowsari K, Zhang W, He X, et al. Projection micro stereolithography based 3D printing and its applications. International Journal of Extreme Manufacturing. 2020;2(2):022004.

359. Tsai A-C, Pacak CA. Bioprocessing of Human Mesenchymal Stem Cells: From Planar Culture to Microcarrier-Based Bioreactors. Bioengineering. 2021;8(7):96.

360. Hollister SJ. Porous scaffold design for tissue engineering. Nat Mater. 2005;4(7):518-24.

361. Yan X, Zhang K, Yang Y, Deng D, Lyu C, Xu H, et al. Dispersible and Dissolvable Porous Microcarrier Tablets Enable Efficient Large-Scale Human Mesenchymal Stem Cell Expansion. Tissue Eng Part C Methods. 2020;26(5):263-75.

362. Dosta P, Ferber S, Zhang Y, Wang K, Ros A, Uth N, et al. Scale-up manufacturing of gelatin-based microcarriers for cell therapy. Journal of Biomedical Materials Research Part B: Applied Biomaterials. 2020;108(7):2937-49.

363. Shekaran A, Lam A, Sim E, Jialing L, Jian L, Wen JTP, et al. Biodegradable ECM-coated PCL microcarriers support scalable human early MSC expansion and in vivo bone formation. Cytotherapy. 2016;18(10):1332-44.

364. Heathman TRJ, Nienow AW, Rafiq QA, Coopman K, Kara B, Hewitt CJ. Agitation and aeration of stirred-bioreactors for the microcarrier culture of human mesenchymal stem cells and potential implications for large-scale bioprocess development. Biochemical Engineering Journal. 2018;136:9-17.

365. Lam AT, Sim EJ, Shekaran A, Li J, Teo KL, Goggi JL, et al. Sub-confluent culture of human mesenchymal stromal cells on biodegradable polycaprolactone microcarriers enhances bone healing of rat calvarial defect. Cytotherapy. 2019;21(6):631-42.

366. Maibohm C, Silvestre OF, Borme J, Sinou M, Heggarty K, Nieder JB. Multi-beam two-photon polymerization for fast large area 3D periodic structure fabrication for bioapplications. Scientific Reports. 2020;10(1).

367. O'Brien J, Wilson I, Orton T, Pognan F. Investigation of the Alamar Blue (resazurin) fluorescent dye for the assessment of mammalian cell cytotoxicity. European Journal of Biochemistry. 2000;267(17):5421-6.

368. Sonnaert M, Papantoniou I, Luyten FP, Schrooten J. Quantitative Validation of the Presto Blue™ Metabolic Assay for Online Monitoring of Cell Proliferation in a 3D Perfusion Bioreactor System. Tissue Engineering Part C: Methods. 2015;21(6):519-29.

369. Hamid R, Rotshteyn Y, Rabadi L, Parikh R, Bullock P. Comparison of alamar blue and MTT assays for high through-put screening. Toxicol In Vitro. 2004;18(5):703-10.

370. Nava MM, Zandrini T, Cerullo G, Osellame R, Raimondi MT. 3D Stem Cell Niche Engineering via Two-Photon Laser Polymerization. Springer New York; 2017. p. 253-66.

371. Nava MM, Di Maggio N, Zandrini T, Cerullo G, Osellame R, Martin I, et al. Synthetic niche substrates engineered via two-photon laser polymerization for the expansion of human mesenchymal stromal cells. Journal of Tissue Engineering and Regenerative Medicine. 2017;11(10):2836-45.

372. Ngandu Mpoyi E, Cantini M, Reynolds PM, Gadegaard N, Dalby MJ, Salmerón-Sánchez M. Protein Adsorption as a Key Mediator in the Nanotopographical Control of Cell Behavior. ACS Nano. 2016;10(7):6638-47.

373. dos Santos RL, de Sampaio GA, de Carvalho FG, Pithon MM, Guênes GM, Alves PM. Influence of degree of conversion on the biocompatibility of different composites in vivo. J Adhes Dent. 2014;16(1):15-20.

374. Hudson DE, Hudson DO, Wininger JM, Richardson BD. Penetration of Laser Light at 808 and 980 nm in Bovine Tissue Samples. Photomedicine and Laser Surgery. 2013;31(4):163-8.

375. Chen C, Garber L, Smoak M, Fargason C, Scherr T, Blackburn C, et al. In Vitro and In Vivo Characterization of Pentaerythritol Triacrylate-co-Trimethylolpropane Nanocomposite Scaffolds as Potential Bone Augments and Grafts. Tissue Engineering Part A. 2015;21(1-2):320-31.

376. Moon JJ, Hahn MS, Kim I, Nsiah BA, West JL. Micropatterning of poly(ethylene glycol) diacrylate hydrogels with biomolecules to regulate and guide endothelial morphogenesis. Tissue Eng Part A. 2009;15(3):579-85.

377. Thorpe J, Nasir A, Burroughs L, Meurs J, Pijuan-Galito S, Irvine DJ, et al. Discovery of a Novel Polymer for Xeno-free, Long-term Culture of Human Pluripotent Stem Cell Expansion. bioRxiv. 2020:2020.09.16.298810.

378. Xu CS, Hayworth KJ, Lu Z, Grob P, Hassan AM, García-Cerdán JG, et al. Enhanced FIB-SEM systems for large-volume 3D imaging. eLife. 2017;6.

379. Weisgrab G, Guillaume O, Guo Z, Heimel P, Slezak P, Poot A, et al. 3D Printing of large-scale and highly porous biodegradable tissue engineering scaffolds from poly(trimethylene-carbonate) using two-photon-polymerization. Biofabrication. 2020;12(4):045036.

380. Ren T, Steiger W, Chen P, Ovsianikov A, Demirci U. Enhancing cell packing in buckyballs by acoustofluidic activation. Biofabrication. 2020;12(2):025033.

381. Sala F, Ficorella C, Martínez Vázquez R, Eichholz HM, Käs JA, Osellame R. Rapid Prototyping of 3D Biochips for Cell Motility Studies Using Two-Photon Polymerization. Frontiers in Bioengineering and Biotechnology. 2021;9.

382. Gadelorge M, Bourdens M, Espagnolle N, Bardiaux C, Murrell J, Savary L, et al. Clinical-scale expansion of adipose-derived stromal cells starting from stromal vascular fraction in a single-use bioreactor: proof of concept for autologous applications. Journal of Tissue Engineering and Regenerative Medicine. 2018;12(1):129-41.

383. Seniutinas G, Weber A, Padeste C, Sakellari I, Farsari M, David C. Beyond 100 nm resolution in 3D laser lithography — Post processing solutions. Microelectronic Engineering. 2018;191:25-31.

384. Minett TW, Tighe BJ, Lydon MJ, Rees DA. Requirements for cell spreading on polyHEMA coated culture substrates. Cell Biology International Reports. 1984;8(2):151-9.

385. Bouchaour T. Dye retention by a photochemical crosslinked poly(2- Hydroxy-Ethyl-Meth-Acrylic) network in water2015.

386. Bardakova KN, Faletrov YV, Epifanov EO, Minaev NV, Kaplin VS, Piskun YA, et al. A Hydrophobic Derivative of Ciprofloxacin as a New Photoinitiator of Two-Photon Polymerization: Synthesis and Usage for the Formation of Biocompatible Polylactide-Based 3D Scaffolds. Polymers. 2021;13(19):3385.

387. Elliott AD. Confocal Microscopy: Principles and Modern Practices. Curr Protoc Cytom. 2020;92(1):e68-e.

388. Clendenon SG, Young PA, Ferkowicz M, Phillips C, Dunn KW. Deep tissue fluorescent imaging in scattering specimens using confocal microscopy. Microsc Microanal. 2011;17(4):614-7.

389. Graf BW, Boppart SA. Imaging and Analysis of Three-Dimensional Cell Culture Models. Humana Press; 2010. p. 211-27.

390. Hupfeld J, Gorr IH, Schwald C, Beaucamp N, Wiechmann K, Kuentzer K, et al. Modulation of mesenchymal stromal cell characteristics by microcarrier culture in bioreactors. Biotechnology and Bioengineering. 2014;111(11):2290-302.

391. Goh TK-P, Zhang Z-Y, Chen AK-L, Reuveny S, Choolani M, Chan JKY, et al. Microcarrier Culture for Efficient Expansion and Osteogenic Differentiation of Human Fetal Mesenchymal Stem Cells. BioResearch Open Access. 2013;2(2):84-97.

392. Teixeira FG, Panchalingam KM, Assunção-Silva R, Serra SC, Mendes-Pinheiro B, Patrício P, et al. Modulation of the Mesenchymal Stem Cell Secretome Using Computer-Controlled Bioreactors: Impact on Neuronal Cell Proliferation, Survival and Differentiation. Scientific Reports. 2016;6(1):27791.

393. Hewitt CJ, Lee K, Nienow AW, Thomas RJ, Smith M, Thomas CR. Expansion of human mesenchymal stem cells on microcarriers. Biotechnol Lett. 2011;33(11):2325-35.

394. Eibes G, dos Santos F, Andrade PZ, Boura JS, Abecasis MMA, da Silva CL, et al. Maximizing the ex vivo expansion of human mesenchymal stem cells using a microcarrier-based stirred culture system. Journal of Biotechnology. 2010;146(4):194-7.

395. Sun LY, Hsieh DK, Syu WS, Li YS, Chiu HT, Chiou TW. Cell proliferation of human bone marrow mesenchymal stem cells on biodegradable microcarriers enhances in vitro differentiation potential. Cell Prolif. 2010;43(5):445-56.

396. Hanley PJ, Mei Z, Durett AG, da Graca Cabreira-Harrison M, Klis M, Li W, et al. Efficient manufacturing of therapeutic mesenchymal stromal cells with the use of the Quantum Cell Expansion System. Cytotherapy. 2014;16(8):1048-58.

397. Hervy M, Weber JL, Pecheul M, Dolley-Sonneville P, Henry D, Zhou Y, et al. Long Term Expansion of Bone Marrow-Derived hMSCs on Novel Synthetic Microcarriers in Xeno-Free, Defined Conditions. PLoS ONE. 2014;9(3):e92120.

398. Levato R, Planell JA, Mateos-Timoneda MA, Engel E. Role of ECM/peptide coatings on SDF-1α triggered mesenchymal stromal cell migration from microcarriers for cell therapy. Acta Biomaterialia. 2015;18:59-67.

399. Lin YM, Lim JFY, Lee J, Choolani M, Chan JKY, Reuveny S, et al. Expansion in microcarrier-spinner cultures improves the chondrogenic potential of human early mesenchymal stromal cells. Cytotherapy. 2016;18(6):740-53.

400. Ma T, Tsai A-C, Liu Y. Biomanufacturing of human mesenchymal stem cells in cell therapy: Influence of microenvironment on scalable expansion in bioreactors. Biochemical Engineering Journal. 2016;108:44-50.

401. Neuhuber B, Swanger SA, Howard L, Mackay A, Fischer I. Effects of plating density and culture time on bone marrow stromal cell characteristics. Experimental Hematology. 2008;36(9):1176-85.

402. Watari S, Hayashi K, Wood JA, Russell P, Nealey PF, Murphy CJ, et al. Modulation of osteogenic differentiation in hMSCs cells by submicron topographically-patterned ridges and grooves. Biomaterials. 2012;33(1):128-36.

403. Shi J, Zhu L, Li L, Li Z, Yang J, Wang X. A TPMS-based method for modeling porous scaffolds for bionic bone tissue engineering. Scientific Reports. 2018;8(1).

404. Castro APG, Pires T, Santos JE, Gouveia BP, Fernandes PR. Permeability versus Design in TPMS Scaffolds. Materials (Basel). 2019;12(8):1313.

405. Wang Y, Gunasekara DB, Reed MI, DiSalvo M, Bultman SJ, Sims CE, et al. A microengineered collagen scaffold for generating a polarized crypt-villus architecture of human small intestinal epithelium. Biomaterials. 2017;128:44-55.

406. Dua HS, Shanmuganathan VA, Powell-Richards AO, Tighe PJ, Joseph A. Limbal epithelial crypts: a novel anatomical structure and a putative limbal stem cell niche. British Journal of Ophthalmology. 2005;89(5):529-32.

407. Park S, Park H-H, Sun K, Gwon Y, Seong M, Kim S, et al. Hydrogel Nanospike Patch as a Flexible Anti-Pathogenic Scaffold for Regulating Stem Cell Behavior. ACS Nano. 2019;13(10):11181-93.

408. Ridley AJ, Schwartz MA, Burridge K, Firtel RA, Ginsberg MH, Borisy G, et al. Cell Migration: Integrating Signals from Front to Back. Science. 2003;302(5651):1704-9.

409. Yang Y, Wang K, Gu X, Leong KW. Biophysical Regulation of Cell Behavior—Cross Talk between Substrate Stiffness and Nanotopography. Engineering. 2017;3(1):36-54.

410. Jeon H, Simon CG, Kim G. A mini-review: Cell response to microscale, nanoscale, and hierarchical patterning of surface structure. Journal of Biomedical Materials Research Part B: Applied Biomaterials. 2014;102(7):1580-94.

411. Clark P, Connolly P, Curtis AS, Dow JA, Wilkinson CD. Topographical control of cell behaviour: II. Multiple grooved substrata. Development. 1990;108(4):635-44.

412. Jeon H, Hidai H, Hwang DJ, Healy KE, Grigoropoulos CP. The effect of micronscale anisotropic cross patterns on fibroblast migration. Biomaterials. 2010;31(15):4286-95.

413. Kim DH, Seo CH, Han K, Kwon KW, Levchenko A, Suh KY. Guided Cell Migration on Microtextured Substrates with Variable Local Density and Anisotropy. Adv Funct Mater. 2009;19(10):1579-86.

414. Cha HD, Hong JM, Kang T-Y, Jung JW, Ha D-H, Cho D-W. Effects of micro-patterns in three-dimensional scaffolds for tissue engineering applications. Journal of Micromechanics and Microengineering. 2012;22(12):125002.

415. McGregor AL, Hsia C-R, Lammerding J. Squish and squeeze — the nucleus as a physical barrier during migration in confined environments. Current Opinion in Cell Biology. 2016;40:32-40.

416. Haase K, Macadangdang JKL, Edrington CH, Cuerrier CM, Hadjiantoniou S, Harden JL, et al. Extracellular Forces Cause the Nucleus to Deform in a Highly Controlled Anisotropic Manner. Scientific Reports. 2016;6(1):21300.

417. Amer MH, Alvarez-Paino M, McLaren J, Pappalardo F, Trujillo S, Wong JQ, et al. Designing Topographically Textured Microparticles for Induction and Modulation of Osteogenesis in Mesenchymal Stem Cell Engineering. 2020.

418. Tan KY, Teo KL, Lim JFY, Chen AKL, Reuveny S, Oh SK. Serum-free media formulations are cell line–specific and require optimization for microcarrier culture. Cytotherapy. 2015;17(8):1152-65.

419. Mishra P, Martin DC, Androulakis IP, Moghe PV. Fluorescence Imaging of Actin Turnover Parses Early Stem Cell Lineage Divergence and Senescence. Scientific Reports. 2019;9(1).

420. Dos Santos F, Campbell A, Fernandes-Platzgummer A, Andrade PZ, Gimble JM, Wen Y, et al. A xenogeneic-free bioreactor system for the clinical-scale expansion of human mesenchymal stem/stromal cells. Biotechnology and Bioengineering. 2014;111(6):1116-27.

421. Timmins NE, Kiel M, Günther M, Heazlewood C, Doran MR, Brooke G, et al. Closed system isolation and scalable expansion of human placental mesenchymal stem cells. Biotechnology and Bioengineering. 2012;109(7):1817-26.

422. Zhu L, Luo D, Liu Y. Effect of the nano/microscale structure of biomaterial scaffolds on bone regeneration. International Journal of Oral Science. 2020;12(1):6.

423. Xie K, Yang Y, Jiang H. Controlling Cellular Volume via Mechanical and Physical Properties of Substrate. Biophysical Journal. 2018;114(3):675-87.

424. Kilian KA, Bugarija B, Lahn BT, Mrksich M. Geometric cues for directing the differentiation of mesenchymal stem cells. Proceedings of the National Academy of Sciences. 2010;107(11):4872-7.

425. Oh S, Brammer KS, Li YSJ, Teng D, Engler AJ, Chien S, et al. Stem cell fate dictated solely by altered nanotube dimension. Proceedings of the National Academy of Sciences. 2009;106(7):2130-5.

426. Shekaran A, Sim E, Tan KY, Chan JKY, Choolani M, Reuveny S, et al. Enhanced in vitro osteogenic differentiation of human fetal MSCs attached to 3D microcarriers versus harvested from 2D monolayers. BMC Biotechnology. 2015;15(1):102.

427. Lee SJ, Choi JS, Park KS, Khang G, Lee YM, Lee HB. Response of MG63 osteoblast-like cells onto polycarbonate membrane surfaces with different micropore sizes. Biomaterials. 2004;25(19):4699-707.

428. Tienen TG, Heijkants RG, de Groot JH, Pennings AJ, Schouten AJ, Veth RP, et al. Replacement of the knee meniscus by a porous polymer implant: a study in dogs. Am J Sports Med. 2006;34(1):64-71.

429. McBeath R, Pirone DM, Nelson CM, Bhadriraju K, Chen CS. Cell shape, cytoskeletal tension, and RhoA regulate stem cell lineage commitment. Dev Cell. 2004;6(4):483-95.

430. Alakpa EV, Burgess KEV, Chung P, Riehle MO, Gadegaard N, Dalby MJ, et al. Nacre Topography Produces Higher Crystallinity in Bone than Chemically Induced Osteogenesis. ACS Nano. 2017;11(7):6717-27.

431. Song I-H, Dennis JE. Simple evaluation method for osteoinductive capacity of cells or scaffolds using ceramic cubes. Tissue Cell. 2014;46(5):372-8.

432. Akay G, Birch MA, Bokhari MA. Microcellular polyHIPE polymer supports osteoblast growth and bone formation in vitro. Biomaterials. 2004;25(18):3991-4000.

433. Hippler M, Lemma ED, Bertels S, Blasco E, Barner-Kowollik C, Wegener M, et al. 3D Scaffolds to Study Basic Cell Biology. Advanced Materials. 2019;31(26):1808110.

434. Yourek G, McCormick SM, Mao JJ, Reilly GC. Shear stress induces osteogenic differentiation of human mesenchymal stem cells. Regen Med. 2010;5(5):713-24.

435. Zhao F, Chella R, Ma T. Effects of shear stress on 3-D human mesenchymal stem cell construct development in a perfusion bioreactor system: Experiments and hydrodynamic modeling. Biotechnology and Bioengineering. 2007;96(3):584-95.

436. Yuan X, Tsai A-C, Farrance I, Rowley JA, Ma T. Aggregation of culture expanded human mesenchymal stem cells in microcarrier-based bioreactor. Biochemical Engineering Journal. 2018;131:39-46.

437. Yang Y-HK, Ogando CR, Wang See C, Chang T-Y, Barabino GA. Changes in phenotype and differentiation potential of human mesenchymal stem cells aging in vitro. Stem Cell Research & Therapy. 2018;9(1).

438. Liu TM, Ng WM, Tan HS, Vinitha D, Yang Z, Fan JB, et al. Molecular basis of immortalization of human mesenchymal stem cells by combination of p53 knockdown and human telomerase reverse transcriptase overexpression. Stem cells and development. 2013;22(2):268-78.

439. Siska EK, Weisman I, Romano J, Ivics Z, Izsvák Z, Barkai U, et al. Generation of an immortalized mesenchymal stem cell line producing a secreted biosensor protein for glucose monitoring. PLOS ONE. 2017;12(9):e0185498.

440. Harvey JB, Phan LH, Villarreal OE, Bowser JL. CD73's Potential as an Immunotherapy Target in Gastrointestinal Cancers. Frontiers in Immunology. 2020;11.

441. Follin B, Juhl M, Cohen S, Pedersen AE, Kastrup J, Ekblond A. Increased Paracrine Immunomodulatory Potential of Mesenchymal Stromal Cells in Three-Dimensional Culture. Tissue engineering Part B, Reviews. 2016;22(4):322-9.

442. Moraes DA, Sibov TT, Pavon LF, Alvim PQ, Bonadio RS, Da Silva JR, et al. A reduction in CD90 (THY-1) expression results in increased differentiation of mesenchymal stromal cells. Stem Cell Research & Therapy. 2016;7(1):97.

443. Kauer J, Schwartz K, Tandler C, Hinterleitner C, Roerden M, Jung G, et al. CD105 (Endoglin) as negative prognostic factor in AML. Scientific Reports. 2019;9(1):18337.

444. Pham LH, Vu NB, Van Pham P. The subpopulation of CD105 negative mesenchymal stem cells show strong immunomodulation capacity compared to CD105 positive mesenchymal stem cells. Biomedical Research and Therapy. 2019;6(4):3131-40.

445. Claeyssens F, Hasan EA, Gaidukeviciute A, Achilleos DS, Ranella A, Reinhardt C, et al. Three-Dimensional Biodegradable Structures Fabricated by Two-Photon Polymerization. Langmuir. 2009;25(5):3219-23.

446. Melissinaki V, Gill AA, Ortega I, Vamvakaki M, Ranella A, Haycock JW, et al. Direct laser writing of 3D scaffolds for neural tissue engineering applications. Biofabrication. 2011;3(4):045005.

447. Raimondi MT, Eaton SM, Nava MM, Laganà M, Cerullo G, Osellame R. Two-photon laser polymerization: from fundamentals to biomedical application in tissue engineering and regenerative medicine. J Appl Biomater Funct Mater. 2012;10(1):55-65.

448. Dendukuri D, Pregibon DC, Collins J, Hatton TA, Doyle PS. Continuous-flow lithography for high-throughput microparticle synthesis. Nat Mater. 2006;5(5):365-9.

449. Geng Q, Wang D, Chen P, Chen S-C. Ultrafast multi-focus 3-D nano-fabrication based on two-photon polymerization. Nature Communications. 2019;10(1).

450. Xue G, Zhai Q, Lu H, Zhou Q, Ni K, Lin L, et al. Polarized holographic lithography system for high-uniformity microscale patterning with periodic tunability. Microsystems & Nanoengineering. 2021;7(1).

451. Bai SW, Herrera-Abreu MT, Rohn JL, Racine V, Tajadura V, Suryavanshi N, et al. Identification and characterization of a set of conserved and new regulators of cytoskeletal organization, cell morphology and migration. BMC Biology. 2011;9(1):54.

452. Kumar S, Lande NV, Barua P, Pareek A, Chakraborty S, Chakraborty N. Proteomic dissection of rice cytoskeleton reveals the dominance of microtubule and microfilament proteins, and novel components in the cytoskeleton-bound polysome. Plant Physiology and Biochemistry. 2022;170:75-86.

453. Balducci L, Blasi A, Saldarelli M, Soleti A, Pessina A, Bonomi A, et al. Immortalization of human adipose-derived stromal cells: production of cell lines with high growth rate, mesenchymal marker expression and capability to secrete high levels of angiogenic factors. Stem Cell Research & Therapy. 2014;5(3):63.

454. Mori T, Kiyono T, Imabayashi H, Takeda Y, Tsuchiya K, Miyoshi S, et al. Combination of hTERT and bmi-1, E6, or E7 Induces Prolongation of the Life Span of Bone Marrow Stromal Cells from an Elderly Donor without Affecting Their Neurogenic Potential. Molecular and Cellular Biology. 2005;25(12):5183-95.

455. Hasan A, Bagnol R, Owen R, Latif A, Rostam HM, Elsharkawy S, et al. Mineralizing Coating on 3D Printed Scaffolds for the Promotion of Osseointegration. Frontiers in Bioengineering and Biotechnology. 2022;10.

456. Burroughs L, Amer MH, Vassey M, Koch B, Figueredo GP, Mukonoweshuro B, et al. Discovery of synergistic material-topography combinations to achieve immunomodulatory osteoinductive biomaterials using a novel in vitro screening method: The ChemoTopoChip. Biomaterials. 2021;271:120740.

457. Galarza Torre A, Shaw JE, Wood A, Gilbert HTJ, Dobre O, Genever P, et al. An immortalised mesenchymal stem cell line maintains mechano-responsive behaviour and can be used as a reporter of substrate stiffness. Scientific Reports. 2018;8(1).

458. Kulebyakin K, Tyurin-Kuzmin P, Efimenko A, Voloshin N, Kartoshkin A, Karagyaur M, et al. Decreased Insulin Sensitivity in Telomerase-Immortalized Mesenchymal Stem Cells Affects Efficacy and Outcome of Adipogenic Differentiation in vitro. Frontiers in Cell and Developmental Biology. 2021;9.

459. Wang Y, Chen S, Yan Z, Pei M. A prospect of cell immortalization combined with matrix microenvironmental optimization strategy for tissue engineering and regeneration. Cell & Bioscience. 2019;9(1):7.

460. Wall I, Santiago Toledo G, Jat P. Recent advances in conditional cell immortalization technology. Cell and Gene Therapy Insights. 2016;2:339-55.

461. El-Kadiry AE-H, Rafei M, Shammaa R. Cell Therapy: Types, Regulation, and Clinical Benefits. Frontiers in Medicine. 2021;8.

462. Yang T, Rycaj K, Liu Z-M, Tang DG. Cancer Stem Cells: Constantly Evolving and Functionally Heterogeneous Therapeutic Targets. Cancer Research. 2014;74(11):2922-7.

463. Serra AT, Serra M, Silva AC, Brckalo T, Seshire A, Brito C, et al. Scalable Culture Strategies for the Expansion of Patient-Derived Cancer Stem Cell Lines. Stem Cells International. 2019;2019:1-7.

464. O'Brien CA, Kreso A, Jamieson CHM. Cancer Stem Cells and Self-renewal. Clinical Cancer Research. 2010;16(12):3113-20.

465. Visvader JE, Lindeman GJ. Cancer stem cells in solid tumours: accumulating evidence and unresolved questions. Nature Reviews Cancer. 2008;8(10):755-68.

# Appendices

## Appendix A: Polymer selection

| Polymer | Molecular weight (kDa) | Structure |
|---|---|---|
| Pentaerythritol triacrylate (PETA) | 298 | 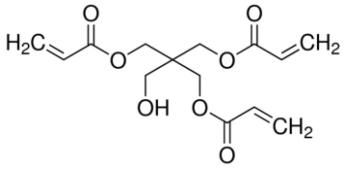 |
| Pentaerythritol tetraacrylate (PETRA) | 352 | 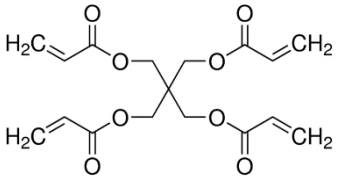 |
| Trimethylolpropane ethoxylate triacrylate (TMPETA) | 428 | 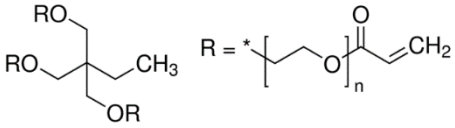 |
| Tricyclodecanedimethanol diacrylate (TCDMDA) | 304 | 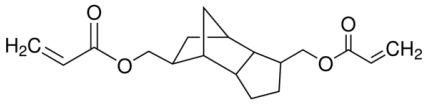 |
| Poly(ethylene glycol) diacrylate (PEGDA) | 700 | 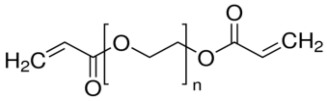 |

***Table A1:*** *The names, abbreviations, MW and chemical structures of the primary and ongoing polymers that underwent further optimisation and continued use within experiments.*

# Appendix B: Woodpile sweep SEM data

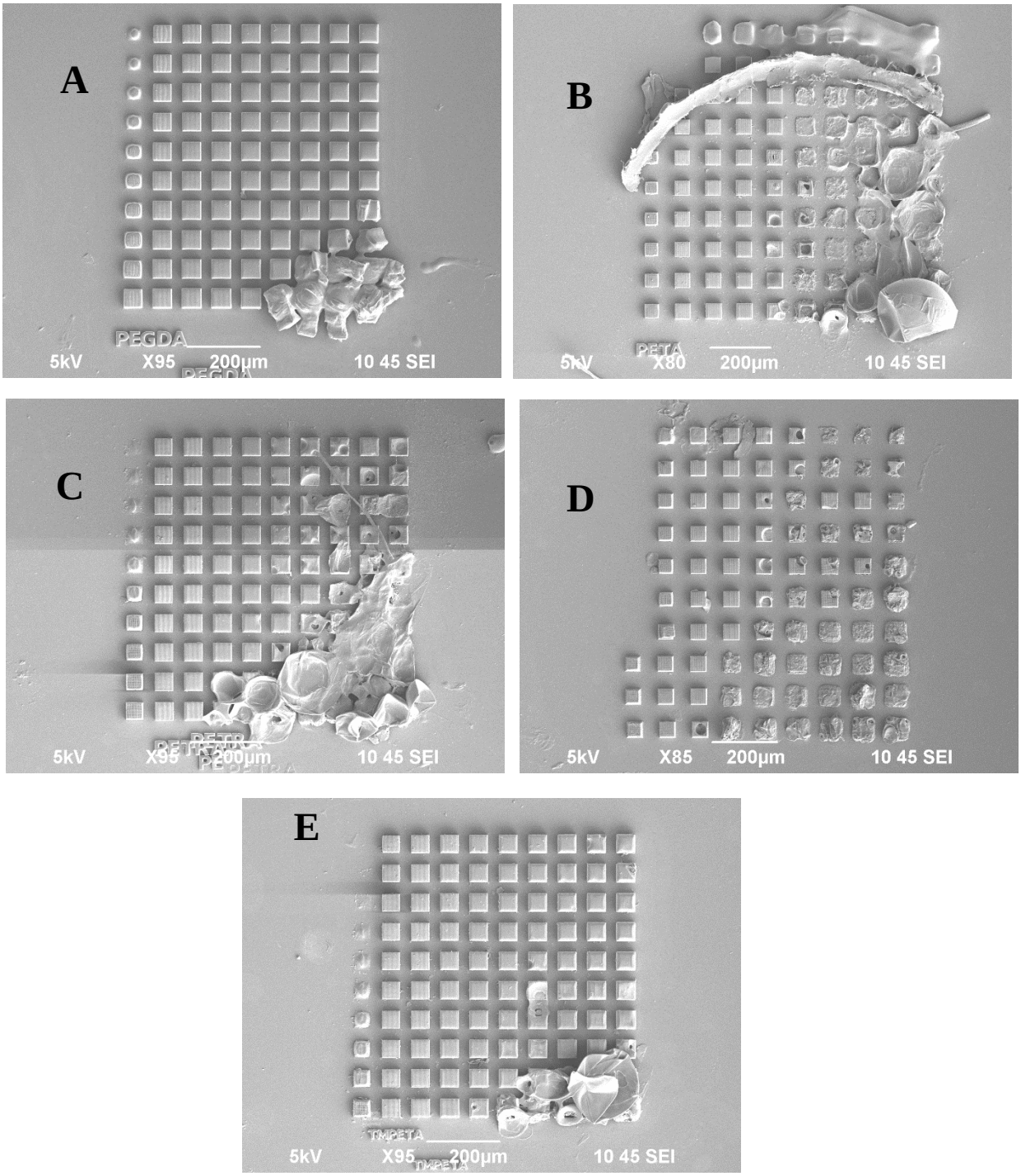


***Figure B1:*** *SEM microscopy of polymer sweeps used to create fabrication suitability heatmaps. Each structure is a repeated 50µm woodpile and laser power is increased left to right whilst writing speed is increased from bottom to top. A) PEGDA, B) PETA, C) PETRA, D) TCDMDA and E) TMPETA.*

# Appendix C: Design SEM sweep microscopy

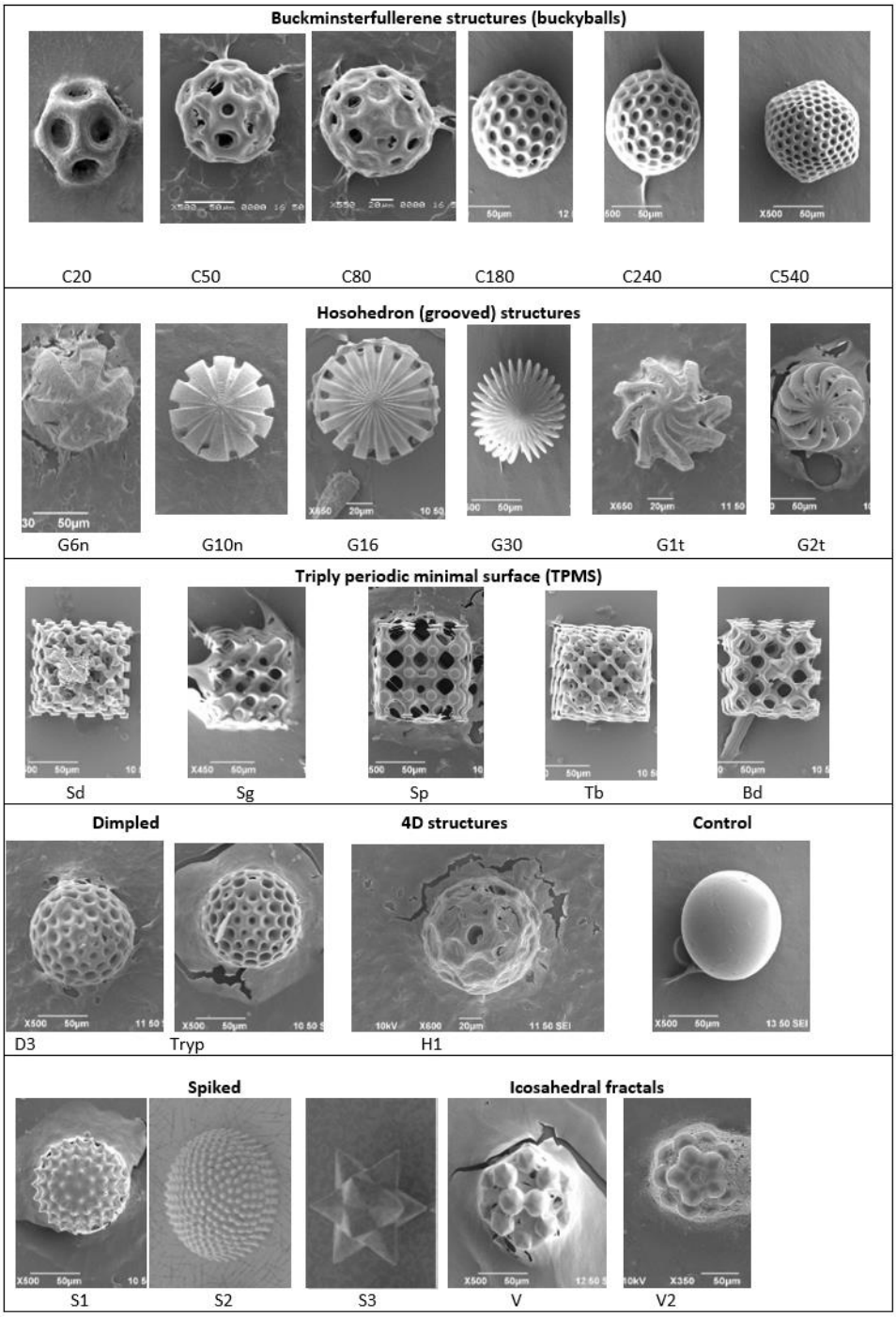


***Figure C1:*** *SEM microscopy of different microcarrier designs after iMSC growth to indicate level of cell interaction with geometry. Certain architectures had high levels of cell interaction in comparison to others. Not all designs conceived were included in these screens as some such as H2 could not be fabricated reliably without damage due to struts being too thin and fragile.*

# Appendix D: ALP activity of MSCs undergoing osteoinduction

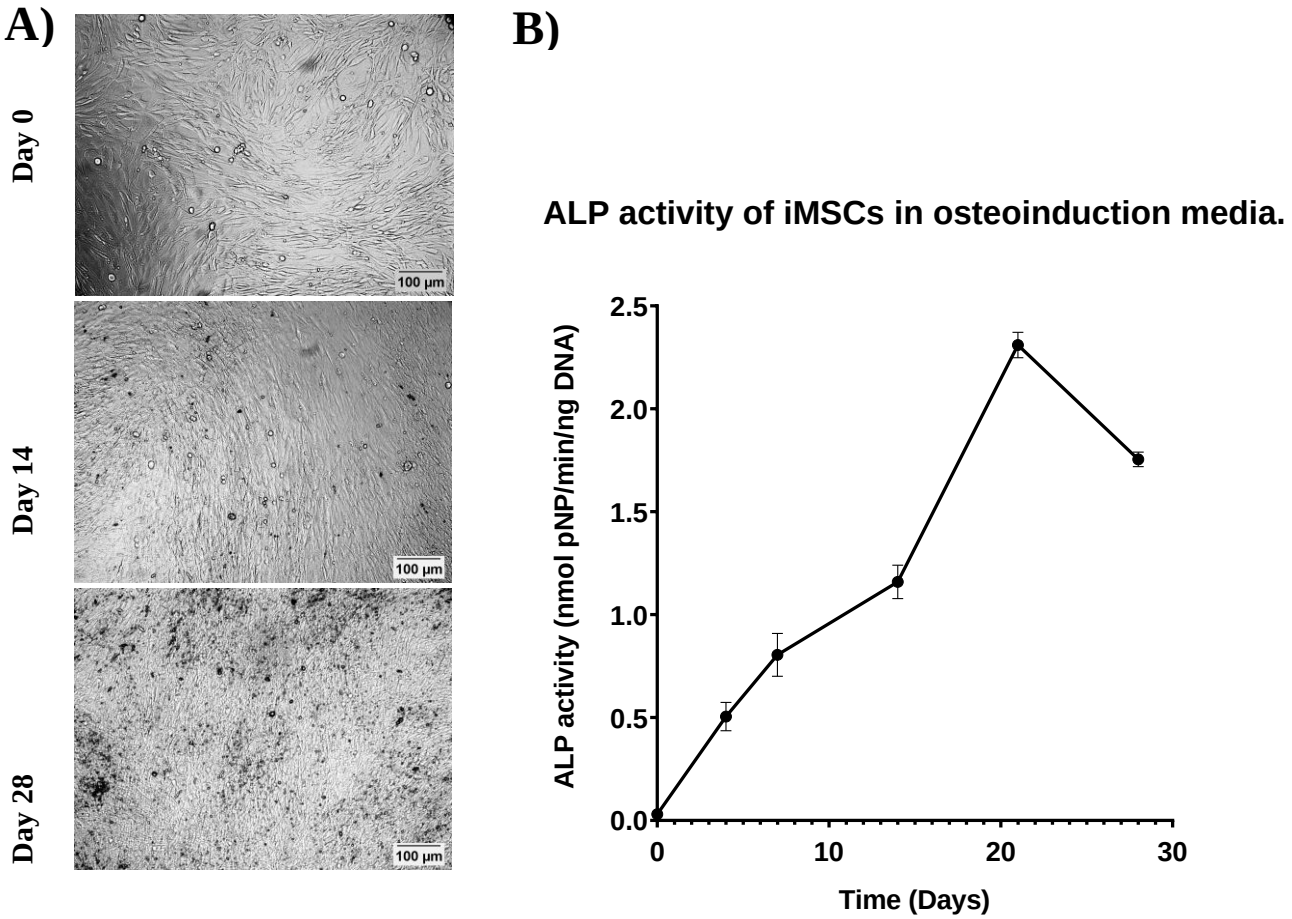


***Figure D1:*** *Characteristics of iMSCs during osteoinduction. ALP activity and microscopy for iMSCs grown in osteoinduction media over 28 days. A) Brightfield microscopy of iMSCs at varying levels of differentiation indicating change in cell morphology and increase in calcium deposits at days 0, 14 and 28. B) ALP activity normalised to DNA amount increasing from 0.21 nmol pNP/min/ng DNA at day 0 and reaching peak levels of 2.31 nmol pNP/min/ng DNA at 21 days before reducing at day 28 to 1.75 nmol pNP/min/ng DNA. Mean ± SD, (n=3).*

# Appendix E: Figure permissions

Most figures were used under a creative commons attribution license which allowed reproduction or modification of material without special permissions as long as proper acknowledgement to original authors is given. Where a CC license was not available permissions were granted via RightsLink. Records of these permissions are in figure E1.


***Figure E1:*** *Figure permissions granted by RightsLink.*